

**Microcircuit Mechanisms Regulating Nucleus Accumbens Circuit Function**

By

Kevin M. Manz

**Dissertation**

Submitted to the Faculty of the  
Graduate School of Vanderbilt University

in partial fulfillment of the requirements

for the degree of

**Doctor of Philosophy**

in

**Neuroscience**

December 14, 2019

Nashville, Tennessee

**Approved:**

Brad A. Grueter, Ph.D.

Danny G. Winder, Ph.D.

Christine Konradi, Ph.D.

Sachin Patel, M.D., Ph.D.

## ACKNOWLEDGMENTS

I would like to acknowledge the loving, patient, and unwavering support from my parents, Janice and Barry Manz, sister, Michelle Statham, and my partner and best friend, Wendy Levine, as I completed this journey. I would also like to acknowledge my doctoral adviser, Dr. Brad Grueter, for giving me the opportunity to engage in what has presently been the most formative and exciting intellectual experience of my life. Dr. Grueter's intensive and meticulous training principles, ambitious experimental pursuits, devoted mentoring style, and passion for scientific discovery have shaped my development as a future physician-scientist. Of course, my initial exposure to neuroscience would not have been possible without the mentorship, guidance, and support from my undergraduate research advisor, Dr. Christian Reich, at Ramapo College. Finally, I would like to thank my doctoral thesis committee, Neuroscience Graduate Program, Vanderbilt Brain Institute, MSTP administration team, and School of Medicine at Vanderbilt University.

## TABLE OF CONTENTS

	<b>Page</b>
ACKNOWLEDGMENTS.....	ii
LIST OF FIGURES.....	iv
 <b>Chapter</b>	
1. <i>Foreword</i> : The nucleus accumbens as the brain’s motivational hub.....	1
2. Microcircuit mechanisms regulating nucleus accumbens circuit function.....	10
2.1. Abstract.....	11
2.2. Introduction.....	11
2.3. Organizational structure of the NAc.....	13
2.4. Microcircuit elements of the NAc.....	18
2.5 Conclusion.....	36
2.6 Overall aims.....	37
3. Heterosynaptic GABA <sub>B</sub> receptor function within feedforward microcircuits gates glutamatergic transmission in the nucleus accumbens core.....	41
3.1. Abstract.....	41
3.2. Significance Statement.....	42
3.3. Introduction.....	42
3.4. Methods and materials.....	45
3.5. Results.....	49
3.6. Discussion.....	80
4. Calcium-permeable AMPA receptors trigger endocannabinoid signaling at parvalbumin interneuron synapses in the nucleus accumbens core.....	86
4.1. Abstract.....	87
4.2. Introduction.....	87
4.3. Methods and materials.....	89
4.4. Results.....	93
4.5. Discussion.....	110
5. Works in progress, concluding remarks, and future directions.....	114
5.1. Noradrenergic signaling engages a dual PV-cholinergic interneuron microcircuit to dampen feedforward inhibition in the nucleus accumbens core.....	115
5.2. State-dependent inhibitory synaptic plasticity at feedforward inhibitory synapses in the nucleus accumbens core.....	131
5.3 Assembling a model of plasticity mechanisms regulating intrinsic and extrinsic network function in the NAc.....	144
5.4 Closing.....	154

**Appendix**

A. Histamine H<sub>3</sub> receptor function biases excitatory gain onto D1 medium spiny neurons in the nucleus accumbens core.....156

    A.1. Abstract.....157

    A.2. Introduction.....157

    A.3. Methods and materials.....159

    A.4. Results.....163

    A.5. Discussion.....183

6. REFERENCES.....189

## LIST OF FIGURES

Figure	Page
2.1. Gross organizational scheme of mesolimbic reward network.....	7
2.2. Feedforward inhibitory microcircuits in the NAc.....	19
2.3. Cholinergic interneuron microcircuit interactions in the NAc.....	27
2.4. Lateral inhibitory networks formed by D1(+) and D1(-) MSNs in the NAc.....	34
2.5. Schematic depicting experimental focus within PV-IN-embedded feedforward microcircuits in the NAc.....	38
3.1. GABA <sub>B</sub> R activity reduces synaptic efficacy at glutamatergic synapses onto D1(+) and D1(-) MSNs in the NAc core.....	51
3.2. GABA <sub>B</sub> R is functionally expressed at presynaptic loci at glutamatergic synapses onto both MSN subtypes in the NAc core.....	54
3.3. GABA <sub>B</sub> R activation recruits a non-canonical intracellular signaling mechanism..	
3.4. GABA <sub>B</sub> R is functionally distinct from mGluRs in the NAc core.....	58
3.5. GABA <sub>B</sub> R is functionally distinct from CB <sub>1</sub> R at glutamatergic synapses in the NAc core.....	60
3.6. Elevating presynaptic Ca <sup>2+</sup> influx abrogates downstream GABA <sub>B</sub> R effector function.....	63
3.7. Genetically reducing the G <sub>βγ</sub> -SNAP-25 interaction blunts the synaptic effect of GABA <sub>B</sub> R.....	66
3.8. GAT-1-regulated ambient GABA acts on GABA <sub>B</sub> R to decrease glutamatergic transmission in the NAc core. ....	69

<b>3.9.</b> Parvalbumin (PV)-expressing interneurons preferentially decrease glutamatergic transmission onto D1(+) MSNs via heterosynaptic GABA <sub>B</sub> R signaling.....	72
<b>3.10.</b> GABAergic transmission at PV-IN-to-D1(+) and D1(-) MSN synapses is largely BAC-insensitive and unchanged by LFS.....	79
<b>4.1.</b> CP-AMPARs are expressed at glutamatergic synapses onto PV(+)-INs but not D1(+) or D1(-) MSNs in the NAc core.....	96
<b>4.2.</b> Low frequency stimulation (LFS) triggers long-term depression of glutamatergic transmission onto PV(+)-INs.....	98
<b>4.3.</b> LFS-induced LTD at PV(+)-IN synapses is CP-AMPAR- and CB <sub>1</sub> R-dependent.....	101
<b>4.4.</b> Tonic AEA signaling is dependent on CP-AMPAR function.....	104
<b>4.5.</b> Cocaine abolishes LFS-induced LTD at PV(+)-IN synapses.....	107
<b>4.6.</b> Cocaine decreases glutamatergic transmission via actions at CB <sub>1</sub> R in a DA-independent manner.....	109
<b>5.1.</b> Noradrenergic signaling regulates glutamatergic synapses onto PV(+)-INs but not MSNs in the NAc core.....	120
<b>5.2.</b> NE and TOM-induced depression in EPSC amplitude in PV(+)-INs in the NAc core-shell interface is putatively postsynaptic.....	121
<b>5.3.</b> Blocking SERT does not elicit similar effects as NET at glutamatergic synapses onto PV(+)-INs.....	123
<b>5.4.</b> Glutamatergic synapses onto PV(+)-INs are minimally regulated by $\alpha$ 1 and $\alpha$ 2 adrenergic receptors.....	125
<b>5.5.</b> The NEergic effects on PV-INs may be due to microcircuit alterations in cholinergic signaling.....	128

<b>5.6.</b> Downstate iLTD at PV-IN-to-MSN synapses is restricted to D1(+) MSNs.....	137
<b>5.7.</b> Upstate iLTD at PV-IN-to-MSN synapses is restricted to D1(-) MSNs.....	138
<b>5.8.</b> State dependent iLTD at PV-IN-to-D1(+) and D1(-) MSN synapses is CB <sub>1</sub> R- and GABA <sub>B</sub> R-independent.....	141
<b>5.9.</b> Pharmacological evidence that ex vivo cocaine modulates glutamatergic transmission onto PV(+)-INs in a $\sigma_1$ R-dependent manner.....	149
<b>A.1.</b> HA differentially modulates glutamatergic transmission onto D1(+) and D1(-) MSNs in the NAc core.....	166
<b>A.2.</b> HA decreases glutamatergic synaptic efficacy onto D1(+) MSNs via a presynaptic locus of action.....	169
<b>A.3.</b> HA acts via H <sub>3</sub> heteroreceptors to elicit long-term depression of glutamatergic transmission onto D1(+) MSNs.....	172
<b>A.4.</b> H <sub>3</sub> R activity tonically regulates glutamatergic synapses onto D1(-) MSNs but not D1(+) MSNs in the NAc.....	173
<b>A.5.</b> G <sub><math>\beta\gamma</math></sub> -dependent recruitment of the PI3K-Akt-GSK3 $\beta$ axis mediates HA-LTD at glutamatergic synapses onto D1(+) MSNs.....	176
<b>A.6.</b> Thalamocortical drive onto D1(+) MSNs in the NAc is differentially regulated by histamine signaling.....	179
<b>A.7.</b> Acute stress recruits endogenous H <sub>3</sub> R signaling at glutamatergic synapses onto D1(+) MSNs in the NAc.....	182

## CHAPTER 1

### ***Foreword: The nucleus accumbens as the brain's motivational hub***

An intriguing question is how common motivational urges, such as having Italian for dinner or choosing to have a night out with friends, begin to occupy conscious awareness. If the desire to engage in an activity is strong enough, or if an urge takes over our internal dialogue for long enough, we are driven to act on that desire. In many cases, the motivation to achieve an outcome is followed in close succession by the requisite behavioral act, such as consuming food when metabolic resources are low. The evolutionary necessity of hardware that orchestrates these responses is clear. Many species, particularly those with weaker executive control centers, rely on basic biological drives to engage in behaviors that promote survival. However, the question that remains is *how* a network of interconnected cells subserving distinct biobehavioral functions transforms motivation into goal-directed behavior. It is this question that has guided decades of research into the neurocircuitry of the brain's intrinsic reward center.

The notion that the brain is equipped with localized regions encoding "reward" emerged from seminal studies conducted in the 1950s. In these experiments, Olds and Milner *et al.* implanted stimulating electrodes along a fiber tract in rats now defined anatomically as the *medial forebrain bundle*. Electrical discharge from these electrodes was coupled to a lever in the animal's cage (Olds and Milner, 1954). An immediate observation was that animals would vigorously self-administer electrical stimuli to this region. Animals would escalate self-stimulation to the point where natural reinforcers, such as food and water, quickly became inconsequential. If animals were

permitted *ad libitum* access to the lever coupled to electrical stimulation, it was not uncommon for animals to self-stimulate to their demise. It became clear that the anatomical locus targeted by the electrode conveys elements of hedonic value, or pleasure, that are characteristic of an intrinsic “reward center.” Future studies revealed that stimulation of the medial forebrain bundle triggered the release of dopamine (DA) into the nucleus accumbens (NAc), a subcortical forebrain structure within the ventral striatum (Fallon and Moore, 1978; Covey and Cheer, 2019). Today, we know that DA, a catecholamine synthesized in evolutionarily-conserved regions of the brainstem, reports reward prediction errors (RPE) to the NAc, where information is then packaged and delivered to downstream limbic-motor centers (Schultz, 1998).

Evidence of a DA-enriched neural conduit encoding reward raised questions as to whether drugs used recreationally exert pharmacological effects on this pathway. It is well-established that virtually every drug of abuse, including cocaine, opiates, marijuana, nicotine, and ethanol, increases DA efflux into the NAc (Lüscher and Malenka, 2011; Lüscher, 2016; Vena et al., 2016). Although several classes of abused drugs share similar pharmacodynamic profiles, a remarkable feature of these compounds is their ability to potentiate “mesoaccumbens” DA release through distinct molecular mechanisms (Bassareo et al., 2017; Yang et al., 2018). For example, cocaine, a psychostimulant with a well-studied neurobiological profile, prevents DA reuptake into NAc-projecting terminals within the medial forebrain bundle. This is partially due to its high affinity for the DA transporter (DAT), which is responsible for clearing DA from the synaptic cleft (Siciliano and Jones, 2017). Alternatively, opiates, such as morphine and heroine, target  $\mu$  opioid receptors (MOR) on inhibitory neurons in the ventral tegmental area (VTA), which results in the disinhibition of mesolimbic DA release into the NAc (Chen et al., 2015; Corre et al., 2018).

It is surprising to note that converging mechanisms of action at NAc-projecting DA terminals fails to explain why drugs of abuse can trigger a debilitating cycle of addiction. *Addiction*, as it is defined here, is a relapsing-remitting motivational disorder characterized by persistent drug use despite harmful consequences (Wise and Koob, 2014; Koob and Volkow, 2016). A well-supported hypothesis is that chronic drug use elicits cellular and synaptic adaptations in the NAc that reorganizes mesolimbic network function (Grueter et al., 2012; Turner et al., 2018a). As drug use progresses, reward-seeking behavior evolves into a compulsive habit that depends more on motor areas in the dorsal striatum than the NAc. This model is supported by anatomical and functional studies showing that the NAc is embedded within a “spiraling” anatomical framework progressing from the VTA to the substantia nigra (SN) and dorsal striatum (nigrostriatal) (Haber et al., 2000). From a broader perspective, substances with high abuse liability appear to “hijack” the brain’s motivational network so that previously “neutral” compounds begin to drive motivational decision making.

Given that synaptic adaptations within the NAc are causally linked to relapse, or *reinstatement*, of drug-seeking behavior, extensive work has been done on how the NAc is remodeled at different withdrawal time-points following chronic drug use (Huang et al., 2015b). A coherent model, referred to as *incubation of drug craving*, has gained traction in describing the neurobehavioral adaptations following cocaine use (Wolf, 2016; Dong et al., 2017). As chronic cocaine use increases in duration, glutamatergic, or excitatory, synapses in the NAc begin to form new connections. This process involves a remarkable return to earlier developmental periods, where molecular machinery necessary for *de novo* synaptogenesis are “reinvigorated.” When cocaine use

is ceased during periods of withdrawal, these new synapses become progressively potentiated with unique synaptic properties (Huang et al., 2015b; Wang et al., 2018a). The progressive remodeling of glutamatergic synapses in the NAc during withdrawal coincides with an increase in drug-seeking (or “drug craving”) behavior, so much so that reversing these adaptations *in vivo* is sufficient to reduce reinstated reward-seeking behavior (Pascoli et al., 2011; Hearing et al., 2016).

It is not surprising that persistent shifts in glutamatergic transmission in the NAc drive reward-related behavioral outcomes. The primary projection neurons in the NAc are GABAergic, or inhibitory, medium spiny neurons (MSNs). In many regions of the brain, a basal rate of neuronal output occurs through molecular pacemaker mechanisms that spontaneously fire action potentials (APs) at a defined rate (He et al., 2014). MSNs lack this property and exhibit passive membrane properties that hyperpolarize the resting membrane potential well below AP threshold (Al-Muhtasib et al., 2018). As a result, MSNs are functionally reliant on glutamatergic input to reach AP threshold. It is reasonable to hypothesize then that biological adaptations at glutamatergic synapses onto MSNs can dramatically influence NAc-directed motivational output (Rothwell et al., 2011). The fundamental role of glutamate in NAc circuit function invites immediate experimental focus on these synapses when examining novel circuit elements contributing to motivated behavior. For this reason, the “glutamate hypothesis” of addiction has prompted considerable research into putative druggable targets regulating glutamate signaling in the central nervous system (CNS) (Kalivas, 2009).

A challenging question that remains is how the NAc integrates reward-related stimuli encoded by DA with information communicated by long-range glutamatergic inputs. Glutamatergic input to

the NAc originates predominately from cortical, limbic and paralimbic brain regions, including the prefrontal cortex (PFC), ventral hippocampus (vHipp), mediodorsal thalamus (MDT), and basolateral amygdala (BLA) (Britt et al., 2012; Zahm, 1999a; Turner et al., 2018a). Although information processed by each afferent is still not entirely clear, several important distinctions have been identified. Whereas inputs from the PFC, vHipp, and BLA largely support adaptive reward behavior, MDT inputs to the NAc overwhelmingly convey elements of aversion and negative emotional valence (Zhu et al., 2016; Sweis et al., 2018). The gross functional dichotomy between these inputs stems from studies where mice are trained to self-administer trains of stimuli to specific inputs to the NAc. Projections that promote reward are vigorously self-stimulated, whereas those that do not are actively avoided or ignored. Much like keynotes on a piano contributing to a composition of music, each glutamatergic input conveys motivationally-relevant information that is transduced by the NAc into a goal-directed appetitive behavior.

As a neuromodulator signaling within a network of glutamatergic synapses, DA likely functions within this circuit as a chemical switchboard, orienting MSN responsiveness to specific glutamatergic inputs. However, defining the precise synaptic actions of DA in the NAc is complicated further by the fact that MSNs are heterogeneous, with populations differentiated according to the expression of the D1 or D2 DA receptors (Grueter et al., 2011; Francis et al., 2015; Francis and Lobo, 2017; Turner et al., 2018b; Manz et al., 2019). The anatomical and functional properties of these MSN subpopulations are described in detail in **Chapter 2**. If what is known about the basic computational elements of the NAc are pieced together, a simplified rendering emerges of how the NAc integrates reward-related information. In general, MSNs, with separable hodological and functional properties, are the primary “receivers” directing information

flow to downstream limbic-motor structures; the “divers” are the glutamatergic corticolimbic inputs onto D1 and D2 MSNs; and the “modulators”, most notably DA, scale the strength and efficacy with which drivers trigger NAc output.

A circuit element historically lacking in the model above is the *microcircuit*, or an intrinsic neuronal network modulating functional circuit output. In the NAc, most microcircuits are comprised of diverse interneuron populations that innervate other cellular components (Burke et al., 2017; Tepper et al., 2018). For years, interneuron-enriched microcircuits were difficult to access due to a lack of cell type-specific genetic targeting techniques. However, advances in biotechnology facilitating the study of defined neuronal subtypes has led to extraordinary growth in our understanding of microcircuit processing in different areas of the brain, including the NAc. The clearest example of a technological advancement providing scientific and intellectual access to these questions is vector-mediated gene transfer of chemo and photoactivatable receptor systems, such as chemo- and optogenetics, respectively. In conjunction with an array of transgenic mouse lines (e.g., *Cre-loxP* systems) enabling tissue-specific genetic manipulations, these tools have transformed, fast-tracked, and transcended experimental barriers critical to understanding the full functional repertoire of NAc microcircuits.

While multiple molecularly and biophysically distinct interneurons exist in the NAc, fast-spiking GABAergic, or inhibitory, parvalbumin (PV)-expressing interneurons (INs) are the primary focus of this dissertation. PV-INs in the NAc mediate a circuit phenomenon referred to as *feedforward inhibition*. Feedforward inhibition occurs through a disynaptic process that serves as the conceptual framework for studies discussed in Chapters 3-6. Briefly, glutamatergic afferents

ramify in the NAc synapse onto D1 and D2 DA receptor-expressing MSNs, resulting in the functional “excitation”. These afferents send collateralizing axons onto contiguous populations of PV-INs, which in turn form inhibitory synapses with MSNs. GABAergic transmission at PV-IN-to-MSN synapses follows the excitation of MSNs in quick temporal succession, narrowing the window during which MSNs sustain AP firing (Wright et al., 2017; Manz et al., 2019). While PV-INs represent only 1-2% of neurons in the NAc, a single PV-IN is connected to numerous MSNs, such that silencing a *single* PV-IN can disinhibit up to 27 distinct MSNs (Hu et al., 2014; Tepper et al., 2018). The time-contingent signaling dynamics of PV-INs suggests that these cells are equipped to exert broad regulatory actions on NAc circuit output.

Despite the importance of the cells in the NAc, basic synaptic mechanisms regulating PV-IN-embedded feedforward inhibitory microcircuits in the NAc are largely unknown. Using the feedforward network as a conceptual framework, my overall hypothesis is that PV-IN-mediated feedforward microcircuits are regulated at two distinct nodes within this circuit: at glutamatergic, or “feedforward”, synapses onto PV-INs and at GABAergic synapses between PV-INs and D1 and D2 MSNs. Although straightforward, this hypothesis challenges the longstanding notion that feedforward inhibition in the striatum is a fixed, aplastic circuit element undergoing minimal change in synaptic strength. Synaptic plasticity within this disynaptic feedforward circuit may significantly shift the manner in which salient- and reward-encoding information in the NAc is transformed into motivated behavior. Indeed, recent work from our research group and others strongly supports this hypothesis, showing that manipulating PV-IN function in the NAc can dramatically influence reward behavior. An optimistic prospect is that deciphering mechanisms

regulating feedforward circuit function in the NAc will uncover novel therapeutic targets for the treatment of addiction and other motivational disorders.

To facilitate experimentation at each synaptic node within this microcircuit, we performed patch-clamp electrophysiology, targeted pharmacology, and optogenetics in multiple transgenic mouse lines. *Chapter 3* provides evidence for a novel arm within the canonical feedforward mechanism mediated by the  $G_{i/o}$ -coupled GABA<sub>B</sub> heteroreceptor (GABA<sub>B</sub>R). We find that PV-INs can heterosynaptically target GABA<sub>B</sub>R expressed on glutamate terminals innervating D1 and D2 MSNs. Furthermore, we provide evidence that GABA<sub>B</sub>R function at this synapse reduces glutamatergic transmission through a unique intracellular signaling mechanism. Unlike GABA<sub>B</sub>R at other synapses in the brain, GABA<sub>B</sub>R at glutamatergic synapses in the NAc proceeds independently of voltage-gated  $Ca^{2+}$  channels, inwardly-rectifying  $K^+$  channels, and adenylyl cyclase function, but instead mobilizes the  $G_{\beta\gamma}$  complex to interact directly with target-SNARE protein, SNAP25. The  $G_{\beta\gamma}$ -SNAP25 interaction prevents the formation of ternary SNARE complexes necessary for vesicular glutamate release. The importance of these studies is underscored by the abundant expression of GABA<sub>B</sub>R through the striatum and recent clinical interest in GABA<sub>B</sub>R-selective pharmacology for the treatment of addiction (Manz et al., 2019).

Chapter 4 describes a previously unknown mechanism of synaptic plasticity at glutamatergic synapses onto PV-INs. We find that PV-INs express a unique stoichiometric profile of AMPA receptors enriched in GluA2-lacking  $Ca^{2+}$ -permeable AMPA receptors (CP-AMPA).  $Ca^{2+}$  influx through these receptors triggers long-term depression (LTD) of glutamatergic transmission

that depends on retrograde endocannabinoid (eCB) signaling via the  $G_{i/o}$ -coupled CB1 receptor (CB<sub>1</sub>R). CP-AMPARs also surprisingly promote tonic eCB signaling through CB<sub>1</sub>R to negatively regulate baseline glutamatergic transmission. This form of plasticity is abolished following acute *in vivo* and *ex vivo* cocaine exposure due to the pharmacological occlusion of CB<sub>1</sub>R-dependent plasticity mechanisms. Together, these findings support the notion that feedforward synapses in the NAc undergo activity-dependent shifts in synaptic strength and that acute drug experience dynamically rearranges these synapses.

Experiments examining additional regulatory mechanisms within PV-IN-embedded microcircuits are currently underway (Chapter 6). Most notably, we have growing evidence that feedforward synapses onto PV-INs are under the control of cholinergic interneurons (CINs), an interneuron subtype that supplies the NAc with its primary source of acetylcholine (ACh). Our findings suggest that norepinephrine (NE) signaling regulates the PV-CIN interaction without concomitantly affecting glutamatergic synapses onto MSNs. These findings point to a potential hierarchical microstructure within the NAc, wherein CINs, by interacting with various circuit elements in the NAc, also govern PV-IN-mediated feedforward inhibition. It is my hope that the completion of these studies will broaden our understanding of how interconnected microcircuits in the NAc gate NAc-dependent motivational behavior. Moreover, these studies may serve as a basis for translational research into microcircuit-specific therapeutics for maladaptive motivational disorders, such as addiction, depression, and autism.

## CHAPTER 2

### Microcircuit mechanisms governing nucleus accumbens circuit function

Authors: Kevin M. Manz<sup>1,2,3</sup> and Brad A. Grueter<sup>†3,4,5,6</sup>

<sup>1</sup>Medical Scientist Training Program, Vanderbilt University, Nashville, TN 37232.

<sup>2</sup>Neuroscience Graduate Program, Vanderbilt University, Nashville, TN 37232.

<sup>3</sup>Vanderbilt Brain Institute, Vanderbilt University, Nashville, TN 37232.

<sup>4</sup>Department of Anesthesiology, Vanderbilt University Medical Center, Nashville, TN 37232.

<sup>5</sup>Vanderbilt Center for Addiction Research, Vanderbilt University, Nashville, TN 37232

<sup>6</sup>Department of Molecular Physiology and Biophysics, Vanderbilt University, Nashville, TN 37232.

#### †Correspondence to:

Brad A. Grueter, Ph.D.

Department of Anesthesiology,

2213 Garland Avenue, P435H MRB IV

Vanderbilt University Medical Center

Nashville, TN 37232-0413

Tel. 615-936-2586

E-Mail: [brad.grueter@vanderbilt.edu](mailto:brad.grueter@vanderbilt.edu)

#### Keywords

Nucleus accumbens, microcircuits, interneurons, reward, feedforward inhibition, lateral inhibition, neuromodulation

## 2.1. Abstract

The nucleus accumbens (NAc) is implicated in the pathogenesis of conditions characterized by maladaptive motivational states, including addiction, depression, and autism. Embedded within the mesolimbic network, the NAc coordinates reward-related behavioral output by integrating ascending neuromodulatory input with glutamatergic afferents from cortical and allocortical limbic structures. These signaling events occur within an interneuron-enriched microcircuit environment that contributes to adaptive and pathological shifts in motivated behavior, such as seeking out natural reinforcers or using illicit drugs despite adverse consequences. While intense research has focused on how extrinsic monoaminergic signaling gates synaptic adaptations in the NAc, comparatively little is known how local microcircuitry within the NAc calibrates mesolimbic circuit output to shape goal-directed behaviors. Here, we survey the cellular and synaptic architecture of NAc microcircuitry, the contribution of these circuit elements to reward-related behaviors, and potential microcircuit-specific avenues for the treatment of relapsing-remitting motivational disorders.

## 2.2. Introduction

The mesolimbic reward pathway, classically defined by ascending neuromodulatory projections from the ventral tegmental area (VTA) to the nucleus accumbens (NAc), transforms reward-related stimuli into goal-directed motivational behavior (Koob and Volkow, 2016; Lüscher, 2016). Circuit-specific adaptations within these regions are implicated in the pathogenesis of pathological motivational states, including addiction, autism, schizophrenia, bipolar disorder, anxiety, and depression (Rothwell et al., 2011; Huang et al., 2015; Dong et al., 2017). For years, emphasis has been placed on experience-dependent shifts in dopamine (DA) signaling in the NAc, as virtually

every drug of abuse, including psychostimulants, opiates, ethanol, GHB, and nicotine, increases mesoaccumbens DA transmission (Cruz et al., 2004; Labouèbe et al., 2007; Bassareo et al., 2017; Siciliano and Jones, 2017). However, increasing evidence suggests that recurring withdrawal-relapse behavior following chronic drug exposure follows time-contingent synaptic rearrangements at glutamatergic inputs to the NAc (Huang et al., 2015b). In the last several years, this model has expanded to include interneuron-enriched microcircuitry embedded within the NAc. *Microcircuits* defined here are intrinsic computational elements in the NAc that modulate how information encoded by monoaminergic and corticolimbic afferents direct NAc circuit output. Microcircuit dynamics within the NAc gate synaptic and cellular processes that facilitate goal-directed behavior.

NAc microcircuits are largely comprised of  $\gamma$ -aminobutyric acid (GABA)-ergic and cholinergic interneurons that interact functionally with medium spiny projection neurons (MSNs), output from which directs reward-related behavior. GABAergic microcircuits in the NAc encompass those formed by parvalbumin (PV) and somatostatin (SST)-expressing interneurons, each characterized by distinct biophysical, molecular, and synaptic properties (English et al., 2011; Burke et al., 2017). These properties equip PV- and SST-expressing interneurons with manifold control over how motivationally-relevant information is propagated through the NAc. Cholinergic interneurons, via three-dimensional interactions with virtually every circuit element in the NAc, release acetylcholine (ACh) to elicit broad modulatory effects on mesolimbic function. Behavioral, electrophysiological, and cell type-specific genetic targeting and labeling techniques, alongside targeted pharmacological and imaging studies, have elucidated mechanisms by which NAc microcircuits shape reward-related behavioral outcomes. In the present review, we summarize

basic anatomical, functional and organizational components of the NAc, establish cellular and synaptic properties of NAc microcircuits, dynamic contributions of these circuits to NAc-dependent motivational behavior, and potential therapeutic targets for the treatment of maladaptive motivational states.

### 2.3 Organizational structure of the NAc

*The NAc is a heterogeneous structure with core and shell subterritories*

The NAc is anatomically divided into *core* and *shell* subregions that subserve distinct but overlapping behavioral functions. Whereas the NAc shell is involved in associative learning mechanisms and unconditioned motivational responding, the NAc core initializes instrumental commands to conditioned reinforcers and supports adaptive motor responses (Zahm, 1999a; Floresco et al., 2006). These functions are supported by gross hodological input-output differences, with projections from the NAc core engaging motor-embedded output centers and those from the shell engaging more visceral and autonomic regions in the brainstem and hypothalamus (Castro and Bruchas, 2019). Furthermore, mesoaccumbens inputs to the core are accompanied by projections from the substantia nigra (SN), whereas the NAc shell is innervated exclusively by dopaminergic (DA) fibers from the ventral tegmental area (VTA) (Ikemoto, 2007; Salgado and Kaplitt, 2015). The NAc core and shell are also differentially targeted by cortical and allocortical afferents. Glutamatergic inputs to the core predominately arise from the prelimbic prefrontal cortex (PFC), dorsal subicular hippocampus, mediodorsal thalamus (MDT), and specific loci within the basolateral amygdala (BLA), whereas the shell receives input from infralimbic PFC, ventral subiculum of the hippocampus (VHipp), MDT and BLA (Zahm, 1999a; Britt et al., 2012; Turner et al., 2018b). Despite functional and anatomical differences between NAc core and shell

subregions, both operate cooperatively in a spiraling anatomical framework that transforms complex motivational states into goal-directed behaviors (Haber et al., 2000).

*Functional NAc output is mediated by distinct D1 and D2-expressing MSNs*

The NAc core and shell are primarily comprised (90-95%) of GABAergic medium spiny projection neurons (MSNs) (Tepper et al., 2018). MSNs in the NAc exhibit similar electrophysiological properties to MSNs in the dorsal striatum, including bistable up- and down-membrane states at  $\sim$ -55-60 mV and -80-90 mV, respectively, relatively low input resistance ( $R_{IN}$ ), quiescent basal action potential (AP) firing, and absent intrinsic pacemaker activity (Grueter et al., 2010; Al-Muhtasib et al., 2018; Willett et al., 2019). These properties render MSNs reliant on concerted excitatory input to sustain plateau potentials near AP spike threshold (Plotkin et al., 2011). Furthermore, excitatory input drives downstate-update transitions via a dynamic interplay between voltage-dependent and independent  $K^+$  conductances, including those mediated by Kir2 and  $K_v1$  channel families (Plenz and Kitai, 1998; Kreitzer and Malenka, 2005). These properties confer critical computational dynamics regulating NAc circuit output to downstream limbic-motor units.

Distinct populations of MSNs in the NAc can be segregated according to the expression of D1 and D2 dopamine (DA) receptors. D1-expressing [D1 or D1(+)] MSNs colocalize with dynorphin and substance P and send collateralizing projections to midbrain DA nuclei (e.g., VTA and SN) and the ventral pallidum (VP). In contrast, D2-expressing MSNs [D2 or D1(-)] MSNs co-express enkephalin and the adenosine 2a (A2a) receptor and project primarily to the VP (Salgado and Kaplitt, 2015; Pardo-Garcia et al., 2019). D1 and D2 MSNs in the NAc exhibit distinguishable

synaptic and membrane properties, with D1 MSNs exhibiting lower intrinsic excitability and glutamatergic inputs containing lower presynaptic release probability than D2 MSNs (Grueter et al., 2010). While cell type-specific anterograde tracing methods indicate that D1 and D2 MSNs receive comparable corticolimbic input, differences are observed in their basal synaptic properties (Barrientos et al., 2018). For example, glutamate release probability at D1 MSNs in the NAc core appears to be highest at synapses from the PFC, whereas glutamate release probability onto D2 MSNs is highest at synapses from the BLA (Britt et al., 2012; Deroche et al., 2019). Data supporting these observations are limited, as surprisingly few studies have utilized MSN subtype-specific labeling to compare the synaptic profile of discrete inputs to the NAc core and shell.

A conventional heuristic is that D1 and D2 MSNs in the NAc differentially regulate reward-related behavioral outcomes, with D1 MSNs promoting appetitive and reward-seeking behavior and D2 MSNs supporting ambivalent or aversive motivational states (Francis and Lobo, 2017; Cole et al., 2018). Indeed, withdrawal from repeated cocaine self-administration elicits robust synaptic adaptations at glutamatergic synapses onto D1 MSNs but not D2 MSNs in the NAc shell (Pascoli et al., 2011, 2014; Graziane et al., 2016). Conversely, negative affect associated with acute morphine withdrawal coincides with increased thalamoaccumbens transmission onto D2 MSNs (Zhu et al., 2016). Collectively, this model shares circuit similarities to the dorsal striatum, where D1 and D2 MSNs activate and inhibit locomotor activity, respectively, by engaging largely non-overlapping effector systems. However, retrolabeling of MSN efferents to the VP colocalize with D1 and D2 MSN mRNA and display high synaptic connectivity, indicating that D1 vs. D2 MSN-mediated behavioral outcomes cannot be explained by segregated projection patterns alone (**Figure 2.1**) (Kupchik et al., 2015). Furthermore, these behaviors cannot be explained by divergent

signaling mechanisms engaged by D1 vs. D2 receptor activation, as intra-NAc D2 blockade attenuates various drug-induced reward behaviors (Pina and Cunningham, 2014; Manvich et al., 2019). Despite growing appreciation of behavioral states supported by D1 and D2 MSN subtypes, considerable work is needed to fully understand how MSNs direct NAc-dependent reward behavior.

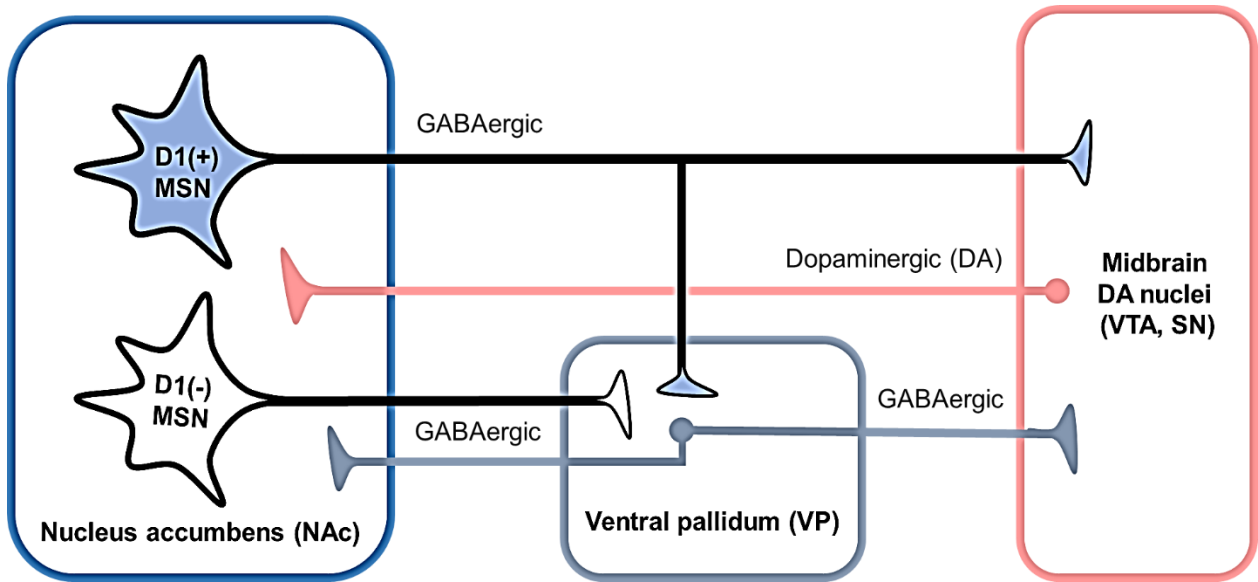


**Figure 2.1. Gross organizational scheme of mesolimbic reward network.** Dopaminergic (DA) projections from midbrain DA nuclei, such as the ventral tegmental area (VTA) and substantia nigra (SN) ramify in the NAc. GABAergic medium spiny neurons (MSNs) in the NAc are differentiated according to the expression of D1 [D1(+)] or D2 [D1(-)] DA receptors. In addition to the VTA and SN, D1(+) MSNs parallel D1(-) projections onto GABAergic projection neurons in VP. GABAergic projection neurons in the VP innervate the VTA alongside other limbic-motor nuclei, such as the thalamus, prefrontal cortex (PFC), and lateral habenula (LHb). Although poorly characterized, a reciprocal GABAergic pallidoaccumbens projection has been identified in the NAc.

## 2.4 Microcircuit elements in the NAc

### *Feedforward inhibitory microcircuits in the NAc constrain MSN output*

An emerging circuit element in the NAc with broad functional implications is the feedforward inhibitory microcircuit. Feedforward inhibition, whereby afferent glutamatergic input to principal output neurons collateralizes onto GABAergic interneurons, gates circuit output by narrowing the spatiotemporal window of principal neuron AP firing (Hu et al., 2014). Similar to the dorsal striatum, cortex, and hippocampus, feedforward inhibition in the NAc is mediated by GABAergic parvalbumin (PV)-expressing fast-spiking interneuron (PV-INs) synapses onto D1 and D2 MSNs (**Figure 2.2**) (Yu et al., 2017; Scudder et al., 2018). While the role of the PV protein in these cells is unclear, PV has  $\text{Ca}^{2+}$ -chelating EF-hand motifs that control intracellular  $\text{Ca}^{2+}$  homeostasis. Disruption of endogenous PV expression has been shown to impair short- and long-term synaptic plasticity mechanisms in PV-expressing cells elsewhere, including PV(+) interneurons in the striatum and Purkinje cells in the cerebellum (Soler-Llavina and Sabatini, 2006; Eggermann and Jonas, 2011; Orduz et al., 2013). PV-INs in the NAc are aspiny with dense varicosities along minimally branching dendritic arbors. Varicosities at distal dendritic branch points represent dendro-dendritic synapses between pairs of PV-INs, as current injection elicits a time-locked shift in membrane potential in distal PV-INs, consistent with intercellular coupling via connexon-containing gap junctions (Wright et al., 2017). In addition, PV-IN axonal fields are spherical and diffuse with numerous branch points emerging from moderately sized somata (16-18  $\mu\text{m}$ ), highlighting the large diameter within which a single PV-IN can influence neighboring cellular activity (Kawaguchi et al., 1995; Tepper et al., 2018).

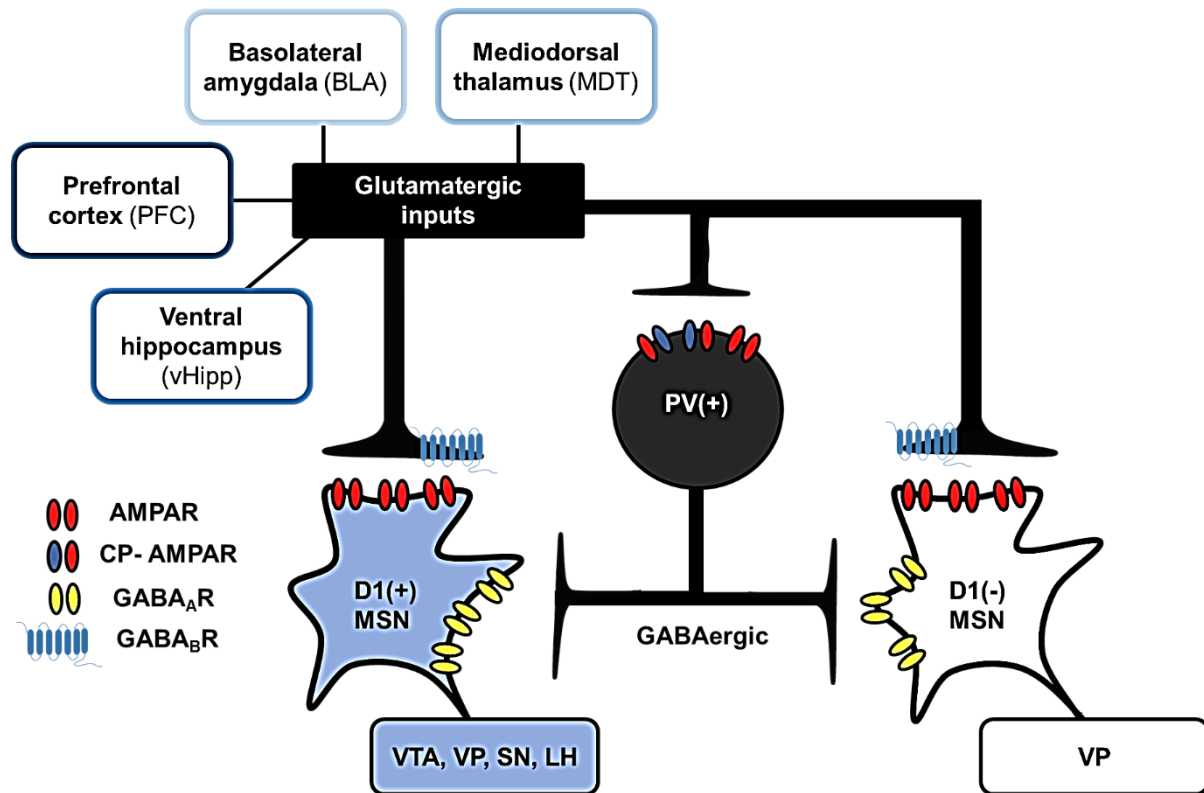


**Figure 2.2. Feedforward inhibitory microcircuits in the NAc.** Feedforward inhibition in the NAc is initiated when AMPAR-mediated glutamatergic transmission onto D1(+) and D1(-) MSNs collateralize onto parvalbumin (PV)-expressing interneurons [PV(+)-INs]. PV(+)-INs then exert robust inhibitory control over D1(+) and D1(-) MSNs via GABA<sub>A</sub>R-mediated GABAergic transmission. GABA<sub>B</sub>R, a G<sub>i/o</sub>-coupled GPCR, expressed presynaptically on glutamate terminals is heterosynaptically targeted by PV(+)-INs. Glutamatergic input predominately arises from the prefrontal cortex (PFC), mediodorsal thalamus (MDT), basolateral amygdala (BLA), and ventral hippocampus (vHipp). Note that glutamatergic synapses onto PV(+)-INs basally express GluA2-lacking Ca<sup>2+</sup>-permeable AMPARs (CP-AMPA). D1(+) MSNs send GABAergic projections to midbrain dopamine (DA) nuclei in the ventral tegmental area (VTA) and substantia nigra (SN), the lateral hypothalamus (LH), and ventral pallidum (VP), whereas D1(-) MSNs project to the ventral pallidum (VP).

PV-INs exhibit striking biophysical properties that support their role in feedforward inhibition, most notable of which is high-fidelity AP firing with maximal sustained firing rates of 200-250 Hz (Yu et al., 2017; Scudder et al., 2018). The AP waveform is defined by short-duration AP half-widths with large amplitude afterhyperpolarizations mediated by delayed-rectifying Kv3.1 K<sup>+</sup> channels. PV-INs undergo distinct output “modes” characterized by periods of rapid burst firing followed by subthreshold “chattering” membrane potential oscillations (English et al., 2011; Scudder et al., 2018). Similar to D1 and D2 MSNs in the NAc, PV-INs rest at a hyperpolarized membrane potential (-75-80 mV) and exhibit relatively low R<sub>IN</sub> (80-180 MΩ) with a linear current-voltage relationship (Yu et al., 2017). Despite increased intrinsic excitability, the rheobase current, or minimum current needed to elicit a single AP, is greater in PV-INs than MSNs and other GABAergic cell types in the NAc, indicating that sequential trains of excitatory input are required to sustain PV-IN output (Taverna et al., 2007). While MSNs and PV-INs receive comparable glutamatergic input, AMPA receptor (AMPA)-mediated excitatory postsynaptic currents (EPSCs) in PV-INs exhibit remarkably fast decay kinetics due to the electronic properties of aspiny dendrites and high baseline expression of GluA2-lacking Ca<sup>2+</sup>-permeable AMPARs (CP-AMPA) (Hainmüller et al., 2014; Yu et al., 2017). These properties enable PV-INs to respond quickly to activity-dependent shifts in circuit function by rapidly summing EPSPs along a broad somatodendritic axis.

PV-INs form robust somatic and proximal dendritic synapses onto D1 and D2 MSNs mediated by fast ionic GABA<sub>A</sub> receptors (GABA<sub>A</sub>R). GABA<sub>A</sub>R-mediated transmission at PV-IN-to-MSN synapses is maintained across a broad dynamic range of firing frequencies that is largely devoid of an autoreceptor feedback system (Gittis et al., 2010; Manz et al., 2019). Furthermore, PV-IN-

elicited inhibitory postsynaptic currents (IPSCs) in MSNs display rapid onset kinetics, minimal failure rates (< 2%), and synaptic connectivity congruent with feedforward synapses in the dorsal striatum (Wright et al., 2017). Unlike hippocampal PV-INs, PV-INs in the NAc express presynaptic cannabinoid receptor type-1 (CB<sub>1</sub>R) that contribute to short- and long-term endocannabinoid (eCB)-dependent plasticity mechanisms (Winters et al., 2012; Graziane et al., 2016; Yu et al., 2017). This plasticity is restricted to PV-IN-to-MSN synapses in the NAc, as GABAergic transmission at PV-IN-to-PV-IN synaptic strength is unaffected by depolarization-induced eCB release (Wright et al., 2017). While other plasticity mechanisms at PV-IN-to-D1 and D2 MSN synapses remain largely unexplored, a small subset of synapses in the NAc core undergo GABA<sub>B</sub> receptor (GABA<sub>B</sub>R)-induced long-term depression (LTD). However, most PV-IN synapses are unresponsive to GABA<sub>B</sub>R-selective pharmacology, indicating that an autoreceptor feedback system may be expressed at select feedforward inhibitory synapses in the NAc (Manz et al., 2019).

A series of experiments describing the temporal properties of feedforward inhibition in the NAc indicate that (a) silencing a single [CB1(+)-expressing] PV-IN strongly disinhibits MSN AP spiking activity and (b) feedforward-evoked IPSCs in MSNs precede peak AP amplitude (Yu et al., 2017). In addition, targeting putative PV-INs by selectively blocking CP-AMPA receptors increases BLA and PFC-evoked MSN AP firing. These findings highlight the close spatiotemporal proximity of PV-IN-to-MSN synapses in the NAc and the robust inhibitory influence PV-INs have on MSN output. Interestingly, PV-INs in the NAc were recently shown to dampen excitatory input onto D1 MSNs by heterosynaptically targeting presynaptic GABA<sub>B</sub>R on glutamate terminals, pointing to a novel arm within the canonical feedforward microcircuit (Manz et al., 2019). An

intriguing hypothesis is whether afferent-directed increases in PV-IN activity triggers GABA<sub>B</sub>R-contingent heterosynaptic crosstalk to maintain MSN output within a preferred physiological range. Despite making up 1-5% of the cells in the NAc, the biophysical properties of PV-INs, alongside GABA<sub>A</sub>R- and GABA<sub>B</sub>R-contingent feedforward mechanisms, enable PV-INs to carefully coordinate and entrain NAc circuit output.

As the cellular and synaptic properties of PV-IN synapses become increasingly clear, the role of these cells in NAc-dependent reward behavior is still largely unknown. Recent studies suggest that modulating glutamatergic input onto PV-INs expedites the development of drug-induced reward learning (Yu et al., 2017; Chen et al., 2019). Specifically, triggering LTP at BLA-to-NAc synapses onto PV-INs *in vivo* without altering glutamatergic transmission onto MSNs expedites the acquisition of cocaine self-administration. Thus, BLA-directed feedforward inhibition in the NAc may serve as a rate-control mechanism governing associative reward learning (Yu et al., 2017). Consistent with this hypothesis, targeted ablation of PV-INs in the NAc decreases D-amphetamine (AMPH)-induced hyperlocomotion and conditioned place preference (CPP), indicating that functional PV-IN output is required for these behaviors (Wang et al., 2018b; Kim et al., 2019a). Furthermore, PV-IN-mediated entrainment of MSN output using chemo- and optogenetic techniques elicits robust CPP, whereas chemogenetic inhibition of PV-INs elicits condition place aversion (CPA) (Chen et al., 2019). However, a previous report utilizing the same optogenetic stimulation protocol found that activation of PV-INs elicits robust CPA, an effect recapitulated by photostimulating glutamatergic VTA-to-PV-IN NAc synapses (Qi et al., 2016). While both studies utilize a 20 Hz optogenetic stimulation protocol, it is worth noting that the former group utilized a PV-2A-Cre transgenic mouse line to conditionally express channelrhodopsin-2 (ChR2), whereas

the latter group utilized a PV-IRES-Cre line that targets fewer PV(+) cells in the NAc. Different Cre-driver lines may lead to varying penetrance of Cre-inducible viral constructs and should be carefully considered when manipulating NAc microcircuits.

A more parsimonious explanation is that PV-INs support diverse behavioral functions unamenable to a simple “rewarding vs. aversive” categorization scheme. For example, disruption of dorsal striatal PV-INs was recently shown to impair action-selection learning without affecting gross motor performance (O’Hare et al., 2017; Owen et al., 2018). Furthermore, fiber photometric analysis of NAc core PV-INs during a 5-choice serial reaction time task to assess attentional impulse control showed a time-locked increase in  $Ca^{2+}$  transients during successfully-executed trials (Pisansky et al., 2019). In contrast, chemo- and optogenetically inhibiting PV-INs in the NAc core increased rates of premature task responding, indicating that PV-INs in the NAc, analogous to PV-INs within executive control networks in the PFC and cingulum, ultimately constrain impulsive behavioral responding. These behavioral findings closely mirror the physiological role of PV-INs within striatal microcircuits as synchronizing “nodes” regulating MSN signal-to-noise computations (Gittis et al., 2010; Damodaran et al., 2014; Moyer et al., 2014). In the NAc, PV-INs likely contribute to reward-related shifts in behavioral flexibility, targeting of which may lead to a novel therapeutic approach to the treatment of maladaptive motivational disorders.

#### *Cholinergic interneurons tonically regulate NAc circuit function*

While the importance of NAc-specific PV-INs only recently garnered appreciation, cholinergic interneurons (CINs), historically defined as tonically-activate giant cells, have received far greater attention. CINs are choline acetyltransferase (ChAT)-positive cells characterized by large, ovoid

somata (17-30  $\mu\text{m}$ ), minimally branching dendrites and widely ramifying axonal networks. Unlike MSNs and PV-INs in the NAc, CINs spontaneously fire APs (between 2-8 Hz) independent of extrinsic glutamatergic input, indicating that CINs are equipped with an autonomous peacemaking mechanism (Kawaguchi et al., 1995; Francis et al., 2019). Consistent with this observation, CINs in the NAc express robust hyperpolarized-activated cationic currents ( $I_h$ ) mediated by HCN2 channels that calibrate CIN responsiveness and excitability (Cheng et al., 2019; Lemos et al., 2019). Spontaneous (or tonic) output along diffuse, far-reaching axonal fields allows CINs to exert broad cholinergic effects on striatal circuit function (Mamaligas and Ford, 2016). Accordingly, CINs serve a complex regulatory role within NAc microcircuitry, as CINs receive (a) convergent glutamatergic input from limbic and paralimbic regions, (b) collateral “feedback” synapses from MSNs, and (c) robust DAergic innervation from mesencephalic DA nuclei (Whitehead et al., 2001; Sullivan et al., 2008; Faust et al., 2016; Augustin et al., 2018). Moreover, CINs diffusely modulate microcircuit dynamics in the NAc, with several reports indicating that CIN-evoked acetylcholine (ACh) release exerts synaptic actions on PV-IN-mediated feedforward transmission (English et al., 2011; Faust et al., 2016). In the dorsal striatum, CINs can modulate spontaneous action potential firing in a subset of neuronal nitric oxide synthase (nNOS)-expressing GABAergic interneurons via M4 muscarinic ACh receptor (mAChR) signaling, an effect recapitulated by stimulating corticostriatal afferents onto CINs (Melendez-Zaidi et al., 2019). Thus, CIN signaling may target diverse GABAergic interneuron subtypes to entrain striatal circuit activity.

Relative to PV-IN synapses, CIN-embedded microcircuit elements in the NAc are more closely linked to mesoaccumbens DA signaling (**Figure 2.3**). Specifically, cholinergic receptor function, including both mAChRs and nicotinic ACh receptors (nAChRs), have been shown to modulate

DA efflux into the NAc via direct presynaptic mechanisms (Rice and Cragg, 2004; Threlfell et al., 2012; Brimblecombe et al., 2018). Most  $\alpha 4\beta 2$ -containing nAChRs elicit a depolarizing current that facilitates voltage-gated calcium (VGCC)-dependent vesicular DA release, whereas mAChRs, notably  $G_{\alpha q}$ -coupled M5 mAChRs, presumably potentiate DA release by mobilizing intracellular  $Ca^{2+}$  stores (Shin et al., 2017; Yorgason et al., 2017; Lemos et al., 2019). CINs are also one of few interneuron subtypes in the NAc to express D2-like DA receptors, activation of which has been shown to offset  $I_h$ -mediated depolarizing currents that promote CIN output (Maurice et al., 2004). A mathematical model summarizing ACh-DA coupling describes how reward-evoked DA release activates D2-like receptors on CINs, which, in turn, transiently reduces ACh tone on DA terminals. Reduced ACh signaling at DA terminals decreases DA efflux, thereby engaging a negative feedback system following experience-dependent shifts in mesolimbic DA signaling (Hoebel et al., 2007; Kim et al., 2019b). Although the role of ACh-DA microcircuit interactions in the NAc remain controversial, this model parallels recent reports that disrupting autonomous CIN activity, selectively ablating CINs, and chemo- or optogenetically inhibiting CINs supports depressive-like behavioral states traditionally associated with reduced NAc DA levels (Cheng et al., 2019).

CINs heterosynaptically modulate glutamatergic transmission onto D1 and D2 MSNs via pre- and postsynaptically-expressed mAChRs (Zhang and Warren, 2002; Shin et al., 2015). Recently, exogenous M1 mAChR activation was shown to elicit a dose-dependent form of eCB-LTD in the NAc core mediated by  $CB_1R$ - and transient receptor potential vanilloid 1 (TRPV1)-dependent signaling mechanisms (Neuhofer et al., 2018). Conversely, high-frequency stimulation of D1 MSNs elicits M1-dependent long-term potentiation (LTP) of glutamatergic transmission onto D2 MSNs via evoked substance P release from CINs (Francis et al., 2019). Although an explanation

for the cell type-specific expression of M1-induced LTP at D2 MSNs is lacking, it is unlikely that CINs differentially innervate D2 MSNs over D1 MSNs, as the synaptic effects of mAChR activation is comparable between MSN subtypes (Pancani et al., 2014). CIN activity may serve an intermediary role within NAc microcircuits by “transferring” excitatory synaptic transmission one MSN cell-type to another.

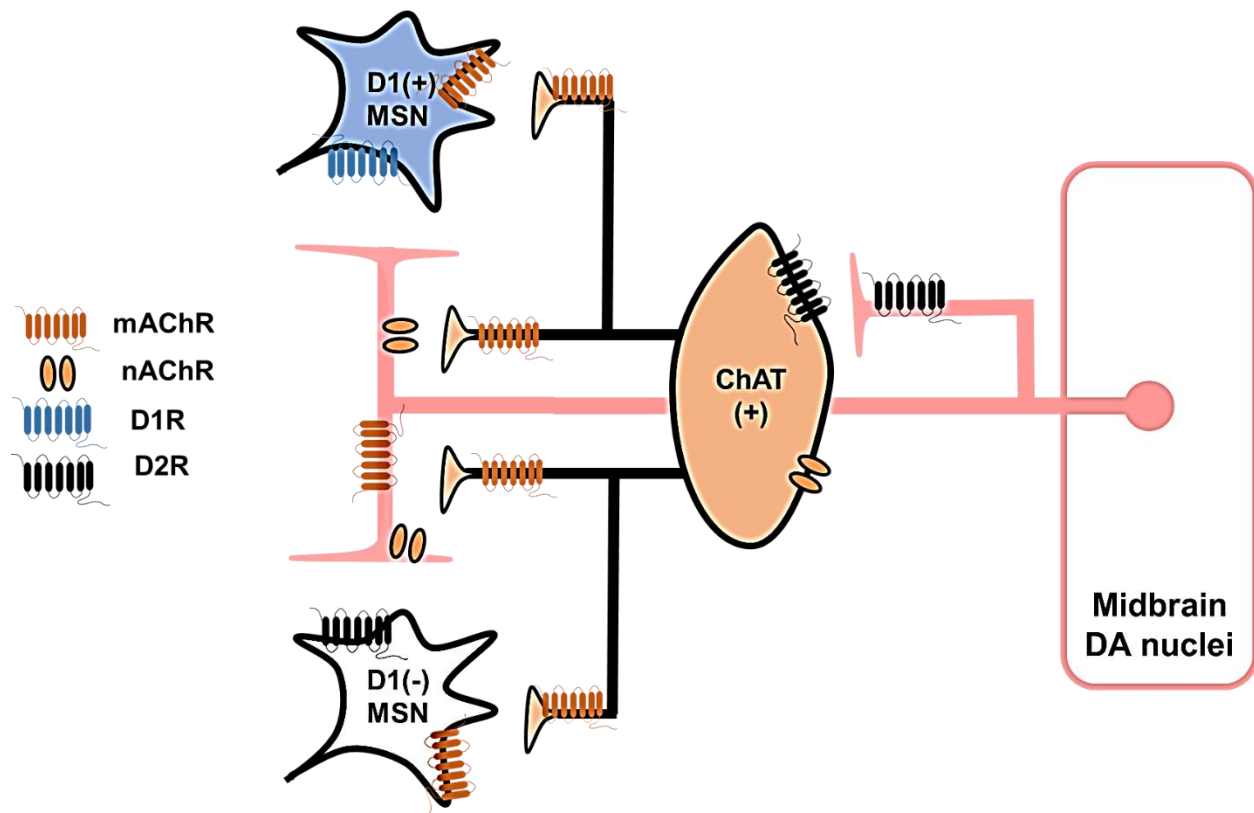


**Figure 2.3. Cholinergic interneuron microcircuit interactions in the NAc.** Cholinergic interneurons (CINs) are identified in the NAc according to their molecular, morphological and electrophysiological properties, including the expression of choline acetyltransferase (ChAT). Dopaminergic (DA) projections from mesencephalic nuclei (e.g., VTA and SN) innervate cholinergic interneurons (CINs) via D2-like DA receptors, which decreases CIN output. CINs reciprocally regulate mesoaccumbens DA release via muscarinic (mAChR) and nicotinic (nAChR) acetylcholine receptors, most notably  $\alpha 4\beta 2$ -containing nAChRs and M1/5  $G_q$ -coupled mAChRs. ACh released from CINs also modulates glutamatergic transmission at D1(+) and D1(-) MSNs via pre- and postsynaptic mAChR signaling. Although CINs have been shown to heterosynaptically regulate GABAergic interneurons, this interaction has not been explicitly demonstrated in the NAc.

In the NAc, cholinergic transmission is largely, but not exclusively, mediated by intrinsic CIN network activity, whereas other regions within the reward network, such as the VTA, rely on extrinsic cholinergic afferents from the mesencephalon, including the pedunculopontine tegmental nucleus (PPTg) laterodorsal tegmentum (LDTg) (Dautan et al., 2016; Zhang et al., 2018). Accumulating evidence suggests that CINs in the NAc form a parallel reward-prediction system directing cue-invigorated motivational output. For example, rats trained in a classical Pavlovian-instrumental transfer (PIT) task, whereby the presence of a food pellet signaled by an auditory cue becomes dependent on an instrumental task (e.g., lever press), exhibit increased cue-motivated behavior when CINs are chemogenetically inhibited. Conversely, optogenetic excitation of CINs decreases PIT behavior in a  $\alpha 4\beta 2$  nAChR-dependent manner, suggesting that CIN microcircuits within the NAc oppose cue-contingent behavior (Laurent et al., 2014; Collins et al., 2019). This conceptual framework is supported by prior studies showing that reward-predictive cues elicit a “pause” in tonic CIN activity that coincides with increased DA transients in the NAc (Zhang and Cragg, 2017; Augustin et al., 2018).

Experience-dependent shifts in CIN activity in the NAc align with the broader functional configuration of CINs within NAc microcircuits. During bouts of acute stress, corticotropin-releasing factor (CRF) in the NAc potentiates DA transmission (a) directly via CRF-2 receptors and (b) indirectly via CRF-1 receptors on CINs (Lemos et al., 2012, 2019). CRF-induced ACh release from CINs augments DA efflux from VTA fibers in the NAc via M5 receptors. Interestingly, a previous report suggests that intra-NAc CRF infusion elicits CPP despite observations that systemic CRF administration causes CPA (Lemos et al., 2012). Alongside data showing that CINs encode general motivational valence to salient environmental stimuli, these

data indicate that transitions in functional CIN output may exert bidirectional influences on goal-directed behavior. Given that therapeutic attempts to modulate mesolimbic DA signaling have largely failed in the treatment of addiction-related disorders, drugs targeting ACh-DA coupling in the NAc remain a viable target. For example, M5 mAChR knockout mice exhibit pronounced reductions in multiple drug-induced reward behaviors, including acquisition and reinstatement of cocaine- and morphine-induced CPP and self-administration, cue-induced reinstatement of ethanol seeking, and opioid withdrawal symptoms, with M5 negative allosteric modulators (NAMs) recapitulating several of these behavioral outcomes (Steidl and Yeomans, 2009; Gunter et al., 2018; Teal et al., 2019). Understanding CIN microcircuit function will likely yield greater therapeutic avenues for the treatment of NAc-dependent motivational disorders.

*Somatostatin interneurons are a source of nitric oxide and neuropeptide Y in the NAc*

Somatostatin-expressing interneurons (SST-INs) in the NAc are an enigmatic GABAergic interneuron subtype containing both neuropeptide Y (NPY) and neuronal nitric oxide synthase (nNOS) (Kawaguchi et al., 1995; Ribeiro et al., 2019). SST-INs throughout the striatum emit few (2-5) non-tortuous dendritic branches with simple axonal arbors that commonly contain two collateralizing processes, though NAc-specific cytological characterizations of SST-IN structure are lacking (Tepper et al., 2018). SST-INs are readily distinguished from other GABAergic cell types in the NAc via distinct electrophysiological properties, including a high  $R_{IN}$  (200 M $\Omega$ -1 G $\Omega$ ), relatively low rheobase current, and a significantly depolarized resting membrane potential (-50-60 mV) relative to MSNs and PV-INs (Smith et al., 2017; Scudder et al., 2018). Importantly, SST-INs exhibit  $Co^{2+}$ -sensitive “low threshold  $Ca^{2+}$  spikes” (LTS) and a persistent depolarizing plateau potential following depolarizing or hyperpolarizing current injection. Unlike PV-INs, SST-INs in

the NAc undergo  $I_h$ -dependent spontaneous activity, indicating that these neurons also do not require afferent glutamatergic input to reach AP threshold (Kawaguchi, 1993).

Few studies have examined synaptic mechanisms by which SST-INs contribute to microcircuit processing in the NAc. While SST-INs form GABA<sub>A</sub>R-mediated GABAergic synapses onto D1 and D2 MSNs, the inhibitory influence of these cells on MSN output is weak due to a distal dendritic innervation pattern (Gittis et al., 2010; Straub et al., 2016). In addition, several biophysical properties of SST-INs preclude them from participating in disynaptic feedforward inhibition mediated by PV-INs (Szydlowski et al., 2013). First, although SST-INs receive monosynaptic glutamatergic input from similar structures as MSNs and PV-INs in the NAc, afferent-evoked EPSCs obtained from SST-INs have a small amplitude and high failure rate (Faust et al., 2016; Scudder et al., 2018; Assous and Tepper, 2019). This is in contrast to glutamatergic transmission recorded from PV-INs in which afferent-evoked EPSCs are stronger than both D1 and D2 MSNs (Wright et al., 2017; Yu et al., 2017). Second, the dendritic structure of SST-INs impedes rapid electrotonic conduction of depolarizing current to the axon initial segment, resulting in latent EPSP-to-AP spike coupling (Elghaba et al., 2016; Fino et al., 2018). Finally, intracellular current injection elicits a reported maximum firing frequency of 10-15 Hz, preventing SST-INs from responding to abrupt shifts in NAc circuit activity (Scudder et al., 2018). Together, these properties indicate that SST-INs regulate NAc circuit function via synaptic mechanisms distinct from interneuron subtypes.

Although SST-INs appear to function outside of feedforward microcircuits, recent reports indicate that they can heterosynaptically regulate synaptic transmission in the NAc core. For example,

mGluR signaling in the NAc core has been shown to drive nNOS-dependent NO production, resulting in the *S*-nitrosylation of matrix metalloproteinases (MMPs) that regulate excitatory synaptic strength. SST-IN-dependent NO release is targeted by *in vivo* cocaine experience, as cued reinstatement to cocaine seeking is attenuated by intra-NAc blockade of the mGluR-nNOS signaling pathway in SST-INs (Smith et al., 2017). Furthermore, the AMPA/NMDA ratio in unlabeled MSNs, a conventional measure of excitatory synaptic strength, is increased following chemogenetic activation of nNOS-expressing INs (putative SST-INs), mirroring synaptic adaptations that evolve during protracted cocaine withdrawal (Smith et al., 2017). Congruent with these findings, optically-recruiting and inhibiting SST-INs enhances and suppresses cocaine-induced locomotor activity, respectively, indicating that SST-IN activity positively regulates cocaine reward behavior (Ribeiro et al., 2018). Furthermore, putative SST-INs in the dorsal striatum have recently been shown to adapt to novel contingencies during instrumental motor learning tasks (Holly et al., 2019). Although not directly tested in NAc *ex vivo* slice preparations, exogenous DA application excites dorsal striatal SST-INs in a D1-dependent manner, suggesting that SST-IN activity may also correlate with drug-induced shifts in DA signaling (Centonze et al., 2002). In addition, NPY, co-expressed in most NAc SST-INs, augments DA release in the NAc shell, though these effects could also result from NPY-expressing afferents from hypothalamic feeding centers (Sørensen et al., 2009). Nevertheless, as microcircuits in the NAc become better characterized, SST-INs will likely emerge as key regulators of NAc-dependent reward behavior.

#### *D1 and D2 MSNs in the NAc form mutually inhibitory collateral microcircuits*

While MSNs in the NAc predominately project to extrastriatal loci, D1 and D2 MSNs form mutual inhibitory synapses in the NAc referred to as lateral inhibition (Pennartz et al., 1991; Dobbs et al.,

2016; Wright et al., 2017). Similar to PV-IN-to-MSN synapses, MSN-to-MSN connectivity is mediated by fast ionotropic GABA<sub>A</sub>Rs without a concomitant GABA<sub>B</sub>R-mediated slow IPSC present at D1 MSN-to-VTA synapses (Czubayko and Plenz, 2002; Burke et al., 2017; Edwards et al., 2017). However, MSN-evoked IPSCs in contiguous MSNs exhibit lower amplitudes with slow activation kinetics, consistent with ultrastructural studies showing that MSNs preferentially synapses along distal dendritic domains. Several reports in the dorsal striatum suggest that MSN-to-MSN connectivity is asymmetric, with D2 MSNs (i.e., indirect pathway MSNs) forming stronger and more frequent synapses onto D1 MSNs. In contrast, D1 MSNs appear to synapse more frequently with other D1 MSNs (Planert et al., 2010). In addition to GABA<sub>A</sub>R-mediated GABAergic transmission, recent evidence suggests that MSNs express presynaptic GABA<sub>B</sub>R receptors that negatively modulate inhibitory synaptic efficacy (Dobbs et al., 2016). Therefore, while GABA<sub>B</sub>R decreases glutamate release probability onto D1 and D2 MSNs in the NAc, GABA<sub>B</sub>R may also be targeted by collateral inhibitory synapses.

For years, the lateral inhibitory framework within the striatum, including the NAc, had been neglected due to the relatively weak GABAergic responses elicited in paired MSN recordings. However, individual MSN-to-MSN synapses may function within a broader network that synchronizes the output of functional MSN ensembles (Cruz et al., 2013) (**Figure 2.4**). The “ensemble” hypothesis of MSN activity has been supported by *in vivo* Ca<sup>2+</sup> imaging studies showing that reward-related cues elicit time-locked population shifts in MSN activity (Cruz et al., 2014; Moyer et al., 2014). MSN-to-MSN lateral inhibition may support NAc output from discrete MSN ensembles and prevent concomitant output from competing pathways, similar to the computational conceptualization of a Go-No Go network (Moyer et al., 2014). Interestingly, lateral

inhibition between putative D1 and D2 MSNs in the NAc appears to gate the stimulant actions of cocaine. Specifically, cocaine-induced DA efflux decreases D2-to-D1 MSN lateral inhibition via laterally-localized D2 receptors, thereby disinhibiting NAc output along the D1 pathway (Dobbs et al., 2016; Burke et al., 2017). This finding may explain why pharmacological blockade of D2 receptors in the NAc attenuates the rewarding properties of canonical DA secretagogues, such as AMPH, methamphetamine, MDMA and cocaine. It is enticing to consider whether reward-related motivational output is generally gated by regulatory mechanisms within the NAc collateral inhibitory network.

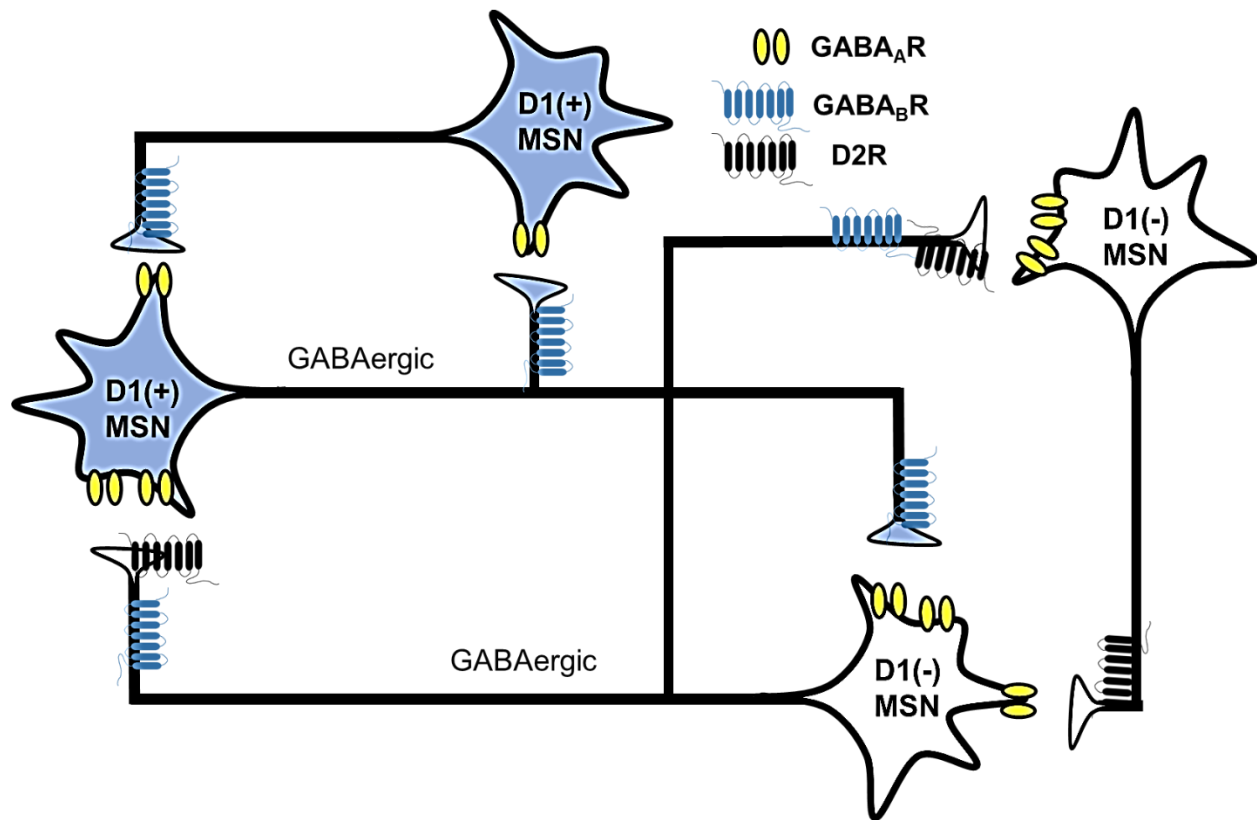


**Figure 2.4. Lateral inhibitory networks formed by D1(+) and D1(-) MSNs in the NAc.** D1(+) and D1(-) MSNs form mutual inhibitory networks via GABAergic collaterals. While phasic GABAergic transmission between MSNs is mediated by GABA<sub>A</sub>R, both MSN subtypes presynaptically express GABA<sub>B</sub>R. D1(-) MSNs express D2 DA receptors that inhibit D1(-) MSN-to-D1(+) MSN transmission, thereby disinhibiting D1(+) MSN output. Lateral inhibition is hypothesized to facilitate functional output of discrete MSN ensembles recruited during experience.

An important distinction between lateral inhibition in the NAc and dorsal striatum is the expression of CB<sub>1</sub>R on presynaptic terminals. Unlike MSN-to-MSN synapses in the dorsolateral striatum, lateral inhibition in the NAc is insensitive to WIN 55-212, a potent CB<sub>1/2</sub>R agonist, and fails to undergo depolarization-induced suppression of inhibition (DSI) (Winters et al., 2012; Wright et al., 2017). In the dorsolateral striatum, CB<sub>1</sub>R function on MSN terminals mediates state-dependent inhibitory LTD (iLTD) – a heterosynaptic form of plasticity in which MSN voltage-state (i.e., up vs. downstate) and afferent excitatory input gates MSN-to-MSN GABAergic transmission (Mathur et al., 2013). Specifically, the eCB anandamide (AEA) released from MSNs clamped in their downstate elicits iLTD of lateral MSN-to-MSN transmission, an effect unobserved at PV-IN-to-MSN feedforward synapses (Mathur et al., 2013). While downstate iLTD is expressed at local GABAergic synapses onto MSNs in the NAc, (a) this plasticity is CB<sub>1</sub>R-independent and (b) paired MSN recordings or optogenetic tools were not used to assess which GABAergic synapses undergo iLTD (Atwood et al., 2014; Patton et al., 2019). Thus, activity-dependent changes in GABAergic synaptic strength onto MSNs in the NAc likely utilizes distinct synaptic mechanisms from those in the dorsal striatum. Furthermore, the lack of CB<sub>1</sub>R on MSNs suggests that eCBs and exogenous cannabinoids, such as  $\Delta^9$ -tetrahydrocannabinol ( $\Delta^9$ -THC) in marijuana or WIN 55-212, likely exert differential effects on NAc and dorsal striatal circuit function.

It is presently unknown to what extent MSNs in the NAc modulate the activity of contiguous interneuron microcircuits. A candidate mediator of direct MSN-microcircuit interactions is the endogenous opioid system, as D1 and D2 MSNs synthesize and release dynorphin and enkephalin, respectively. In the dorsal striatum, antidromic stimulation of globus pallidus (GP)-projecting

MSNs decreases corticostriatal transmission via presynaptic  $\mu$ -opioid receptors (MOR) and GABA<sub>B</sub>R (Blomeley and Bracci, 2011; Logie et al., 2013). The former effect is probably mediated by endogenous enkephalin release, as dynorphin acts predominately via  $\kappa$ -ORs (KORs) with negligible affinity for MORs (Shang and Filizola, 2015). While endogenously-released opioid signaling in the NAc has not been explicitly demonstrated, glutamatergic transmission onto D1 and D2 MSNs is exquisitely sensitive to exogenous opioid receptor agonists, indicating that these synapses are likely also targeted by retrograde opioid signaling (Iremonger and Bains, 2009; Tejada et al., 2017). It would be interesting to examine whether GABAergic interneurons, such as PV-INs or SST-INs, undergo opioid-dependent forms of synaptic plasticity. Similar to the MSN-to-CIN interaction mediated by D1 MSN-evoked substance P release, MSN-induced modulation of PV-IN synapses by G<sub>i/o</sub>-coupled ORs would functionally disinhibit discrete MSN ensembles. A similar tripartite interaction has been shown between MSN collaterals and CINs, where presynaptic mAChR signaling decreases GABAergic transmission at MSN-to-MSN collateral synapses (Witten et al., 2010; Yamamoto et al., 2013). Future studies will be needed to define intrinsic and extrinsic modulatory actions within lateral inhibitory microcircuits in the NAc.

## 2.5 Conclusion

The NAc contains an interconnected microcircuit network regulating goal-directed motivational output. While PV-IN-directed feedforward microcircuits form a robust regulatory unit within the NAc, CINs, via expansive ACh-containing axonal arborizations, uniquely influence NAc circuit dynamics at the interface between GABAergic interneurons, mesoaccumbens DA signaling, and afferent glutamatergic transmission. In contrast, SST-INs appear to influence NAc circuit function through more furtive means, as SST-INs exhibit a weak hodological input-output profile that may

rely more on NO and NPY-dependent signaling mechanisms than GABA. Although D1 and D2 MSNs predominately innervate mesencephalic and pallidal output systems, lateral inhibition between reciprocal MSN synapses gate which MSN ensembles direct functional NAc output. Defined by distinct biophysical, morphological, and molecular phenotypes, interneuron-enriched microcircuits in the NAc collectively function by adapting to environmental and situational contexts in which NAc-dependent behaviors are recruited. As more sophisticated computational modeling, *in vivo* recording, and behavioral techniques emerge, microcircuit contributions to NAc circuit function may become viable therapeutic targets for the treatment of various pathological motivational states, including addiction and depression.

## 2.6 Overall aims

The overall objective of this dissertation is to broaden our understanding of the synaptic, cellular, and molecular mechanisms governing intrinsic circuit function in the NAc core. Intrinsic circuits refer to interneuron-embedded networks that regulate NAc circuit dynamics, whereas extrinsic circuits are apical neuromodulatory afferents capable of modulating overall NAc activity. These terms are operationally defined according to the current conceptualization of NAc circuit function. The intrinsic circuit interrogated here is the feedforward inhibitory microcircuit mediated by parvalbumin (PV)-expressing INs (PV-INs), with precise experimental focus on disynaptic plasticity mechanisms regulating feedforward transmission (**Fig. 2.5**).

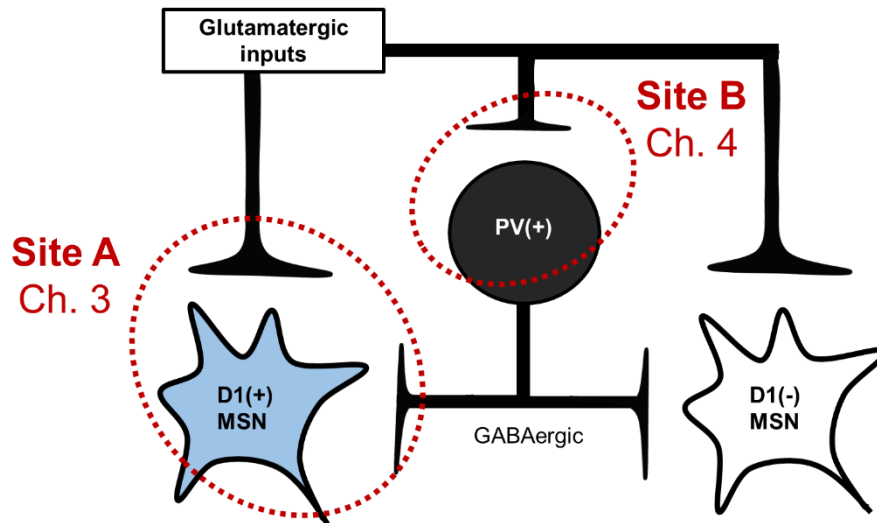


**Figure 2.5. Schematic depicting experimental focus within PV-IN-embedded feedforward microcircuits in the NAc.** Feedforward inhibition in the NAc occurs via fast-spiking, parvalbumin (PV)-expressing interneurons (PV-INs). Glutamatergic inputs from corticolimbic brain regions form monosynaptic connections with D1 [D1(+)] and D2 [D1(-)] DA receptor-expressing medium spiny neurons (MSNs). Collateralizing axons from these regions synapse onto contiguous PV-INs. PV-INs form GABAergic synapses with D1(+) and D1(-) MSNs to provide precise spatiotemporal regulation of MSN output. *Note:* for the remainder of chapters in this Dissertation, D1(+) and D1(-) nomenclature is used for MSNs to align with our experimental reporter strategy in D1tdTomato mice.

Chapter 2 describes a heterosynaptic phenomenon in which PV-INs target presynaptically-expressed GABA<sub>B</sub> receptors (GABA<sub>B</sub>R) on glutamate terminals. GABA<sub>B</sub>R elicits a non-canonical form of short-term plasticity mediated largely by a Gβγ-SNAP25 interaction with the vesicular release machinery. Chapter 3 describes a novel plasticity mechanism at feedforward synapses onto PV-INs, whereby Ca<sup>2+</sup>-permeable AMPA receptors (CP-AMPA) trigger a novel, CB<sub>1</sub>R-dependent form of long-term depression (LTD). Chapters 3 and 4 both describe activity-dependent mechanisms by which PV-IN-mediated feed-forward inhibition modulate NAc circuit function.

*Note:* In the Appendix, the extrinsic circuit interrogated is the neuromodulatory interactions between histamine (HA) and glutamatergic transmission in the NAc core, with emphasis placed on the H<sub>3</sub> heteroreceptor (H<sub>3</sub>R). Appendix A describes the synaptic and molecular mechanism by which HA elicits H<sub>3</sub>R-dependent LTD of glutamatergic transmission onto D1(+) MSNs. HA-induced LTD proceeds through a novel intracellular signaling mechanism mediated by the Akt-GSK3β axis that is preferentially expressed at corticoaccumbens synapses. Chapter 4 represents a turning point in my scientific development, as central HA signaling in the tuberomammillary nucleus (TMN) is where I intend to take my skillset as an electrophysiologist. My future scientific pursuits aim to understand how disruptions to sleep-wake circuit mechanisms within the TMN contribute to neuropsychiatric disease states, including depression, addiction, and anxiety.

Intrinsic and extrinsic neuromodulatory function in the NAc converges on signaling mechanisms recruited by G protein-coupled receptors (GPCRs). By studying how PV-INs and HA in the NAc elicit discrete circuit adaptations, GPCR function, particularly “inhibitory” G<sub>i/o</sub>-coupled GPCRs [e.g., GABA<sub>B</sub>R (Ch. 2), and CB<sub>1</sub>R (Ch. 3), and H<sub>3</sub>R (Appendix A)], became increasingly

characterized in parallel. Thus, studies examining NAc circuit dynamics led to concomitant discoveries of novel effector systems targeted by therapeutically-relevant GPCRs. It is my hope that this dissertation encourages others to define detailed mechanisms regulating anatomically-defined circuit maps of the mesolimbic reward network so that future treatments for maladaptive motivational disorders can be developed.

## CHAPTER 3

### **Heterosynaptic GABA<sub>B</sub> receptor function within feedforward microcircuits gates glutamatergic transmission in the nucleus accumbens core**

*Note:* The following chapter was titled as published in the *Journal of Neuroscience*:

Manz KM, Baxley AG, Zurawski Z, Hamm HE, Grueter BA. (2019). Heterosynaptic GABA<sub>B</sub> receptor function within feedforward microcircuits gates glutamatergic transmission in the nucleus accumbens core. *Journal of Neuroscience*.

#### 3.1 Abstract

Complex circuit interactions within the nucleus accumbens (NAc) facilitate goal-directed behavior. Medium spiny neurons (MSNs) mediate NAc output by projecting to functionally divergent brain regions, a property conferred, in part, by the differential projection patterns of D1- and D2 dopamine receptor-expressing MSNs. Glutamatergic afferents to the NAc direct MSN output by recruiting feedforward inhibitory microcircuits comprised of parvalbumin (PV)-expressing interneurons (INs). Furthermore, the GABA<sub>B</sub> heteroreceptor (GABA<sub>B</sub>R), a G<sub>i/o</sub>-coupled G protein-coupled receptor, is expressed at glutamatergic synapses throughout the mesolimbic network, yet its physiological context and synaptic mechanism within the NAc remains unknown. Here, we explored GABA<sub>B</sub>R function at glutamatergic synapses within PV-IN-embedded microcircuits in the NAc core of male mice. We found that GABA<sub>B</sub>R is expressed presynaptically and recruits a non-canonical signaling mechanism to reduce glutamatergic synaptic efficacy at D1(+) and D1(-) [putative D2] MSN subtypes. Furthermore, PV-INs, a robust source of neuronal GABA in the NAc, heterosynaptically target GABA<sub>B</sub>R to selectively modulate

glutamatergic transmission onto D1(+) MSNs. These findings elucidate a new mechanism of feedforward inhibition and refine mechanisms by which GABA<sub>B</sub> heteroreceptors modulate mesolimbic circuit function.

### 3.2. Significance Statement

Glutamatergic transmission in the nucleus accumbens (NAc) critically contributes to goal-directed behaviors. However, intrinsic microcircuit mechanisms governing the integration of these synapses remain largely unknown. Here, we show that parvalbumin-expressing interneurons within feedforward microcircuits heterosynaptically target GABA<sub>B</sub> heteroreceptors (GABA<sub>B</sub>R) on glutamate terminals. Activation of presynaptically-expressed GABA<sub>B</sub>R decreases glutamatergic synaptic strength by engaging a non-canonical signaling pathway that interferes with vesicular exocytotic release machinery. These findings offer mechanistic insight into the role of GABA<sub>B</sub> heteroreceptors within reward circuitry, elucidate a novel arm to feedforward inhibitory networks, and inform the growing use of GABA<sub>B</sub>R-selective pharmacotherapy for various motivational disorders, including addiction, major depressive disorder, and autism.

### 3.3 Introduction

The nucleus accumbens (NAc) is a critical node within the mesolimbic reward network implicated in maladaptive motivational states, including addiction and major depressive disorder (Lüscher and Malenka, 2011; Koob and Volkow, 2016). The NAc orchestrates goal-directed motivational behavior by integrating glutamatergic input from cortical and limbic brain structures (Kalivas, 2009; Turner et al., 2018). While experience-driven adaptations at glutamatergic inputs drive reward-related behavioral outcomes (Pascoli et al., 2014; LeGates et al., 2018), microcircuit

mechanisms governing excitatory gain in the NAc remain largely unidentified. A putative gain control mechanism in the NAc are feedforward inhibitory microcircuits mediated by fast-spiking parvalbumin (PV)-expressing interneurons (PV-INs). Glutamatergic afferents onto medium spiny projection neurons (MSNs), differentiated based on the expression of D1 [D1(+) MSNs] or D2 dopamine receptors [D1(-) MSNs], collateralize onto PV-INs, which exert robust GABAergic control over MSN output (Wright et al., 2017; Scudder et al., 2018). PV-IN-directed feedforward inhibition gates NAc-dependent behavioral output by coordinating time-contingent changes in MSN action potential activity (Yu et al., 2017).

A potential candidate bridging glutamatergic transmission in the NAc to PV-IN-embedded feedforward microcircuits is the GABA<sub>B</sub> heteroreceptor (GABA<sub>B</sub>R), a G<sub>i/o</sub>-coupled G protein-coupled receptor (GPCR) expressed highly at synapses throughout mesolimbic and striatal networks (Lacey et al., 2005; Edwards et al., 2017). Clinical and preclinical studies of addiction indicate that baclofen (BAC), a selective GABA<sub>B</sub>R agonist, attenuates drug-seeking behavior, drug craving, and relapse (Hotsenpiller and Wolf, 2003; Kahn et al., 2009). *In vivo* BAC treatment attenuates cocaine-induced dopamine (DA) efflux into the NAc and is accompanied by decreased psychostimulant-induced hyperlocomotion, self-administration, and conditioned place preference (CPP) (Di Ciano & Everitt, 2003; Li et al., 2001; Roberts & Andrews, 1997; Voigt et al., 2011). Congruent with these findings, GABA<sub>B</sub>R activity recruits postsynaptic inward-rectifying K<sup>+</sup> channels (Kir) channels in the ventral tegmental area (VTA) to hyperpolarize NAc-projecting dopamine (DA) neurons, reducing functional mesoaccumbens DA output (Cruz et al., 2004; Labouèbe et al., 2007; Edwards et al., 2017). In the NAc, GABA<sub>B</sub>R is likely targeted by GABA from contiguous GABAergic circuits, such as PV-IN microcircuits, to elicit heterosynaptic

changes in neurotransmission (Uchimura and North, 1991). In parallel with MSNs, PV-INs receive robust glutamatergic inputs that are required to drive activity-dependent feedforward inhibition (Yu et al., 2017; Scudder et al., 2018). Despite making up 0.5-1.0% of cells in the NAc, PV-INs extensively innervate MSN ensembles to regulate NAc-directed motivational output (Tepper & Koós, 2017; Winters et al., 2012; Wright et al., 2017). For example, silencing PV-INs impairs amphetamine-induced locomotor sensitization and CPP, whereas strengthening of synapses onto PV-INs expedites cocaine self-administration (Yu et al., 2017; Wang et al., 2018). While PV-INs critically regulate NAc-dependent motivational behavior, the synaptic repertoire utilized by these cells to entrain MSN output is unclear.

We hypothesized that PV-IN-embedded feedforward microcircuits regulate glutamatergic transmission in the NAc by heterosynaptically targeting GABA<sub>B</sub>R. Utilizing transgenic mice, optogenetics, and whole-cell patch-clamp electrophysiology, in combination with rigorous pharmacology, we demonstrate that presynaptic GABA<sub>B</sub>R activity in the NAc core reduces glutamate release probability non-canonically in a SNAP-25-dependent manner that is distinct from similar G<sub>i/o</sub>-GPCRs in the NAc core. We find that PV-INs within feedforward inhibitory circuits are a heterosynaptic source of GABA regulating glutamatergic synapses by targeting presynaptically-expressed GABA<sub>B</sub>R. Congruent with the absence of autonomous PV-IN action potential activity, our findings indicate a lack of tonic GABA<sub>B</sub>R activity, suggesting that heterosynaptic targeting of GABA<sub>B</sub>R is activity-dependent. Together, our results provide insight into mechanisms by which GABA<sub>B</sub>R is recruited within a novel feedforward microcircuit to regulate glutamatergic transmission in the NAc.

### 3.4 Methods and Materials

#### *Animals*

Animals were bred and housed at Vanderbilt University Medical Center in accordance to IACUC. Male mice 8-12 weeks of age were used for all electrophysiological experiments. Mice were housed according to sex in groups of 2-5/cage on a 12-hr light-dark cycle with *ad lib* access to food and water. Breeding cages were given 5LOD chow (PicoLab ®, 28.7% protein, 13.4 % fat, 57.9 % carbohydrate) to improve litter viability. For all electrophysiological experiments, C57BL/6J mice were bred to harbor a bacterial artificial chromosome (BAC) carrying the tdTomato fluorophore under control of the *Drd1a* (D1 receptor) promoter. For a subset of experiments, parvalbumin (PV)-IRES-Cre mice ( $Pvalb^{tm1(cre)Arbr}$ ) were crossed with conditional channelrhodopsin-2 (ChR2) mice (Ai32(RCL-ChR2(H134R)/EYFP) and *Drd1a*-tdTomato mice, generating triple transgenic PV<sup>Cre</sup>-cChR2-D1tdTomato (abbreviated as PV<sup>Cre</sup>) mice. SNAP25 $\Delta$ 3 transgenic mice lacking the G $\beta\gamma$ -binding motif at the C-terminus of SNAP-25 and WT littermate controls were generously donated to our lab by the Heidi Hamm lab and colleagues (Vanderbilt University).

#### *Electrophysiology*

Whole-cell voltage clamp recordings were obtained from D1tdTomato or PV<sup>Cre</sup> mice, as described previously (Joffe and Grueter, 2016; Turner et al., 2018b). Mice were euthanized under isoflurane anesthesia. Briefly, parasagittal slices (250  $\mu$ M) containing the NAc core were prepared from whole brain tissue using a Leica Vibratome in oxygenated (95% O<sub>2</sub>; 5% CO<sub>2</sub>) ice-cold *N*-methyl-*D*-glucamine (NMDG)-based solution (in mM: 2.5 KCl, 20 HEPES, 1.2 NaH<sub>2</sub>PO<sub>4</sub>, 25 Glucose, 93 NMDG, 30 NaHCO<sub>3</sub>, 5.0 sodium ascorbate, 3.0 sodium pyruvate, 10 MgCl<sub>2</sub>, and 0.5 CaCl<sub>2</sub>-2H<sub>2</sub>O).

Slices were then recovered in NMDG-based recovery solution for 10-15-min at 32 °C before being transferred to a chamber containing artificial cerebral spinal fluid (ACSF, in Mm: 119 NaCl, 2.5 KCl, 1.3 MgCl<sub>2</sub>-6H<sub>2</sub>O, 2.5 CaCl<sub>2</sub>-2H<sub>2</sub>O, 1.0 NaH<sub>2</sub>PO<sub>4</sub>-H<sub>2</sub>O, 26.2 NaHCO<sub>3</sub>, and 11 glucose). All experiments were performed using a Scientifica Slicescope Pro System with continuously-perfused 32 °C ACSF at 2 mL/min. MSNs in the NAc core were visualized using Scientifica PatchVision software and patched with 3–6 MΩ recording pipettes (P1000 Micropipette Puller) filled with a cesium (Cs<sup>+</sup>)-based internal solution (in mM: 120 CsMeSO<sub>3</sub>, 15 CsCl, 8 NaCl, 10 HEPES, 0.2 EGTA, 10 TEA-Cl, 4.0 Mg-ATP, 0.3 Na-GTP, 0.1 spermine, and 5.0 QX 314 bromide).

D1(+) and D1(-) MSNs were differentiated according to the expression of the tdTomato fluorophore via 530 nm LED light. D1(-) MSNs were distinguished from interneuron cell types based on morphological (size, shape) and biophysical properties (e.g., capacitance, membrane resistance, and AMPAR decay kinetics). In SNAP25Δ3 and WT littermate mice, MSNs were unlabeled and carefully differentiated from other NAc cell types according to the above criteria. Isolated electrically-evoked excitatory postsynaptic currents (eEPSCs) were performed in the continuous presence of GABA<sub>A</sub>R antagonist, picrotoxin (PTX, 50 μM). In PV<sup>Cre</sup> mice, optically-evoked inhibitory postsynaptic currents (oIPSCs) were isolated by continuously superfusing pan-AMPA antagonist, NBQX (5 μM), and NMDAR antagonist, D-APV (50 μM), into the ACSF bath. Paired pulse ratios (PPR) were obtained within-experiment by delivering two 0.3-ms duration pulses with a 50-ms interstimulus interval and calculating the amplitude ratio of the second eEPSC to the first eEPSC (eEPSC<sub>2</sub>/eEPSC<sub>1</sub>). Coefficient of variance (CV) analysis was conducted within-experiment by calculating  $\sigma/\mu$  of PSC amplitudes during specified time intervals. To assess CB<sub>1</sub>R

short-term plasticity, depolarization-induced suppression of excitation (DSE) was performed by depolarizing the postsynaptic cell from -70 to +40 mV for 10-sec. eEPSCs obtained pre- and post-DSE were obtained with a 5-sec interstimulus interval to capture synaptically-evoked short-term plasticity. To quantify the kinetics of the  $\text{Cd}^{2+}$ -induced blockade of eEPSC amplitude, each experiment was fit with a non-linear curve to capture the specific time point, T, at which eEPSC amplitude was 50% from baseline. T was then subtracted from the time point coinciding with the end of the baseline to obtain  $T_{1/2}$ . mEPSC analysis was performed with Clampfit 10.4 using a stringent best-fit template obtained from preliminary 10-min recording bouts in D1(+) and D1(-) MSNs. Each recording bout yielded a rise/day time ( $\leq 3$ -ms) and amplitude ( $\geq 5$  pA) selection criteria that was reflected in the overall template score. Series resistance ( $R_s$ ) was monitored continuously during all experiments, with  $>20\%$  change in  $R_s$  resulting in the omission of that experiment. Execution of experimental protocols, stimulus control, and data collection were accomplished using Molecular Devices pClamp 10 Analysis software. Monitoring electrical properties of cells was achieved using Axopatch 500B Multiclamp amplifier and Axon Digidata 1550 low-noise data acquisition digitizer. Responses were filtered at 2 kHz and digitized at 10 kHz. Optical stimulation of ChR2-expressing cells was achieved using a CoolLED pE-100 LED excitation system. 480 nm light at variable intensities (5-40%) was pulsed through the 40X high-power objective at 0.1 Hz with a duration of 0.3-0.5 ms.

### *Pharmacology*

(RS)-Baclofen, SCH 50911, CGP 7930, Forskolin,  $\text{CdCl}_2$ ,  $\text{BaCl}_2$ , LY 341495, LY 379268,  $\omega$ -Conotoxin GVIA,  $\omega$ -Agatoxin IVA, WIN 55,212-2, H89, 4-aminopyridine, and tiagabine were

purchased from Tocris Biosciences. Picrotoxin and *N*-ethylmaleimide were purchased from Sigma Aldrich.

### *Statistics and Data Analysis*

Electrophysiological experiments were analyzed using Clampfit 10.4 and GraphPad Prism v7.0. Changes in baseline eEPSC/oIPSC amplitude, coefficient of variance (CV), and PPR were calculated by comparing mean values during 5 min intervals specified in each time-course to baseline PPR and CV values. A depression was defined as a significant difference in eEPSC or oIPSC amplitude from baseline calculated during the time interval specified in the recording. For specific oIPSC experiments at PV-IN-to-MSN synapses, cells were rendered BAC-responsive (+) if BAC application resulted in a significant depression in oIPSC amplitude from baseline. To separate BAC(+) from BAC(-) negative synapses, a threshold criterion was set at >35% depression from baseline. Long-term depression (LTD) was defined as a significant difference in eEPSC or oIPSC amplitude from baseline that persisted in the presence of GABA<sub>B</sub>R antagonist, SCH 50911. After obtaining each data set, Shapiro-Wilk tests were performed to assess normality. Data depicted in Figures 1-8 were determined to be normally distributed. Thus, paired or unpaired *t*-tests were used to analyze statistical differences between data sets. Sidak's post-hoc analyses were used for analyses requiring multiple comparisons. Figure 9 depicts data that were determined to not be normally distributed, consistent with separable populations of PV-IN-to-MSN synapses. Power analyses were performed with preliminary data during the acquisition of each new data set. The sample size obtained from each power analysis calculation was then compared to sample sizes reported in the literature for similar experiments. Errors bars depicted in figures represent SEM. For all analyses,  $\alpha$  was set as 0.05, with P values <  $\alpha$  indicating a statistically significant difference.

### 3.5 Results

#### *Presynaptic GABA<sub>B</sub>R activity reduces synaptic efficacy at glutamatergic synapses onto D1(+) and D1(-) MSNs in the NAc core*

To determine if GABA<sub>B</sub>R activity modulates synaptic efficacy at glutamatergic synapses in the NAc core, we performed whole-cell voltage clamp recordings in *ex vivo* brain slice preparations from D1tdTomato BAC transgenic reporter mice. Expression of the red-fluorescent protein, tdTomato (tdT), is driven by the D1 dopamine receptor promoter, with tdT-expressing cells indicating D1(+) MSNs and tdT-lacking cells indicating D1(-) MSNs (putative D2 receptor-expressing MSNs) (**Fig. 3.1A**) (Joffe & Grueter, 2016; Kashima & Grueter, 2017; Lim et al., 2012; Rothwell et al., 2014; Turner et al., 2018). Electrically-evoked excitatory postsynaptic currents (eEPSCs) were isolated by incorporating GABA<sub>A</sub> receptor (GABA<sub>A</sub>R) antagonist, picrotoxin (50 μM), into the ACSF bath. Following a stable 10-min eEPSC baseline, GABA<sub>B</sub>R agonist, baclofen (BAC, 3 μM), was superfused into the bath for 10-min, resulting in a robust depression in eEPSC amplitude at D1(+) and D1(-) MSNs that was indistinct between cell types (**Fig. 1B-E**, D1(+) BAC: 35.7±4.1%, n=7, p<0.0001; D1(-) BAC: 32.9±3.8%, n=7, p<0.0001). Subsequent application of GABA<sub>B</sub>R antagonist, SCH 50911 (5 μM), reversed the BAC-induced depression to baseline at D1(+) and D1(-) MSNs, indicating a lack of GABA<sub>B</sub>R-induced long-term depression (GABA<sub>B</sub>R-LTD) at local glutamatergic synapses (**Fig. 3.1B-E**, D1(+): 103.5±6.9%, n=6, p=0.61; D1(-): 99.6±1.7%, n=6, p=0.80).

We next examined whether GABA<sub>B</sub>R activity modulates pharmacologically-isolated *N*-methyl-D-aspartate receptor (NMDAR)-mediated eEPSCs obtained at +40 mV in D1(+) and D1(-) MSNs.

Indeed, BAC application resulted in a robust decrease in NMDAR eEPSC amplitude at D1(+) and D1(-) MSN synapses (**Fig. 3.1G,H**, D1(+):  $35.29 \pm 10.2\%$ ,  $n=4$ ,  $p=0.0052$ ; D1(-):  $36.27 \pm 9.36\%$ ,  $n=6$ ,  $p=0.0007$ ). To determine if synapses onto D1(+) and D1(-) MSNs are differentially sensitive to GABA<sub>B</sub>R activation, we obtained a dose-response curve with BAC concentrations ranging from 200 nM-10  $\mu$ M. While higher concentrations (3-10  $\mu$ M) resulted in an equivalent decrease in eEPSC amplitude at both MSN subtypes, lower concentrations (200-600 nM) resulted in a greater decrease in eEPSC amplitude at D1(+) than D1(-) MSN synapses (**Fig. 1F**, 200 nM, D1(+):  $55.55 \pm 4.80\%$ ,  $n=5$ ; D1(-):  $72.46 \pm 4.35\%$ ,  $n=6$ ; 600 nM, D1(+):  $43.10 \pm 5.72\%$ ,  $n=5$ ; D1(-):  $59.82 \pm 2.76\%$ ,  $n=4$ ; 3  $\mu$ M, reported above; 10  $\mu$ M, D1(+):  $18.21 \pm 4.16\%$ ,  $n=3$ ; D1(-):  $21.38 \pm 1.29\%$ ,  $n=4$ ; 2-way ANOVA, effect of MSN subtype:  $F_{1,28} = 8.688$ ,  $p=0.006$ ). Prior application of SCH 50911 did not alter basal eEPSC amplitude and completely blocked the BAC-induced depression at both MSN subtypes (**Fig. 3.11I**, D1(+):  $99.39 \pm 3.95\%$ ,  $n=5$ ,  $p=0.74$ ;  $100.66 \pm 3.78\%$ ,  $n=4$ ,  $p=0.21$ ).

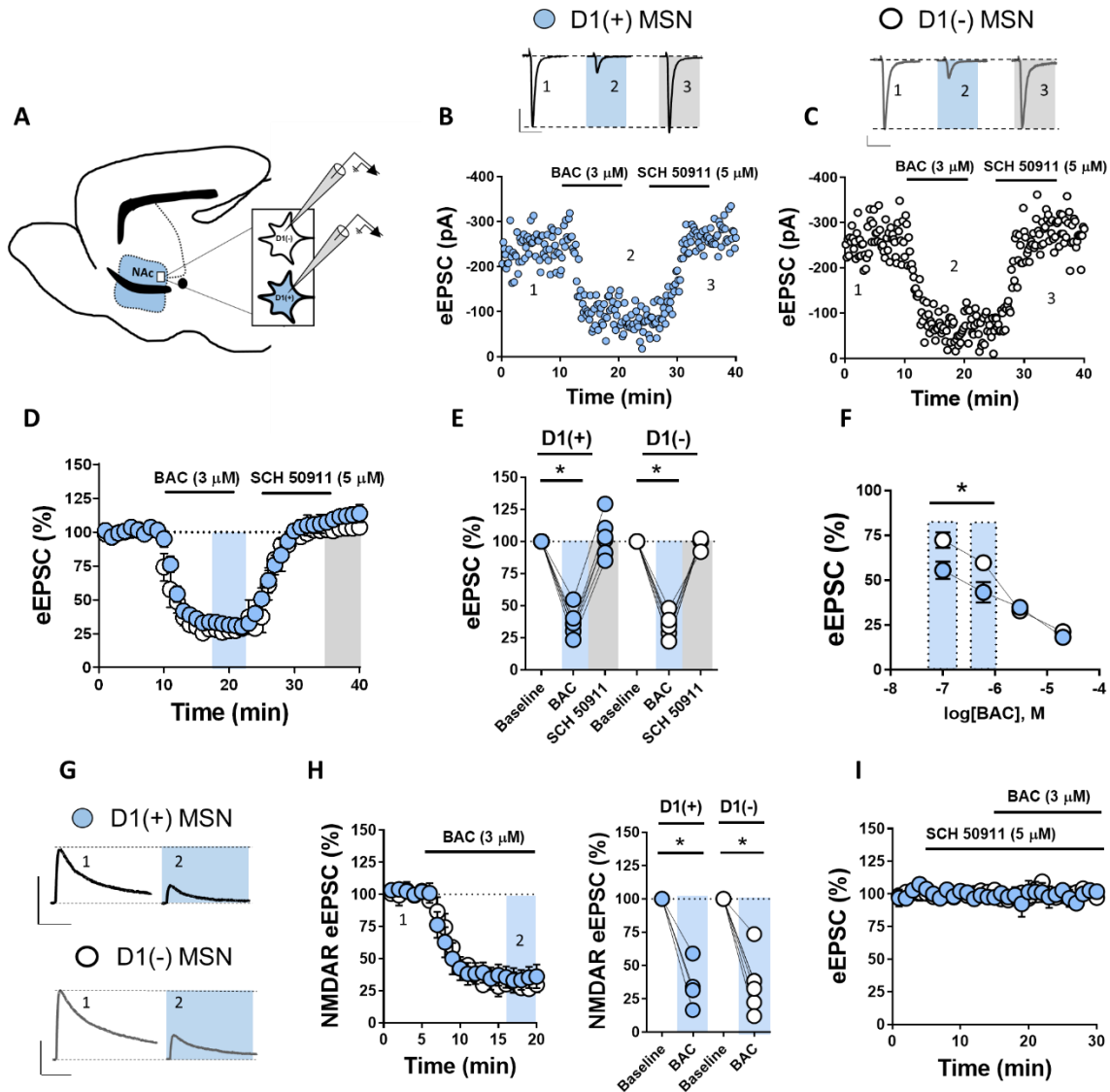


**Figure 3.1. GABA<sub>B</sub>R activity reduces synaptic efficacy at glutamatergic synapses onto D1(+) and D1(-) MSNs in the NAc core.** (A) Schematic of parasagittal D1tdTomato mouse brain slice outlining the recording area. (B, C) Representative eEPSCs obtained from D1(+) (blue circles) and D1(-) MSNs (open circles). Scale bar, left: 300 pA/50 ms; Scale bar, right: 100 pA/50 ms. (D) Normalized eEPSCs obtained from D1(+) and D1(-) MSNs in the presence of GABA<sub>B</sub>R agonist, BAC (3 μM), followed by GABA<sub>B</sub>R antagonist, SCH 50911 (5 μM). BAC decreased eEPSC amplitude that returns to baseline in SCH 50911. (E) Average eEPSC amplitude following BAC SCH 50911. (F) BAC dose-response curve (200 nM, 600 nM, 3 μM and 10 μM) obtained from D1(+) MSNs and D1(-) MSNs showing increased sensitivity to BAC at D1(+) MSNs. Note: 3 μM values obtained from averaged eEPSC values in (D). (G) NMDA eEPSCs obtained at +40 mV from D1(+) and D1(-) MSNs in the presence of NBQX. Scale bars (top, bottom): 100 pA/100 ms. (H) Time-course summary and average NMDAR eEPSCs following BAC. (I) SCH 50911 alone does not significantly alter eEPSC amplitude and blocks BAC. Error bars indicate SEM. \*  $p < 0.05$ .

GABA<sub>B</sub>R is expressed throughout the mesolimbic reward network with diverse pre- and postsynaptic sites of action (Cruz et al., 2004; Pitman et al., 2014; Edwards et al., 2017). Given that GABA<sub>B</sub>R is presynaptically-expressed at MSN-to-MSN collateral synapses (Dobbs et al., 2016), we performed multiple electrophysiological measurements to determine the synaptic locus of GABA<sub>B</sub>R at glutamatergic synapses in the NAc core. We first assessed changes in paired-pulse ratio (PPR) and coefficient of variance (CV), metrics which inversely correlate with presynaptic neurotransmitter release probability. BAC significantly increased PPR and CV at D1(+) and D1(-) MSN synapses that returned to baseline in the presence of SCH 50911 (**Fig. 3.2A-B**, PPR = D1(+) baseline:  $1.19 \pm 0.04$ , D1(+) BAC:  $1.8 \pm 0.2$ , D1(+) SCH:  $1.16 \pm 0.08$ , n=8, 1-way RM ANOVA, drug effect:  $F_{2,21} = 13.85$ , p=0.0001; Sidak's post-hoc analysis, BAC: p = 0.004; D1(-) baseline:  $0.97 \pm 0.07$ , D1(-) BAC:  $1.69 \pm 0.20$ , D1(-) SCH:  $1.02 \pm 0.08$ , n=8, 1-way RM ANOVA, drug effect:  $F_{2,21} = 11$ , p=0.0005; Sidak's post-hoc analysis, BAC: p=0.008; CV = D1(+) baseline:  $0.06 \pm 0.01$ , D1(+) BAC:  $0.51 \pm 0.07$ , D1(+) SCH:  $0.09 \pm 0.02$ , n=8, 1-way RM ANOVA, drug effect:  $F_{2,18} = 37.48$ , p<0.0001; Sidak's post-hoc analysis, BAC: p=0.001; D1(-) baseline:  $0.05 \pm 0.01$ , D1(-) BAC:  $0.55 \pm 0.05$ , D1(-) SCH:  $0.13 \pm 0.03$ , n=8, 1-way RM ANOVA, drug effect:  $F_{2,18} = 68.36$ , p<0.0001; Sidak's post-hoc analysis, BAC: p=0.001). This experiment performed in a Cs<sup>+</sup>/tetraethylammonium (TEA)-free, K<sup>+</sup>-loaded internal solution resulted in a similar change in PPR and CV without altering holding current or membrane resistance, suggesting a presynaptic change in glutamate release probability that is unaccompanied by a postsynaptic K<sup>+</sup> conductance (data not shown). We next examined the effects of BAC on tetrodotoxin (TTX, 500 nM)-insensitive miniature EPSCs (mEPSCs). Consistent with a presynaptic site of action, BAC significantly decreased mEPSC frequency without altering mEPSC amplitude (**Fig. 3.2C-F**, *mEPSC frequency* = D1(+) baseline:  $1.38 \pm 0.022$  Hz, D1(+) BAC:  $0.82 \pm 0.08$  Hz, n=9, p=0.027;

D1(-) baseline:  $2.53 \pm 0.0332$  Hz, D1(-) BAC:  $1.28 \pm 0.15$  Hz,  $n=9$ ,  $p=0.0014$ ; *mEPSC amplitude* =  
D1(+) baseline:  $-19.61 \pm 0.88$  pA, D1(+) BAC:  $-19.35 \pm 0.82$  pA,  $n=9$ ,  $p=0.846$ ; D1(-) baseline: -  
 $20.49 \pm 0.61$  pA, D1(-) BAC:  $-20.13 \pm 0.82$  pA,  $n=9$ ,  $p=0.666$ ). These data rigorously support a  
presynaptic localization of GABA<sub>B</sub>R at glutamatergic synapses onto D1(+) and D1(-) MSNs in  
the NAc core.

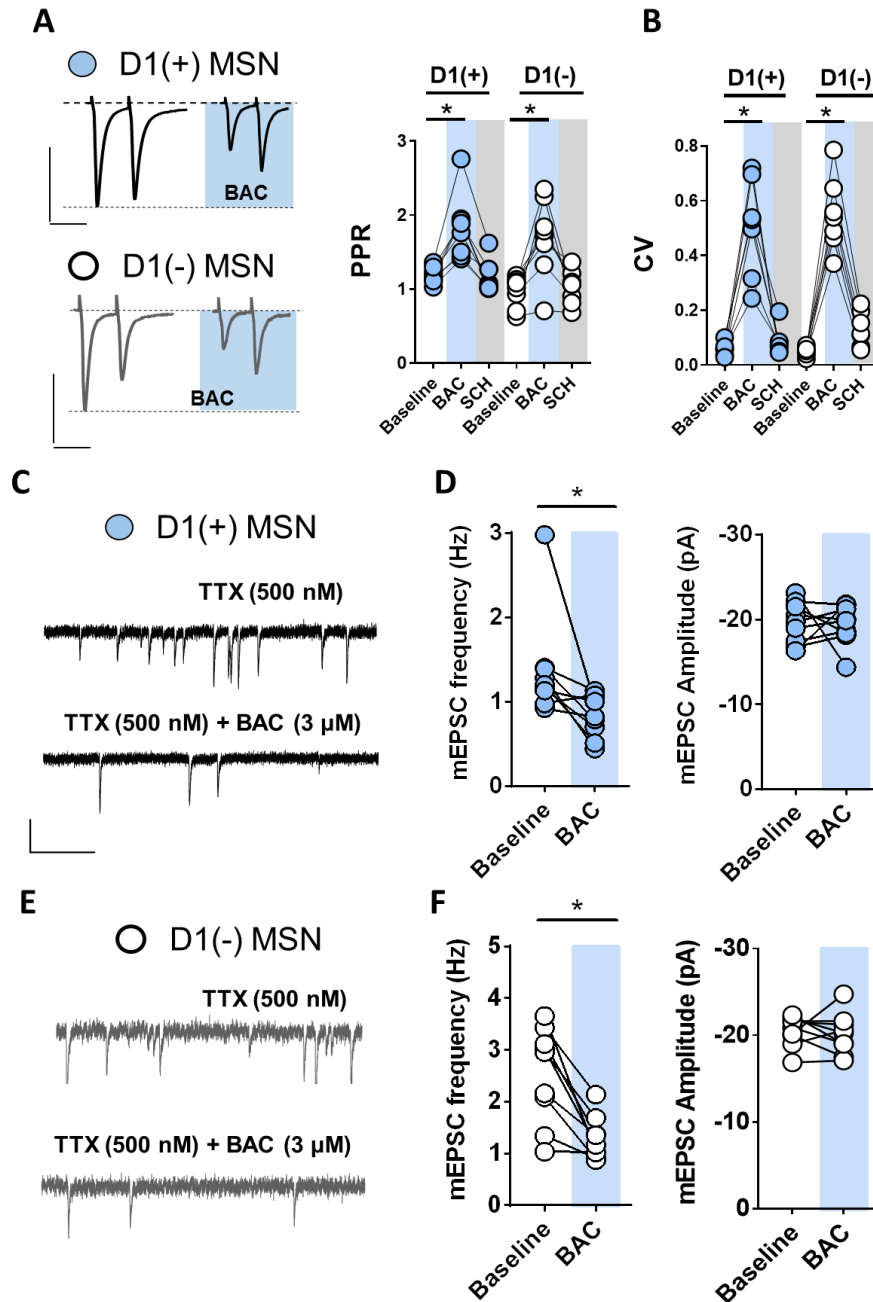


**Figure 3.2. GABA<sub>p</sub>R is functionally expressed at presynaptic loci at glutamatergic synapses onto both MSN subtypes in the NAc core.** (A) Representative traces of 50-ms ISI paired pulse eEPSCs obtained from D1(+) (blue circles) and D1(-) (open circles) MSNs at baseline and in the presence of BAC. Scale bar, top: 200 pA/50 ms; Scale bar, bottom: 100 pA/50 ms. BAC application increases PPR and (B) CV at D1(+) and D1(-) MSNs. (C, E) Representative traces of TTX-insensitive mEPSCs pre- and post-BAC application at D1(+) [black] and D1(-) MSNs [grey]. Scale bar: 20 pA/1-sec. (D, F) BAC decreases mEPSC frequency but not amplitude at D1(+) MSNs and D1(-) MSNs. Error bars indicate SEM. \*  $p < 0.05$ .

*GABA<sub>B</sub>R activation recruits non-canonical intracellular signaling mechanisms to reduce glutamate release probability at both MSN subtypes*

Presynaptic GABA<sub>B</sub> heteroreceptors canonically reduce neurotransmitter release probability by shifting the voltage dependence of voltage-gated Ca<sup>2+</sup> channels (VGCCs) (Kupferschmidt & Lovinger, 2015; Terunuma, 2018). To begin to interrogate this mechanism in the NAc core, we first tested whether prior GABA<sub>B</sub>R activation diminishes broad-spectrum blockade of VGCCs by cadmium (Cd<sup>2+</sup>, 100 μM). Prior application of BAC had no effect on the amplitude or kinetics (Cd<sup>2+</sup>-blockade T<sub>1/2</sub>, see Methods) with which Cd<sup>2+</sup> blocked evoked glutamatergic transmission (**Fig. 3.3.A-D**, pooled MSNs, BAC: 9.08±3.15%, n=5; ACSF: 10.11±1.35%, n=5, p=0.509; BAC Cd<sup>2+</sup>-T<sub>1/2</sub>: 0.67±0.15-min, n=6; ACSF Cd<sup>2+</sup>-T<sub>1/2</sub>: 0.65±0.13-min, n=6, p=0.907). To specifically rule out subtype-selective actions at VGCCs, we tested whether GABA<sub>B</sub>R reduces glutamate release probability by inhibiting N- or P/Q-type voltage-gated Ca<sup>2+</sup> channels (VGCCs). We examined the contribution of N-type VGCCs by superfusing selective N-type VGCC blocker, ω-conotoxin GVIA (ω-CTx, 800 nM), into the ACSF bath prior to BAC. ω-CTx significantly reduced eEPSC amplitude at D1(+) and D1(-) MSNs but failed to occlude the effects of BAC (**Fig. 3.3.E,J**, D1(+): 35.11±3.35%, n=4, p=0.9953; D1(-) 34.83±3.99%, n=4, p=0.9999). To determine if GABA<sub>B</sub>R instead couples selectively to P/Q-type VGCCs, we repeated the above experiment with selective P/Q-type VGCC blocker, ω-agatoxin IVA (ω-AgTx, 200 nM). ω-AgTx also resulted in a significant reduction in baseline eEPSC amplitude at D1(+) and D1(-) MSN synapses, consistent with previous reports showing that glutamatergic transmission in the NAc is mediated by N- and P/Q-type VGCCs. Prior ω-AgTx application also had no effect on the BAC-induced decrease in eEPSC amplitude at both MSN subtypes (**Fig. 3.3.E,J**, pooled MSNs: 29.08±3.15%, n=3,

p=0.593). These findings suggest that GABA<sub>B</sub>R reduces glutamate release probability independently of N- and P/Q-type VGCCs. Collectively, these findings suggest that the presynaptic mechanism of GABA<sub>B</sub>R at glutamatergic synapses in the NAc core is largely VGCC-independent.

We next asked if GABA<sub>B</sub>R activity reduces synaptic efficacy by activating G protein-coupled inward-rectifying K<sup>+</sup> (Kir) channels, a downstream effector targeted by several classes of G<sub>i/o</sub>-coupled GPCRs, including GABA<sub>B</sub>R (Ladera et al., 2008). BAC application in the presence of Ba<sup>2+</sup> (1 mM), a nonselective Kir channel blocker, resulted in a decrease in eEPSC amplitude at D1(+) and D1(-) MSNs that was similar to control conditions (**Fig. 3.3.F,J**, D1(+): 27.12±5.67%, n=4, p=0.4038; D1(-) 31.71±6.67, n=5, p=0.9976). Having ruled out mechanisms mediated by classical G<sub>βγ</sub> signaling, we next determined if GABA<sub>B</sub>R activation mobilizes G<sub>αi</sub> to inhibit adenylyl cyclase (AC) function. Bath-application of AC activator, forskolin (1 μM), had no effect on the BAC-induced decrease in eEPSC amplitude at both MSN subtypes (**Fig. 3.3.G,J**, D1(+): 35.99±5.11%, n=4, p=0.9994; D1(-) 32.72±3.91%, n=4, p=0.9999). Furthermore, prior application of cell-permeant protein kinase A (PKA) inhibitor, H89 (10 μM), did not occlude the effects of BAC at D1(+) and D1(-) MSN synapses (**Fig 3.3.H,J**, D1(+): 30.65±3.36%, n=5, p<0.001; D1(-): 26.89± 6.04%, n=5, p=0.8871). These data collectively suggest a mechanism by which GABA<sub>B</sub>R engages a non-canonical signaling pathway to influence presynaptic function. In line with this hypothesis, disabling G<sub>i/o</sub>-GPCR function with *N*-ethylmaleimide (NEM, 50 μM) diminished but did not block the BAC-induced decrease in eEPSC amplitude (**Fig. 3.4.,J**, D1(+): 58.38±10.27%, n=6, 1-way RM ANOVA, BAC effect: F<sub>2,16</sub> = 33.49, p<0.001; D1(+) Sidak's post-hoc analysis for BAC in ACSF vs. BAC in NEM, p=0.035 ; D1(-): 63.49±6.54%, n=6, 1-way RM ANOVA,

BAC effect:  $F_{2,16} = 73.13$ ,  $p < 0.001$ ; D1(-) Sidak's post-hoc analysis for BAC in ACSF vs. BAC in NEM,  $p = 0.001$ ).

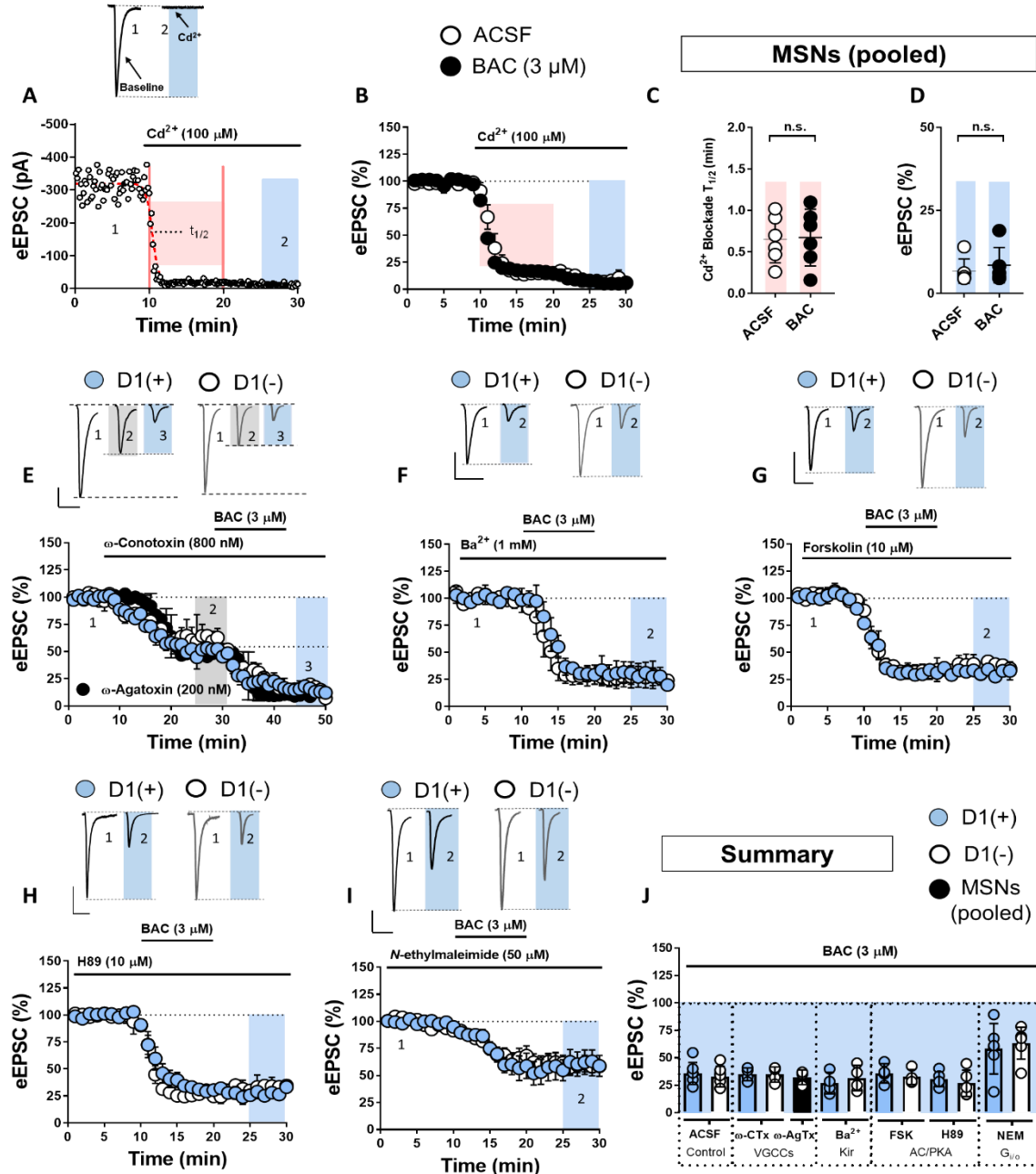


**Figure 3.3. GABA<sub>A</sub>R activation recruits a non-canonical intracellular signaling mechanism.** (A)

Representative Cd-induced blockade of eEPSC from pooled MSNs the time interval from which T<sub>1/2</sub> is obtained. (B) Time-course summary in ACSF and BAC (3 μM)-infused ACSF. (C, D) Quantified kinetics and magnitude of the Cd block. Scale bar for all traces: 100 pA/50 ms. (E) N-type VGCC blocker, ω-conotoxin GVIA (ω-CTx, 800 μM), failed to occlude the effects of BAC on eEPSC amplitude at D1(+) (blue circles) and D1(-) MSNs (open circles). ω-AgTx also failed to occlude the effects of BAC. (F) Effect of Ba (1 mM), on BAC. (G) Time-course summary and representative traces showing effect of AC activator, forskolin (10 μM), on BAC. (H) Effect of cell-permeant PKA inhibitor, H89, (10 μM), on BAC-induced decrease in eEPSC amplitude. (I) N-ethylmaleimide (NEM, 50 μM) blunted but did not block the effects of BAC on eEPSC amplitude at D1(+) and D1(-) MSNs. (J) Summary graph of BAC-induced decrease in eEPSC amplitude synapses

We next examined if group II mGluRs interact functionally with GABA<sub>B</sub>R at presynaptic loci to reduce glutamate release probability. Presynaptically-expressed mGluRs in the NAc have previously been shown to decrease vesicular release by selectively targeting P/Q-type VGCCs (Robbe et al., 2002; Mato et al., 2008). Given that  $\omega$ -AgTx failed to occlude the effects of BAC, we predicted that GABA<sub>B</sub>R functions through a different pathway than group II mGluRs. Bath-application of selective group II mGluR agonist, LY379268 (200 nM), resulted in a significant reduction in eEPSC amplitude that was accompanied by an increase in PPR and CV, consistent with the presynaptic localization of group II mGluRs in the NAc core (**Fig. 3.4.A,B**, PPR = D1(+) 8baseline:  $1.19 \pm 0.07$ , D1(+) LY,  $1.70 \pm 0.14$ , n=4, p=0.007; D1(-) baseline:  $1.08 \pm 0.064$ , D1(-) LY:  $1.64 \pm 0.14$ , n=5, p = 0.0246; CV = D1(+) baseline:  $0.03 \pm 0.01$ , D1(+) LY:  $0.41 \pm 0.09$ , n=5, p=0.0198; D1(-) baseline:  $0.12 \pm 0.01$ , D1(-) LY:  $0.35 \pm 0.07$ , n=4, p=0.0141). Subsequent application of BAC decreased eEPSC amplitude at D1(+) and D1(-) MSNs that was also indistinct from control conditions, suggesting that presynaptic group II mGluRs and GABA<sub>B</sub>R recruit distinct intracellular effectors to reduce glutamatergic transmission in the NAc core (**Fig. 3.4.C,E**, D1(+):  $34.45 \pm 6.91\%$ , n=4, p=0.6412; D1(-):  $32.02 \pm 4.53\%$ , n=4, p=0.1032). In the cerebellum, GABA<sub>B</sub>R couples to presynaptic metabotropic glutamate receptors (mGluR<sub>1</sub>) such that GABA<sub>B</sub>R activation augments mGluR sensitivity to synaptic glutamate levels (Tabata and Kano, 2006, 2010). To determine if a similar relationship exists in the NAc, LY3431495 was superfused at a concentration that antagonizes all mGluRs (100  $\mu$ M). In the presence of LY3431495, BAC application resulted in a similar reduction in eEPSC amplitude at D1(+) and D1(-) MSNs relative to control conditions (**Fig. 3.4.D,E**, D1(+):  $39.74 \pm 4.2\%$ , n=5, p=0.999; D1(-)  $43.07 \pm 5.55\%$ , n=5, p=0.4951). These data strongly suggest that GABA<sub>B</sub>R functions independently of mGluRs in the NAc core.

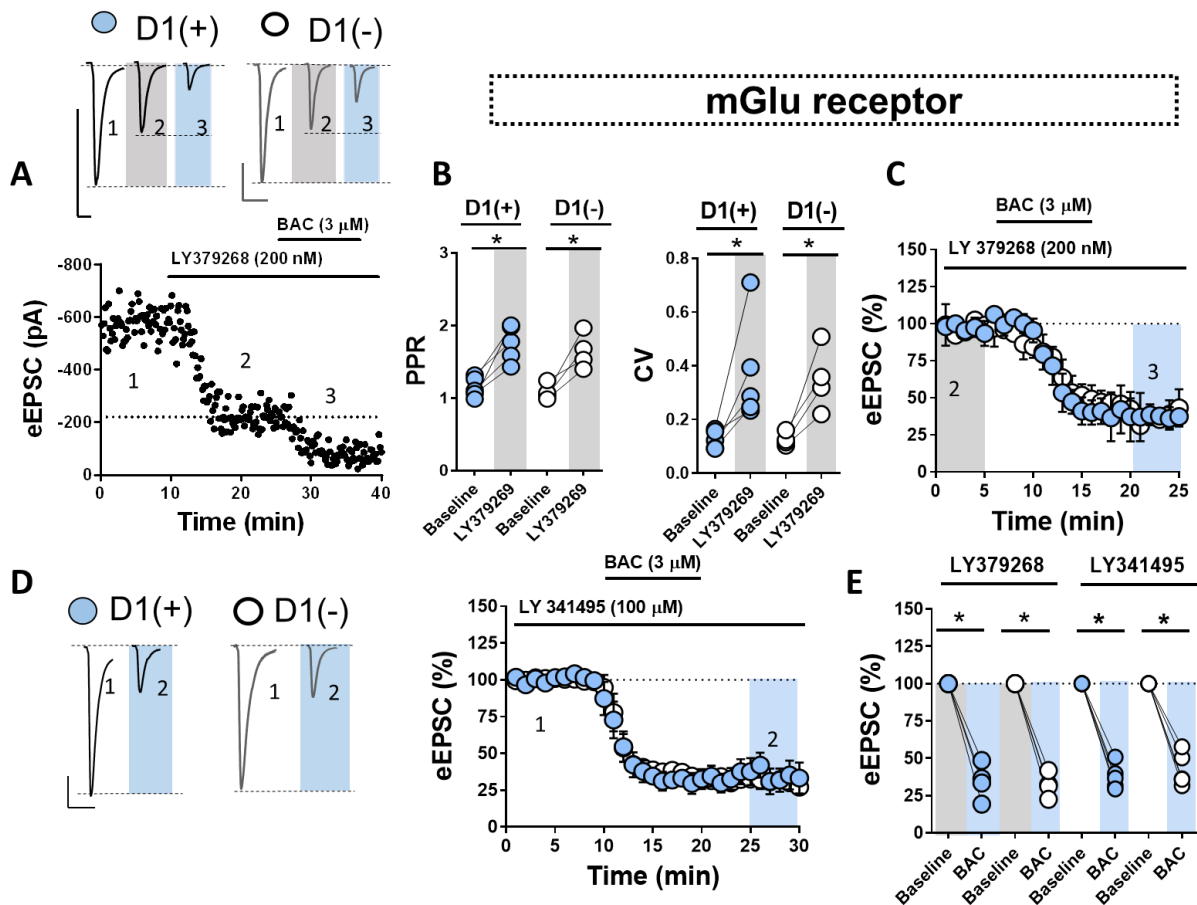


**Figure 3.4. GABA<sub>B</sub>R is functionally distinct from mGluRs in the NAc core.** (A) Representative experiment and traces showing that group II mGluR agonist, LY379268 (200 nM), fails to occlude the effects of BAC on eEPSC amplitude at D1(+) and D1(-) MSNs. Scale bar for all traces in figure: 100 pA/50 ms. (B). LY379268 application increases PPR and CV at D1(+) and D1(-) MSNs, consistent with a presynaptic locus of expression (C) Time-course summary showing the effects of BAC on eEPSC amplitude renormalized to stabilized baseline in the presence of LY379268 (grey). (D) Representative traces and time-course summary showing that prior application of pan-mGluR antagonist, LY341495, does not prevent the BAC-induced decrease in eEPSC amplitude (E) Summary graph quantifying the effects of mGluR-specific pharmacological manipulations on GABA<sub>B</sub>R function [averaged at t=35-40 min (blue)].

We next examined whether GABA<sub>B</sub>R shares a common intracellular mechanism with cannabinoid receptor type-1 (CB<sub>1</sub>R), the cognate receptor for endogenous cannabinoids (eCBs), such as 2-arachidonylglycerol (2-AG) and anandamide. We selected CB<sub>1</sub>R because it is the most ubiquitously expressed G<sub>i/o</sub>-GPCR in the mammalian CNS, generally restricted to presynaptic domains, and critically regulates excitatory transmission in the striatum (Robbe et al., 2003; Grueter et al., 2010; Castillo et al., 2012). To ascertain the functional difference between CB<sub>1</sub>R and GABA<sub>B</sub>R, we first looked at whether CB<sub>1/2</sub>R agonist, WIN 55-212 (1 μM), occludes the effects of BAC on eEPSC amplitude. WIN 55-212 resulted in a significant decrease in eEPSC amplitude that was accompanied by an increase in PPR and CV (**Fig. 3.5.F,G**, PPR = D1(+) baseline: 1.31±0.09, D1(+) WIN: 1.55±0.15, n=4, p=0.0439); D1(-) baseline: 1.44±0.80, D1(-) WIN: 1.75±0.18, n=5, p=0.0336); CV = D1(+) baseline: 0.010±0.003, D1(+) WIN 0.22±0.05, n=4, p=0.02771; D1(-) baseline: 0.12±0.018, D1(-) WIN: 0.29±0.28, n=5, p=0.0079). However, WIN 55-212 failed to occlude BAC at synapses onto both MSN subtypes, suggesting that presynaptically-expressed CB<sub>1</sub>R and GABA<sub>B</sub>R also modulate presynaptic release probability via distinct intracellular mechanisms (**Fig. 3.5.H**, D1(+): 35.60±6.78%, n=4, p=0.6412; D1(-) 38.07±4.71%, n=5, p=0.1032). We next tested the effects of BAC on depolarization-induced suppression of excitation (DSE), a CB<sub>1</sub>R-dependent form of short-term plasticity that transiently decreases glutamate release probability. N- and P/Q-type VGCCs have been implicated in the expression of CB<sub>1</sub>R-induced DSE in various regions, providing us with an additional means to assess the contribution of VGCCs in the mechanism of GABA<sub>B</sub>R (Kreitzer and Regehr, 2001; Heifets et al., 2008; Castillo et al., 2012). Postsynaptic depolarization from -70 to +40 mV for 10-sec resulted in a significant reduction in eEPSC amplitude at D1(+) and D1(-) MSN synapses, confirming the presence of DSE (**Fig. 3.5, I-L**, D1(+) DSE-ACSF: 64.97±2.69%, n=8, p<0.0001;

D1(-) DSE-ACSF:  $74.13 \pm 1.61\%$ ,  $n=9$ ,  $p < 0.0001$ ). Following a triplicate DSE baseline, BAC was superfused into the ACSF bath, resulting in a significant decrease in eEPSC amplitude that stabilized at the 20-min time-point. Subsequent trials of DSE were then performed in the presence of BAC. DSE remained completely intact following BAC application at D1(+) and D1(-) MSN synapses, indicating that BAC did not occlude the expression of DSE (**Fig. 3.5, I-L**, D1(+) DSE-BAC:  $59.1 \pm 4.38$ ,  $n=8$ ,  $p=0.2321$ ; D1(-) DSE-BAC:  $71.56 \pm 1.69$ ,  $n=$ ,  $p=0.1779$ ).

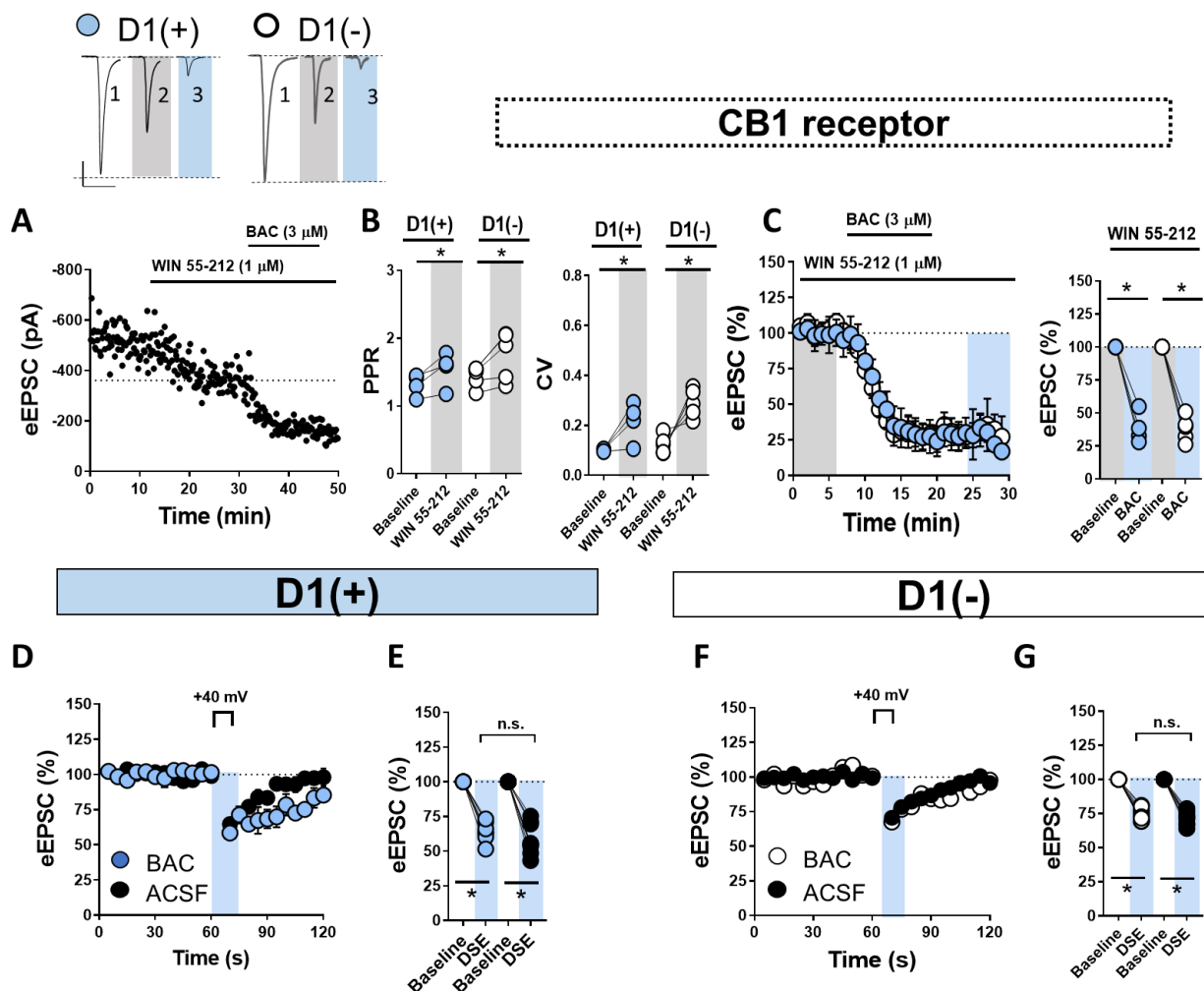


**Figure 3.5.  $GABA_pR$  is functionally distinct from  $CB_1R$  at glutamatergic synapses in the NAc core.** (A) Representative experiment and traces showing that  $CB_1/2$  agonist, WIN 55-212 (1  $\mu M$ ), depresses eEPSC amplitude at D1(+) and D1(-) MSNs but fails to occlude the effects of BAC. Scale bar for all traces in figure: 50 pA/50 ms. (B) Bath application of WIN 55-212 increased PPR and CV at glutamatergic synapses onto D1(+) and D1(-) MSNs, confirming the canonical presynaptic expression of  $CB_1R$  in the NAc. (C) Time-course summary and quantification showing the effects of BAC on eEPSC amplitude renormalized to stabilized baseline in the presence of WIN 55-212 (grey). (D-G). Time-course summaries and quantification (obtained at  $t=60$ -sec) of DSE followed by DSE in the presence of BAC for D1(+) and D1(-) MSNs. All DSE experiments performed in pairs such that DSE was repeated within-cell in the presence of BAC. Error bars indicate SEM. \*  $p < 0.05$ .

*Elevating presynaptic Ca<sup>2+</sup> influx abrogates downstream GABA<sub>B</sub>R effector function*

The above data suggest that presynaptic GABA<sub>B</sub>R function at glutamatergic synapses in the NAc core is distinct from the actions of GABA<sub>B</sub>R elsewhere in the CNS. One possibility is that GABA<sub>B</sub>R activation interferes with vesicular release machinery. To gain insight into how GABA<sub>B</sub>R may be involved in vesicular release, we asked if increasing presynaptic Ca<sup>2+</sup> influx during the electrically-evoked fiber volley modulates the effects of BAC. We accomplished this by bath-applying K<sup>+</sup> channel blocker, 4-aminopyridine (4-AP, 100 μM), at a concentration selective for voltage-gated K<sup>+</sup> channels (K<sub>v</sub>) (**Fig. 3.6.A**). Selective blockade of K<sub>v</sub> channels elongates action potential half-width, increasing VGCC open probability and presynaptic Ca<sup>2+</sup> conductance (Solis and Nicoll, 1992; Iremonger and Bains, 2009). Application of 4-AP alone significantly increased eEPSC amplitude at D1(+) and D1(-) MSNs (**Fig. 3.6.B,C**, D1(+) 4-AP: 142.26±12.38, n=6, p<0.001; D1(-) 4-AP: 143.55±11.34, n=6, p<0.001) and was accompanied by a reduction in PRR, consistent with a Ca<sup>2+</sup>-dependent enhancement of presynaptic release probability (**Fig. 3.6.D**, PPR = D1(+) baseline: 1.26±0.13, D1(+) 4-AP: 0.52±0.28, n=5, p=0.0468; D1(-) baseline: 1.16±0.09, D1(-) 4-AP: 0.76±0.13, n=4, p=0.0169). Subsequent application of BAC in the presence of 4-AP resulted in a depression in eEPSC amplitude at D1(+) and D1(-) MSNs that was significantly attenuated relative to control conditions (**Fig. 3.6.A-C**, D1(+): 66.71±3.09%, n=5, p=0.0001; D1(-): 69.35±7.02%, n=4, p=0.0003). 4-AP also negated BAC-induced changes in PPR and fully reversed the depression in eEPSC amplitude elicited by BAC (**Fig. 3.6.D-F**, PPR = D1(+) 4-AP + BAC: 0.79±0.12, n=5, p=0.214; D1(-) 4-AP±BAC: 0.73±0.11, n=4, p=0.4374; D1(+) 4-AP reversal: 116.40±7.89%, n=5, p=0.0033; D1(-) 4-AP reversal: 107.08±10.85%, n=4, p=0.0093). To verify that 4-AP increased Ca<sup>2+</sup> influx secondary to its action

at  $K_v$  channels, we repeated this experiment in low- $Ca^{2+}$  ACSF (1 mM  $Ca^{2+}$ /3 mM  $Mg^{2+}$ ). Prior application of 4-AP in low- $Ca^{2+}$  ACSF returned the BAC-induced decrease in eEPSC amplitude back to baseline conditions at MSN [pooled D1(+) and D1(-)] synapses, suggesting that increased  $Ca^{2+}$  influx via  $K_v$  channel blockade can successfully overcome the inhibitory actions of BAC at glutamatergic synapses in the NAc core (**Fig. 3.6.C**, MSNs (pooled):  $40.58 \pm 9.28\%$ ,  $n=11$ ,  $p=0.3533$ ).

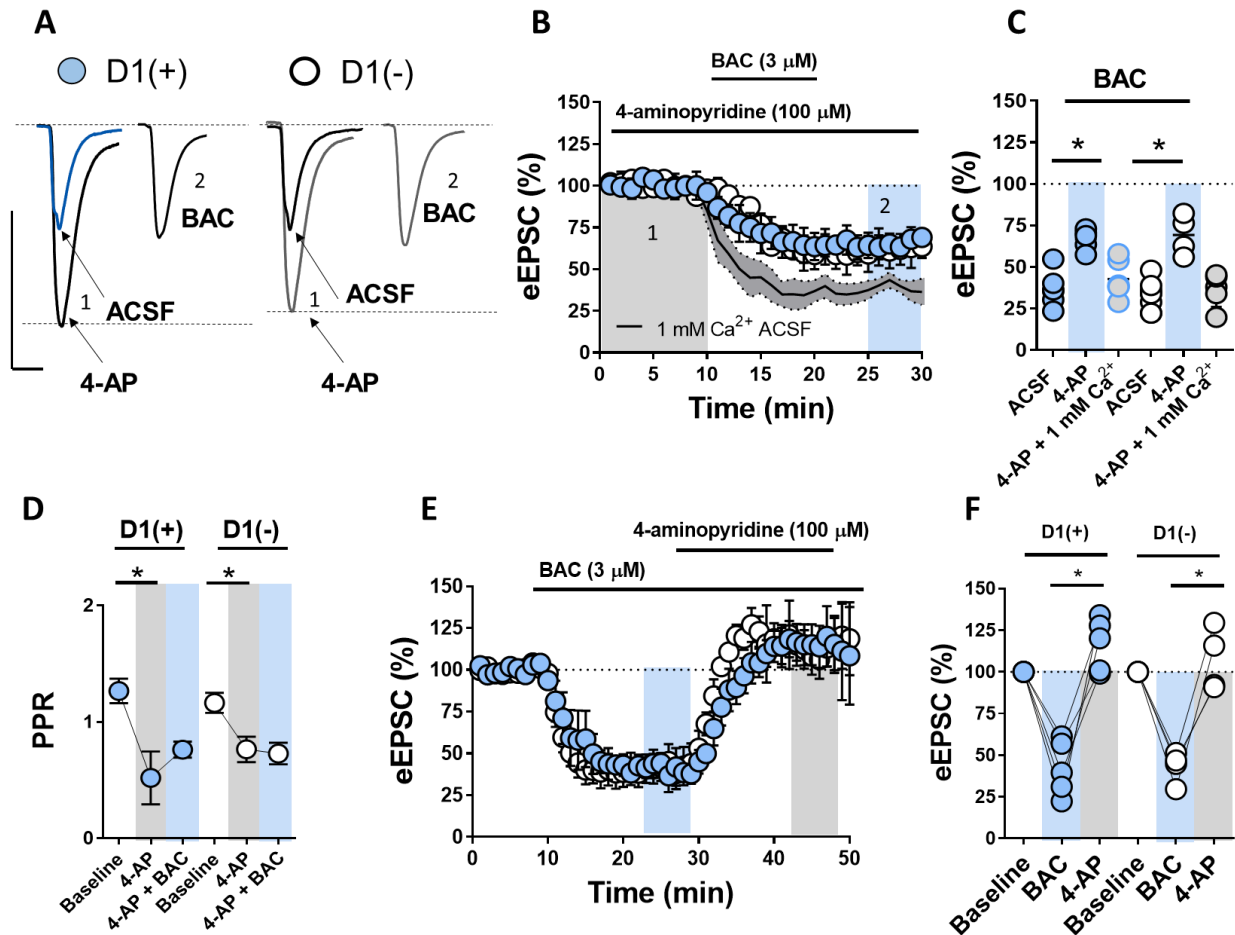


**Figure 3.6. Elevating presynaptic  $\text{Ca}^{2+}$  influx abrogates downstream  $\text{GABA}_B$  R effector function.** (A) 1: Representative traces showing that 4-AP application increases eEPSC amplitude and decay time at glutamatergic synapses onto D1(+) and D1(-) MSNs. 2: eEPSC amplitude at D1(+) and D1(-) MSN synapses in the presence of BAC. Scale bar: 200 pA/20 ms (B) Prior bath application of 4-AP blunts the BAC-induced decrease in eEPSC amplitude at D1(+) and D1(-) MSNs. Low calcium (1 mM) ACSF returns BAC-induced decrease in eEPSC amplitude to control conditions (pooled D1(+) and D1(-) MSNs, line with shaded grey area within SEM). (C) Graph of average eEPSC amplitude in the presence of BAC with 4-AP, 4-AP + low Ca ACSF, and ACSF-only control conditions. (D) 4-AP application alone decreases PPR and negates the increase in PPR elicited by BAC. (E) Time course summary showing that 4-AP application reverses eEPSC amplitude in the presence of BAC at D1(+) and D1(-) MSNs. (F) Graph of average eEPSC amplitude following 4-AP reversal in the presence of BAC and 4-AP + BAC for D1(+) and D1(-) MSNs. (G, H) Error bars indicate SEM. \*  $p < 0.05$ .

*Genetically disrupting the Gβγ-SNAP-25 interaction blunts the synaptic effect of GABA<sub>B</sub>R on glutamatergic transmission in the NAc core*

G<sub>i/o</sub>-coupled GPCR-induced mobilization of Gβγ at the presynaptic active zone has been shown to interfere with exocytotic fusion mediated by ternary SNARE complexes. Gβγ-dependent targeting of membrane-associated target SNARE proteins (t-SNAREs), such as SNAP-25, has been shown to prevent the association of synaptotagmin with the SNARE complex to reduce vesicular release probability (Wells et al., 2012; Zurawski et al., 2019). The Gβγ-SNARE interaction is Ca<sup>2+</sup>-sensitive, as pharmacological enhancement of presynaptic [Ca<sup>2+</sup>] can offset Gβγ binding to restore baseline synaptic transmission (Gerachshenko et al., 2005). Given that GABA<sub>B</sub>R heteroreceptor function in the NAc core is (a) putatively VGCC, Kir, AC, PKA, and mGluR-independent and (b) blunted by 4-AP-induced increases in presynaptic Ca<sup>2+</sup> influx, we hypothesized that GABA<sub>B</sub>R engages a presynaptic Gβγ-SNARE mechanism at glutamatergic synapses onto MSNs. To test this hypothesis, we utilized transgenic mice lacking the C-terminally-located Gβγ-binding motif of SNAP-25 (**Fig. 3.7.A**). Inserting the SNAP25Δ3 allele into the wild-type (WT) SNAP-25 locus attenuates Gβγ-SNAP-25 complex formation by ~47% without significantly disrupting evoked synaptic transmission (Zurawski et al., 2019).

We prepared acute *ex vivo* brain slices from SNAP25Δ3 and WT mice and recorded eEPSCs in unlabeled MSNs. Interestingly, baseline PPR of glutamatergic transmission in SNAP25Δ3 mice was significantly elevated relative to WT controls, consistent with a SNAP-25-specific reduction in vesicular exocytosis (**Fig. 3.7.**, MSNs (unlabeled), 3 μM, WT baseline 50-ms ISI, PPR:

0.99±0.14, n=7; SNAP25Δ3: 1.56±0.09, n=5, p=0.0021). Bath-application of BAC (3 μM) in slices obtained from littermate (WT) control mice decreased eEPSC amplitude comparably to D1tdTomato mice. However, BAC application (3 μM) in SNAP25Δ3 mice resulted in a significantly blunted decrease in eEPSC amplitude (**Fig. 3.7.C**, MSNs (unlabeled), WT: 27.54±1.14%, n=10; SNAP25Δ3: 55.45±4.94%, n=5, p=0.0003). To discern the functional relationship between GABA<sub>B</sub>R and SNAP25 more clearly, we superfused BAC at lower concentrations to elicit submaximal GABA<sub>B</sub>R activity. While the BAC-induced decrease in eEPSC amplitude was modestly reduced at higher BAC concentrations (3 μM, 10 μM), the effect was significantly attenuated at lower concentrations (200 nM, 600 nM) in SNAP25Δ3 mice (**Fig. 3.7.E,G**, 200 nM, WT: 79.35±2.09, n=6; SNAP25Δ3: 92.64±7.92, n=4, p=0.0083; 600 nM, WT: 62.71±4.10, n=7; SNAP25Δ3: 83.03±4.12%, n=5, p=0.0074). Furthermore, BAC application in WT mice was accompanied by a time-locked increase in PPR at all concentrations tested, whereas BAC application in SNAP25Δ3 mice did not significantly alter PPR (**Fig. 3.7.D,F,H**, 200 nM, WT baseline: 1.12±0.05, BAC: 1.34±0.08, n=4, p=0.0208; SNAP25Δ3 baseline: 1.35±0.11, BAC: 1.44±0.19, n=4, p=0.0964; 600 nM, WT baseline: 1.16±0.11, BAC: 1.36±0.15, n=6, p=0.0306; SNAP25Δ3 baseline: 1.46±0.17, BAC: 1.61±0.16, n=5, p=0.1419; 3 μM, WT baseline: 1.04±0.19, BAC: 1.73±0.13, n=4, p=0.0054; SNAP25Δ3 baseline: 1.76±0.16, BAC: 1.79±0.14, n=8, p=0.6367). These findings indicate that presynaptic GABA<sub>B</sub>R function at glutamatergic synapses in the NAc core is impaired in mice lacking the G<sub>βγ</sub>-targeting motif of SNAP-25.

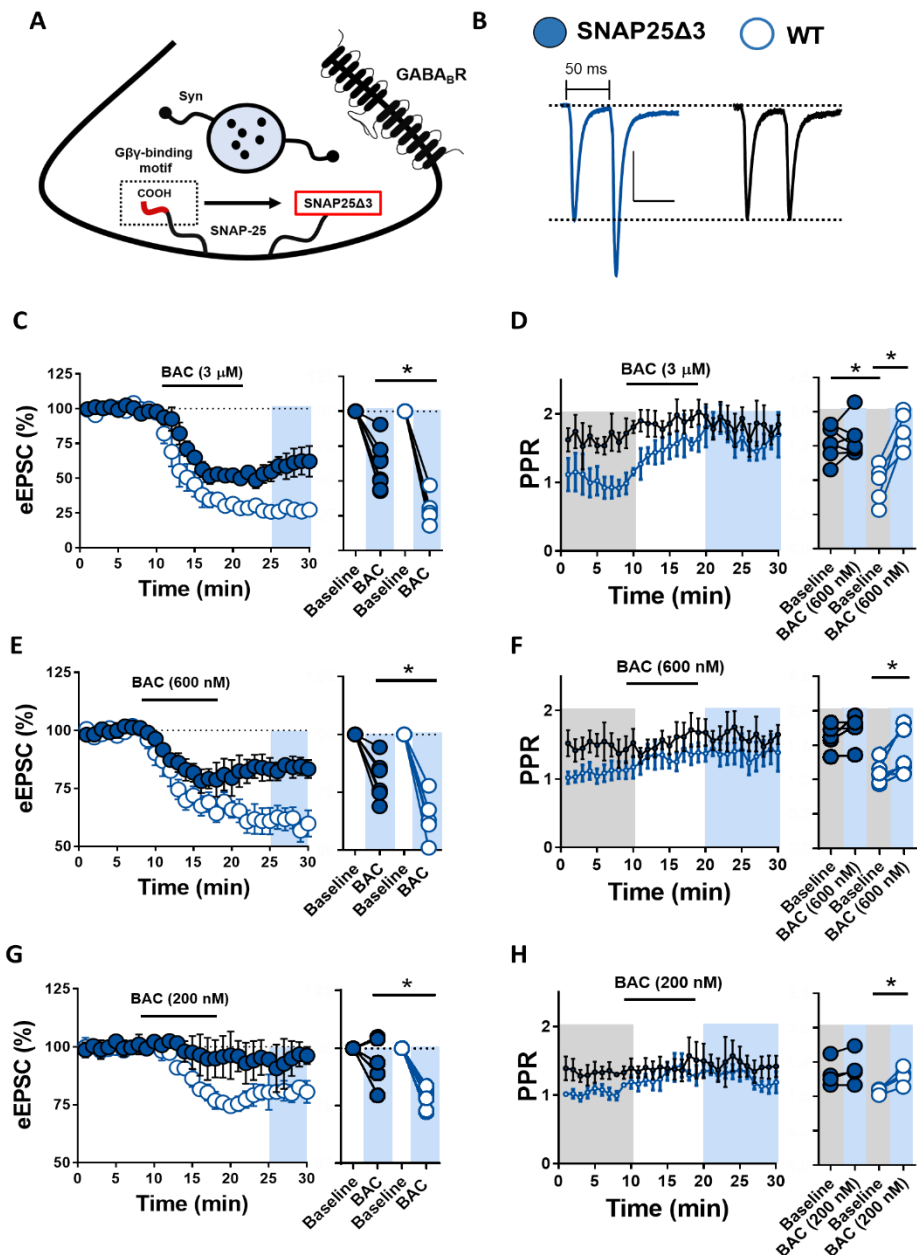


**Figure 3.7. Genetically reducing the  $G_{\beta\gamma}$ -SNAP-25 interaction blunts the synaptic effect of  $GABA_B R$ .** (A) Schematic of presynaptic terminal with C-terminally truncated SNAP-25 in transgenic SNAP25 $\Delta$ 3 mouse. (B) 50-ms paired-pulse eEPSCs in SNAP25 $\Delta$ 3 (left, blue circle) and WT mice (right, open circle). Basal PPR at 50-ms is increased in SNAP25 $\Delta$ 3 mice relative to WT littermate controls. Scale bars: 100 pA/50-ms. (C) eEPSC amplitude obtained from unlabeled MSNs in SNAP25 $\Delta$ 3 mutant mice (blue circles) and WT littermate control mice (open circles) in 3  $\mu$ M BAC. (D) PPR summary and averages pre-BAC (grey area) and post-BAC (blue area). (E) eEPSC amplitude obtained from unlabeled MSNs in SNAP25 $\Delta$ 3 mutant mice (blue circles) and WT littermate control mice (open circles) in 600 nM BAC. (F) PPR summary and averages pre-BAC (grey area) and post-BAC (blue area). (G) eEPSC amplitude obtained from unlabeled MSNs in SNAP25 $\Delta$ 3 mutant mice (blue circles) and WT littermate control mice (open circles) in 200 nM BAC. (H) PPR time-course summary and averages pre-BAC (grey area) and post-BAC (blue area).

*GAT-1-regulated ambient GABA acts on GABA<sub>B</sub>R to decrease glutamatergic transmission in the NAc core*

GABA<sub>B</sub>R expressed on glutamate terminals may serve as a heteroreceptor for GABA released from contiguous GABAergic synapses in the NAc. To assess whether circuit-wide elevations in ambient GABA modulate glutamatergic synapses in the NAc core, we bath-applied tiagabine (20 μM), a blocker of GABA reuptake transporter type-1 (GAT-1), the CNS expression of which is high in the striatum relative to other subcortical regions (Augood et al., 1995; Kirmse et al., 2008). Tiagabine resulted in a significant decrease in eEPSC amplitude at D1(+) and D1(-) MSNs (**Fig. 3.8A-C,F**, D1(+): 62.00±3.61%, n=5, p=0.0143; D1(-): 63.67±5.13%, n=6, p=0.00244). To determine if this effect was due to GABA<sub>B</sub>R heteroreceptor function, we incorporated SCH 50911 into the superfusate prior to the application of tiagabine. SCH 50911 significantly decreased the tiagabine-induced decrease in eEPSC amplitude in both MSN subtypes (**Fig. 3.8.D,F**, D1(+) SCH: 88.93±10.16%, n=9, 1-way RM ANOVA, tiagabine effect:  $F_{3,19} = 13.03$ , p=0.0009; Sidak's post-hoc analysis, ACSF vs. SCH: p=0.0256; D1(-) SCH: 88.57±5.60%, n=10, 1-way RM ANOVA, tiagabine effect:  $F_{3,20} = 18.66$ , p<0.0001; Sidak's post-hoc analysis, ACSF vs. SCH: p=0.0134). If neuronal GAT-1 blockade promotes heterosynaptic crosstalk between GABA- and glutamatergic synapses via GABA<sub>B</sub>R, then CGP 7930, a potent, well-characterized GABA<sub>B</sub>R positive allosteric modulator (PAM) (Adams and Lawrence, 2007), should enhance the tiagabine-induced decrease in eEPSC amplitude. Indeed, prior application of CGP 7930 (30 μM) enhanced the tiagabine-induced decrease in eEPSC amplitude at D1(+) and D1(-) MSN synapses (**Fig. 3.8.E,F**, D1(+) CGP: 42.81±3.51%, n=5, 1-way RM ANOVA; Sidak's post-hoc analysis, ACSF vs. CGP: p=0.0486; D1(-) CGP: 44.77±4.26%, n=7; Sidak's post-hoc analysis, ACSF vs. CGP: p=0.0144).

CGP 7930 alone had no effect on basal eEPSC amplitude at either MSN subtype (data not shown), consistent with a lack of effect of SCH 50911 alone on basal eEPSC amplitude. These findings suggest that elevations in GAT-1-regulated GABA levels in the NAc core modulate glutamatergic transmission onto D1(+) and D1(-) MSNs via GABA<sub>B</sub>R.

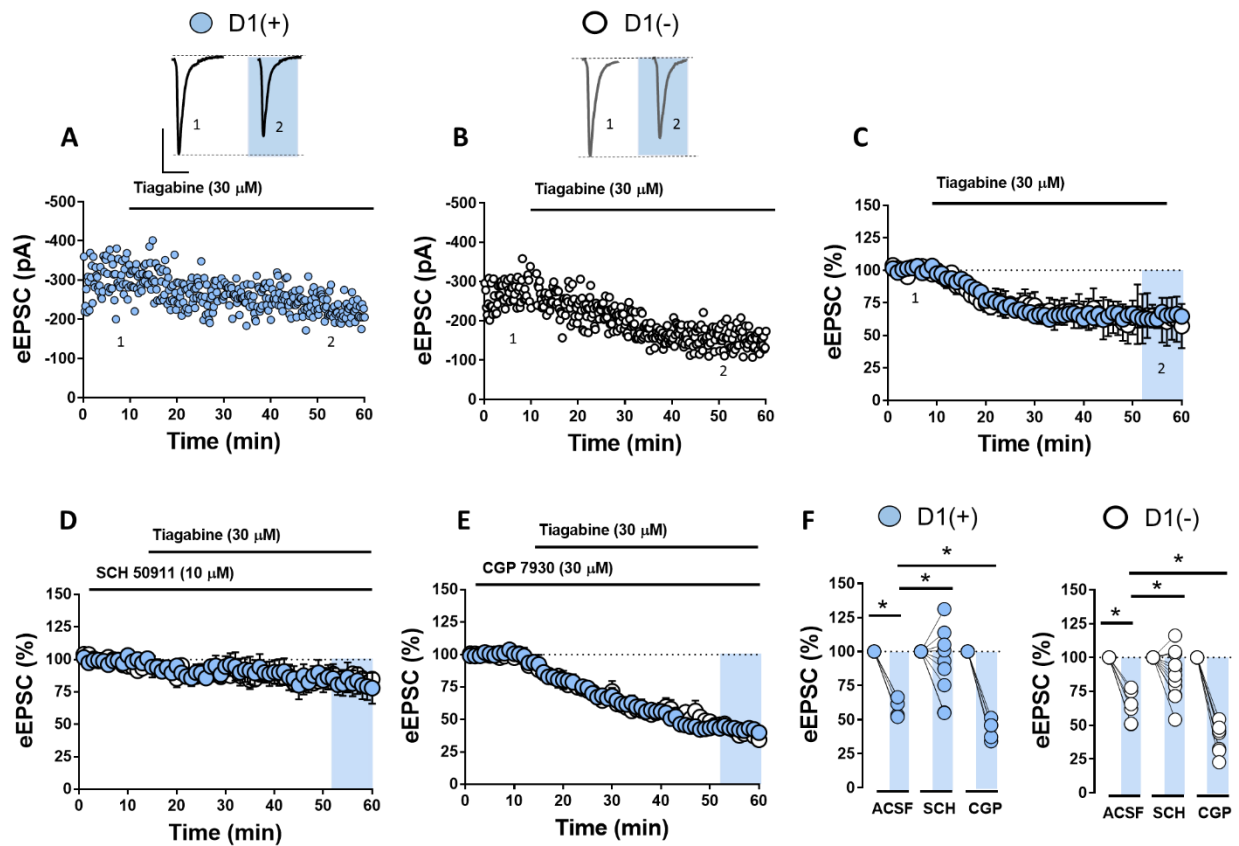


**Figure 3.8. GAT-1-regulated ambient GABA acts on GABA<sub>B</sub>R to decrease glutamatergic transmission in the NAc core.** (A, B) Representative experiment and traces of eEPSCs obtained from D1(+) MSNs (blue circles) and D1(-) MSNs (open circles) in the NAc core. Scale bar: 200 pA/50 ms. (C) Time-course of normalized eEPSC amplitude from D1(+) and D1(-) MSNs in the presence of GABA reuptake (GAT-1) inhibitor, tiagabine (30 μM). (D) Time-course of normalized eEPSC amplitude from D1(+) and D1(-) MSNs in the presence of tiagabine + SCH 50911 (5 μM). (E) Time-course of normalized eEPSC amplitude from D1(+) and D1(-) MSNs in the presence of tiagabine (30 μM) and GABA<sub>B</sub>R positive allosteric modulator (PAM), CGP 7930 (30 μM). (F) Quantification of average eEPSC amplitude of tiagabine in normal ACSF, CGP 7930 and SCH 50911 at D1(+) MSNs and D1(-) MSNs. Error bars indicate SEM. \* p < 0.05.

*Parvalbumin-expressing interneurons preferentially decrease glutamatergic transmission onto D1(+) MSNs via heterosynaptic GABA<sub>B</sub>R signaling*

While various sources of GABA exist in the NAc, we hypothesized that fast-spiking interneurons, the majority of which express the Ca<sup>2+</sup>-binding protein parvalbumin, contribute to elevations in extrasynaptic GABA concentration as a consequence of their fast-spiking activity. PV-INs in the NAc coordinate MSN spiking activity through feedforward inhibition, wherein glutamatergic synapses onto MSNs collateralize onto nearby PV-INs, which exert robust GABAergic control over MSN output (Wright et al., 2017; Yu et al., 2017; Scudder et al., 2018). In comparison to MSNs and other GABAergic interneuron subtypes in the NAc, PV-INs receive stronger and more extensive excitatory input from afferents that drive MSN activity, providing them with greater temporal authority over information propagated through the NAc (Yu et al., 2017; Scudder et al., 2018). Furthermore, the lack of tonic GABA<sub>B</sub>R activity at glutamatergic synapses suggests a neuronal source of GABA driven by acute shifts in circuit activity. To determine if PV-INs exert heterosynaptic control over glutamatergic synapses onto D1(+) and D1(-) MSNs, we bred PV-Cre mice, in which Cre recombinase expression is driven by the PV promoter, with Ai32 conditional ChR2 (cChR2) and D1tdTomato BAC transgenic mouse lines, generating PV<sup>Cre</sup>-cChR2-D1tdTomato mice (abbreviated PV<sup>Cre</sup>) (**Fig. 3.9A**). This breeding strategy confers optogenetic control over PV-expressing cells in the NAc, which are GABAergic PV-INs. Indeed, optically-evoked inhibitory postsynaptic currents (oIPSCs) recorded from D1(+) and D1(-) MSNs were abolished by picrotoxin (PTX, 50 μM), indicating that PV-IN-to-MSN transmission in the NAc core is mediated by GABA<sub>A</sub>R (**Fig. 3.9B**, D1(+) PTX: 4.5±3.11%, n=5, p=0.8851; D1(-) 5.96±2.07%, n=6, p=0.6500).

To determine if PV-IN activity modulates glutamatergic transmission onto D1(+) and D1(-) MSNs, we prepared acute brain slices from PV<sup>Cre</sup> mice and recorded eEPSCs from D1(+) and D1(-) MSNs in PTX-containing ACSF. PV-INs were stimulated optically at 30 Hz to resemble a PV-IN-directed, low-range gamma frequency stimulation (LFS<sup>PV</sup>) pattern. Prior to using this induction protocol, we first wanted to confirm that optical excitation of PV-INs at 30 Hz yielded high-fidelity oIPSCs in MSNs. Indeed, LFS<sup>PV</sup> resulted in oIPSCs in MSNs throughout the induction period, indicating that ChR2(H134R) is a suitable opsin for these experiments (**Fig. 3.9B**). Following a stable 10-min eEPSC baseline, LFS<sup>PV</sup> was delivered for 5-min, after which eEPSCs were recorded up to 30-min post-LFS. LFS<sup>PV</sup> resulted in a significant decrease in eEPSC amplitude at D1(+) but not D1(-) MSNs that was accompanied by an increase in CV, consistent with a presynaptic locus of action (**Fig. 3.9C-F**, D1(+): 79.71±5.12%, n=5, p=0.0481; D1(-): 102.86±5.26%, n=5, p=0.5762; CV = D1(+) baseline: 0.05±0.01, D1(+) post-LFS<sup>PV</sup>: 0.072±0.015, n=5, p=0.0352; D1(-) baseline: 0.05±0.01, D1(-) post-LFS<sup>PV</sup>: 0.04±0.004, n=5, p=0.3665). The effect of LFS<sup>PV</sup> on eEPSC amplitude was significantly different between D1(+) and D1(-) MSNs (2-way RM ANOVA, LFS<sup>PV</sup>-MSN subtype interaction:  $F_{1,4} = 14.48$ , p=0.0170). To determine if this plasticity was mediated by GABA<sub>B</sub>R, SCH 50911 was incorporated into the ACSF bath prior to the induction protocol. SCH 50911 completely abolished the LFS<sup>PV</sup>-induced depression of eEPSC amplitude at D1(+) MSN synapses (**Fig. 3.9G-I**, D1(+) SCH: 91.46±7.63%, n=6, p=0.2751). Furthermore, prior application of CGP 7930 enhanced the LFS<sup>PV</sup>-induced depression at D1(+) MSNs and unmasked a significant depression in D1(-) MSNs that was accompanied by an increase in CV (**Fig. 3.9G-L**, D1(+) CGP: 48.14±8.56%, n=6, 1-way RM ANOVA, Sidak's post-hoc analysis ACSF vs. CGP: p=0.0043; D1(-) CGP: 73±10.03%, n=6, p=0.0325; CV = D1(+) baseline:

0.048±0.008, D1(+) post-LFS<sup>PV</sup> CGP: 0.226±0.053, n=5, p=0.0069; D1(-) baseline: 0.048±0.11, D1(-) post-LFS<sup>PV</sup> CGP: 0.18±0.067, n=7, p=0.0475). These data indicate that PV-INs can heterosynaptically regulate glutamatergic transmission onto D1(+) MSNs and, less so, D1(-) MSNs by targeting presynaptically-expressed GABA<sub>B</sub>R, identifying a novel arm within feedforward inhibitory microcircuits in the NAc core.

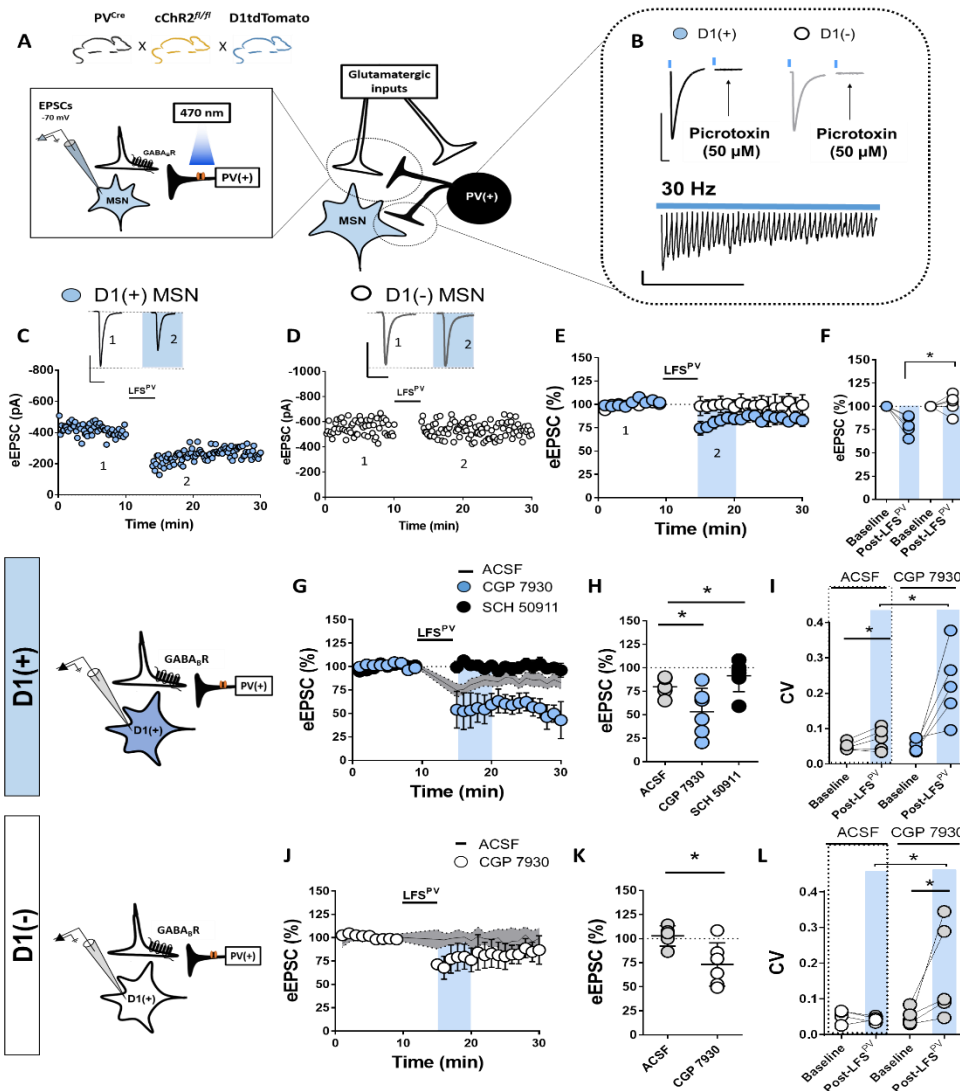


**Figure 3.9. Parvalbumin (PV)-expressing interneurons preferentially decrease glutamatergic transmission onto D1(+) MSNs via heterosynaptic GABA<sub>B</sub> signaling.** (A)

Left: model depicting breeding scheme of triple transgenic mouse line. Right: synaptic model of heterosynaptic electrophysiological configuration. (B) Top: Representative traces of picrotoxin (PTX, 50  $\mu$ M)-sensitive oIPSCs recorded in D1(+) and D1(-) MSNs. Scale bar: 300 pA/50 ms. Bottom: High-fidelity train of oIPSCs delivered at 30 Hz recorded in MSNs. Scale bar: 30 pA/0.5-sec (C, D) Representative experiments and traces of eEPSCs obtained from D1(+) (blue circles) and D1(-) MSNs (open circles) pre- and post-LFSPV (in PTX). LFS denotes optically-evoked stimulation at 30 Hz for 5-min. Scale bar: 200 pA/50 ms. (E) Time-course of normalized eEPSCs obtained from D1(+) and D1(-) MSNs pre- and post-LFSPV. (F) Graph of average eEPSC amplitude post-LFS (G, H) Time-course summary and graph of normalized eEPSCs obtained from D1(+) MSNs in normal ACSF (line), SCH 50911 (black dots), and CGP 7930 (blue). (I) Graph depicting CV post-LFSPV in normal ACSF and CGP 7930 (J, K) Time-course summary and graph of normalized eEPSCs obtained from D1(+) MSNs in normal ACSF (line) and CGP 7930 (open circles). (L) Graph depicting CV post-LFSPV in normal ACSF and CGP 7930.

PV-IN-to-MSN synapses in the striatum maintain synaptic efficacy across a broad dynamic range of firing frequencies (Gittis et al., 2010). We hypothesized that this property may permit heterosynaptic crosstalk between PV-INs and glutamate terminals without altering GABAergic transmission at PV-IN-to-MSN synapses. To address this, we recorded oIPSCs elicited from PV-INs in D1(+) and D1(-) MSNs (**Fig. 3.10A**). We first tested if GABA<sub>B</sub>R autoregulates PV-IN-to-D1(+) and D1(-) MSN synapses. Interestingly, only a subset of PV-IN-to-MSN synapses were responsive to BAC [BAC(+)], with BAC(+) synapses exhibiting a significant decrease in oIPSC amplitude at both MSN subtypes and BAC(-) synapses exhibiting no change in oIPSC amplitude. Subsequent application of SCH 50911 incompletely reversed oIPSC amplitude to baseline at BAC(+) synapses, indicating the presence of inhibitory long-term depression (iLTD) at a subset of synapses (**Fig. 3.10B-E**, *BAC(+) cells* = D1(+) BAC: 41.73±6.03%, D1(+) SCH: 58.76±3.49%, n=4, 1-way RM ANOVA, drug effect:  $F_{2,10} = 70.94$ ,  $p < 0.0001$ , Sidak's post hoc analysis, baseline vs. BAC:  $p < 0.001$ , vs. SCH:  $p < 0.001$ ; D1(-) BAC: 38.96±6.17%, D1(-) SCH: 63.09±5.37%, n=4, 1-way RM ANOVA, drug effect:  $F_{2,10} = 93.97$ ,  $p < 0.0001$ , Sidak's post hoc analysis, baseline vs. BAC:  $p < 0.001$ , vs. SCH:  $p < 0.001$ ; *BAC(-) cells* = D1(+): 98.42±2.76%, n=3 of 11 cells,  $p = 0.1169$ ; D1(-): 99.36±2.86%, n=3 of 9 cells,  $p = 0.2690$ ). We next asked if GABA<sub>B</sub>R activity tonically inhibits PV-IN-to-D1(+) and D1(-) MSN synapses via presynaptic autoreceptor function. SCH 50911 added to the ACSF following a 10-min oIPSC baseline did not significantly alter oIPSC amplitude at D1(+) or D1(-) MSN synapses (**Fig. 3.10.F,G**, D1(+): 100.05±7.64%, n=4,  $p = 0.9981$ ; D1(-) 101.56±4.23%, n=5,  $p = 0.6900$ ). Given these findings, we predicted that LFS<sup>PV</sup> would not elicit a GABA<sub>B</sub>R-dependent change in synaptic strength at PV-IN-to-MSN synapses. Indeed,

GABAergic transmission at PV-IN-to-MSN (pooled) synapses remained completely unchanged 40-min post-LFS<sup>PV</sup> (**Fig. 3.10.H,I**, MSNs (pooled):  $103.56 \pm 7.62\%$ ,  $n=4$ ,  $p=0.3138$ ). Together, these data suggest that PV-INs are well-suited to functionally regulate glutamatergic transmission via GABA<sub>B</sub> heteroreceptors on glutamate terminals in the NAc core.

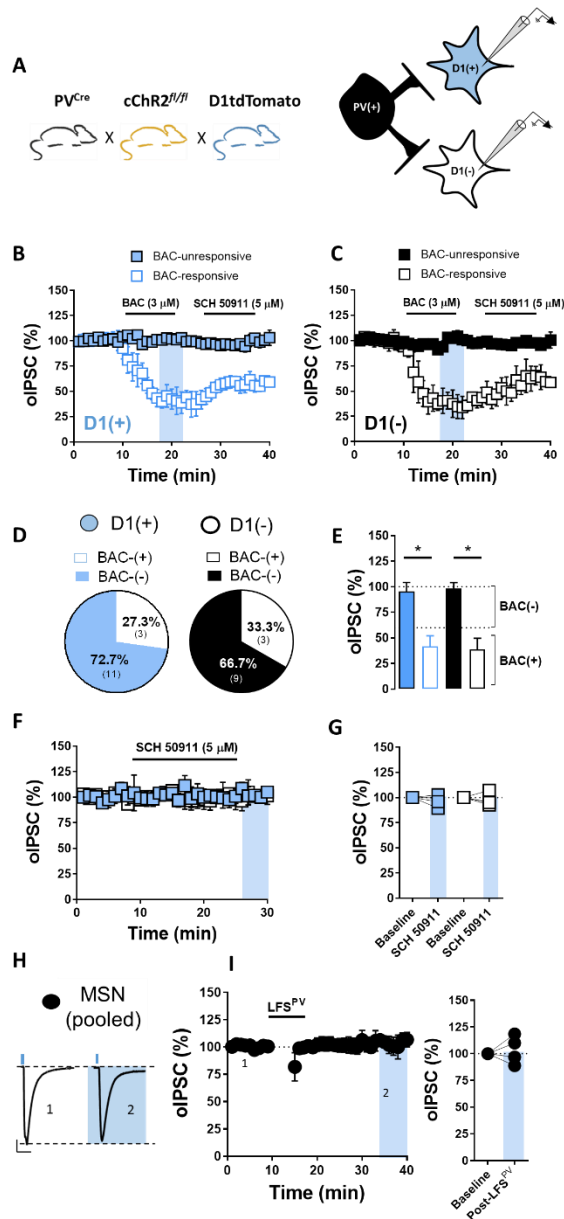


**Figure 3.10. GABAergic transmission at PV-IN-to-D1(+) and D1(-) MSN synapses is largely BAC-insensitive and unchanged by LFS.** (A) Schematic of breeding scheme and electrophysiological configuration (B) Time-course summary at PV-IN-to-D1(+) MSN synapses showing that BAC decreases oIPSC amplitude to elicit inhibitory long-term depression at a minority of synapses. (C) Time-course summary at PV-IN-to-D1(-) MSN synapses showing that BAC decreases oIPSC amplitude. (D) Pie chart representation of BAC+/BAC- synapses onto D1(+) and D1(-) MSNs. (E) Quantification of average oIPSC amplitude depicting separation between BAC(+) and BAC(-) PV-IN-to-MSN synapses. (F, G) Time course summary and average oIPSC amplitude showing that bath application of GABAB antagonist, SCH 50911, alone does not alter oIPSC amplitude at PV-IN-to-D1(+) and D1(-) MSN synapses. (H) Representative traces of oIPSCs pre- and post-LFS at pooled MSN synapses. (I) Time-course summary and quantification of average oIPSC amplitude pre- and post-LFS showing that LFS does not alter oIPSC amplitude at PV-IN-to-MSN (pooled) synapses.

### 3.6 Discussion

We elucidate cell type- and microcircuit-specific mechanisms by which GABA<sub>B</sub>R dynamically regulates glutamatergic synapses in the NAc core. We report that presynaptically-expressed GABA<sub>B</sub>R activation elicits a robust decrease in glutamatergic synaptic transmission onto D1(+) and D1(-) MSNs by engaging a non-canonical signaling mechanism that is distinct from other G<sub>i/o</sub>-coupled GPCRs in the NAc, including CB<sub>1</sub>R and group II mGluRs. Instead, GABA<sub>B</sub>R activity interferes with vesicular exocytosis in a SNAP-25-dependent manner. Furthermore, we show that GABA<sub>B</sub> heteroreceptors at D1(+) MSN synapses are preferentially recruited by PV-INs within feedforward inhibitory microcircuits. Alongside data showing a lack of GABA<sub>B</sub>R tone at glutamatergic synapses, these data offer rigorous support for a new, activity-dependent GABA<sub>B</sub>R-contingent arm within feedforward circuits in the NAc core.

*Presynaptic GABA<sub>B</sub>R recruits a non-canonical, SNAP-25-dependent signaling mechanism to regulate glutamatergic transmission in the NAc core*

We find that GABA<sub>B</sub>R activation elicits a robust decrease in synaptic efficacy at glutamatergic synapses onto D1(+) and D1(-) MSNs. Following pharmacological examination of GABA<sub>B</sub>R function, our findings suggest that GABA<sub>B</sub>R recruits a signaling mechanism that is N- and P/Q-type VGCC, Kir, mGluR, and AC/cAMP-independent, suggesting that GABA<sub>B</sub>R recruits a non-canonical signaling pathway at these synapses. Anomalous GABA<sub>B</sub>R function has been described in regions where the synaptic effects of BAC are insensitive to G<sub>i/o</sub>-GPCR-disabling agents, such as pertussis toxin or NEM (Colmers and Pittman, 1989). We hypothesized that GABA<sub>B</sub>R directly interferes with vesicular release machinery, such as membrane-associated t-SNARE, SNAP-25, to reduce glutamate release probability onto MSNs. SNAP-25 facilitates transmitter exocytosis by

binding  $\text{Ca}^{2+}$ -sensing SNARE protein, synaptotagmin, to establish ternary SNARE complexes that authorize vesicular release (Wells et al., 2012; Zurawski et al., 2019). The C-terminally-located botulinum toxin type-A (BoNT/A) cleavage site of SNAP-25 has previously been shown to mediate the inhibitory actions of  $\text{G}\beta\gamma$  on SNAP-25 (Gerachshenko et al., 2005). Thus, we utilized SNAP25 $\Delta$ 3 transgenic mice partially deficient (~47%) in the SNAP-25- $\text{G}\beta\gamma$  interaction. Consistent with reduced synaptic efficacy of  $\text{GABA}_{\text{B}}\text{R}$ , the actions of BAC were dose-dependently reduced in SNAP25 $\Delta$ 3 mutant mice. While targeted mutations in SNAP-25 will affect other neuromodulatory systems in the NAc, the BAC-induced reduction in mEPSC frequency supports a direct synaptic effect of  $\text{GABA}_{\text{B}}\text{R}$  on glutamatergic transmission. The pronounced increase in PPR induced by BAC was also abolished in SNAP25 $\Delta$ 3 mice, strongly supporting the hypothesis that  $\text{GABA}_{\text{B}}\text{R}$ -induced decrease in glutamate release probability is partially mediated by the SNAP-25- $\text{G}\beta\gamma$  interaction.

Several key findings also support a VGCC-independent interaction with vesicular release machinery. Low  $\text{Ca}^{2+}$  ACSF and pharmacological blockade of N- and P/Q-type VGCCs failed to occlude the effects of BAC on glutamatergic transmission. The non-linear relationship between VGCCs and transmitter release at corticostriatal synapses complicates the interpretation of this finding, as a modest reduction in presynaptic  $\text{Ca}^{2+}$  influx can substantially impact neurotransmitter release (Kupferschmidt and Lovinger, 2015). Therefore, we examined the functional interaction between  $\text{GABA}_{\text{B}}\text{R}$  and VGCC-targeting  $\text{G}_{i/o}$ -coupled GPCRs in the NAc, such as  $\text{CB}_1\text{R}$  and group II mGluRs. Presynaptically-expressed  $\text{CB}_1\text{R}$  and mGluRs trigger short- and long-term plasticity can be attributed in part to their actions on presynaptic  $\text{Ca}^{2+}$  entry via VGCCs. For example, group II mGluRs in the NAc trigger presynaptic LTD by attenuating downstream P/Q-type VGCC

function (Robbe et al., 2002). Similarly, activity-dependent release of eCBs can transiently activate presynaptic CB<sub>1</sub>R<sub>s</sub> on glutamate terminals to elicit VGCC-dependent reductions in neurotransmitter release (Hoffman and Lupica, 2000; Kreitzer and Regehr, 2001). Our data collectively suggest that GABA<sub>B</sub>R recruits different intracellular effectors than either group II mGluRs or CB<sub>1</sub>R, corroborating the hypothesis that GABA<sub>B</sub>R mobilizes Gβγ to interact directly with exocytotic machinery at the presynaptic active zone.

Blocking K<sub>v</sub> channels significantly attenuated and reversed the actions of GABA<sub>B</sub>R, consistent with previous studies showing that Gβγ-SNARE interactions can be overcome by increasing presynaptic Ca<sup>2+</sup> levels (Wells et al., 2012; Lia et al., 2016). Although we cannot definitively rule out GABA<sub>B</sub>R-induced changes in K<sup>+</sup> channel function, the observation that GABA<sub>B</sub>R activity returns to normal in 4-AP-containing low-Ca<sup>2+</sup> ACSF, is resistant to extracellular Ba<sup>2+</sup> application, and produces no detectable change in PPR following 4-AP treatment points to a 4-AP-induced enhancement in presynaptic Ca<sup>2+</sup> conductance. While it is possible that GABA<sub>B</sub>R initiates functionally redundant mechanisms to reduce glutamate release, this hypothesis is less likely given that the effects of BAC on eEPSC amplitude remained intact following each pharmacological manipulation. Taken together, we propose a novel mechanism by which GABA<sub>B</sub>R in the NAc core reduces presynaptic glutamate release probability downstream of VGCCs by interfering with the assembly of core SNARE complexes in a SNAP-25-dependent manner.

#### *PV-INs heterosynaptically regulate glutamatergic transmission via GABA<sub>B</sub>R*

While heterosynaptic regulation of GABAergic synapses by glutamate has been characterized in the striatum, the reverse relationship in which GABA regulates glutamatergic transmission has not

been demonstrated (Mathur et al., 2013; Patton et al., 2019). We report that optogenetic stimulation of PV(+) cells reduces glutamatergic transmission onto D1(+) and, less so, D1(-) MSNs in a GABA<sub>B</sub>R-dependent manner, offering physiological context for GABA<sub>B</sub> heteroreceptor function within the NAc. This finding is striking for several reasons. First, striatal PV-INs form monosynaptic connections with MSNs at somatic and proximal dendritic domains, whereas glutamatergic afferents target distal dendrites (Hu et al., 2014; Tepper and Koós, 2017; Yu et al., 2017). The privileged anatomical positioning of PV-IN-to-MSN synapses confers optimal GABAergic control over MSN spiking activity, supporting the role of PV-INs in feedforward inhibition. Second, PV-INs, unlike somatostatin-expressing interneurons (SST-INs), lack autonomous action potential (AP) firing that could contribute to tonic GABA<sub>B</sub> heteroreceptor function (Smith et al., 2017; Tepper and Koós, 2017; Trouche et al., 2019). However, PV-INs receive significantly greater excitatory innervation than SOM-INs and sustain afferent-evoked firing rates of up to 250 Hz, indicating that acute shifts in circuit activity are likely to recruit PV-INs over other GABAergic cell types in the NAc (Tepper and Koós, 2017; Scudder et al., 2018; Tepper et al., 2018; Trouche et al., 2019). SST-INs also exhibit biophysical limitations that prevent them from responding to time-locked changes in glutamatergic transmission, including a lower AP frequency, prolonged latency to spike, and accommodating AP firing pattern (Scudder et al., 2018; Tepper et al., 2018). While tonic GABA<sub>A</sub>R and GABA<sub>B</sub>R activity is observed at heterosynaptic loci on DA terminals in the dorsal striatum, NAc DA release is comparatively unaffected by GABA<sub>B</sub>R blockade (Tritsch et al., 2014; Melchior et al., 2015; Lopes et al., 2019). Similarly, we do not detect GABA<sub>B</sub>R tone at glutamatergic synapses onto D1(+) or D1(-) MSNs, supporting a distinct role for GABAergic neurons requiring afferent excitatory input to fire. Therefore, PV-INs

may be better equipped than other GABAergic cell types in the NAc to modulate activity-dependent increases in glutamatergic activity.

PV-INs entrain principal neuron output via gamma frequency oscillations (25-100 Hz) that are sustained by the coordinated recruitment of electrically-connected PV-INs (Hu et al., 2014). We elected to activate PV-INs at 30 Hz (LFS<sup>PV</sup>) to resemble a physiologically relevant gamma frequency stimulation pattern that can be achieved with the transgenically-encoded opsin, ChR2(H134R). Our data suggests that LFS<sup>PV</sup> for 5-min is sufficient to heterosynaptically target GABA<sub>B</sub>R at glutamatergic synapses onto D1(+) MSNs. Interestingly, we find that LFS<sup>PV</sup> targets GABA<sub>B</sub>R at synapses onto D1(-) MSNs only in the presence of a GABA<sub>B</sub>R PAM, suggesting that LFS<sup>PV</sup> may be subthreshold to elicit changes in glutamatergic transmission at synapses onto D1(-) MSNs. One possibility is that PV-IN-to-D1(+) and D1(-) MSN synapses are differentially regulated by GABA<sub>B</sub>R, with synapses onto D1(-) MSNs exhibiting greater GABA<sub>B</sub>R-dependent autoinhibitory feedback than synapses onto D1(+) MSNs. Differences in autoreceptor function at these synapses would limit the efficacy with which prolonged PV-IN stimulation elevates extracellular GABA levels. However, the majority of PV-IN-to-D1(+) and D1(-) MSN synapses were BAC-insensitive and LFS<sup>PV</sup> of oIPSCs failed to elicit homosynaptic plasticity at PV-IN-to-MSN synapses. Having ruled out intrinsic mechanisms at PV-IN-to-MSN synapses, the most probable explanation is a synapse-specific difference in GABA sensitivity. This hypothesis is strongly supported by the BAC dose-response relationship in which glutamatergic synapses onto D1(+) MSNs exhibited increased sensitivity to BAC at lower concentrations (200-600 nM) relative to D1(-) MSNs. Another intriguing possibility is whether differences in GABA reuptake kinetics between D1(+) and D1(-) synapses create synapse-specific microdomains that modulate

glutamatergic inputs onto distinct cell types in the NAc. Future studies will be needed to elucidate fully the intricate mechanisms by which PV-INs sculpt cell type-specific circuit output in the NAc core.

### *Concluding remarks*

The NAc coordinates motivated behaviors by integrating PV-IN-directed inhibitory networks with glutamatergic inputs from various salience-encoding brain regions. While GABA<sub>B</sub>R function is well characterized at upstream loci within the mesolimbic reward network, a comprehensive analysis of GABA<sub>B</sub> heteroreceptor function in the NAc is lacking. Here, we revise and expand knowledge on the role of GABA<sub>B</sub>R function within PV-IN-embedded feedforward microcircuits in the NAc core. Our findings rigorously support a novel mechanism by which GABA<sub>B</sub>R modulates glutamatergic transmission and define an activity-dependent source of GABA within PV-IN-embedded feedforward circuits. Understanding the role of GABA<sub>B</sub>R within NAc microcircuits paints a more complete picture of how GABA<sub>B</sub>R-specific pharmacological agents can be used to treat neuropsychiatric disorders characterized by aberrant motivational states, including addiction, major depressive disorder, and autism (Cousins et al., 2002; Kahn et al., 2009; Jacobson et al., 2018; Stoppel et al., 2018; Pisansky et al., 2019).

## CHAPTER 4

### **Calcium-permeable AMPA receptors trigger endocannabinoid signaling at parvalbumin interneuron synapses in the nucleus accumbens core**

Authors: Kevin M. Manz<sup>1,2,3</sup>, Dipanwita G. Ghose, Brandon D. Turner, Anne Taylor, Jennifer  
Becker, Carrie A. Grueter, and Brad A. Grueter<sup>†3,4,5,6</sup>

<sup>1</sup>Medical Scientist Training Program, Vanderbilt University, Nashville, TN 37232.

<sup>2</sup>Neuroscience Graduate Program, Vanderbilt University, Nashville, TN 37232.

<sup>3</sup>Vanderbilt Brain Institute, Vanderbilt University, Nashville, TN 37232.

<sup>4</sup>Department of Anesthesiology, Vanderbilt University Medical Center, Nashville, TN 37232.

<sup>5</sup>Vanderbilt Center for Addiction Research, Vanderbilt University, Nashville, TN 37232

<sup>6</sup>Department of Molecular Physiology and Biophysics, Vanderbilt University, Nashville, TN  
37232.

**†Correspondence to:**

Brad A. Grueter, Ph.D.

Department of Anesthesiology,

2213 Garland Avenue, P435H MRB IV

Vanderbilt University Medical Center

Nashville, TN 37232-0413

Tel. 615-936-2586

E-Mail: [brad.grueter@vanderbilt.edu](mailto:brad.grueter@vanderbilt.edu)

## 4.1 Abstract

Feedforward inhibitory microcircuits in the nucleus accumbens (NAc) facilitate reward-related motivational behavior by regulating time-contingent shifts in medium spiny neuron (MSN) activity. Feedforward inhibition in the NAc is initiated when glutamatergic afferents onto MSNs collateralize onto fast-spiking parvalbumin (PV)-expressing interneurons (PV-INs), which exert GABAergic control over MSN spiking activity. Here, we find that glutamatergic synapses onto PV-INs in the NAc core selectively express  $\text{Ca}^{2+}$  permeable AMPA receptors (CP-AMPA receptors).  $\text{Ca}^{2+}$  influx through CP-AMPA receptors on PV-INs triggers long-term depression (LTD) via endocannabinoid (eCB) signaling at presynaptic  $\text{CB}_1$  receptors ( $\text{CB}_1\text{R}$ ). Moreover, CP-AMPA receptors authorize tonic eCB signaling to negatively regulate glutamate release probability. This plasticity is abolished following acute *in vivo* and *ex vivo* cocaine exposure by competitively engaging  $\text{CB}_1\text{R}$  function, pointing to a novel substrate of cocaine action in the NAc. These findings elucidate mechanisms by which PV-IN-embedded feedforward microcircuits in the NAc undergo activity- and experience-dependent shifts in synaptic strength.

## 4.2 Introduction

The nucleus accumbens (NAc) contains a complex circuit architecture that orchestrates reward-related motivational output (Turner et al., 2018a). Microcircuit dynamics, such as feedforward inhibition, gate synaptic and cellular processes that coordinate goal-directed behavior (Winters et al., 2012; Burke et al., 2017). Feedforward inhibition in the NAc is mediated by GABAergic fast-spiking parvalbumin (PV)-expressing interneurons (PV-IN), output from which exerts robust inhibitory control over D1- and D2 dopamine (DA) receptor-expressing medium spiny projection neurons (MSNs) (Wright et al., 2017; Scudder et al., 2018). PV-IN-mediated feedforward

inhibition, whereby NAc-projecting glutamatergic inputs from cortical and limbic structures collateralize onto PV-INs, synchronizes and entrains D1 and D2 MSN output. While GABAergic transmission at PV-IN-to-MSN synapses is a recognized regulatory element within striatal microcircuits, mechanisms regulating feedforward glutamatergic transmission *onto* PV-INs in the NAc remain unexplored.

PV-INs in the NAc display hodological similarities to D1 and D2 MSNs, receiving glutamatergic afferents primarily from the ventral hippocampus, prefrontal cortex, mediodorsal thalamus, and basolateral amygdala (BLA) (Yu et al., 2017). An important distinction between PV-IN and MSN synapses is the selective expression of GluA2-lacking Ca<sup>2+</sup>-permeable AMPA receptors (CP-AMPARs) on PV-INs at baseline (Hu et al., 2014; Yu et al., 2017). CP-AMPARs exhibit greater single-channel conductance, faster deactivation kinetics, and an inwardly rectifying biophysical profile (Liu and Cull-Candy, 2000; Nissen et al., 2010). The fast-spiking, **electronic**, and synaptic properties of PV-INs allows these cells to rapidly transduce shifts in corticolimbic circuit activity into a GABAergic signal regulating MSN output (O'Hare et al., 2017; Tepper et al., 2018). Similar to CP-AMPAR-expressing synapses elsewhere, synaptic plasticity at feedforward synapses onto PV-INs may have broad regulatory consequences on NAc circuit function (Soler-Llavina and Sabatini, 2006). Congruent with this hypothesis, a recent study suggests that potentiating glutamatergic transmission at BLA synapses onto PV-INs expedites the acquisition of cocaine self-administration (Yu et al., 2017). In contrast, synaptic and membrane properties at GABAergic PV-IN-to-MSN synapses following cocaine withdrawal remained largely unchanged, supporting the notion that a modulatory locus within feedforward microcircuits in the NAc is excitatory drive onto PV-INs (Winters et al., 2012).

In the present study, we employed whole-cell patch-clamp electrophysiology in cell type-specific reporter mice to interrogate synaptic plasticity mechanisms at glutamatergic synapses onto PV-INs in the NAc core. Adapting a low-frequency stimulation (LFS) protocol used to elicit long-term depression (LTD) at synapses onto D2 MSNs, we find that LFS triggers LTD of glutamatergic transmission onto PV(+)-INs via CP-AMPARs expressed uniquely at this synapse. LFS-induced LTD mediated by increased intracellular  $Ca^{2+}$  via CP-AMPARs evokes endocannabinoid (eCB) signaling at presynaptic cannabinoid type-1 receptors (CB<sub>1</sub>R). In addition, CP-AMPARs gate tonic CB<sub>1</sub>R signaling by regulating the production of anandamide (AEA). Finally, LTD at PV(+)-IN synapses is a substrate of acute cocaine exposure, as *in vivo* and *ex vivo* cocaine exposure abolishes this plasticity by engaging presynaptic CB<sub>1</sub>R function. These findings elucidate a previously unknown mechanism regulating synaptic strength within PV-IN-embedded feedforward microcircuits, a physiological process subserved by CP-AMPARs on PV-INs, and a novel synaptic target of acute cocaine experience in the NAc core.

#### 4.3 Materials and methods

##### *Animals*

Animals were bred and housed at Vanderbilt University Medical Center in accordance with IACUC. Male mice 8-16 weeks of age were used for all electrophysiological and *in vivo* experiments. Mice were housed according to sex in groups of 3-5/cage on a 12-hr light-dark cycle with *ad lib* access to standard food and water. Breeding cages were given 5LOD chow (PicoLab®, 28.7% protein, 13.4 % fat, 57.9 % carbohydrate) to improve litter viability. For all electrophysiological experiments examining PV(+)-INs, Cre-induced STOP<sup>fl/fl</sup>-tdTomato mice

(Ai9, *Gt(ROSA)26Sor<sup>tm9(CAG-tdTomato)Hze</sup>*) obtained from Jackson Laboratory (Stock No.: 007909) were crossed with PV-IRES-Cre (*PV<sup>Cre</sup>, Pvalb<sup>tm1(cre)Arbr/J</sup>*, Stock No.: 008069), generating PV<sup>Cre</sup>-tdTomato<sup>fl/fl</sup> (PV<sup>tdT</sup>) mice. For all experiments examining D1 and D2 MSN physiology, C57BL/6J mice were bred to harbor a bacterial artificial chromosome (BAC) carrying the tdTomato fluorophore under control of the *Drd1a* (D1 receptor) promoter. In a subset of experiments, PV<sup>tdT</sup> mice received an injection of saline or cocaine HCl (15 mg/kg) administered intraperitoneal (IP) in a novel environment.

### *Electrophysiology*

Whole-cell patch-clamp electrophysiological recordings were obtained in acute brain slice preparations from PV<sup>tdT</sup> and D1tdTomato BAC transgenic mice. Mice were euthanized under isoflurane anesthesia after which parasagittal slices (250  $\mu$ M) containing the NAc core were prepared from whole brain tissue using a Leica Vibratome in oxygenated (95% O<sub>2</sub>; 5% CO<sub>2</sub>) ice-cold *N*-methyl-*D*-glucamine (NMDG)-based solution (in mM: 2.5 KCl, 20 HEPES, 1.2 NaH<sub>2</sub>PO<sub>4</sub>, 25 Glucose, 93 NMDG, 30 NaHCO<sub>3</sub>, 5.0 sodium ascorbate, 3.0 sodium pyruvate, 10 MgCl<sub>2</sub>, and 0.5 CaCl<sub>2</sub>·2H<sub>2</sub>O). Slices were then recovered in NMDG-based recovery solution for 10-15-min at 30-32 °C before being transferred to a chamber containing artificial cerebral spinal fluid (ACSF, in mM: 119 NaCl, 2.5 KCl, 1.3 MgCl<sub>2</sub>·6H<sub>2</sub>O, 2.5 CaCl<sub>2</sub>·2H<sub>2</sub>O, 1.0 NaH<sub>2</sub>PO<sub>4</sub>·H<sub>2</sub>O, 26.2 NaHCO<sub>3</sub>, and 11 glucose; 287-295 mOsm). All experiments were performed using a Scientifica Slicescope Pro System with continuously-perfused 28-32 °C ACSF at 2 mL/min. PV-INs or MSNs in the NAc core were visualized using Scientifica PatchVision software and patched with 3–6 M $\Omega$  recording pipettes (P1000 Micropipette Puller). For current-clamp recordings, experiments were performed in K<sup>+</sup>-based intracellular solution: (in mM: 135 K<sup>+</sup>-gluconate, 5 NaCl, 2 MgCl<sub>2</sub>, 10 HEPES, 0.6

EGTA, 3 Na<sub>2</sub>ATP, 0.4 Na<sub>2</sub>GTP; 290 mOsm). For voltage-clamp recordings, a Cs<sup>+</sup>-based intracellular solution was used (in mM: 120 CsMeSO<sub>3</sub>, 15 CsCl, 8 NaCl, 10 HEPES, 0.2 EGTA, 10 TEA-Cl, 4.0 Mg-ATP, 0.3 Na-GTP, 0.1 spermine, and 5.0 QX 314 bromide). In PV<sup>tdT</sup> or D1tdTomato mice, PV(+)-INs and D1(+) and D1(-) (putative D2) MSNs were differentiated according to the expression of the red tdTomato fluorophore via 530 nm LED light. D1(-) MSNs were distinguished from interneuron cell types based on morphological (size, shape) and biophysical properties (e.g., capacitance, membrane resistance, and AMPAR decay kinetics).

For *voltage-clamp* recordings, electrically-evoked excitatory postsynaptic currents (eEPSCs) were obtained at a command voltage of -70 mV and isolated by incorporating GABA<sub>A</sub>R antagonist, picrotoxin (PTX, 50 μM), into the ACSF bath. To obtain the current-voltage (I-V) function of AMPAR-mediated EPSCs, AMPAR-mediated EPSCs were isolated by also including NMDAR antagonist, APV (50 μM), into the ACSF bath, though NMDAR-mediated EPSCs contribute minimally to EPSC amplitude at -70 mV. EPSC decay kinetics were obtained from  $t_{1/2}$  obtained time, T, following peak EPSC amplitude. In experiments examining local glutamatergic transmission, a bipolar electrode was placed at the corticoaccumbens interface and stimulated at 0.1 Hz. Paired pulse ratios (PPR) were obtained within-experiment by delivering two 0.3-ms duration pulses with a 50-ms interstimulus interval and calculating the amplitude ratio of the second eEPSC to the first eEPSC ( $eEPSC_2/eEPSC_1$ ) at the indicated time-point. sEPSC analysis was performed with Clampfit 10.4 using a stringent best-fit template obtained from preliminary 10-min recording bouts in D1(+) and D1(-) MSNs. Each recording bout yielded a rise/day time ( $\leq 3$ -ms) and amplitude ( $\geq 5$  pA) selection criteria that was reflected in the overall template score. For *current-clamp* recordings, cells were permitted 5-min after entering whole-cell configuration to equilibrate to the

intracellular dialysate, after which a depolarizing plateau potential was established to maintain cells at approximately -70 mV. To assess intrinsic membrane excitability, action potentials (APs) were elicited in PV(+)-INs or MSNs following 50 pA current steps increasing from -400 to 400 pA with an 800-ms step duration. Membrane resistance and series resistance ( $R_s$ ) were monitored continuously during all experiments, with >20% change in  $R_s$  resulting in the omission of that experiment.

### *Pharmacology*

NASPM, (RS)-DHPG, LY341495, URB597, AM251, WIN 55,212-2, NBQX disodium, APV, sulpiride, SCH 23390, and atropine were purchased from Tocris Biosciences. Picrotoxin, cocaine HCl, and pirenzepine were purchased from Sigma Aldrich.

### *Statistics and Data Analysis*

Electrophysiological experiments were analyzed using Clampfit 10.4 and GraphPad Prism v7.0. Changes in baseline EPSC amplitude, coefficient of variance (CV), and PPR were calculated by comparing mean values during 5 min intervals specified in each time-course to baseline PPR and CV values. A depression was defined as a significant difference in eEPSC amplitude from baseline calculated during the time interval specified in the recording. After obtaining each data set, Shapiro-Wilk tests were performed to assess normality. Data depicted in Figures were determined to be normally distributed. Thus, paired or unpaired *t*-tests were used to analyze statistical differences between data sets. Sidak's post-hoc analyses were used for analyses requiring multiple comparisons. Power analyses were performed with preliminary data during the acquisition of each new data set. The sample size obtained from each power analysis calculation was then compared

to sample sizes reported in the literature for similar experiments. Error bars depicted in figures represent SEM. For all analyses,  $\alpha$  was set as 0.05, with P values  $< \alpha$  indicating a statistically significant difference.

#### 4.4 Results

##### *Calcium-permeable AMPA receptor expression is restricted to PV-expressing interneurons in the NAc core*

Fast-spiking interneurons, the majority of which contain  $\text{Ca}^{2+}$ -binding protein parvalbumin, highly express GluA2-lacking  $\text{Ca}^{2+}$ -permeable AMPA receptors (CP-AMPA) throughout the forebrain (Hu et al., 2014). CP-AMPA receptors exhibit greater single-channel conductance, inward rectification, and sharp activation-deactivation kinetics that confer specialized synaptic properties (Twomey et al., 2017, 2018). To determine if PV-INs in the NAc core are unique from D1 dopamine receptor [(D1(+))- and D2 dopamine receptor [D1(-)]-expressing medium spiny neurons (MSNs) in functional CP-AMPA content, we prepared acute brain slices from  $\text{PV}^{\text{Cre}}\text{-tdTomato(tdT)}^{\text{fl/fl}}$  ( $\text{PV}^{\text{tdT}}$ ) and D1tdTomato transgenic reporter mice (**Fig. 4.1A**). This strategy allows PV(+) and D1(+) cells in the NAc to be visualized *ex vivo*, as described previously (Scudder et al., 2018; Manz et al., 2019). To confirm that tdT(+) cells in  $\text{PV}^{\text{tdT}}$  mice were indeed PV-INs, we first performed current-clamp recordings in tdT(+) cells to assess whether tdT(+) cells exhibited a fast-spiking electrophysiological profile. Depolarizing current injection exceeding action potential (AP) threshold in tdT(+) cells elicited high-frequency AP firing with short-duration waveforms and steep afterhyperpolarizations (AHPs), consistent with fast-spiking PV-INs in the NAc. In contrast, D1(+) and D1(-) MSNs in D1tdTomato mice exhibited a regular-spiking spiking electrophysiological profile, hyperpolarized resting membrane potential ( $V_{\text{RMP}}$ ), and prolonged

AHPs, consistent with MSN properties described previously (**Fig. 4.1B**, AP frequency at I<sub>INJ</sub> 350 pA, PV(+): 157.5±8.7 Hz, n=10; D1(+): 22.8±1.4 Hz, n=12; D1(-): 26.2±3.5 Hz, n=9, 1-way ANOVA, p<0.001).

We next obtained electrically-evoked excitatory postsynaptic currents (EPSCs) in PV(+)-INs of PV<sup>tdT</sup> mice and D1(+) and D1(-) MSNs of male D1tdTomato mice. AMPAR-mediated EPSCs were pharmacologically-isolated by incorporating GABA<sub>A</sub> receptor (GABA<sub>A</sub>R) antagonist, picrotoxin (50 μM), and NMDAR antagonist, APV (50 μM), into the ACSF bath. To assess stoichiometric differences in AMPAR content at glutamatergic synapses onto PV(+)-INs relative to D1(+) and D1(-) MSNs, we examined the current-voltage (I-V) relationship of AMPAR-mediated EPSCs in PV(+)-INs, D1(+) and D1(-) MSNs in the NAc core. The rectification index (RI), calculated as the amplitude ratio of EPSCs obtained at -70 mV relative to +40 mV, was significantly higher in PV(+)-INs than both MSN subtypes, indicating the presence of inwardly-rectifying GluA2-lacking CP-AMPA receptors in PV(+)-INs (**Fig. 4.1C,D**, RI, PV(+): 4.32±0.57, n=7; D1(+): 1.83±0.30, n=6; D1(-): 1.79±0.17, n=6, 1-way ANOVA, p=0.002). Bath-application of CP-AMPA-selective AMPAR antagonist, NASPM (200 μM), also significantly decreased EPSC amplitude in PV(+)-INs without altering EPSC amplitude in D1(+) or D1(-) MSNs (**Fig. 4.1E,F**, NASPM, PV(+): 54.45±6.57%, n=5; D1(+): 98.68±6.74%, n=5; D1(-): 94.04±1.91%, n=5, 1-way ANOVA, p<0.001). Furthermore, AMPAR-mediated EPSCs in PV(+)-INs exhibited significantly faster decay kinetics (t<sub>1/2</sub>) in PV(+)-INs relative to D1(+) and D1(-) MSNs (**Fig. 4.1F-J**, T<sub>1/2</sub>, PV(+): 4.04±0.18 ms, n=15; D1(+): 7.35±0.35 ms, n=10; D1(-): 7.23±0.50, n=11, 1-way ANOVA p<0.001). The t<sub>1/2</sub> of EPSCs in PV(+)-INs was increased in the presence of NASPM but was still less than the t<sub>1/2</sub> of EPSCs in D1(+) and D1(-) MSNs, pointing to potential electrotonic differences

in dendritic charge transfer in PV(+)-INs (**Fig. 4.1J**, NASPM  $T_{1/2}$ , ACSF PV(+):  $4.04 \pm 0.18$  ms,  $n=15$ ; NASPM PV(+):  $5.12 \pm 0.33$ ,  $n=12$ ,  $p=0.004$ ). Other than increased spontaneous EPSC (sEPSC) frequency, we did not observe any other differences in excitatory synaptic properties between PV(+)-INs and MSNs. Together, these data suggest that CP-AMPA receptors contribute to feedforward transmission onto PV(+)-INs but not MSNs in the NAc core.

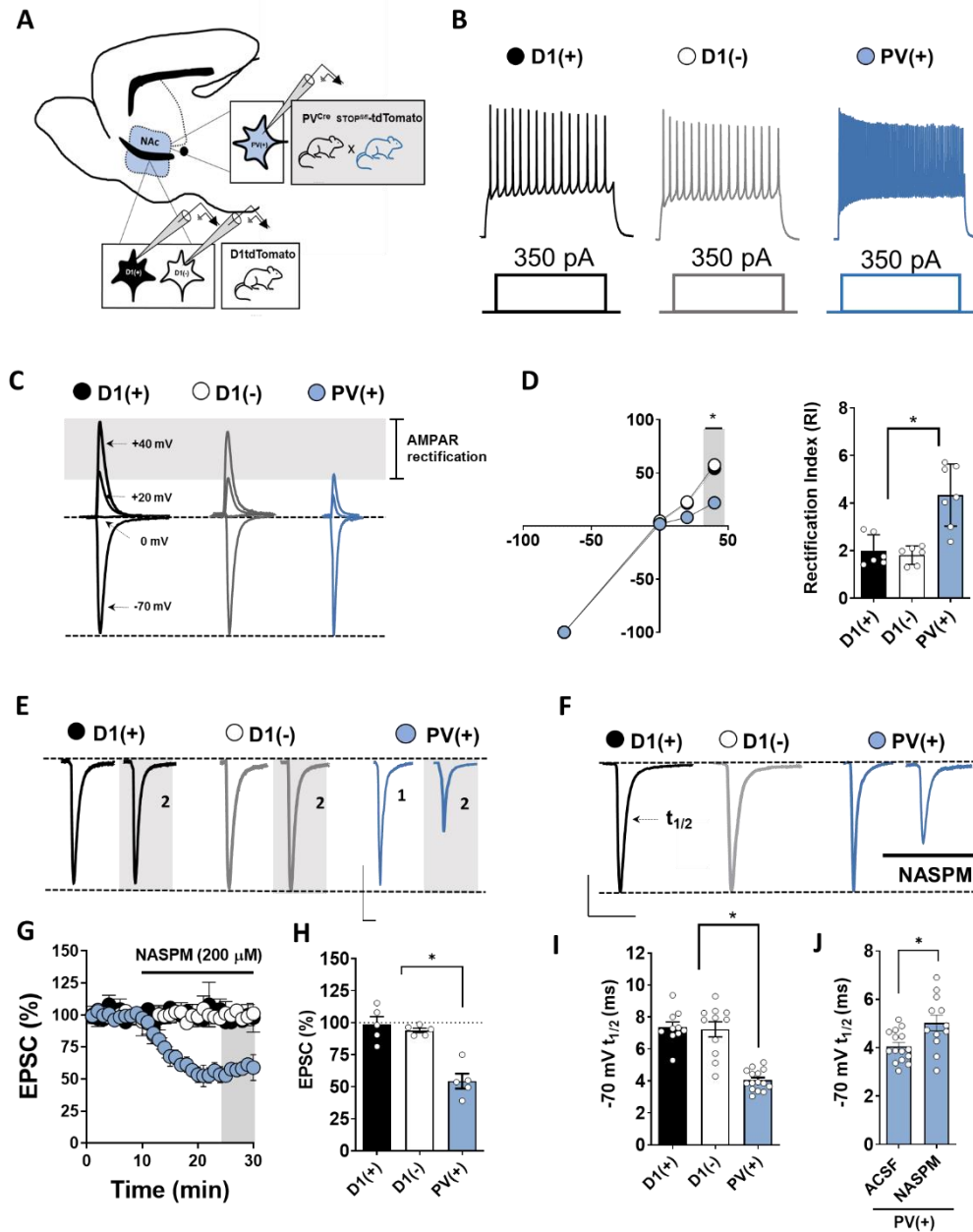


**Figure 4.1. CP-AMPA receptors are expressed at glutamatergic synapses onto PV(+)-INs but not D1(+) and D1(-) MSNs in the NAc core.** (A) Schematic depicting transgenic reporter strategy and electrophysiological configuration. (B) Representative traces of APs elicited in PV(+), D1(+) and D1(-) cells following 350 pA somatic current injection. (C) Representative AMPAR-mediated EPSCs in PV(+), D1(+) and D1(-) cells when clamped at -70, 0, +20 and +40 mV. (D) AMPAR I-V relationship and RI quantified in PV(+), D1(+) and D1(-) cells. (E) EPSCs in PV(+), D1(+) and D1(-) cells showing differential sensitivity to NASPM. (F) EPSCs in PV(+), D1(+) and D1(-) cells showing differences in AMPAR decay kinetics and the contribution of CP-AMPA receptors. (G) Normalized EPSCs in PV(+), D1(+) and D1(-) cells in the presence of NASPM. (H) Quantification of EPSC amplitude in the presence of NASPM. (I, J) I: T<sub>1/2</sub> obtained from PV(+), D1(+) and D1(-) cells. J: Shift in T<sub>1/2</sub> in PV(+)-INs by NASPM. Error bars indicate SEM. \* p<0.05.

*Low-frequency stimulation (LFS) elicits CP-AMPA-dependent LTD at feedforward synapses onto PV-INs*

PV(+)-INs receive collateralizing glutamatergic input from corticolimbic afferents that target D1(+) and D1(-) MSNs. At synapses onto D2-GFP(+) [D1(-)] MSNs in the NAc core, low-frequency stimulation (LFS, 10 Hz) triggers robust long-term depression (LTD) (Grueter et al., 2010; Turner et al., 2018b). To determine if LFS similarly modulates glutamatergic synaptic strength onto PV(+)-INs, LFS was delivered for 5-min following a stable 10-min EPSC baseline. LFS resulted in a persistent decrease in EPSC amplitude throughout the recording period, indicating the induction of LTD (**Fig. 4.2.A-D**, LTD, PV(+):  $54.67 \pm 6.79\%$ ,  $n=9$ ,  $p < 0.001$ ). Given that group I mGluRs are required for the induction of LTD in the NAc core and shell, we first assessed the contribution of mGluRs to LTD at PV(+)-IN synapses (PV-LTD) by incorporating pan-mGluR antagonist, LY341495 (100  $\mu$ M), into the ACSF bath prior to LFS. LFS-induced LTD remained intact in the presence of LY341495 (**Fig. 4.3A,I**, mGluRs,  $41.30 \pm 15.67\%$ ,  $n=4$ ,  $p=0.163$ ). Furthermore, bath-application of group I mGluR agonist, (*RS*)-dihydroxyphenylglycine (DHPG, 100  $\mu$ M), elicited a transient depression in EPSC amplitude at PV(+)-IN synapses that returned to baseline, indicating a lack of group I mGluR-induced LTD at these synapses (**Fig. 4.3B,I**, DHPG,  $100.37 \pm 5.75\%$ ,  $n=4$ ,  $p=0.454$ ). These findings indicate that LFS-induced LTD of glutamatergic transmission onto PV(+)-INs is mGluR-independent.

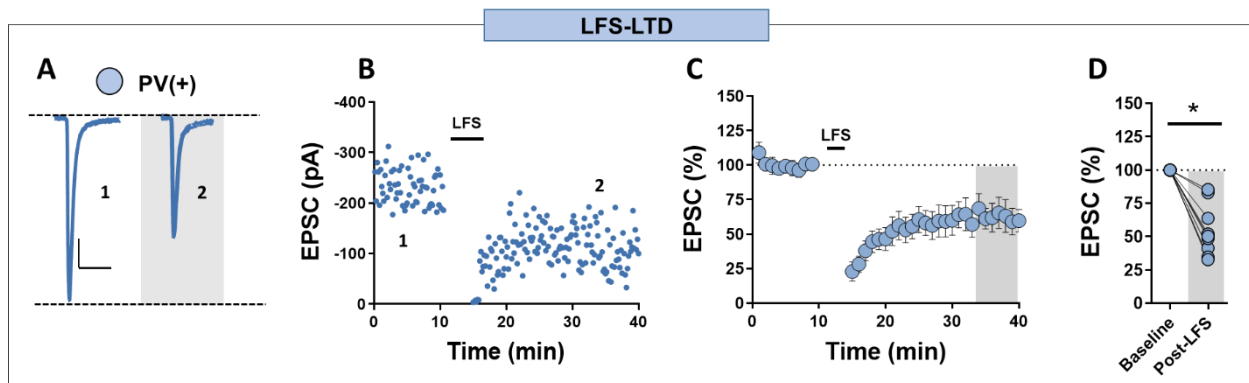


**Figure 4.2. Low frequency stimulation (LFS) triggers long-term depression of glutamatergic transmission onto PV(+)-INs.** (A, B) Representative traces and experiment in PV(+)-INs at baseline and post-LFS showing that LFS induces robust LTD. (C) Time-course summary of normalized EPSCs in PV(+)-INs. (D) Quantification of normalized EPSC amplitude post-LFS t(grey) = 35-40-min. Note: all experiments performed in the dorsomedial NAc core near corticoaccumbens interface. Error bars indicate SEM. \*  $p < 0.05$

To determine if LFS instead recruits postsynaptic NMDAR function, we repeated these experiments in the presence of NMDAR antagonist, APV (50  $\mu$ M). APV also failed to block LFS-induced LTD at PV(+)-IN synapses (**Fig. 4.3C,I**, APV,  $45.34 \pm 13.3\%$ ,  $n=5$ ,  $p=0.232$ ). We then asked whether intracellular  $Ca^{2+}$  signaling in PV(+)-INs is required for the induction of PV-LTD, as activity-dependent shifts in  $Ca^{2+}$  dynamics underlie various forms of plasticity in the NAc (Grueter et al., 2010; Francis et al., 2019). To address this possibility, we included fast-acting  $Ca^{2+}$  chelator, BAPTA (30 mM), in the intracellular solution of the patch pipette during the plasticity protocol. BAPTA completely blocked LFS-induced LTD, indicating that a rise in intracellular  $Ca^{2+}$  in PV(+)-INs is required for PV-LTD (**Fig. 4.3D,I**, BAPTA,  $76.37 \pm 9.86\%$ ,  $n=6$ ,  $p=0.032$ ). Given that NASPM-sensitive CP-AMPA receptors are expressed at PV(+)-IN synapses, we hypothesized that  $Ca^{2+}$  influx through CP-AMPA receptors contributes to the rise in intracellular  $Ca^{2+}$  necessary for PV-LTD. To test this hypothesis, we incorporated CP-AMPA receptor antagonist, NASPM (200  $\mu$ M), into the ACSF bath for 30-min prior to establishing an EPSC baseline. LFS delivered in NASPM-containing ACSF failed to elicit LTD of glutamatergic transmission onto PV(+)-INs, indicating that LTD is triggered at these synapses via CP-AMPA receptor-mediated  $Ca^{2+}$  entry (**Fig. 4.3E,I**, NASPM,  $97.72 \pm 7.40\%$ ,  $n=6$ ,  $p=0.003$ ).

Increased intracellular  $Ca^{2+}$  signaling often contributes to the induction of signaling events that are required for the expression of LTD (Winder and Sweatt, 2001; Fitzjohn and Collingridge, 2002). Given that glutamatergic afferents to the NAc highly express presynaptic  $CB_1R$  and eCB signaling underlies LFS-induced LTD at D2(+) MSN synapses, we assessed whether increased  $Ca^{2+}$  signaling triggers  $CB_1R$ -dependent LTD at PV(+)-IN synapses (Grueter et al., 2010). To investigate this mechanism, we first examined the integrity of LTD in the presence of  $CB_1R$  inverse

agonist, AM251 (5  $\mu$ M). Pre-incubation of slices in AM251 blocked LFS-induced LTD and unmasked a modest potentiation in EPSC amplitude (**Fig. 4.3F,I**, AM251,  $109.48 \pm 11.89\%$ ,  $n=5$ ,  $p=0.002$ ). If the expression of LTD at these synapses requires CB<sub>1</sub>R activity, then prior activation of CB<sub>1</sub>R with CB<sub>1/2</sub>R agonist, WIN 55-212 (1  $\mu$ M), should also occlude LFS-induced LTD. Consistent with this idea, prior application of WIN 55-212 abolished the subsequent LTD, indicating that CB<sub>1</sub>R activity mediates synaptic plasticity at PV(+)-IN synapses (**Fig. 4.3G,I**, WIN,  $92.70 \pm 5.27\%$ ,  $n=6$ ,  $p=0.002$ ). To determine if CB<sub>1</sub>R activation alone is sufficient to induce LTD at PV(+)-IN synapses, we superfused WIN 55-212 into the ACSF bath followed by AM251 once the WIN 55-212-induced depression in EPSC amplitude stabilized. WIN 55-212 significantly decreased EPSC amplitude in PV(+)-INs, an effect that persisted in the presence of AM251, indicating that pharmacological activation of CB<sub>1</sub>R triggers LTD of feedforward glutamatergic transmission (**Fig. 4.3H,I**, WIN-AM251,  $63.49 \pm 5.49\%$ ,  $n=5$ ,  $p<0.001$ ). Collectively, these data strongly support that eCB signaling via CB<sub>1</sub>R mediates the expression of LTD triggered by CP-AMPARs.

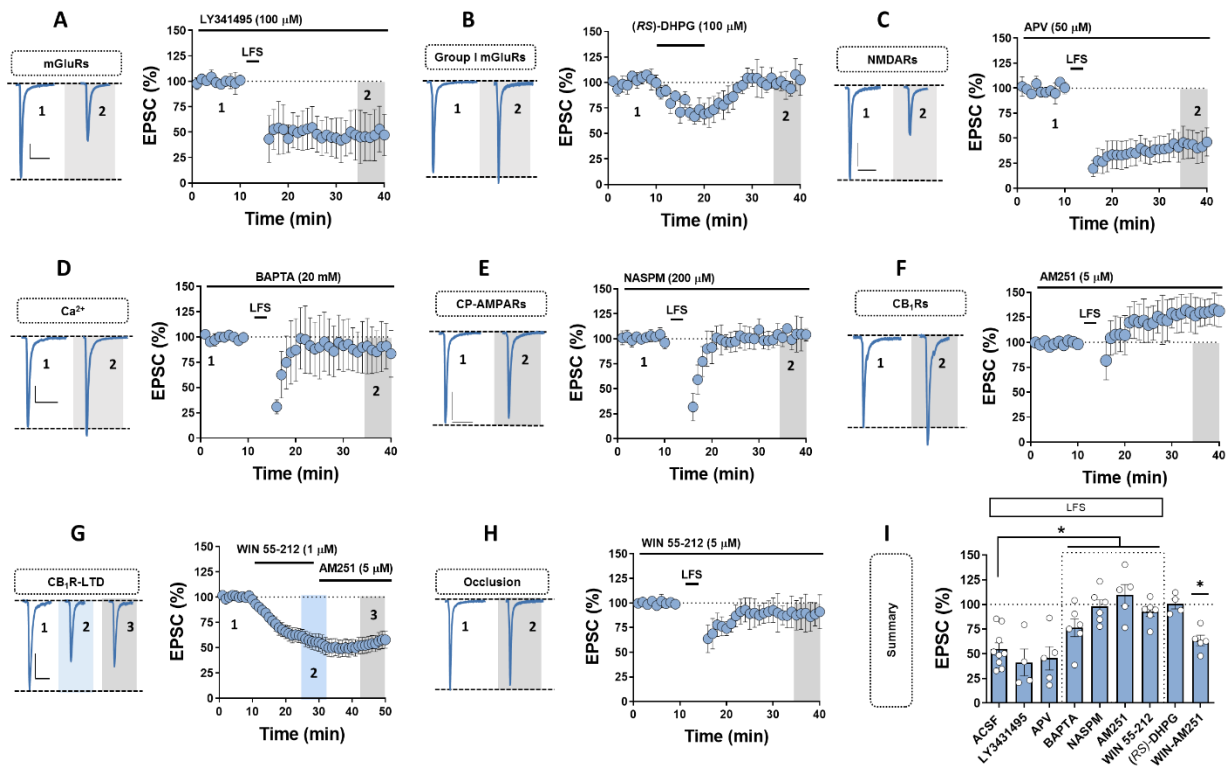


**Figure 4.3. LFS-induced LTD at PV(+)–IN synapses is CP-AMPA- and CB<sub>1</sub>R-dependent.** (A) Representative EPSCs and normalized time-course of LFS-induced LTD assessed in the presence of pan-mGluR antagonist, LY341495. (B) Representative EPSCs and normalized time-course showing that group I mGluR agonist, DHPG, fails to elicit LTD at synapses onto PV(+)–INs. (C) Representative EPSCs and normalized time-course of LFS-induced LTD assessed in the presence of NMDAR antagonist, APV. (D) Representative EPSCs and normalized time-course of LFS-induced LTD assessed with Ca<sup>2+</sup> chelator, BAPTA, included in the internal solution. (E) Representative EPSCs and normalized time-course of LFS-induced LTD assessed in the presence of NASPM. (F) Representative EPSCs and normalized time-course of LFS-induced LTD assessed in the presence of CB<sub>1</sub> receptor inverse agonist, AM251. (G) Representative EPSCs and normalized time course showing that CB<sub>1</sub> agonist, WIN 55-212, depresses EPSC amplitude that persists when chased with AM251. (H) Representative EPSCs and normalized time-course of LFS-induced LTD assessed in WIN 55-212-containing ACSF, showing that prior CB<sub>1</sub> activation occludes LFS-LTD. (I) Summary of average EPSC amplitude post-LFS during each pharmacological manipulation.

*CP-AMPA<sub>s</sub> on PV(+)-INs trigger tonic eCB signaling via CB<sub>1</sub>R at feedforward synapses in the NAc core*

Our data suggest that Ca<sup>2+</sup> influx via CP-AMPA<sub>s</sub> triggers eCB signaling via presynaptic CB<sub>1</sub>R<sub>s</sub>. We next asked whether tonic eCB signaling occurs at glutamatergic synapses onto PV(+)-INs. To interrogate this possibility, we first assessed whether tonic CB<sub>1</sub>R function negatively regulates glutamate release probability at these synapses. Following a 10-min EPSC baseline, AM251 was superfused into the ACSF bath for a prolonged exposure period (40-min) to capture changes in EPSC amplitude. Bath-application of AM251 resulted in an increase in EPSC amplitude that was accompanied by a decrease in the paired-pulse ratio (PPR), consistent with a presynaptic enhancement of glutamate release probability (**Fig. 4.4A**, EPSCs, 128.27±6.06%, n=6, p<0.001; PPR baseline = 1.11±0.180, PPR post-AM251 = 0.83±0.17, n=6, paired *t*-test, p<0.001). The most likely eCBs contributing to tonic CB<sub>1</sub>R function are the arachidonic acid-derived ligands anandamide (AEA) and 2-arachidonylglycerol (2-AG), the former of which is commonly associated with tonic CB<sub>1</sub>R function (Kreitzer and Malenka, 2005; Lee et al., 2015). To determine if 2-AG signaling tonically inhibits presynaptic glutamate release, we superfused DO34 (1 μM), a selective inhibitor of the 2-AG synthetic enzyme, DAG lipase (DAGL), into the ACSF bath. EPSC amplitude remained unchanged in the presence of DO34, indicating that 2-AG signaling does not tonically regulate PV(+)-IN synapses (**Fig. 4.4C**, DO34, 98.64±5.36%, n=7, p=0.396).

To determine if tonic eCB signaling is mediated instead by AEA, we treated slices with URB597 (1 μM), an inhibitor of the AEA catabolic enzyme, fatty acid amide hydrolase (FAAH). Pharmacological inhibition of FAAH should increase endogenous AEA signaling in synaptic environments where tonic CB<sub>1</sub>R activity is submaximal. After obtaining a 10-min EPSC baseline

in URB597-pretreated slices, AM251 was superfused into the ACSF bath for 40-min. AM251 application in URB597-pretreated slices resulted in a robust enhancement of EPSC amplitude relative to AM251-treated slices alone (**Fig. 4.4B**, URB+AM251,  $146.63 \pm 5.06\%$ ,  $n=7$ ,  $p=0.011$ ). Thus, these data suggest that AEA signaling negatively regulates glutamatergic transmission onto PV(+)-INs by acting on presynaptic CB<sub>1</sub>R. Similar to activity-dependent eCB release, tonic eCB signaling often requires phasic shifts in intracellular Ca<sup>2+</sup> levels. Given the importance of CP-AMPARs in LFS-LTD at PV(+)-IN synapses, we assessed whether CP-AMPARs are also a source of Ca<sup>2+</sup> driving tonic AEA-mediated CB<sub>1</sub>R activity. This hypothesis stems from data showing that prolonged NASPM application elicits a late-phase increase in EPSC amplitude once the NASPM-induced depression has stabilized. To address this question directly, we bath-applied AM251 in slices pre-treated with NASPM for 30-min. Remarkably, in the presence of NASPM, AM251 failed to evoke an increase in EPSC amplitude, indicating that CP-AMPARs regulate both tonic and phasic forms eCB-dependent plasticity at glutamatergic synapses onto PV(+)-INs (**Fig. 4.4D**, NASPM,  $91.29 \pm 6.37\%$ ,  $n=4$ ,  $p=0.012$ )

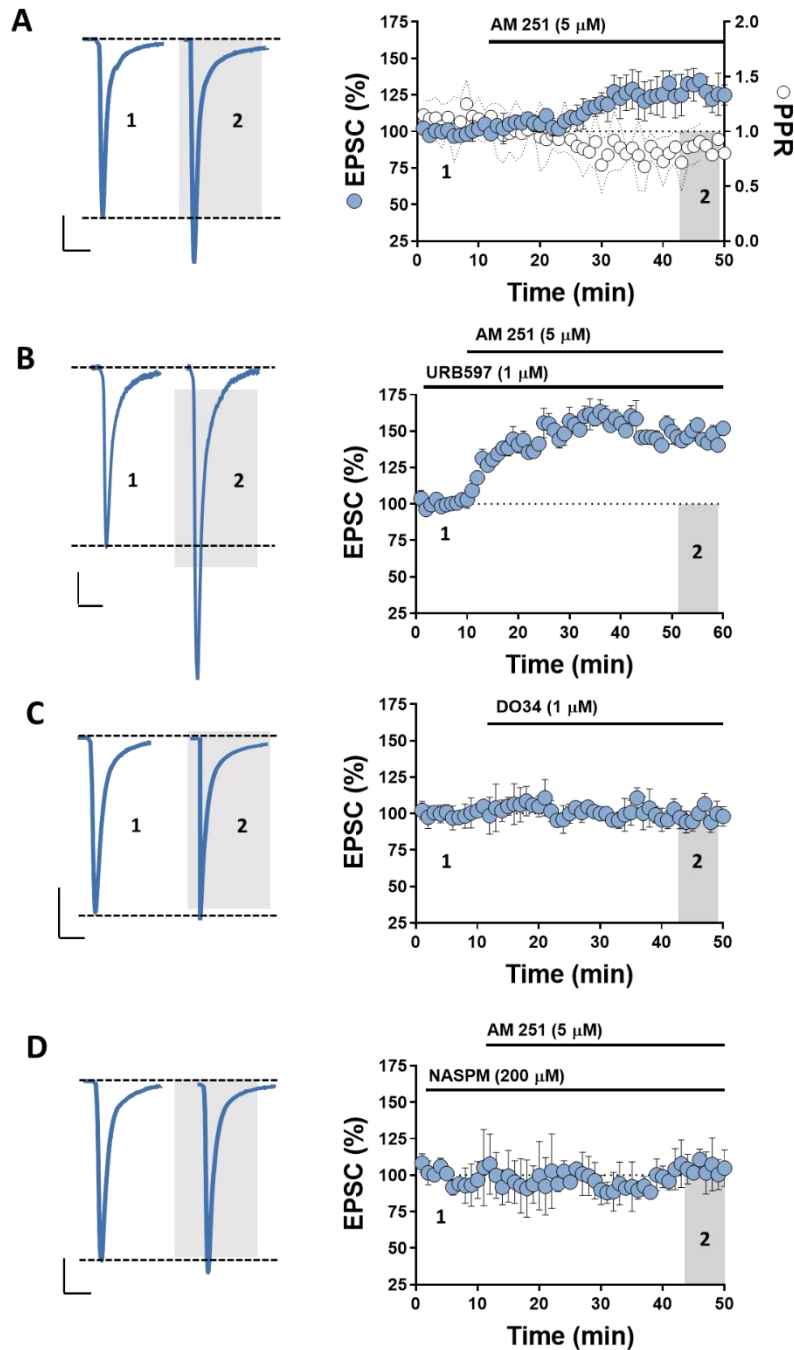


**Figure 4.4. Tonic AEA signaling is dependent on CP-AMPA function.** (A) Left Y axis: Representative traces and normalized time-course of average EPSC amplitude in PV(+)-INs during bath-application of AM251. Right Y axis: raw PPR time-course during AM251 superfusion (open circles). (B) Representative traces and normalized EPSCs during AM251 bath-application in slices continuously perfused with FAAH inhibitor, URB597. (C) Representative traces and normalized EPSCs during the bath-application of DAGL inhibitor, DO34. (D) Representative traces and normalized EPSCs during AM251 bath-application in slices continuously perfused with NASPM. Error bars indicate SEM. \*  $p < 0.05$

*Acute cocaine exposure occludes LTD at feedforward synapses onto PV(+)-INs in the NAc core*

Experience-dependent adaptations at glutamatergic synapses in the NAc contribute to persistent pathological shifts in motivated behavior, including those elicited by drugs of abuse (Kalivas, 2009; Dong et al., 2017). A single exposure to cocaine alters eCB-LTD at D2(+) MSN synapses in the NAc core (Grueter et al., 2010; Huang et al., 2015a). Furthermore, eCB-dependent LTD in the NAc, as well as afferent-specific glutamatergic properties onto MSNs, is abolished following a single exposure to  $\Delta^9$ -tetrahydrocannabinol ( $\Delta^9$ -THC) (Mato et al., 2004; Hwang and Lupica, 2019). Thus, salient experience evoked by drugs of abuse modulate the expression of CB<sub>1</sub>R-induced LTD at glutamatergic synapses in the NAc. Given that PV(+)-INs within feedforward inhibitory microcircuits regulate MSN responsiveness to acute shifts in circuit activity, we hypothesized that *in vivo* exposure to a salient experience, such as cocaine, would also alter the magnitude of LTD at PV(+)-IN synapses. To test this hypothesis, we exposed mice to a single dose of cocaine (15 mg/kg I.P.) or saline and prepared *ex vivo* brain slices 24-hrs later (**Fig. 4.5A**). In cocaine-treated mice, LTD at feedforward synapses onto PV(+)-INs was completely abolished, whereas LTD in saline-treated mice was indistinguishable from experiments in naïve mice (**Fig. 4.5B,C**, LTD saline:  $43.01 \pm 9.71\%$ , n=6, LTD cocaine *in vivo*,  $89.30 \pm 7.61\%$ , n=6,  $p < 0.001$ ).

To begin to understand the mechanism by which a single exposure to cocaine abolishes LTD at PV(+)-IN synapses, we asked if synaptic mechanisms engaged by the pharmacological actions of cocaine were responsible for this effect. We bath-applied cocaine *ex vivo* (COC, 10  $\mu$ M) at a concentration with minimal anesthetic effects at voltage-gated Na<sup>+</sup> channels. Superfusion of COC elicited a robust decrease in EPSC amplitude that returned to baseline following drug washout (**Fig. 4.5G-I**, COC,  $64.98 \pm 3.12\%$ , n=7,  $p < 0.001$ ). The COC-induced decrease in EPSC amplitude

coincided with an increase in PPR and coefficient of variance (CV), indicating a presynaptic site of action (**Fig. 4.5J-L**, PPR baseline =  $1.37 \pm 0.06$ , PPR COC =  $1.51 \pm 0.05$ ,  $n=9$ ,  $p=0.016$ ; CV baseline =  $0.013 \pm 0.01$ , CV COC =  $0.20 \pm 0.02$ ,  $n=9$ ,  $p=0.001$ ). Surprisingly, the synaptic effects of COC remained completely intact in the presence of a D1 receptor antagonist (SCH 23390, 4  $\mu\text{M}$ ) and D2 receptor antagonist (sulpiride, 10  $\mu\text{M}$ ), pointing to dopamine (DA)-independent actions of COC at these synapses (**Fig. 4.6A,B**, COC in sulpiride,  $68.26 \pm 6.06\%$ ,  $n=5$ ; COC in SCH 23390,  $75.24 \pm 5.47\%$ ,  $n=5$ ). Furthermore, superfusion of a selective DA transporter (DAT) blocker, GBR12783 (1  $\mu\text{M}$ ), failed to recapitulate the effects of COC at these synapses (**Fig. 4.6C**, GBR,  $94.75 \pm 3.63$ ,  $n=7$ ,  $p=0.489$ ). The effects were also unlikely caused by indirect actions via muscarinic acetylcholine receptor (mAChR) activity, as prior application of a mAChR antagonist cocktail (pirenzepine, 1  $\mu\text{M}$ ; atropine, 10  $\mu\text{M}$ ) had no effect on the COC-induced decrease in EPSC amplitude (Supplemental data, not shown).

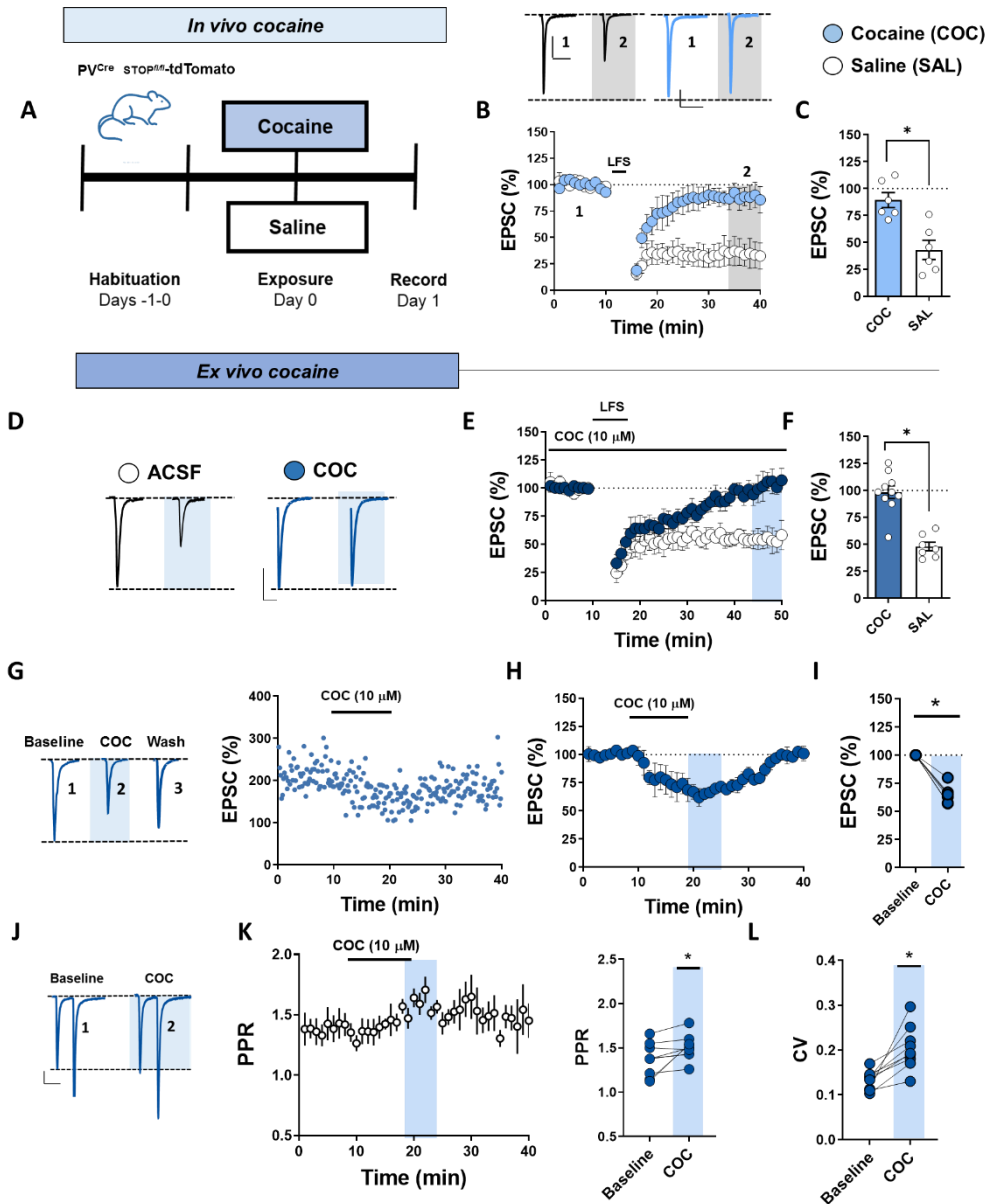


**Figure 4.5. Cocaine abolishes LFS-induced LTD at PV(+)-IN synapses.** (A) Schematic depicting experimental timeline of *in vivo* cocaine exposure paradigm. (B) Representative traces and normalized EPSCs of LFS-induced LTD in cocaine (COC, light blue) and saline-treated mice (open circles). (C) Quantification of average EPSC amplitude post-LFS in COC and saline-treated mice. (D) Representative traces pre- and post-LFS in slices incubated in COC or ACSF alone. (E, F) Normalized and average EPSCs showing the effects of *ex vivo* COC on LFS-induced LTD. (G) Representative traces and experiment showing the acute synaptic effects of *ex vivo* COC application on EPSC amplitude. (H, I) Normalized and average EPSCs in PV(+)-INs during COC superfusion. COC was used at a concentration previously shown to be subthreshold for voltage-gated Na<sup>+</sup> channels. (J) Representative PPR traces depicting effects of COC on release probability. (K) Raw PPR time course with average PPRs. (L) CV pre- and post-COC. Error bars indicate SEM. \**p*<0.05

*Ex vivo* COC-induced activity at CB<sub>1</sub>R has been demonstrated at glutamatergic synapses onto MSNs in the NAc (Jedynak et al., 2016; Ingebretson et al., 2018) . Given that LFS-induced LTD at PV(+)-IN synapses is CB<sub>1</sub>R-dependent, we first asked if the effects of COC are mediated, in part, by an eCB-dependent process via CB<sub>1</sub>R. Consistent with this hypothesis, the COC-induced decrease in EPSC amplitude was completely blocked by prior application of AM251 and occluded by WIN 55-212 (5  $\mu$ M) (**Fig. 4.6D,E**, COC in AM251,  $99.90 \pm 3.56\%$ ,  $n=5$ ,  $p=0.003$ ; COC in WIN,  $97.17 \pm 4.89\%$ ,  $n=3$ ,  $p=0.004$ ). Thus, the acute pharmacological actions of COC recruit a CB<sub>1</sub>R-dependent process. To determine whether COC engages a 2-AG or AEA signaling mechanism, we first treated slices with either an inhibitor of 2-AG synthesis, DO34, or an inhibitor of AEA catabolism, URB 597. The COC-induced depression remained intact in the presence of DO34 but was significantly blunted by URB597, point to an AEA-dependent mechanism recruited by COC at PV(+)-IN synapses (**Fig. 4.6F-H**, 1-way ANOVA, ACSF vs. drug interaction,  $F(7, 35) = 13.85$ , COC in DO34,  $65.41 \pm 5.59\%$ ,  $n=4$ ,  $p>0.999$ ; COC in URB 597,  $84.54 \pm 4.77\%$ ,  $n=7$ ,  $p=0.0016$ ). If the pharmacological actions of COC alone are sufficient to occlude presynaptic CB<sub>1</sub>R activity, *ex vivo* application of COC should also reduce the expression of LTD at these synapses. Indeed, incorporation of COC into the ACSF bath blocked the expression of LTD at PV(+)-IN synapses in the NAc core (**Fig. 4.5D-F**, LFS in COC,  $98.39 \pm 6.37$ ,  $n=10$ ; LFS in ACSF,  $48.02 \pm 4.48$ ,  $n=7$ ,  $p<0.001$ ). Together, these data suggest that CP-AMPA-dependent LTD within this microcircuit is a substrate for COC in the NAc core.

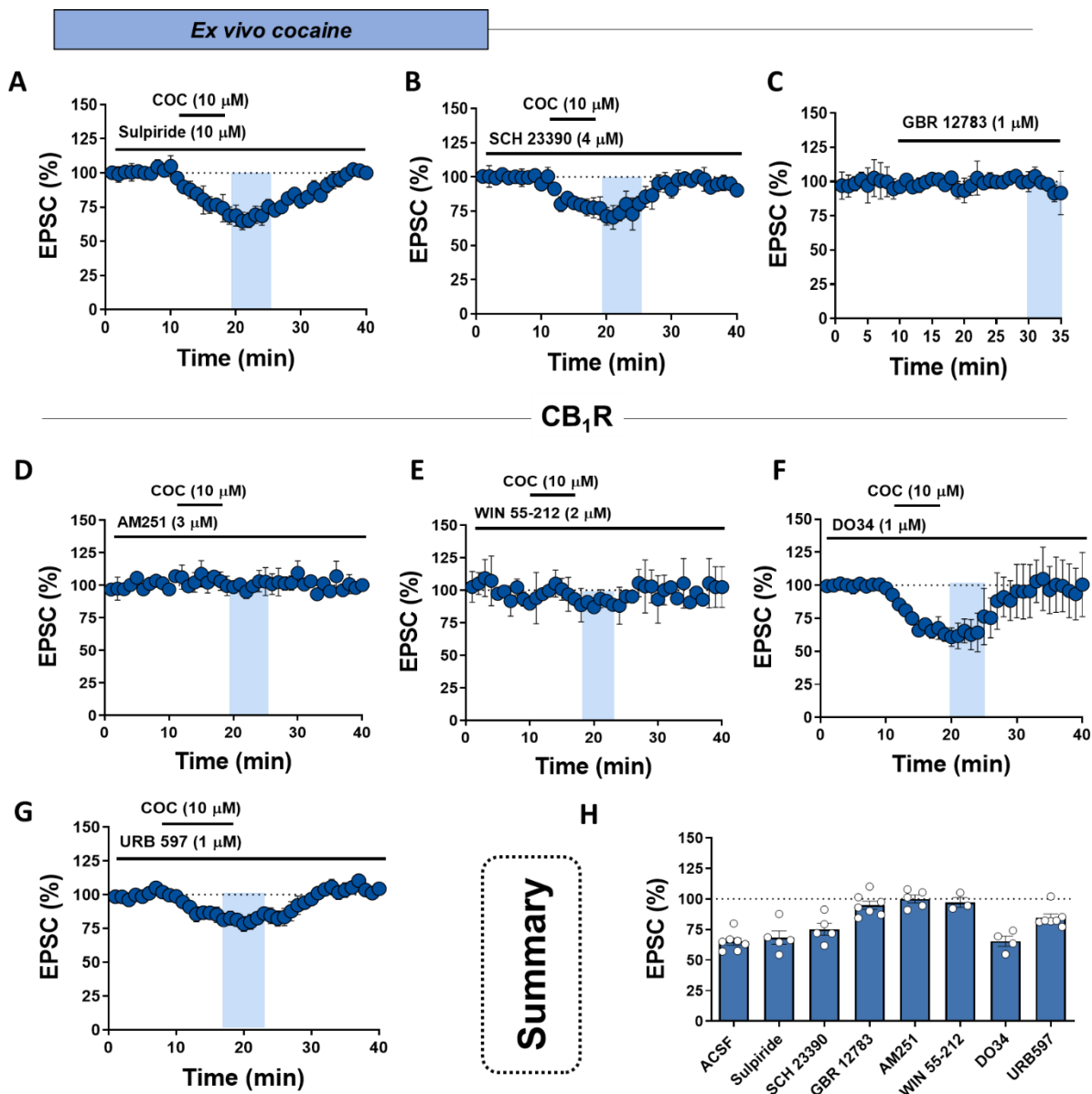


**Figure 4.6. Cocaine decreases glutamatergic transmission via actions at CB<sub>1</sub>R in a DA-independent manner.** (A) Normalized EPSCs showing the effects of COC in the presence of D2-like DA receptor antagonist, sulpiride. (B) Normalized EPSCs showing the effects of COC in the presence of D1-like DA receptor antagonist, SCH 23390. (C) Normalized EPSCs showing that selective DAT inhibitor, GBR 12783, has no effect on EPSC amplitude. (D) Normalized EPSCs showing the effects of COC in the presence of AM251. (E) Normalized EPSCs showing the effects of COC in the presence of WIN 55-212. Both D and E show that COC modulates glutamatergic transmission in a CB<sub>1</sub>R-dependent manner. (F) Normalized EPSCs showing the effects of COC in the presence of DAGL inhibitor, DO34. (D) Normalized EPSCs showing the blunted effects of COC in slices incubated in URB597. (G) Summary of average EPSC amplitude following COC during various pharmacological manipulations.

## 4.5 Discussion

We offer rigorous functional evidence that CP-AMPARs on PV(+)-INs dynamically regulate feedforward synaptic transmission in the NAc core. Utilizing PV- and D1-specific transgenic reporter mice, we report that CP-AMPARs are functionally expressed at glutamatergic synapses onto PV(+)-INs but not D1(+) or D1(-) MSNs.  $\text{Ca}^{2+}$  influx via CP-AMPARs at PV(+)-IN synapses is recruited during LFS to trigger eCB-dependent LTD, contrasting with LFS-induced LTD at MSN synapses in the NAc. Additionally, we find that tonic eCB signaling via  $\text{CB}_1\text{R}$  at PV(+)-IN synapses is mediated by AEA, the production of which is constitutively regulated by  $\text{Ca}^{2+}$  entry through CP-AMPARs. The synaptic plasticity mechanism elucidated at PV(+)-IN synapses is targeted by acute cocaine exposure, as both *in vivo* and *ex vivo* COC abolishes PV-LTD by recruiting presynaptic  $\text{CB}_1\text{R}$  function in a DA-independent manner. To our knowledge, this is the first study directly examining physiological processes governed by CP-AMPARs within PV-IN-embedded feedforward microcircuits in the NAc core.

The stoichiometric profile of AMPARs at glutamatergic synapses in the NAc has important implications for reward-related behavior (Ferrario et al., 2011; Graziane et al., 2016; Wolf, 2016). Withdrawal from repeated cocaine exposure leads to the progressive incorporation of GluA2-lacking CP-AMPARs on MSNs in a cell type- and input-specific manner (Lee et al., 2013; Pascoli et al., 2014). Time-contingent adaptations at these synapses contribute to the “incubation of cocaine craving” that drives the reinstatement of reward-seeking behavior. In the present study, we provide electrophysiological evidence that CP-AMPARs are expressed basally at glutamatergic synapses onto PV(+)-INs but not D1(+) or D1(-) MSNs, consistent with prior assessments of excitatory transmission in the NAc core (Yu et al., 2017). Although CP-AMPAR on MSNs have

been implicated in the pathogenesis of both rewarding- and depressive-like behavioral phenotypes, a significant gap remains as to how CP-AMPARs actually influence synaptic physiology. We find that CP-AMPARs on PV(+)-INs contributes to the fast kinetics of AMPAR-mediated EPSCs detected at these synapses. Rapid detection of glutamatergic input, alongside the electrotonic properties of PV(+)-IN dendrites, supports the role of PV(+)-INs in disynaptic feedforward inhibition. As a synaptic intermediate between afferent-directed excitation of MSNs, PV(+)-INs transduce shifts in corticolimbic circuit activity into feedforward GABAergic output. Thus, the biophysical properties of CP-AMPARs may permit rapid integration of the same corticolimbic inputs driving NAc output.

CP-AMPARs expressed at discrete synapses have been associated with the expression of homeostatic and Hebbian plasticity mechanisms (Liu and Cull-Candy, 2000; Soler-Llavina and Sabatini, 2006). A relatively unexplored question, however, is how CP-AMPARs redefine the molecular requirements for activity-dependent shifts in synaptic strength. We provide evidence that CP-AMPARs on PV(+)-INs trigger a form of LTD mediated by eCB signaling. We also find that CP-AMPARs authorize the release of tonic eCBs which act on presynaptic CB<sub>1</sub>R to regulate glutamate release probability. To our knowledge, this is the first study reporting a link between CP-AMPAR-mediated Ca<sup>2+</sup> influx and eCB signaling mechanisms in the reward network. Although mechanistically distinct, a similar emergent property has been described at NAc synapses enriched in GluN2B-containing NMDARs, a developmentally regulated NMDAR subunit associated with drug-induced silent synapse formation (Neumann et al., 2016; Kashima and Grueter, 2017; Joffe et al., 2018). GluN2B, characterized by delayed deactivation kinetics permitting increased Ca<sup>2+</sup> influx, drives homeostatic scaling of MSN excitability (Kalivas, 2009;

Wang et al., 2018a). Our data here supports the broader hypothesis that subunit-specific synaptic profiles at glutamatergic synapses in the NAc underlie various forms of synaptic and behavioral plasticity.

It is well-established that forms of salient stimuli, particularly to drugs of abuse, can elicit synaptic rearrangements in the NAc (Turner et al., 2018a). A frequent challenge is determining whether a “loss” of synaptically-evoked plasticity is due to an experience-dependent adaptation in the induction or expression system, or whether there is a competing synaptic event occurring in parallel. Our data suggests that acute cocaine exposure abolishes CP-AMPA-mediated LTD by engaging a synaptic mechanism that disrupts the expression of this plasticity at CB<sub>1</sub>R. Indeed, we find that COC evokes a CB<sub>1</sub>R-dependent process that decreases glutamatergic synaptic strength onto PV(+)-INs. The observation that LTD at PV(+)-IN synapses is abolished 24-hrs following cocaine exposure indicates that COC-induced shifts in synaptic function are long-lasting. However, COC has a half-life of 30-min to 1-hr following IP administration, making it less likely that the direct pharmacological actions of COC are still on board (Benuck et al., 1987). Our data showing that inhibiting 2-AG synthesis fails to block the COC-induced depression in excitatory transmission leaves open the possibility that COC instead mobilizes AEA release. Indeed, preventing the degradation of AEA by inhibiting FAAH significantly blunted the COC effect, raising the hypothesis that elevating tonic eCB signaling saturates presynaptic CB<sub>1</sub>R. While this hypothesis remains untested in this study, our data provide a mechanistic step forward in understanding how COC exposure disrupts plasticity mechanisms within NAc microcircuitry.

### *Conclusion*

PV(+)-INs in the NAc are fast-spiking GABAergic neurons embedded within a feedforward inhibitory network that coordinates functional NAc circuit output. We report that PV(+)-INs, unlike D1(+) and D1(-) MSNs, are enriched in GluA2-lacking CP-AMPARs that confer specialized synaptic properties to feedforward glutamatergic synapses. Importantly, we find that  $\text{Ca}^{2+}$  influx through CP-AMPARs triggers (a) eCB-dependent LTD via presynaptic  $\text{CB}_1\text{R}$  and (b) tonic eCB signaling via retrograde AEA signaling. This plasticity is abolished following acute exposure to COC by occluding the  $\text{CB}_1\text{R}$ -dependent expression of LTD. These findings are the first to provide functional evidence that CP-AMPARs are linked to the release of eCBs that gate tonic- and phasic-dependent shifts in glutamatergic synaptic strength. Understanding how CP-AMPARs contribute to synaptic function will likely contribute to ways in which this AMPAR profile can be targeted *within* interneuron microcircuits for the treatment of maladaptive motivational states, such as addiction and depression.

## CHAPTER 5

### Works in progress, concluding remarks and future directions

The prior chapters provide evidence that feedforward inhibitory microcircuits in the NAc are capable of both initiating and undergoing shifts in synaptic strength. Whereas PV-INs can heterosynaptically regulate glutamatergic transmission via GABA<sub>B</sub>R, synapses *onto* PV-INs are subject to CB<sub>1</sub>R-dependent LTD triggered by CP-AMPA<sub>s</sub>, indicating that both synaptic loci within the feedforward network are modifiable. These findings prompted investigation into additional mechanisms regulating these microcircuits, focusing again on the disynaptic framework that organized the prior two projects. Chapter 4 concluded with studies looking at *how* cocaine, a potent monoamine secretagogue within the reward network, evokes CB<sub>1</sub>R signaling independently of its actions on monoamine transporters. Having ruled out canonical actions of cocaine on this circuit, it became increasingly clear through multiple pharmacological analyses that glutamatergic synapses onto PV-INs, but not MSNs, are targeted by the noradrenergic (NE) system.

The observation that specific microcircuits may be targeted by an ascending neuromodulatory system, such as the NEergic arousal system, dramatically increases the complexity of NAc circuit function. In contrast to DA and serotonin (5-HT) signaling in the NAc, NEergic innervation of the NAc is sparse, with relatively few studies looking at how NEergic transmission modulates mesolimbic reward output (Fallon and Moore, 1978; Berridge et al., 1997; Zahm, 1999b). An enticing hypothesis is that the modest NE innervation pattern in the NAc corresponds to the density of interneurons, such that PV-IN-embedded microcircuits receive privileged synaptic input from NEergic afferents. In the subsection below, we provide preliminary evidence that the NE system

indirectly dampens feedforward inhibition by recruiting cholinergic interneurons (CINs). Targeted recruitment of a PV-CIN circuit motif by the NEergic system parallels the effects of DA on cholinergic transmission in the NAc, where mesolimbic DA output is functionally coupled to the spontaneous firing rate of CINs (Yorgason et al., 2017). Therefore, an exciting, broader hypothesis is that NE and DA-containing afferents converge on CINs to differentially regulate PV-IN microcircuits and MSN output, respectively. If correct, this model positions CINs as the primary gatekeepers of neuromodulatory signaling in the NAc, distributing information encoded by NE- and DA-containing loci to the appropriate circuit elements in the NAc. Although incomplete, section 5.1 examines this possibility using a pharmacological and dynamic electrophysiological approach in multiple transgenic mouse lines.

### 5.1 Noradrenergic signaling engages a dual PV-cholinergic interneuron microcircuit to dampen feedforward inhibition in the nucleus accumbens

The NAc core and shell receive extensive monoaminergic input from mesencephalic brain structures, including the VTA and dorsal raphe nucleus (DRN). However, norepinephrine (NE), synthesized in dopamine- $\beta$ -hydroxylase (DBH)-containing cells in the nucleus of the solitary tract (NTS) and locus coeruleus of the brainstem, has received only modest attention regarding NAc circuit function (Fallon and Moore, 1978; Allin et al., 1988). Relative to other subcortical regions within the reward network, the NAc is only sparsely innervated by DBH-(+) noradrenergic fibers, with immunoreactivity for DBH highest in the NAc shell-core transition zone (Berridge et al., 1997; Delfs et al., 1998). While evoked NE content in the NAc is low at baseline, amphetamine (AMPH)-induced NE efflux is detectable in both core and shell subterritories, indicating the presence of functional NEergic input to the NAc (McKittrick and Abercrombie, 2007; Alsene et

al., 2010). Furthermore,  $\alpha$ - and  $\beta$ -adrenergic receptors (ARs) are expressed in the NAc along a rostral-caudal gradient that extends heavily into the NAc core (Kerfoot and Williams, 2011; Mitrano et al., 2012). How NE signaling via  $\alpha$ - and  $\beta$ -ARs modulates NAc circuit function, however, remains unexplored.

It is well-established that noradrenergic transmission gates stress-induced reinstatement to various drugs of abuse (Harris et al., 2018; Giustino et al., 2019). This is partially attributed to extrastriatal NE signaling in the bed nucleus of the stria terminalis (BNST), prefrontal cortex (PFC), and VTA, though prominent effects are also observed at noradrenergic loci in the brainstem (Mantsch et al., 2016). Prior studies in the NAc suggest that NE negatively regulates glutamatergic synaptic efficacy onto GABAergic medium spiny projections (MSNs) mediated by presynaptic  $\alpha$ -ARs (Nicola and Malenka, 1998; Peng et al., 2018). These studies coincide with ultrastructural analyses showing that  $\alpha$ -ARs are expressed on presynaptic elements in the NAc (Mitrano et al., 2012; Park et al., 2017). The extent to which NE regulates presynaptic DA efflux in the NAc is more controversial, as several studies indicate that locus coeruleus projections to the VTA increase mesoaccumbens DA transmission, whereas NE attenuates DA efflux in experiments restricted to the NAc (Mitrano et al., 2012; Park et al., 2017). NE may therefore engage diverse neuromodulatory mechanisms within the NAc to elicit contextually-specific changes in appetitive behavior.

Given the sparse noradrenergic (NEergic) innervation pattern in the NAc relative to other aminergic systems, it is enticing to speculate that NE elicits specific microcircuit adaptations in the NAc. Indeed, a symmetrical relationship exists in the population density of interneurons in the

NAc (i.e., 5% of neurons) and terminal expression levels of DBH (Berridge et al., 1997). We hypothesized that NE signaling in the NAc engages feedforward inhibitory microcircuits mediated by parvalbumin (PV)-expressing interneurons (INs). As described in earlier chapters, PV-INs exert robust GABAergic control over D1- [D1(+)] and D2-expressing MSN [D1(-)] output to constrain activity-dependent increases in corticolimbic input to the NAc (Chapter 2). In light of data from our lab and others showing that (a) CP-AMPA receptors on PV-INs trigger presynaptically-expressed eCB-dependent LTD (Chapter 3), (b) potentiating glutamatergic transmission onto putative PV-INs gates drug reward learning, and (c) PV-IN-to-MSN synapses undergo limited forms of synaptic plasticity (Chapter 2), we hypothesized that NE selectively modulates glutamatergic synaptic strength onto PV-INs.

To determine if NE modulates glutamatergic synaptic efficacy onto PV-INs and MSNs in the NAc core, we prepared acute *ex vivo* brain slices from PV<sup>Cre</sup>-tdTomato<sup>fl/fl</sup> mice in which Cre-dependent tdTomato (tdT) expression is driven by the parvalbumin (PV) promoter. This transgenic strategy distinguishes PV-INs from MSNs and other interneuron subtypes in the NAc. To confirm that tdT(+) cells were indeed PV-INs, we first performed current-clamp recordings in tdT(+) cells and tdT(-) cells [putative MSNs] to assess whether tdT(+) cells exhibited a fast-spiking electrophysiological profile. Depolarizing current injection exceeding action potential (AP) threshold (350 pA) in tdT(+) cells elicited high-frequency AP firing with characteristic short-duration waveforms and steep afterhyperpolarizations (AHPs), consistent with fast-spiking PV-INs in the NAc. AP firing and passive membrane properties in tdT(-) cells were distinct from those of tdT(+) PV-INs and were representative of MSNs in the NAc (see data shown in Chapter 4).

*Noradrenergic signaling modulates glutamatergic transmission onto PV(+)-INs but not MSNs in the NAc*

We first examined whether NE modulates electrically-evoked excitatory postsynaptic currents (EPSCs) onto PV-INs and MSNs in the NAc core. EPSCs were pharmacologically-isolated by incorporating GABA<sub>A</sub> receptor (GABA<sub>AR</sub>) antagonist, picrotoxin (50 μM), into the ACSF bath, as described previously (Chapters 3-4). Following a stable 10-min EPSC baseline, NE (20 μM) was superfused into the ACSF bath, resulting in a robust depression in EPSC amplitude at PV-IN synapses that persisted following drug wash-out (**Fig. 5.1.,AE**, NE PV(+), 66.17±6.63%, n=6, p<0.001) EPSC amplitude at tdT(-) MSN synapses was unaffected by NE, suggesting that NE modulates glutamatergic transmission in the NAc via PV-IN-specific mechanisms (**Fig. 5.1.,CE**, MSNs, 97.91±4.34%, n=4, p=0.671). To assess whether endogenously-released NE from NET-containing NEergic terminals recapitulates this effect, we bath-applied selective NET inhibitor, tomoxetine (TOM, 10 μM). TOM triggered a robust decrease in EPSC amplitude at PV-IN synapses without affecting synapses onto MSNs, suggesting that NET-regulated NE release in the NAc selectively modulates excitatory synapses onto PV-INs (**Fig. 5.1.,BF**, TOM PV(+), 50.59±4.68%, n=10, p<0.001; **Fig. 5.1.,DF** TOM MSN, 99.52±2.83%, n=6, p=0.862). NE signaling via α- and β-ARs can exert pre- and postsynaptic effects at synapses throughout the CNS. To determine if the NE- and TOM-induced depression in EPSC amplitude is expressed at pre- or postsynaptic loci, we measured changes in the paired-pulse ratio (PPR) and coefficient of variance (CV). The NE- and TOM-induced depression in EPSC amplitude did not accompany a shift in PPR or CV, suggesting that the pharmacological actions of NE at PV-IN synapses are likely postsynaptic or subthreshold for detection using PPR and CV measurements alone (**Fig. 5.2., A-**

**D**, PV(+) NE: PPR baseline =  $1.20 \pm 0.06$ , PPR NE =  $1.22 \pm 0.05$ , n=11, p=0.447; CV baseline =  $0.145 \pm 0.01$ , CV NE =  $0.162 \pm 0.01$ , n=9, p=0.0849. PV(+) TOM: PPR baseline =  $1.28 \pm 0.06$ , PPR TOM =  $1.35 \pm 0.08$ , n=17, p=0.495; CV baseline =  $0.156 \pm 0.01$ , CV TOM =  $0.17 \pm 0.07$ , n=12, p=0.051).

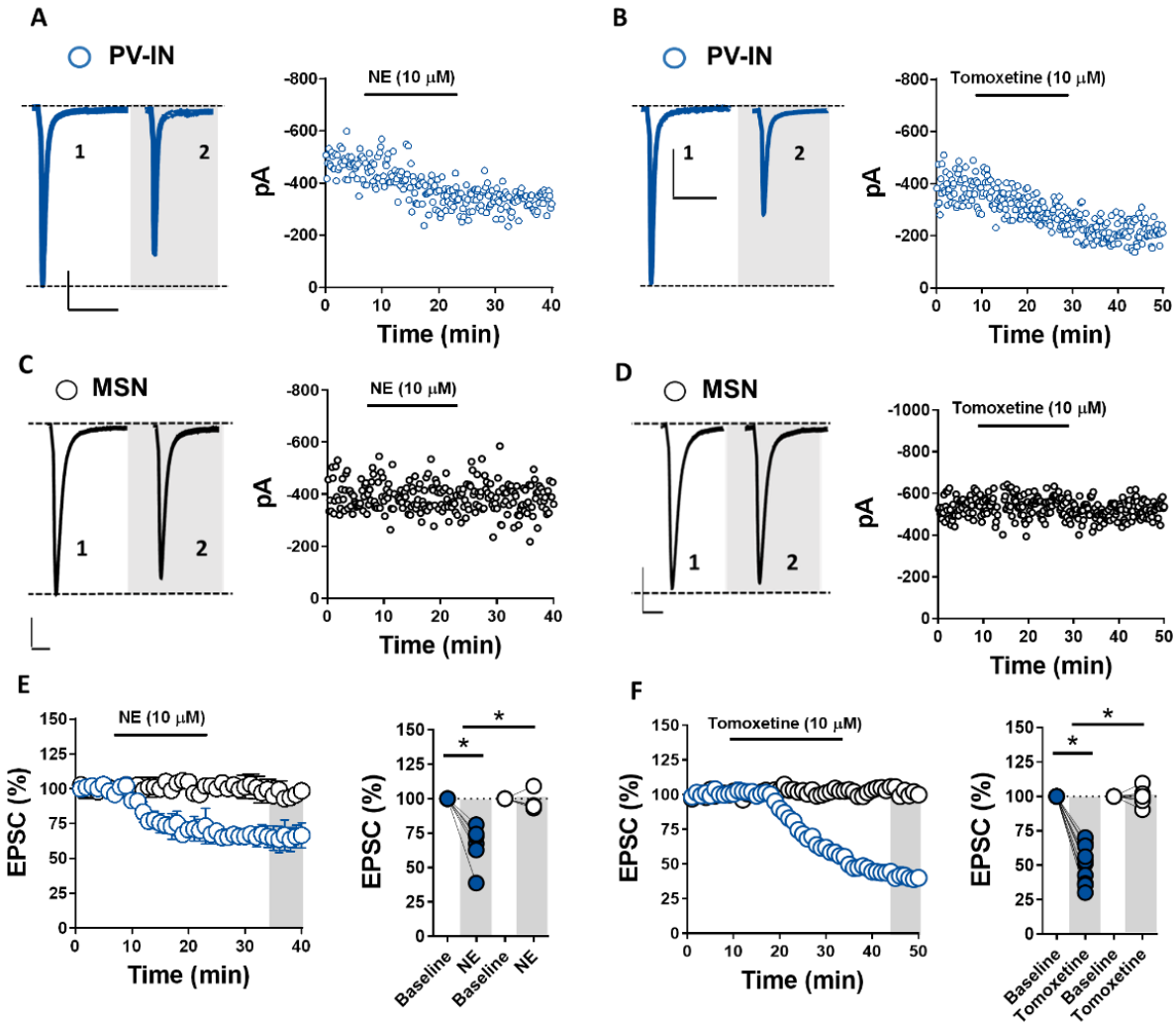


**Figure 5.1. Noradrenergic signaling regulates glutamatergic synapses onto PV(+)-INs but not MSNs in the NAc core.** (A) Representative traces and experiments depicting the effects of exogenous NE on EPSC amplitude in PV(+)-INs (blue open circles). (B) Representative traces and experiments depicting the effects of NET inhibitor, tomoxetine, on EPSC amplitude in PV(+)-INs. (C) Representative traces and experiments depicting the effects of exogenous NE on EPSC amplitude in MSNs (open black circles). (D) Representative traces and experiments depicting the effects of NET inhibitor, tomoxetine, on EPSC amplitude in MSNs. (E) Left: Normalized EPSC amplitude during NE application in PV(+) and PV(-) MSN synapses in the NAc core. Right: Quantification of average EPSC amplitude following NE at PV(+) and MSN synapses. (F) Left: Normalized EPSC amplitude during NE application in PV(+) and PV(-) MSN synapses in the NAc core. Right: Quantification of average EPSC amplitude following NE at PV(+) and MSN synapses. (F) Left: Normalized EPSC amplitude during TOM application in PV(+) and PV(-) MSN synapses in the NAc core. Right: Quantification of average EPSC amplitude following TOM at PV(+) and MSN synapses. Error bars indicate SEM. \*  $p < 0.05$

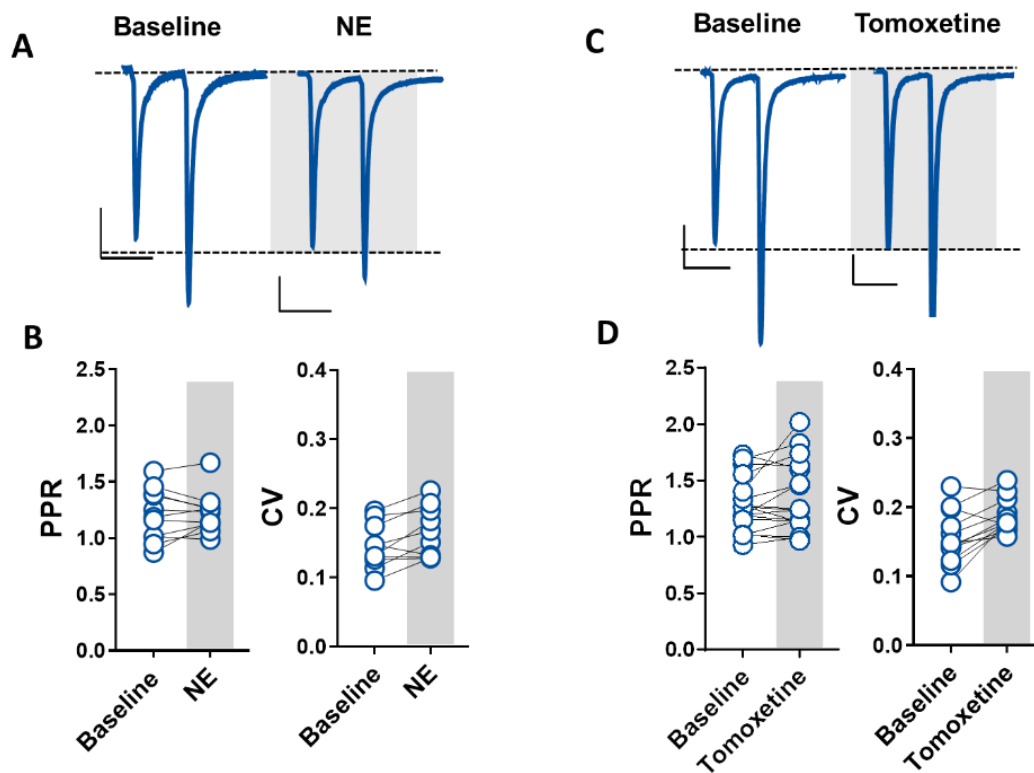


**Figure 5.2. NE and TOM-induced depression in EPSC amplitude in PV(+)-INs in the NAc core-shell interface is putatively postsynaptic.** (A) Representative traces of 50-ms paired pulse EPSCs obtained in PV(+)-INs at baseline and in the presence of NE. (B) Average PPR and CV at baseline and post-NE. (C) Representative traces of 50-ms paired pulse EPSCs obtained in PV(+)-INs at baseline and in the presence of TOM. (D) Average PPR and CV at baseline and post-TOM. No significant differences in PPR and CV is observed at synapses onto PV(+)-INs in the presence of NE or TOM. Error bars indicate SEM. \*  $p < 0.05$

*Blockade of other monoamine reuptake transporters does not alter feedforward transmission onto PV-INs*

Pharmacological blockade of monoamine transporters, including the serotonin transporter (SERT) and dopamine transporter (DAT), is targeted by clinically- and recreationally-used compounds, such as antidepressant medications and cocaine, respectively (Conti et al., 2017). To ensure that the effects of TOM were not due to atypical properties of the drug itself, we bath-applied the tricyclic NET inhibitor, desipramine (10  $\mu$ M), at a concentration with minimal actions at DAT or SERT (Matsui and Alvarez, 2018). Desipramine reproduced the effects of TOM on EPSC amplitude, strengthening data that TOM facilitates NEergic effects at PV-IN synapses (**Fig. 5.3.A-C**, DESIP,  $37.16 \pm 5.05\%$ ,  $n=5$ ,  $p<0.001$ ). We next examined whether this effect was specific to NET blockade by superfusing selective SERT inhibitor, fluoxetine (1  $\mu$ M). SERT-containing 5-HT terminals densely innervate the striatal network, including the NAc. In contrast to TOM, fluoxetine had no appreciable effect on EPSC amplitude (**Fig. 5.3.D-F**, fluoxetine,  $92.84 \pm 3.33\%$ ,  $n=6$ ,  $p=0.065$ ). Moreover, data presented in Chapter 4 indicates that selective inhibition of DAT by GBR 12897 also has no effect at glutamatergic synapses onto PV(+)-INs. Together, these data suggest that selectively inhibiting NE reuptake in the NAc heterosynaptically regulates glutamatergic transmission onto PV-INs in the NAc.

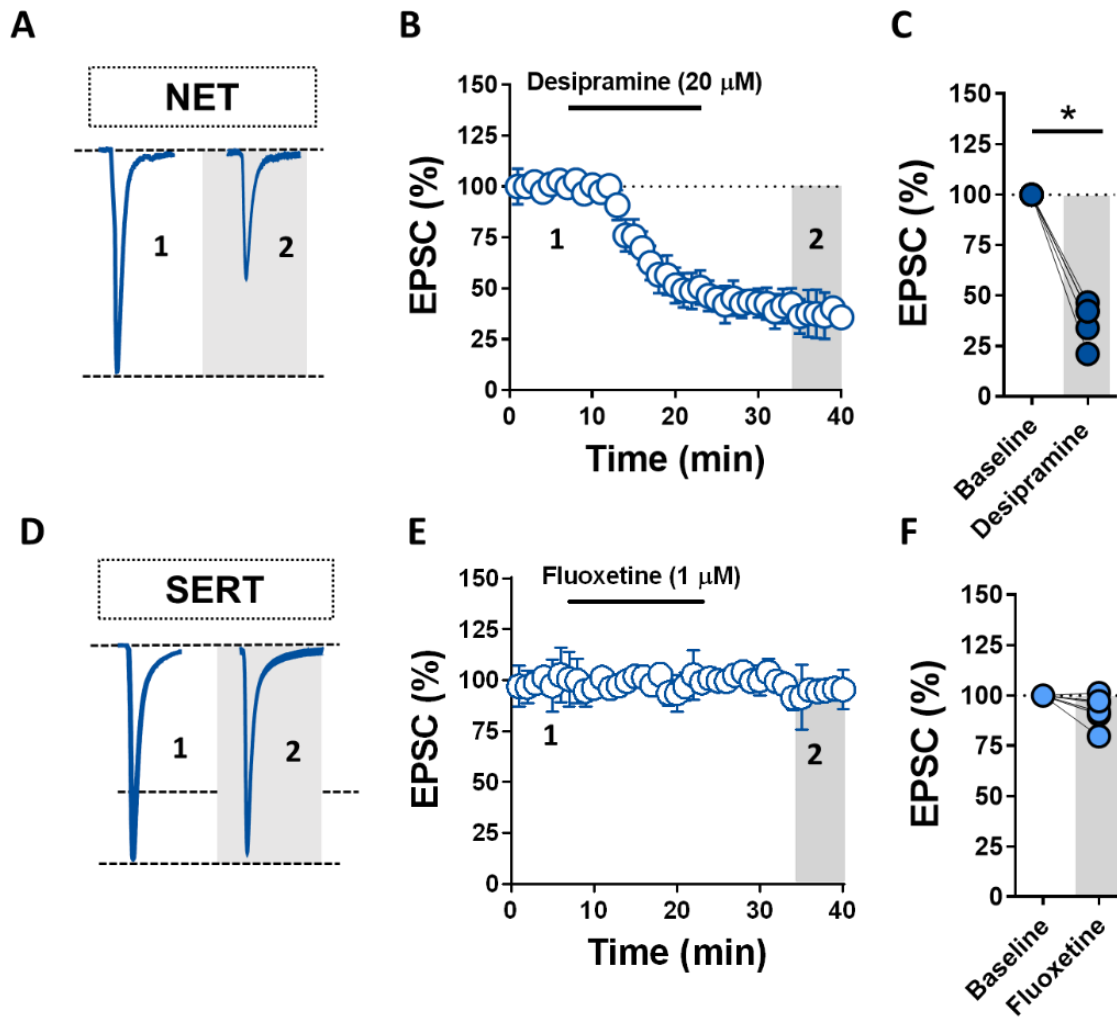


**Figure 5.3. Blocking SERT does not elicit similar effects as NET at glutamatergic synapses onto PV(+)-INs.** (A) Representative traces of EPSCs in PV(+)-INs pre- and post-desipramine application. (B) Normalized EPSC amplitude showing that tricyclic NET inhibitor, desipramine, reproduces the effects of TOM on EPSC amplitude, indicating that the TOM effect is not due to an atypical property of the drug. (C) Quantification of average EPSC amplitude pre- and post-desipramine. (A) Representative traces of EPSCs pre- and post-fluoxetine application. (B) Normalized EPSC amplitude showing that the SSRI antidepressant (SERT inhibitor), fluoxetine, fails to elicit a change in EPSC amplitude at PV(+)-IN synapses, indicating that the effect is specific to NET blockade. (C) Quantification of average EPSC amplitude pre- and post-desipramine. Error bars indicate SEM. \* $p < 0.05$

*β-adrenergic receptor function mediates the effects of norepinephrine signaling on glutamatergic transmission*

To interrogate which class of ARs mediates the effect of NE and TOM at PV-IN synapses, we first bath-applied TOM in the presence of pan- $\alpha$ -AR antagonist, phentolamine (1  $\mu$ M). We elected to use TOM for the remainder of experiments, as TOM-induced NET blockade encourage endogenous NE signaling, mimicking physiological NEergic transmission in the *ex vivo* slice preparation. In addition, NET is a pharmacological target of multiple clinically-used antidepressant medications, including the tricyclic antidepressants (e.g., desipramine,  $K_i = 0.63$ - $3.5$  nM), and is one of many monoamine reuptake transports targeted by cocaine (Owens et al., 1997; Tatsumi et al., 1997). In the presence of phentolamine, the TOM-induced depression in EPSC amplitude was blunted but not blocked (**Fig. 5.4E-G**, TOM + phentolamine,  $58.44 \pm 6.64$ ,  $n=7$ ,  $p=0.301$ ). Consistent with a predominately  $\alpha$ -AR-independent effect, bath-application of selective  $\alpha_2$ -AR agonist, clonidine (10  $\mu$ M), modestly depressed EPSC amplitude, whereas  $\alpha_1$ -AR agonist, phenylephrine (PE, 1  $\mu$ M), had no effect on EPSC amplitude (**Fig. 5.4A-D**, clonidine,  $87.04 \pm 8.81\%$ ,  $n=6$ ,  $p=0.0495$ ; PE,  $97.04 \pm 1.59\%$ ,  $n=6$ ,  $p=0.098$ ). To determine if NEergic signaling at PV-IN synapses instead engages  $\beta$ -AR signaling, TOM was superfused into the ACSF bath in the presence of non-selective  $\beta$ -AR antagonist, propranolol (1  $\mu$ M). Propranolol significantly reduced the TOM-induced decrease in glutamatergic transmission onto PV-INs, indicating that NEergic signaling engages a mixed adrenergic response mediated primarily by  $\beta$ -ARs (data still in progress). Future studies are underway to determine whether NE recruits  $\beta_1$  or  $\beta_2$ -AR isoforms at PV-IN synapses in the NAc.

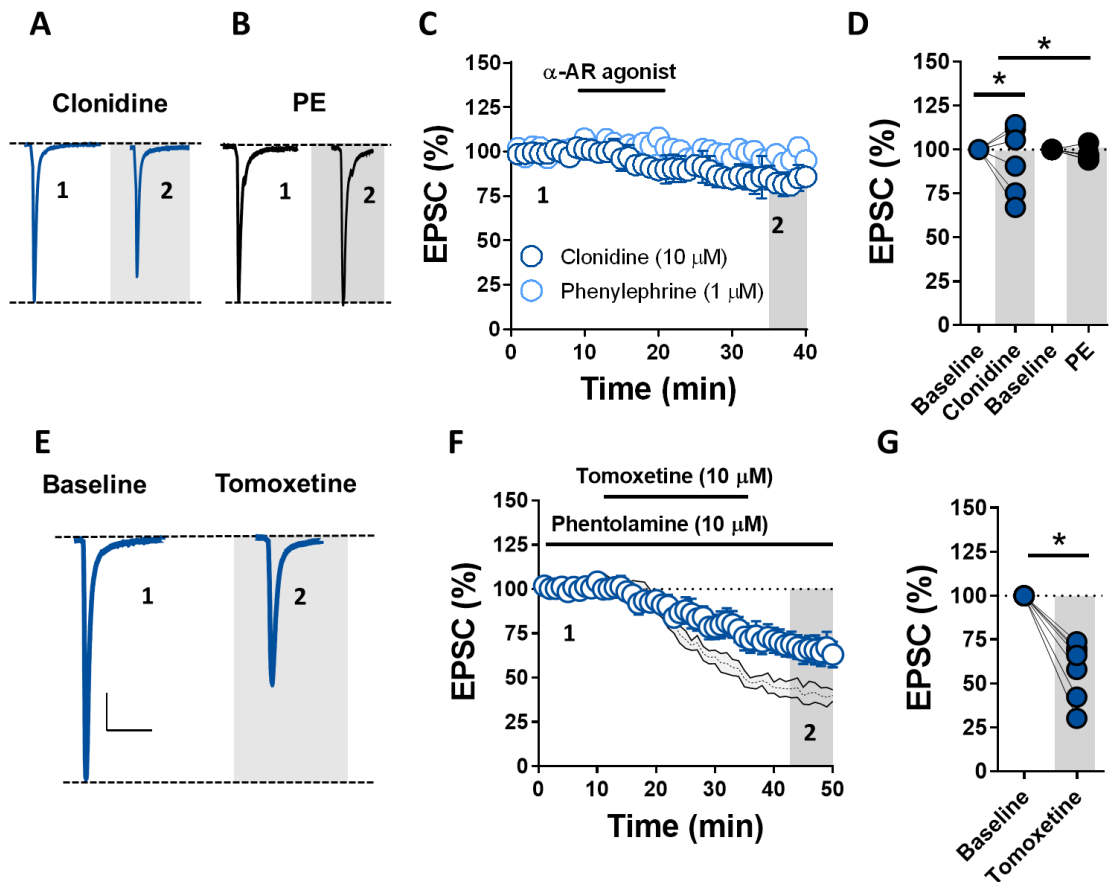


**Figure 5.4. Glutamatergic synapses onto PV(+)-INs are minimally regulated by  $\alpha_1$  and  $\alpha_2$  adrenergic receptors.** (A, B) A: Representative traces of EPSCs obtained from PV(+)-INs at baseline and in the presence of  $\alpha_2$  agonist, clonidine (dark blue). B: Representative traces of EPSCs obtained from PV(+)-INs at baseline and in the presence of  $\alpha_1$  agonist, phenylephrine (PE, black). (C) Normalized EPSC amplitude showing the effects of clonidine and PE. (D) Quantification of average EPSC following bath-application of clonidine and PE. (E) Representative traces of EPSCs at baseline and following TOM in the presence of pan- $\alpha$ -AR antagonist, phentolamine. (F) Normalized EPSC amplitude showing the effects of TOM in the presence of phentolamine. The TOM-induced depression is blunted but clearly not blocked by phentolamine. (G) Quantification of average EPSC following bath-application of TOM in phentolamine. Error bars indicate SEM, \*  $p < 0.05$

*Norepinephrine engages cholinergic interneurons to elicit muscarinic ACh receptor signaling at glutamatergic synapses onto PV-INs*

$\beta$ -ARs are  $G_{\alpha s}$ -coupled GPCRs that increase neuronal excitability in the striatum via cAMP/PKA-dependent intracellular signaling mechanisms (Meitzen et al., 2011). Although  $G_{\alpha s}$ -coupled GPCRs have been shown to reduce neurotransmitter release probability (e.g., presynaptic D1 receptors), we reasoned that NE may be altering other microcircuit elements in the NAc that is being detected at PV-IN synapses (Nicola and Malenka, 1997, 1998). For example, NE signaling shifts cholinergic interneuron (CIN) output in the dorsal striatum via  $\beta_1$ -ARs (Pisani et al., 2003). Therefore, we hypothesized that NE signaling is functioning through a cholinergic intermediary to elicit changes in glutamatergic transmission onto PV-INs. We speculated that NE signaling is increasing spontaneous ACh release from CINs, thereby acting at nAChR or mAChRs on PV-INs. To begin to interrogate this disynaptic mechanism without a CIN-specific reporter line, we first asked whether glutamatergic synapses onto PV-INs are regulated by mAChR signaling. Following a 10-min EPSC baseline, mAChR agonist, oxotremorine (Oxo-M, 10  $\mu$ M) was incorporated into the ACSF bath. Oxo-M application evoked a robust depression in EPSC amplitude that persisted following drug wash-out, suggesting that mAChR induces long-term depression (LTD) (**Fig. 5.5.A-D**, Oxo-M,  $70.97 \pm 5.40\%$ ,  $n=7$ ,  $p<0.001$ ). Additionally, the Oxo-M depression in EPSC amplitude elicited an increase in PPR, indicating that mAChR signaling regulates glutamatergic synaptic strength at PV-IN synapses in the NAc via presynaptic actions due either to presynaptic mAChRs or mAChR-induced retrograde signaling (e.g.,  $CB_1R$ ) (**Fig. 5.5.C**, Oxo-M, PPR baseline =  $1.45 \pm 0.13$ , PPR Oxo-M =  $1.73 \pm 0.18$ ,  $n=7$ ,  $p<0.001$ ).

To determine if mAChR signaling contributes to the TOM-induced decrease in glutamatergic transmission, pan-mAChR antagonist, scopolamine (1  $\mu$ M), was added to the ACSF bath prior to superfusing TOM. Subsequent application of TOM failed to elicit a change in EPSC amplitude (**Fig. 5.5EH**, 1-way ANOVA,  $102.81 \pm 3.93\%$ ,  $n=7$ ,  $p < 0.001$ ). Moreover, prior application of Oxo-M completely occluded the TOM-induced depression in EPSC amplitude (**Fig. 5.5FH**, 1-way ANOVA,  $97.39 \pm 3.98\%$ ,  $n=4$ ,  $p=0.002$ ). At glutamatergic synapses onto MSNs in the NAc, M1 mAChR activation triggers retrograde eCB signaling onto presynaptic CB<sub>1</sub>Rs (Neuhofer et al., 2018). To determine if CB<sub>1</sub>R activity contributes to the expression mechanism elicited by TOM-induced NE signaling and the PPR shift following Oxo-M, slices were first pre-incubated in CB<sub>1</sub>R inverse agonist, AM251 (2-5  $\mu$ M). Prior application of AM251 also completely blocked the TOM-induced depression in glutamatergic transmission onto PV-INs (**Fig. 5.5FH**, 1-way ANOVA,  $93.56 \pm 5.09\%$ ,  $n=4$ ,  $p=0.009$ ). Together, these data suggest that NE acts on CINs, which triggers eCB release via mAChRs on PV-INs. (**Fig. 5.5E-H**, 1-way ANOVA, ACSF vs. drug interaction,  $F(3, 18) = 11.96$ ,  $p < 0.001$ )

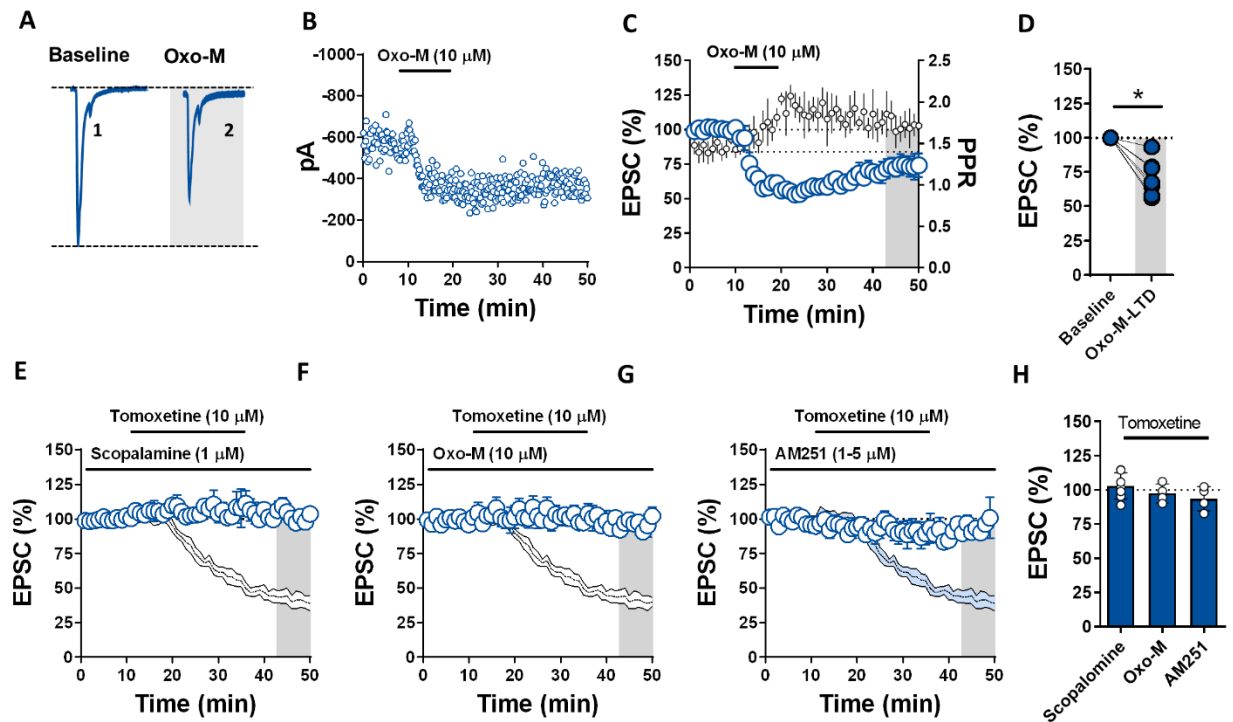


**Figure 5.5. The NEergic effects on PV-INs may be due to microcircuit alterations in cholinergic signaling.** (A, B) A: Representative traces of EPSCs obtained from PV(+)-INs at baseline and in the presence of pan-mAChR agonist, oxotremorine (Oxo-M). B: Representative experiment depicting the effect of Oxo-M on EPSC amplitude. (C) Normalized EPSC amplitude showing the effects of Oxo-M on EPSC amplitude (left Y axis) and PPR (open white circles). PPR is increased during Oxo-M application that returns to baseline during LTD timepoint. (D) Quantification of average EPSC following bath-application of Oxo-M (E) Normalized EPSC amplitude showing the effects of TOM in the presence of mAChR antagonist, scopolamine. (F) Occlusion: Normalized EPSC amplitude showing the effects of TOM in the presence of Oxo-M. (G) Normalized EPSC amplitude showing the effects of TOM in the presence of CB1 inverse agonist, AM251. (H) Summary graph depicting average EPSC amplitude following TOM application in the presence of various pharmacological manipulations. Error bars indicate SEM. \*  $p < 0.05$

Utilizing Cre-inducible transgenic male reporter mice, whole-cell patch-clamp electrophysiology, and targeted pharmacological manipulations, our preliminary data indicates that exogenous NE application and norepinephrine transporter (NET) blockade negatively regulates glutamatergic transmission onto PV-INs but not MSNs. Although we do not rule out direct synaptic actions at feedforward synapses onto PV-INs, we find that the actions of NE may be mediated, in part, by ARs on tonically-active cholinergic interneurons (CINs). Specifically, these findings encourage the hypothesis that NET blockade modulates tonic cholinergic transmission in the NAc, leading to mAChR activation on PV-INs. As the synaptic mechanisms regulating NE transmission at feedforward PV-IN synapses become better delineated, the next steps in this project are to (1) explore behavioral adaptations evoked by intra-NAc NE transmission and (2) utilize anatomical tracing methods to characterize which brainstem nuclei target NAc microcircuits.

These data provide functional evidence that NE signaling in the NAc engages PV-IN-embedded feedforward inhibitory microcircuits without concomitantly modulating glutamatergic synapses onto MSNs. This finding is striking, as the modest NEergic innervation pattern in the NAc core and shell, minimal NEergic tone in the NAc at baseline, and robust behavioral effects of other catecholamine systems have diverted research into how NE regulates NAc circuit function. Furthermore, blocking NE reuptake with TOM, which should theoretically increase NE content throughout the NAc, *only* affected synapses onto PV-INs, strongly supporting the hypothesis that NEergic transmission is engaging microcircuit-specific synaptic mechanisms. These preliminary data offer promising evidence that NEergic transmission in the NAc elicits microcircuit-specific

adaptations at a dual PV-CIN motif embedded within feedforward inhibitory networks. Future behavioral and anatomical studies are needed to discern the behavioral relevance of NEergic signaling in the NAc and identify which NE-containing afferents target the NAc, with emphasis placed on projections originating from the NTS.

While these studies begin to elucidate the disynaptic mechanism by which NE modulates PV-IN synapses in the NAc, several important gaps remain. Most notably, we presently have no direct evidence that NE augments CIN output in a  $\beta$ -AR-dependent manner. Preliminary blind cell-attached recordings of putative CINs, identified by large, elongated somata with tonic, rhythmic AP firing patterns, indicate that NE + TOM co-application dramatically changes CIN firing (Kawaguchi, 1993; Tepper et al., 2018). However, these experiments await replication in ChAT<sup>Cre</sup>-tdTomato<sup>fl/fl</sup> mice to ensure that prior experiments in unlabeled CINs are reproducible. Additionally, a CIN circuit mechanism should be corroborated with spontaneous EPSC and TTX-insensitive mESPC measurements, as NE-induced ACh release should be abolished in TTX-containing *ex vivo* recording conditions. Furthermore, if CIN-evoked ACh release is acting at PV-IN synapses, the TOM- and NE-induced depression in EPSC amplitude would likely be enhanced in the presence of an acetylcholinesterase (AChE) inhibitor, such as physostigmine. To ascertain whether AR or mAChR signaling is occurring within PV-INs and/or presynaptic elements, future experiments should also be performed using an intracellularly-confined GPCR disabling agent, such as the non-hydrolyzable GDP analog, GDP $\beta$ S.

The prospect of a PV-CIN motif within the NAc points to a broader organizational theme in which distinct interneuron subtypes communicate with one another. Although examined in the context of

NE, a more impactful question is whether the PV-CIN circuit interaction is generalizable to other neuromodulators targeting CINs, such as the recently described actions of corticotropin-releasing factor (CRF) on CIN output (Lemos et al., 2019). Given that NE signaling is associated with stress-evoked arousal strategies, it is possible that a CIN-directed reduction in feedforward transmission leads to an adaptive desynchronization of behavioral output. NE signaling via CINs may authorize an escape from feedforward inhibition, leading to a generalized increase in appetitive behavioral output. If correct, this mechanism centralizes CINs within NAc microcircuitry to exert manifold control over how information is propagated through the mesolimbic reward network. Alongside behavioral pharmacology experiments, it will be fascinating to discern the functional implications of NE signaling in the NAc and how and *why* noradrenergic inputs to the NAc selectively regulate feedforward transmission.

## 5.2. State-dependent inhibitory synaptic plasticity at feedforward inhibitory synapses in the nucleus accumbens core

In the NAc, PV-INs are the only intrinsic neuron type to express CB<sub>1</sub>R, the cognate receptor for endogenous cannabinoids (eCBs) in the central nervous system (CNS) (Winters et al., 2012; Wright et al., 2017). CB<sub>1</sub>R is a presynaptic G<sub>i/o</sub>-coupled GPCR that decreases neurotransmitter release probability through various intracellular effectors, including decreased Ca<sup>2+</sup> influx via N- and P/Q-type voltage-gated Ca<sup>2+</sup> channels and opening of inward-rectifying K<sup>+</sup> channels (Hoffman and Lupica, 2001; Chevaleyre et al., 2006; Augustin and Lovinger, 2018). eCBs, such as 2-arachidonylglycerol (2-AG) and anandamide (AEA), are mobilized on-demand from postsynaptic neurons and travel retrogradely across the synapse where they act on CB<sub>1</sub>R (Cohen et al., 2019). At GABAergic synapses, CB<sub>1</sub>R activation reduces release probability at short and long time-

scales, referred to as depolarization-induced suppression of excitation or inhibition (DSI) and long-term depression (iLTD), respectively (Heifets et al., 2008; Turner et al., 2018a). While functional consequences of CB<sub>1</sub>R on PV-INs have yet to be reported, inhibitory synaptic plasticity at PV-IN-to-MSN synapses may serve as a gain control mechanism regulating information flow through the NAc.

CB<sub>1</sub>R has been extensively implicated in addiction-related behavioral adaptations. Systemic administration of WIN 55-212, a potent CB<sub>1/2</sub>R agonist, has been shown to have rewarding properties, while CB<sub>1</sub>R antagonists, such as rimonabant, have been used clinically to treat addiction-related conditions in patients (Houchi et al., 2005; Martín-García et al., 2016). *In vivo* drug exposure has been shown to alter eCB-dependent plasticity mechanisms in the NAc, an effect mediated by the intracellular sequestration of the group I metabotropic glutamate receptor, mGluR5 (Knackstedt et al., 2010; Huang et al., 2011, 2015a). Single exposure to cocaine abolishes eCB-dependent LTD of glutamatergic inputs onto D2 [D1(-)] MSNs, potentially through a similar mechanism (Szumlinski et al., 2008; Grueter et al., 2010). In addition, acute systemic  $\Delta^9$ -THC exposure abolishes eCB-LTD in the NAc by desensitizing CB<sub>1</sub>R activity at presynaptic terminals (Mato et al., 2004). While these data suggest that eCB signaling in the NAc contributes to behavioral states associated with drugs of abuse, no studies have specifically examined how CB<sub>1</sub>R signaling within PV-IN microcircuits regulates functional NAc output.

MSNs in the NAc are quiescent GABAergic projection neurons that oscillate between “up” (-60 mV) and “down” (-80 mV) membrane states, as described previously (Chapters 1-3). MSN spiking activity requires coincident glutamatergic input to transition from their downstate at -80 mV to

their upstate at -60 mV (Plenz and Kitai, 1998; Kreitzer and Malenka, 2005; Plotkin et al., 2011). In the dorsal striatum, MSN membrane state dictates which synapses undergo inhibitory long-term depression (iLTD) and the subcellular processes which subserve this process. Specifically, a 1 Hz, 80-sec low-frequency stimulation (LFS) protocol elicits CB<sub>1</sub>R-dependent iLTD of PV-IN-to-D1 MSN synapses when MSNs are voltage clamped in their downstate at -80 mV. This form of plasticity is insensitive to tetrahydrolipstatin (THL), a potent inhibitor of the 2-AG synthetic enzyme, diacylglycerol lipase (DAGL), indicating that it is putatively mediated by AEA. However, lateral inhibition at MSN-to-MSN synapses undergo iLTD when MSNs are voltage-clamped in either membrane state (Mathur et al., 2013).

Few studies in the NAc have examined whether GABAergic synapses, particularly PV-IN-to-MSN feedforward synapses, undergo activity-dependent iLTD. An earlier study in the NAc shell indicates that putative PV-IN-to-MSN synapses undergo LFS-induced iLTD when MSNs are clamped in their upstate but not in their downstate (Wright et al., 2017). Unlike the dorsal striatum, the expression of iLTD at these synapses requires pre- and postsynaptic CB<sub>1</sub>R and TRPV1 activity, respectively (Wright et al., 2017). Given that TRPV1-mediated LTD at glutamatergic synapses onto D2 MSNs in the NAc is AEA-dependent, multiple eCBs likely mediate upstate iLTD at PV-IN-to-MSN synapses. More recently, it was shown that local GABAergic synapses onto D1 and D2 MSNs undergo downstate CB<sub>1</sub>R-independent iLTD mediated by brain-derived neurotrophic factor (BDNF) at postsynaptic TrkB receptors (Patton et al., 2019). Interestingly, both studies utilize electrical stimulation to induce iLTD, indicating that both glutamate-dependent and independent circuit mechanisms are being recruited in the induction process. Nevertheless, several important mechanistic questions remain: (1) is local field stimulation necessary to evoke iLTD at

PV-IN-specific and -nonspecific GABAergic synapses onto MSNs? (2) is upstate iLTD expressed at both MSN subtypes? (3) if glutamatergic synapses onto MSNs undergo 2-AG and AEA-dependent LTD and GABAergic synapses undergo CB<sub>1</sub>R- and TRPV1-dependent iLTD, which physiological events dictate which synapses are targeted by eCBs? Answering these questions will improve our understanding of how feedforward inhibition in the NAc may be targeted during salient behavioral experiences, such as stress and drug use.

We asked if GABAergic transmission at PV-IN-to-D1(+) and D1(-) MSNs in the NAc core undergo state-dependent iLTD. To address this question, we bred triple transgenic PV<sup>Cre</sup>-ChR2<sup>fl/fl</sup>-D1tdTomato mice to gain optogenetic access to PV-INs in the NAc (Manz et al., 2019). This strategy allows synaptic plasticity events to be surveyed at most synaptically-connected feedforward synapses in the NAc, rather than a single PV-IN-to-MSN synapse sampled via paired unitary recordings. So far, our findings suggest that homosynaptic LFS (1 Hz, 80-sec)-induced iLTD is expressed in a cell type- *and* state-dependent manner. Whereas PV-IN-to-D1(+) MSN synapses undergo downstate iLTD, PV-IN-to-D1(-) MSN synapses undergo upstate iLTD, with neither synapse exhibiting both up- and downstate forms of plasticity. Utilizing PV-IN-specific CB<sub>1</sub>R conditional knockout mice (PV<sup>Cre</sup>-Cnr1<sup>fl/fl</sup>), we found that both up- and downstate iLTD is CB<sub>1</sub>R-independent, deviating from a previous report that upstate iLTD is partially mediated by CB<sub>1</sub>R. Furthermore, up- and downstate iLTD at D1(-) and D1(+) MSN synapses is GABA<sub>B</sub>R-independent. Alongside a complete synaptic profile of PV-IN-to-MSN synapses in the NAc, the mechanism underlying state-dependent iLTD at PV-IN synapses in the NAc continues to be thoroughly examined. Understanding the dynamic processes by which these synapses undergo

activity-dependent changes in synaptic strength will inform how signal propagation through the NAc is regulated by distinct microcircuits.

*Voltage state directs MSN subtype-specific plasticity at feedforward inhibitory synapses in the NAc core*

To determine if PV-IN-to-D1(+) and D1(-) MSNs undergo membrane voltage state-dependent plasticity, we performed whole-cell voltage clamp recordings in D1(+) and D1(-) MSNs of transgenic PV<sup>Cre</sup>-Chr2<sup>fl/fl</sup>-D1tdTomato mice. Optically (473 nm LED)-evoked IPSCs (oIPSCs) from Chr2-expressing PV-INs in the NAc were recorded from D1(+) and D1(-) [putative D2] MSNs in the NAc core at -70 mV. Congruent with previous work from our lab using this mouse line, oIPSCs obtained in D1(+) and D1(-) MSNs were abolished by picrotoxin (50  $\mu$ M), indicating that GABAergic transmission at PV-IN-to-MSN synapses is GABA<sub>A</sub>R-mediated. Furthermore, optical excitation of Chr2(+) cells at 20 Hz in current-clamp mode elicited high-frequency AP firing, consistent with the fast-spiking biophysical profile of PV-INs in the NAc (data not shown). Following a stable 10-min oIPSC baseline in D1(+) MSNs, LFS was delivered while voltage clamping cells in their up- (-60 mV) or downstate (-80 mV). When D1(+) MSNs were held in their upstate, LFS failed to alter oIPSC amplitude throughout the 40-min recording period (**Fig. 5.7.A-D**, D1(+) -60 mV, 59.74 $\pm$ 7.69%, n=9, p<0.001). However, LFS delivered when D1(+) MSNs were held in their downstate resulted in a significant decrease in oIPSC amplitude (**Fig. 5.6.A-D**, D1(+) -80 mV, 100.43 $\pm$ 4.38%, n=7, p=0.449). To determine if voltage state also gates the expression of iLTD at D1(-) MSNs, we replicated these experiments in D1(-) MSNs. Surprisingly, when D1(-) MSNs were clamped in their upstate but not downstate (**Fig. 5.7.A-D**, D1(-) -60 mV, 62.78 $\pm$ 2.59%, n=6, p<0.001), LFS resulted in a significant reduction in oIPSC amplitude (**Fig. 5.6.A-D**, D1(-) -

80 mV,  $91.86 \pm 7.46\%$ ,  $n=8$ ,  $p=0.113$ ). LFS-induced iLTD did not significantly shift CV in D1(+) or D1(-) MSNs at -80 mV and -60 mV, respectively (**Fig. 5.6-5.7E**, D1(+) -80 mV, CV pre-LFS =  $0.071 \pm 0.01$ , CV post-LFS =  $0.063 \pm 0.02$ ,  $n=8$ ,  $p=0.454$ ; D1(-) -60 mV, CV pre-LFS =  $0.062 \pm 0.017$ , CV post-LFS =  $0.08 \pm 0.02$ ,  $n=7$ ,  $p=0.159$ ). The data suggest that downstate-iLTD is expressed at D1(+) MSNs, whereas upstate-iLTD is expressed at D1(-) MSNs, indicating that voltage state *and* MSN subtype dictates the expression of inhibitory synaptic plasticity at PV-IN-to-MSN synapses in the NAc core.

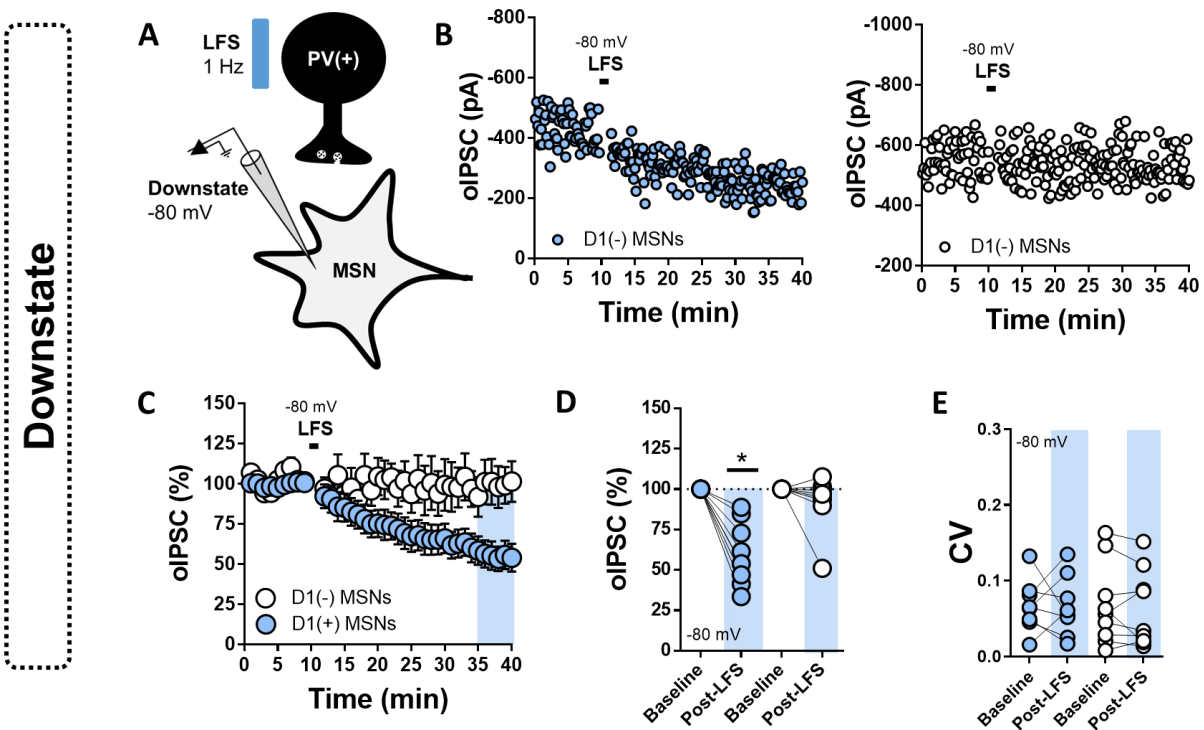


**Figure 5.6. Downstate iLTD at PV-IN-to-MSN synapses is restricted to D1(+) MSNs.** (A) Schematic depicting homosynaptic recording strategy at PV-to-D1(+) and D1(-) MSN synapses in the NAc core. (B) Representative experiments in D1(+) [blue circles] and D1(-) MSNs [open circles] showing that LFS (1 Hz, 80-sec) induces iLTD at D1(+) but not D1(-) MSNs when MSNs are voltage clamped in the downstate (-80 mV) during the induction protocol. (C) Normalized oIPSC amplitude in D1(+) and D1(-) MSNs clamped in the downstate. (D) Average oIPSC amplitude pre- and post-LFS in both MSN subtypes. (E) CV assessed pre- and post-LFS in D1(+) and D1(-) MSNs. Error bars indicate SEM. \*  $p < 0.05$

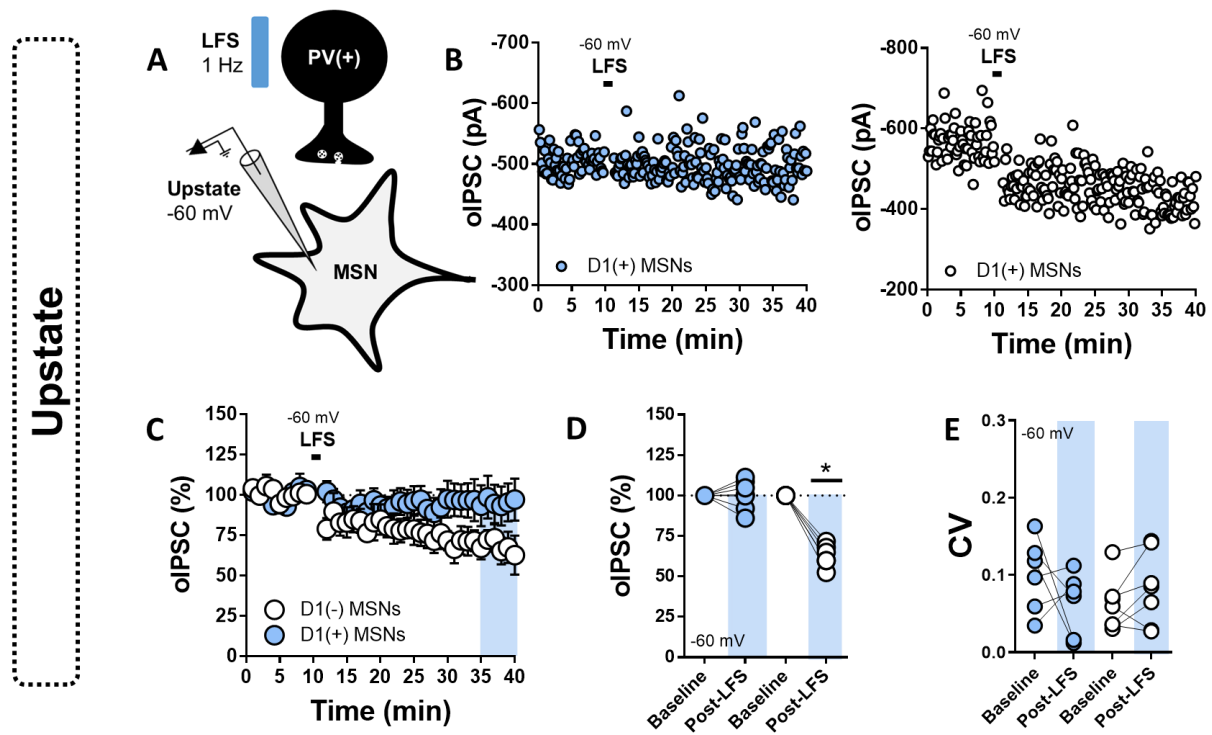


**Figure 5.7. Upstate iLTD at PV-IN-to-MSN synapses is restricted to D1(-) MSNs.** (A) Schematic depicting homosynaptic recording strategy at PV-to-D1(+) and D1(-) MSN synapses in the NAc core. (B) Representative experiments in D1(+) [blue circles] and D1(-) MSNs [open circles] showing that LFS (1 Hz, 80-sec) induces iLTD at D1(-) but not D1(+) MSNs when MSNs are voltage clamped in the upstate (-60 mV) during the induction protocol. (C) Normalized oIPSC amplitude in D1(+) and D1(-) MSNs pre- and post-LFS induction when clamped in the upstate. (D) Average oIPSC amplitude pre- and post-LFS in both MSN subtypes. (E) CV assessed pre- and post-LFS in D1(+) and D1(-) MSNs. Error bars indicate SEM. \*  $p < 0.05$

*State-dependent plasticity at feedforward inhibitory synapses is CB<sub>1</sub>R- and GABA<sub>B</sub>R-independent*

We next interrogated the synaptic mechanism underlying iLTD at D1(+) and D1(-) MSN synapses in the NAc. Given that previous reports suggest that upstate-dependent iLTD requires presynaptic CB<sub>1</sub>R, we tested this possibility by crossing PV<sup>Cre</sup>-ChR2<sup>fl/fl</sup>-D1tdTomato mice with conditional *Cnr1*(CB<sub>1</sub>)<sup>fl/fl</sup> mice, resulting in PV<sup>Cre</sup>-ChR2<sup>fl/fl</sup>-*Cnr1*<sup>fl/fl</sup>-D1tdTomato mice (PV<sup>CB1-/-</sup>). To functionally validate that CB<sub>1</sub>R expression is downregulated in these mice, we bath-applied CB<sub>1/2</sub>R agonist, WIN 55-212 (1 μM), in PV<sup>CB1-/-</sup> and PV<sup>Cre</sup>-negative litter-mate control mice. WIN 55-212 elicited a robust depression of IPSC amplitude in MSNs (pooled) that was absent in PV<sup>CB1-/-</sup> mice (data not shown). Interestingly, LFS-induced downstate iLTD in D1(+) MSNs remained completely intact in PV<sup>CB1-/-</sup> mice, as did LFS-induced upstate iLTD in D1(-) MSNs, indicating that homosynaptic iLTD at these synapses is CB<sub>1</sub>R-independent (**Fig. 5.8BE**, D1(+) PV<sup>CB1-/-</sup>, 59.47±10.9%, n=7, p=0.755; D1(-) PV<sup>CB1-/-</sup>, 63.81±9.19%, n=6, p=0.889). We next asked if LFS is mediated by GABA<sub>B</sub>R autoreceptors, though previous work from our lab suggests that only a small subset of PV-IN-to-D1(+) and D1(-) MSN synapses undergo presynaptic GABA<sub>B</sub>R-induced LTD. Furthermore, CV post-LFS remained unchanged during both up- and downstate iLTD, indicating that the expression of this plasticity is likely postsynaptic whereas GABA<sub>B</sub>R function in the NAc is mostly presynaptic (Uchimura and North, 1991; Manz et al., 2019). Nevertheless, a subset of PV-IN synapses sensitive to GABA<sub>B</sub>R activity may be contributing to this mechanism. To test this possibility, upstate and downstate iLTD at D1(-) and D1(+) MSN synapses, respectively, was assessed in the presence of selective GABA<sub>B</sub>R antagonist, SCH 50911 (5 μM). Blockade of GABA<sub>B</sub>R also had no effect on the expression of iLTD at D1(+) and D1(-) MSN synapses (**Fig. 5.8BE**, D1(+) GABA<sub>B</sub>R, 49.56±18.93%, n=4, p=0.369; D1(-) GABA<sub>B</sub>R, 63.85±15.97%, n=3, p=0.883). Together, these data suggest that state-dependent iLTD at PV-IN

synapses onto both MSN subtypes is CB<sub>1</sub>R- and GABA<sub>B</sub>R-independent. *Note:* experiments investigating the role of GABA<sub>B</sub>R are what ultimately led to the project in **Chapter 2**.

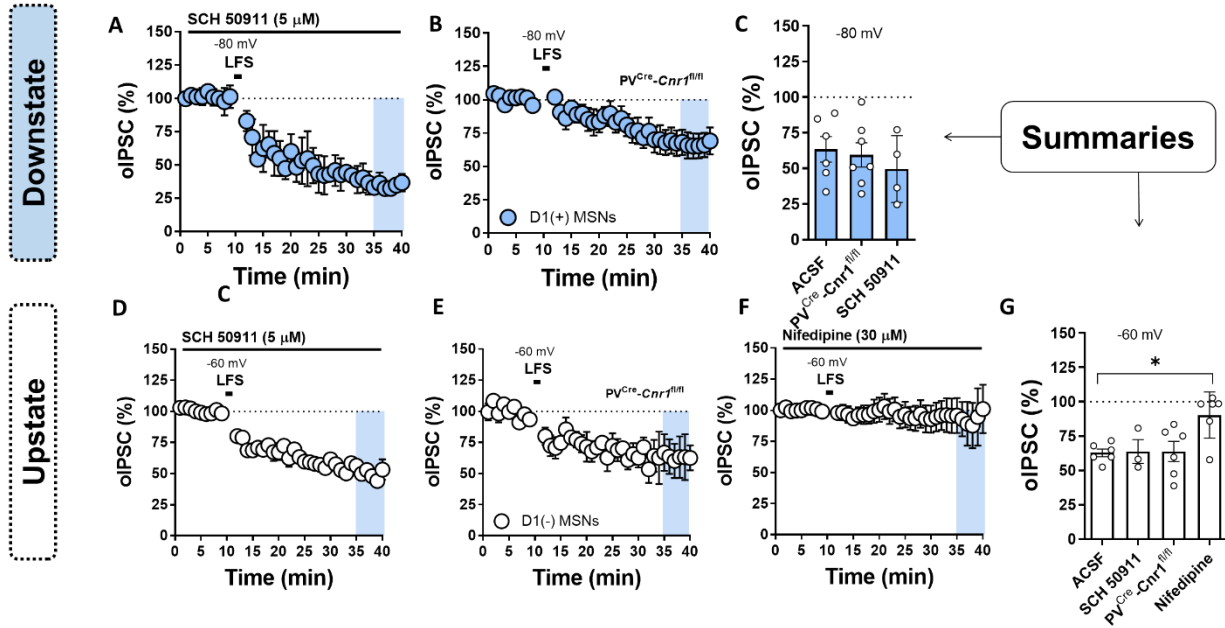


**Figure 5.8. State dependent iLTD at PV-IN-to-D1(+) and D1(-) MSN synapses is CB<sub>1</sub>R- and GABA<sub>B</sub>R-independent.** (A) Normalized oIPSC amplitude pre- and post-LFS in D1(+) MSNs elicited in the presence of GABA<sub>B</sub>R antagonist, SCH 50911, when clamped in their downstate. (B) Normalized oIPSC amplitude pre- and post-LFS elicited in D1(+) MSNs of PV-conditional CB<sub>1</sub>R knockout mice (PV<sup>Cre</sup>-Cnr1<sup>fl/fl</sup>) clamped in their downstate. (C) Average oIPSC amplitude following each manipulation at PV-IN-to-D1(+) MSN synapses. (D) Normalized oIPSC amplitude pre- and post-LFS in D1(-) MSNs elicited in the presence of GABA<sub>B</sub>R antagonist, SCH 50911, when clamped in their downstate. (E) Normalized oIPSC amplitude pre- and post-LFS elicited in D1(-) MSNs of PV-conditional CB<sub>1</sub>R knockout mice (PV<sup>Cre</sup>-Cnr1<sup>fl/fl</sup>) clamped in their downstate. (F) Normalized oIPSC amplitude pre- and post-LFS in D1(+) MSNs elicited in the presence of L-type voltage-gated Ca<sup>2+</sup> channel antagonist, nifedipine, when clamped in their downstate (G) Average oIPSC amplitude following each manipulation at PV-IN-to-D1(-) MSN synapses. Error bars indicate SEM. \* p < 0.05

Transitioning MSN membrane state to a depolarized potential (-60 mV) is sufficient to activate L-type voltage-gated  $\text{Ca}^{2+}$  channels (L-type VGCCs) (Mathur et al., 2013; Augustin et al., 2018). Therefore, we hypothesized that upstate iLTD at PV-IN-to-D1(-) MSN synapses is dependent on L-type VGCCs. To test this hypothesis, we repeated experiments in the presence of selective L-type VGCC antagonist, nifedipine (30  $\mu\text{M}$ ). Nifedipine blocked the LFS<sub>-60 mV</sub>-induced decrease in oIPSC amplitude, indicating that  $\text{Ca}^{2+}$  entry via postsynaptic L-type VGCCs likely contributes to the induction of this plasticity at PV-IN-to-D1(-) MSN synapses (**Fig. 5.8FG**, D1(-) L-type VGCCs,  $90.29 \pm 9.18\%$ ,  $n=6$ ,  $p=0.004$ ). In contrast, preliminary data suggests that prior application of nifedipine had no effect on the expression of downstate iLTD at D1(+) MSN synapses, consistent with a depolarization-induced activation of L-type VGCCs when MSNs are held in their upstate (data in progress).

While these data only rule out candidate effectors contributing to this plasticity, it diverges from previous publications in several ways. First, our findings indicate that the expression of state-dependent iLTD is dictated by specific MSN subtypes, with PV-IN-to-D1(-) MSNs undergoing upstate iLTD and D1(+) MSNs undergoing downstate iLTD. Previous work using a heterosynaptic induction protocol (i.e., LFS delivered via local electrical stimulation) suggests that downstate iLTD is expressed at D1(+) and D1(-) MSN synapses via postsynaptic TrkB receptors, whereas upstate iLTD only occurs if intracellular  $\text{Ca}^{2+}$  is chelated (Patton et al., 2019). Although this study coincides with our data that iLTD is fundamentally  $\text{CB}_1\text{R}$ -independent, it is clear that homosynaptically activating GABAergic PV-IN-to-MSN synapses elicits distinct plasticity mechanisms. It is our overall objective that characterizing state-dependent plasticity at PV-IN

GABAergic synapses in the NAc will improve our understanding of ways in which feedforward synapses undergo changes in synaptic strength.

To our knowledge, no studies have examined the functional relevance of state-dependent plasticity at striatal feedforward synapses. Furthermore, it is unknown under which circuit conditions this form of iLTD would be recruited. One possibility is that afferent glutamatergic input targeting the D1(+) MSN pathway is sustained by simultaneously reducing cell type-specific GABAergic input from PV-INs. A reduction in inhibitory transmission at PV-IN-to-D1(+) MSNs without affecting PV-IN-to-D1(-) MSN synapses would theoretically increase the excitatory-inhibitory (E/I) balance at D1(+) MSNs, thereby driving D1(+) MSN output to nuclei in the VP and/or VTA. When glutamatergic transmission in the NAc is recruited acutely following experience, MSNs will undergo probabilistic shifts to the upstate, which would release the gate at PV-IN-to-D1(-) MSN synapses (Plenz and Kitai, 1998). Congruent with an activity-dependent switch in D1(+)/D1(-) MSN output mediated by PV-IN synapses, optical stimulation of PV-INs at 20 Hz increases cFos mRNA expression only in D1(+) MSNs (Chen et al., 2019).

It is worth arguing that retrofitting the mechanism described here into a coherent circuit model may be inappropriate. This stems from a decades-long argument that the electrophysiological protocols used to study synaptic plasticity in the brain *ex vivo* are also operating *in vivo* (Malenka and Bear, 2004). For example, is iLTD occurring in the NAc when PV-INs are briefly entrained at 1 Hz, or is this an induction protocol designed simply to study plasticity mechanisms at this synapse? Both possibilities have merit that are difficult to disentangle from one another. Established induction protocols delivered *in vivo* to specific glutamatergic afferents to the NAc

can mitigate specific relapse behaviors to drugs of abuse. Whereas LTD at vHipp-to-NAc synapses reduces cue-induced reinstatement of cocaine-seeking, a similar protocol applied to MDT-to-NAc synapses reduces behavioral adaptations associated with naloxone-precipitated morphine withdrawal (Zhu et al., 2016; LeGates et al., 2018). Thus, the physiological mechanisms observed *ex vivo* can have specific behavioral consequences with potential translational utility. Nevertheless, demonstrating that specific effector systems underlie synaptic plasticity in an awake, behaving organism is a daunting task requiring molecular detection systems not-yet available.

An intriguing possibility arising from these data is whether upstate-dependent iLTD at PV-IN-to-D1(-) MSN synapses accompanies other plasticity mechanisms restricted to D1(-) MSNs. At local glutamatergic synapses onto D2-GFP(+) [D1(-)] MSNs, LFS (5-min, 10 Hz) triggers LTD mediated by retrograde and autocrine eCB signaling at CB<sub>1</sub>R and TRPV1 receptors, respectively (Grueter et al., 2010). Furthermore, unpublished work from our lab (Chapter 4) suggests that the same LFS induction protocol triggers CP-AMPA-dependent LTD at glutamatergic synapses onto PV-INs. While not explicitly tested, afferent glutamatergic input to the NAc may be sufficient to depolarize D1(-) MSNs to the upstate, thereby permitting iLTD to occur at PV-IN-to-D1(-) MSN synapses. Therefore, one possibility is that the expression of iLTD at D1(-) MSNs allows D1(-) MSNs to maintain E/I balance within a defined physiological range. More studies are clearly needed to elucidate the functional basis of iLTD within NAc microcircuits.

5.3 Assembling a model of plasticity mechanisms regulating intrinsic and extrinsic network function in the NAc

Despite extensive research conducted on the circuit and synaptic mechanisms underlying NAc-dependent reward behavior, remarkably little attention has been paid to interneuron-enriched microcircuits in the NAc. This is particularly surprising given the broad regulatory influence each interneuron subtype has on NAc circuit output and the disproportionate work done on interneurons in other cortical and subcortical structures. However, biotechnology facilitating the study of defined neuronal subtypes has only recently become accessible and easily implemented. As the physiological relevance of these interneuron populations become increasingly evident, it is my hope that potential therapeutic avenues for the treatment of maladaptive motivational disorders, such as addiction, depression, schizophrenia, autism, and chronic pain syndromes, will target interneuron-contingent neuromodulatory mechanisms.

The work presented in previous chapters and subsections herein provide several significant contributions to our understanding of NAc microcircuits. First, GABA<sub>B</sub>R is expressed throughout the striatal and mesolimbic reward networks, yet few studies have examined the physiological relevance of GABA<sub>B</sub>R outside of slow inhibitory transmission at symmetrical synapses in the VTA. Data presented in Chapter 3 indicate that presynaptically-expressed GABA<sub>B</sub>R on glutamatergic inputs to the NAc represent a novel target within PV-IN-directed feedforward inhibitory microcircuits. In addition to monosynaptic GABA<sub>A</sub>R-mediated inhibitory synapses onto D1(+) and D1(-) MSNs, PV-INS, when recruited at a relatively low-frequency (30 Hz) for fast-spiking PV-INS, can lead to a rise in extracellular GABA that targets GABA<sub>B</sub>R on glutamate terminals in the NAc core. This finding is conceptually challenging, as PV-IN-to-MSN synapses frequently target proximal somatodendritic sites on MSNs, whereas distal glutamate synapses are oriented radially around the dendritic sphere (Yu et al., 2017; Assous and Tepper, 2019). A

GABA<sub>B</sub>R-dependent arm to feedforward inhibition not only increases the inhibitory control PV- INs exert on activity-driven MSN output, but also significantly prolongs the timescale during which PV-INs can regulate excitatory input onto MSNs in the NAc. Furthermore, presynaptic GABA<sub>B</sub>R function is frequently used as a control in experimental manipulations of presynaptic G<sub>i/o</sub>-GPCR signaling, such as presynaptic KORs on BLA terminals and D2 receptors on A2a-expressing MSNs (Dobbs et al., 2016; Tejada et al., 2017). Using GABA<sub>B</sub>R as a control requires the assumption that GABA<sub>B</sub>R in the NAc functions through conventional effector systems, such as the inhibition of presynaptic voltage-gated Ca<sup>2+</sup> channels (VGCCs) (Uchimura and North, 1991; Solís and Nicoll, 1992; Li et al., 2016). However, we find that GABA<sub>B</sub>R elicits a robust depression in glutamatergic transmission that is VGCC, AC/cAMP/PKA, mGluR, and Kir-independent, indicating that GABA<sub>B</sub>R targets a distinct intracellular pathway to reduce glutamate release probability at glutamatergic synapses in the NAc. Acknowledging that it is challenging to definitively rule out a VGCC-dependent mechanism using electrophysiology alone, we supplemented these findings with mEPSC and low-Ca<sup>2+</sup> recordings and comparative analyses of other VGCC-targeting GPCRs in the NAc. Data from each of these experiments supported the hypothesis that the mechanism of GABA<sub>B</sub>R is primarily VGCC-independent. Instead, our findings point to a direct interaction between GABA<sub>B</sub>R-mobilized Gβγ signaling and the t-SNARE, SNAP-25 (Gerachshenko et al., 2005). Together, these findings characterize the functional consequences and molecular mechanism underlying GABA<sub>B</sub> heteroreceptor function in the NAc and point to a physiological source of GABA within a recently-defined GABAergic microcircuit.

In the NAc core, stimulating glutamatergic inputs onto D1(-) MSNs for 5-min at 10 Hz results in robust LTD mediated by presynaptic CB<sub>1</sub>R and postsynaptic TRPV1 receptor function. AEA-

induced TRPV1 activation results in  $\text{Ca}^{2+}$  and dynamin-dependent AMPAR endocytosis, whereas presynaptic  $\text{CB}_1\text{R}$  activation results in a shift in the phosphorylation state of proteins authorizing vesicular transmitter release, such as RIM1 $\alpha$  (Grueter et al., 2010). Given that the same glutamatergic inputs onto MSNs often collateralize onto synaptically-connected PV-INs, we asked whether glutamatergic synapses onto PV-INs also undergo LFS-induced LTD. We initially hypothesized that LTD is unlikely to occur at these synapses, as (a) the electronic properties of PV-IN dendrites rapidly transfers membrane potential shifts along the somatodendritic axis and (b) the lack of a dendritic spines fails to confine intracellular effectors recruited during the induction and/or expression of LTD (Eggermann and Jonas, 2011; Hu et al., 2014).

To our surprise, LFS- LTD triggered robust LTD at synapses onto PV-INs. However, unlike LFS-LTD at D1(-) MSN synapses, the induction of this plasticity was mGluR-independent, instead relying on  $\text{Ca}^{2+}$  influx through postsynaptic CP-AMPARs. In contrast to D1(+) and D1(-) MSNs in the NAc, PV-INs express GluA2-lacking CP-AMPARs at baseline, conferring distinct synaptic properties to feedforward synapses. We found that  $\text{Ca}^{2+}$  influx triggers the release of eCBs, which diffuse presynaptically to act on  $\text{CB}_1\text{Rs}$ . This plasticity is dependent on retrograde 2-AG signaling, as pharmacological inhibition of AEA hydrolysis failed to shift the magnitude of LTD (data still in progress). Moreover, tonic eCB signaling via  $\text{CB}_1\text{R}$  negatively regulates glutamatergic transmission onto PV-INs, an effect that requires CP-AMPAR-mediated  $\text{Ca}^{2+}$  influx and AEA release. These data highlight a novel regulatory mechanism at feedforward synapses in the NAc. Additionally, feedforward transmission onto PV-INs may serve as a gain control center regulating the expression of discrete motivated behaviors. Given the PV-IN-specific expression of CP-AMPARs and the role of this AMPAR types in the induction of LFS-LTD, targeting this plasticity

*in vivo* may become a viable mechanistic target for the treatment of NAc-dependent reward processing disorders.

It is worth noting the considerable effort invested into understanding the mechanism by which acute *in vivo* and *ex vivo* cocaine exposure abolished this plasticity. The purpose of this was not so much for future publication sake, but instead to personally understand what cocaine is *actually* doing to synaptic transmission in the NAc. Despite accumulating evidence that it is the composite drug experience that evokes time-dependent synaptic adaptations in the NAc, we still lack a precise understanding of how drugs of abuse initiate these changes. The notion that the NAc is substrate for drug-induced changes in DA signaling is inadequate, as one of the primary cellular adaptations following chronic cocaine use – decreased intrinsic membrane excitability of MSNs – appears to be entirely monoamine-independent (Kourrich et al., 2013; Wang et al., 2018a). For example, exposure to cocaine *in* or *ex vivo* dramatically reduces the gain of the current input-output relationship in MSNs by recruiting intracellular sigma-1 receptor signaling ( $\sigma$ 1R).  $\sigma$ 1R decreases excitability by facilitating the trafficking and incorporation of specific voltage-gated  $K^+$  channels, thereby enhancing  $K^+$  efflux during repolarization and delaying neuronal output (Kourrich, 2017; Delint-Ramirez et al., 2018). Although it is well-recognized that clinically and recreationally-used psychotropic drugs interact with  $\sigma$ 1R, this was the first mechanistic explanation for cocaine's effects on MSN membrane properties since the early 1990s (Cai et al., 2017).

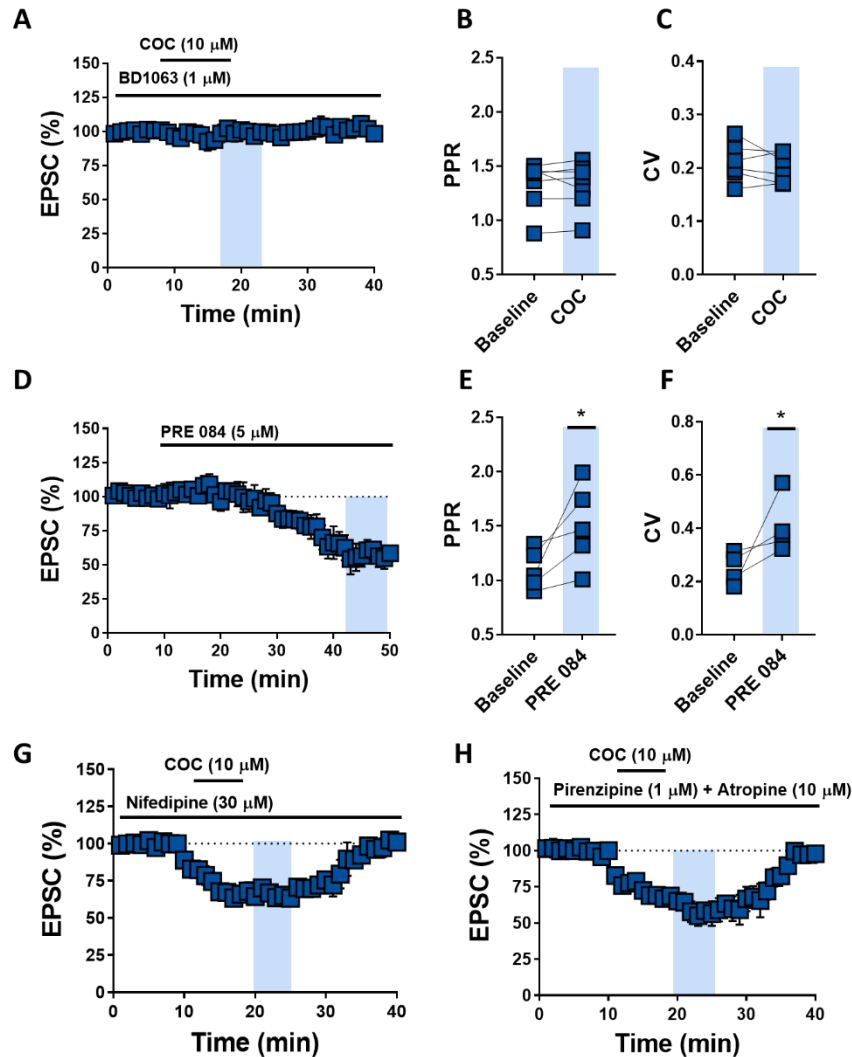


**Figure 5.9. Pharmacological evidence that *ex vivo* cocaine modulates glutamatergic transmission onto PV(+)-INs in a  $\sigma$ 1R-dependent manner.** (A) Normalized EPSCs obtained in PV-INs showing that  $\sigma$ 1R antagonist, BD1063, completely blocks COC-induced depression in EPSC amplitude. (B, C) BD1063 also blocks COC-induced increase in PPR and CV. (D)  $\sigma$ 1R agonist, PRE084, elicits a delayed depression in EPSC amplitude that coincides with an increase in (E) PPR and (F) CV. (G) L-type VGCC blocker, nifedipine, has no effect on COC-induced decrease in EPSC amplitude. (H) M1 antagonist, pirenzepine, and pan-mAChR antagonist, atropine, also fail to block effects of COC. Error bars indicate SEM. \*  $p < 0.05$ . *Note:* part of larger data set showing that COC modulates excitatory transmission independently of monoamine function.

Following a pharmacological odyssey of cocaine's actions on glutamatergic synapses onto PV(+)-INs, we also have evidence that cocaine recruits a monoamine-independent mechanism. To be thorough, we ruled out mechanistic actions of cocaine at NET, SET, DAT, D1 and D2-like DA receptors,  $\beta$ -ARs,  $\alpha 1$  and  $\alpha 2$ -ARs, mAChRs, TRPV1 receptors, 5-HT receptors, and L-type VGCCs (**Fig. 5.9** and **Fig. 4.6**. [Ch. 4]). However, we found that (1) blockade and occlusion of CB<sub>1</sub>R signaling completely abolished the effects of cocaine, (2) FAAH inhibition, but not 2-AG synthesis, diminishes the effect of cocaine, and (3) prior application of  $\sigma 1$ R antagonist, BD1063, also blocked the effects of cocaine (**Fig. 5.9A-C**, BD1063,  $98.82 \pm 2.13\%$ ,  $n=7$ ,  $p=0.596$ ). Additionally,  $\sigma 1$ R agonist, PRE084, elicits a delayed reduction in glutamatergic transmission that coincides with an increase in PPR and CV, similar to the actions of cocaine in ACSF alone (**Fig. D-F**,  $58.65 \pm 10.08\%$ ,  $n=5$ ,  $p=0.009$ ; PPR pre-PRE =  $1.15 \pm 0.09$ , PPR post-PRE =  $1.63 \pm 0.24$ ,  $n=5$ ,  $p=0.028$ ; CV pre-PRE =  $0.23 \pm 0.07$ , CV post-PRE =  $0.43 \pm 0.13$ ,  $n=4$ ,  $p=0.049$ , underpowered). These data encouraged the working hypothesis that cocaine acts on  $\sigma 1$ R to augment IP<sub>3</sub>R-dependent intracellular Ca<sup>2+</sup> mobilization in PV(+)-INs, thereby promoting retrograde AEA signaling. This hypothesis was abandoned until a recent study showed that  $\sigma 1$ R signaling triggers endosomal vesicle release of eCBs at synapses in the VTA (Nakamura et al., 2019). Altogether, these findings point to the rudimentary stage at which we understand how drugs of abuse commandeer the brain's intrinsic reward circuits to create a relapsing-remitting cycle of addiction.

*Note on histaminergic function at glutamatergic synapses in the NAc (Appendix A)*

Histamine (HA), an aminergic neurotransmitter derived from amino acid L-histidine, is synthesized primarily in L-histidine decarboxylase (HDC)-expressing neurons in the tuberomammillary nucleus (TMN) of the posterior hypothalamus (Saito et al., 2018). HA signaling

engages wake-related arousal states, as pharmacological blockade of specific HA receptor subtypes in the CNS triggers sleep-wake transitions, sedation, and drowsiness, and is a major side-effect of first-generation antihistamines, including diphenhydramine and hydroxyzine (Williams et al., 2014; Yu et al., 2015; Rapanelli et al., 2018). HA acts on H<sub>1</sub>, H<sub>2</sub>, and H<sub>3</sub> receptors, each of which is a G-protein coupled receptor (GPCR) with differential effects on wake-promoting neurocircuitry. H<sub>1</sub> and H<sub>2</sub> are G<sub>q</sub>- and G<sub>s</sub>-coupled GPCRs, respectively, with largely excitatory actions on principal neuron output (Ji et al., 2018; Zhuang et al., 2018). In contrast, H<sub>3</sub> is a G<sub>i/o</sub>-coupled GPCR that negatively regulates neurotransmitter release probability as an inhibitory hetero- and autoreceptor (Ellender et al., 2011). HA fibers innervate the entire neuraxis, with terminal density highest in the striatum, including the NAc (Yu et al., 2018). While evidence suggests that central HA signaling attenuates drug-induced reward behavior, few studies have examined how HA modulates NAc circuit function and motivated behavior. Thus, we hypothesized that HA, similar to DA, serotonin (5-HT) and other monoaminergic systems innervating the NAc, modulates glutamatergic transmission onto D1(+) and D1(-) MSNs in a cell-type and input-specific manner.

Using whole-cell patch-clamp electrophysiology in D1tdTomato BAC transgenic mice, we first asked if HA modulates glutamatergic transmission onto D1(+) and D1(-) MSNs in the NAc. HA selectively depressed glutamatergic synapses onto D1(+) MSNs via presynaptically-expressed H<sub>3</sub> without concomitant cholinergic involvement. H<sub>3</sub> receptor activation was sufficient to induce long-term depression (HA-LTD) of excitatory transmission onto D1(+) MSNs. HA-LTD recruited a unique intracellular signaling pathway mediated by the PI3K-Akt-GSK3 $\beta$  axis. Surprisingly, HA also depolarized and increased the intrinsic excitability of both MSN subtypes via postsynaptic H<sub>1</sub>

and H<sub>2</sub> receptors (data omitted). To reconcile the apparent divergent effects of HA on NAc circuit output, we hypothesized that HA tunes D1(+) MSN responsiveness to specific glutamatergic afferents. To address this, we assessed if glutamatergic inputs with “opposing” roles in motivated behavior, such as the prefrontal cortex (PFC) and mediodorsal thalamus (MDT), are differentially regulated by HA (Joffe and Grueter, 2016; Turner et al., 2018b). While the PFC-to-D1(+) MSN synapses underwent robust HA-LTD, MDT synapses were only modestly affected by HA, indicating a gain control mechanism that imposes a high-pass filter on specific inputs onto D1(+) MSNs.

This difference was specific to HA receptor function, as presynaptic GABA<sub>B</sub>R activation induced a depression that was indistinct between inputs. A potent activator of HA signaling via TMN projections is acute stress (Taylor and Snyder, 1971; Dismukes and Snyder, 1974; Miklós and Kovács, 2003). To begin to determine if acute stress exposure recruits endogenous HA signaling in the NAc, mice underwent acute immobilization stress prior to sacrifice for *ex vivo* electrophysiology. In stressed mice, H<sub>3</sub>-dependent HA-LTD was completely abolished at D1(+) MSN synapses. This effect was likely due to the endogenous recruitment of HA signaling in the NAc, as *in vivo* administration of an H<sub>3</sub> antagonist prior to stress rescued HA-LTD at D1(+) MSN synapses. Collectively, these findings elucidate mechanisms by which HA modulates NAc circuit function and point to a potential physiological trigger of HA signaling in the NAc.

A question that remains unanswered is the behavioral context in which endogenous HA signaling is engaged in the NAc. The lack of focused research on this question in the NAc requires potential hypotheses to be adapted from structurally similar regions, such as the dorsal striatum. In the dorsal

striatum, HA signaling has recently garnered considerable interest in the context of tic-related pathological conditions, such as Tourette's syndrome. Recent studies suggest that *Hdc* knockout mice, used to model the loss-of-function W317X point mutation in *Hdc* observed in a subset of patients with this condition, exhibit various motor-related behavioral abnormalities (Rapanelli et al., 2018; Pittenger, 2019). While tic-like repetitive behaviors appeared grossly absent at baseline, acute administration of psychostimulants or the H<sub>3</sub> agonist, RAMH, triggered stereotypies, excessive grooming, and repeated sniffing behavior (Rapanelli et al., 2017). The behavioral shifts observed in RAMH-treated *Hdc* knockout mice is consistent with molecular studies showing increased H<sub>3</sub> receptor protein and mRNA expression in HA-depleted mice. Furthermore, *Hdc* knockout mice display biochemical abnormalities in the intracellular signaling pathways engaged by H<sub>3</sub>, including both the MAPK- and Akt-GSK3 $\beta$  axis (Moreno et al., 2011; Rapanelli et al., 2014). Thus, HA and H<sub>3</sub> function in the dorsal striatum appears to regulate sensorimotor-gating and coordinated motor output, alterations in which lead to disorganized behavioral expression patterns frequently observed in tic-predominant neuropsychiatric disorders (Kononoff Vanhanen et al., 2016).

A tic-related behavioral pathology associated with NAc circuit function is impulse control. Goal-directed executive behaviors require decisional economic strategies encoded by NAc-projecting top-down control centers, such as the prefrontal cortex (PFC) and MDT. Interestingly, our data indicates that HA differentially regulates MDT- and PFC-to-D1(+) MSN NAc synapses. One hypothesis is that HAergic transmission in the NAc serves as a gain control mechanism directing behavioral responding to information encoded by distinct inputs, thereby gating which reward outcomes are sought out by the organism. In this case, the “wake-promoting” actions of HA in the

NAc is expanded to include targeted execution of specific behavioral outcomes (Venner et al., 2019). This may explain, in part, why pharmacological blockade of specific HA receptor subtypes, including H<sub>1</sub> and H<sub>3</sub>, “enhance” the rewarding properties of drugs of abuse (Brabant et al., 2016). For example, co-administration of H<sub>3</sub> antagonist, thioperamide, with cocaine, morphine, and ethanol enhances CPP, self-administration, and drug discrimination assays (Brabant et al., 2005; Nuutinen et al., 2012). Most studies, however, have not looked at whether the effects of these HA-targeting drugs are due to NAc-specific changes in HA signaling. Future studies in our lab are currently underway to assess the behavioral effects of intra-NAc HA infusion.

#### 5.4 Closing

From a broader systems perspective, studies conducted here highlight the specialized synaptic environments regulating information transfer in the CNS. Each circuit is structurally, molecularly and electrically programmed to undertake the biological needs of that system. PV-INs in the NAc, for example, coordinate time-contingent shifts in circuit output, so they express specialized AMPARs with rapid gating kinetics and minimal functional contingencies, SNARE proteins with fast, synchronous release properties, and voltage-gated ion channel families with fast-spiking biophysical capabilities. While various interneuron subtypes contribute to NAc circuit function, PV-INs are the primary circuit element with cable properties enabling efficient, high-fidelity microcircuit processing. As this dissertation addresses in detail, PV-IN-dependent microcircuit processing is required to scale mesolimbic reward input into goal-directed motivational behavior. A guiding motivational strategy of my work hereafter will be to dissect the detailed organizational properties of other limbic-related brain structures, such as the tuberomammillary nucleus (TMN). The stringent, meticulous, and intensive scientific training principles set forth by my doctoral

adviser, Dr. Brad Grueter, has provided me with a unique set of skills to elucidate these properties in arousal-associated microcircuit networks implicated in sleep-wake pathological states encountered in critical care environments.

It is clear from the studies presented here that future work is needed to truly understand how intrinsic- and extrinsic circuit mechanisms contribute to NAc-dependent behavioral outcomes. However, there has rarely been a scientific pursuit in modern history that can be characterized as “finished,” as every set of experimental findings engenders subsequent research, reappraisal, and analysis. It is my sincere hope that my work encourages research interest into the detailed intrinsic circuit mechanisms contributing to maladaptive “biopsychological” states, particularly those with considerable public health attention, including addiction, chronic pain, depression, schizophrenia, anxiety, and autism. As the sociopolitical conversation regarding neuropsychiatric conditions shifts, the importance of biomedical research into why these conditions arise, how to best treat them, and how to improve public awareness will likely enter the forefront of scientific discourse.

## Appendix A

### **Histamine H<sub>3</sub> receptor function biases thalamocortical gain onto D1 medium spiny neurons in the nucleus accumbens core**

Authors: Kevin M. Manz<sup>1,2,3</sup> and Brad A. Grueter<sup>†3,4,5,6</sup>

<sup>1</sup>Medical Scientist Training Program, Vanderbilt University, Nashville, TN 37232.

<sup>2</sup>Neuroscience Graduate Program, Vanderbilt University, Nashville, TN 37232.

<sup>3</sup>Vanderbilt Brain Institute, Vanderbilt University, Nashville, TN 37232.

<sup>4</sup>Department of Anesthesiology, Vanderbilt University Medical Center, Nashville, TN 37232.

<sup>5</sup>Vanderbilt Center for Addiction Research, Vanderbilt University, Nashville, TN 37232

<sup>6</sup>Department of Molecular Physiology and Biophysics, Vanderbilt University, Nashville, TN 37232.

#### **†Correspondence to:**

Brad A. Grueter, Ph.D.

Department of Anesthesiology,

2213 Garland Avenue, P435H MRB IV

Vanderbilt University Medical Center

Nashville, TN 37232-0413

Tel. 615-936-2586

E-Mail: [brad.grueter@vanderbilt.edu](mailto:brad.grueter@vanderbilt.edu)

## A.1 Abstract

The nucleus accumbens (NAc) integrates diverse neuromodulatory inputs to coordinate reward-related behavioral output. Histamine (HA), a wake-promoting neuromodulator, is synthesized in hypothalamic neurons of the tuberomammillary nucleus (TMN). While the NAc expresses various HA receptor subtypes and is innervated by HA-containing varicosities from the TMN, mechanisms by which HA modulates NAc circuit function remain undefined. Here, we interrogate cellular and synaptic mechanisms recruited by HA signaling in the NAc core of male D1tdTomato reporter mice. We find that HA preferentially modulates excitatory gain onto D1 receptor-expressing medium spiny neurons [D1(+)] via H<sub>3</sub> receptor-dependent long-term depression (HA-LTD) that requires G<sub>βγ</sub>-directed Akt-GSK-3β signaling. Furthermore, HA asymmetrically regulates glutamatergic inputs from the prefrontal cortex (PFC) and mediodorsal thalamus (MDT). Finally, we report that acute immobilization stress attenuates HA-LTD by recruiting endogenous H<sub>3</sub>R signaling. These findings elucidate a novel role for HA within the mesolimbic reward network and implicate a physiological trigger of HA function in the NAc core.

## A.2 Introduction

The nucleus accumbens (NAc) coordinates goal-directed behavior by integrating input encoded by distinct neuromodulatory systems. While monoaminergic influences on mesolimbic network activity have been well-characterized, less is known how other aminergic neuromodulators, such as histamine (HA), contribute to NAc circuit function. HA, synthesized primarily in L-histidine decarboxylase (HDC)-expressing hypothalamic neurons of the tuberomammillary nucleus (TMN), promotes wakefulness, sleep-wake transitions, and attention, with a purported regulatory role in appetitive and motivational behavior (Bunney and Aghajanian, 1975; Passani and Blandina, 2011;

Yu et al., 2015). Although HA-containing varicosities moderately innervate the NAc, multiple HA receptor subtypes, including H<sub>1</sub>, H<sub>2</sub> and H<sub>3</sub>, are abundantly expressed in the NAc, indicating that HA may broadly influence NAc circuit dynamics (Takagi et al., 1986; Shoblock and O'Donnell, 2000).

Functional NAc output is gated by the strength of glutamatergic synapses onto D1 and D2 dopamine (DA) receptor-expressing GABAergic medium spiny projection neurons (MSNs) (Turner et al., 2018a; Baimel et al., 2019). Whereas D1-expressing MSNs [D1(+) MSNs] canonically promote reward-seeking behavior, D2-expressing MSNs [D1(-) MSNs] support aversive-like behavioral states (Bock et al., 2013; Francis et al., 2015). Thus, experience-dependent adaptations at corticolimbic synapses onto D1(+) and D1(-) MSNs drive distinct reward-related motivational outcomes (Britt et al., 2012; Pascoli et al., 2014). An unexplored mechanism that may scale excitatory gain in the NAc is the TMN-embedded ascending arousal system. Indeed, HA has been shown to heterosynaptically regulate glutamatergic synaptic strength in various limbic and paralimbic regions, including the striatum, insular cortex, and hippocampus (Brown and Reymann, 1996; Ellender et al., 2011; Takei et al., 2017). While the effects of HA on NAc glutamate homeostasis remain unknown, intra-NAc HA infusion elicits biphasic effects on locomotor activity mediated by various HA receptor subtypes, including H<sub>1</sub> and H<sub>3</sub> (Bristow and Bennett, 1988). Furthermore, manipulating endogenous HA signaling *in vivo* modulates NAc-dependent motivational responding to drugs of abuse (Brabant et al., 2010). Altogether, these observations suggest that HAergic transmission likely engages complex cell type- and synapse-specific circuit adaptations capable of shifting NAc output.

Utilizing D1-specific transgenic reporter mice, whole-cell patch clamp electrophysiology, and optogenetics, we employed a targeted pharmacological approach to interrogate cellular and synaptic mechanisms by which HA signaling modulates NAc circuit function. We find that HA differentially modulates glutamatergic synapses onto D1(+) and D1(-) MSNs in the NAc core via presynaptically-expressed H<sub>3</sub> heteroreceptors (H<sub>3</sub>R). Surprisingly, H<sub>3</sub>R activity is sufficient to induce long-term depression (HA-LTD) of glutamatergic transmission by mobilizing the G<sub>βγ</sub> complex to recruit the Akt-GSK3β effector pathway. Subsequent optogenetic analysis revealed that HA biases excitatory gain to enhance thalamoaccumbens coupling onto D1(+) MSNs. Finally, we provide evidence that heightened wake states *in vivo*, such as during acute immobilization stress, recruits endogenous H<sub>3</sub>R function at glutamatergic synapses in the NAc core. This study sheds light on an unexplored neuromodulatory system in the NAc that has therapeutic potential in treating maladaptive motivational disorders.

### A.3 Methods and materials

#### *Animals*

Animals were bred and housed at Vanderbilt University Medical Center in accordance with IACUC. Male mice 7-14 weeks of age were used for all electrophysiological and *in vivo* experiments. Mice were housed according to sex in groups of 3-5/cage on a 12-hr light-dark cycle with *ad lib* access to standard food and water. Breeding cages were given 5LOD chow (PicoLab®, 28.7% protein, 13.4 % fat, 57.9 % carbohydrate) to improve litter viability. For all electrophysiological experiments, C57BL/6J mice were bred to harbor a bacterial artificial chromosome (BAC) carrying the tdTomato fluorophore under control of the *Drd1a* (D1 receptor)

promoter. For a subset of experiments, mice underwent closely monitored 30-min acute immobilization in an aerated cylindrical holding tube.

### *Electrophysiology*

Whole-cell patch-clamp electrophysiological recordings were obtained in acute brain slice preparations from D1tdTomato BAC transgenic mice, as described previously. Briefly, mice were euthanized under isoflurane anesthesia after which parasagittal slices (250  $\mu$ M) containing the NAc core were prepared from whole brain tissue using a Leica Vibratome in oxygenated (95% O<sub>2</sub>; 5% CO<sub>2</sub>) ice-cold *N*-methyl-*D*-glucamine (NMDG)-based solution (in mM: 2.5 KCl, 20 HEPES, 1.2 NaH<sub>2</sub>PO<sub>4</sub>, 25 Glucose, 93 NMDG, 30 NaHCO<sub>3</sub>, 5.0 sodium ascorbate, 3.0 sodium pyruvate, 10 MgCl<sub>2</sub>, and 0.5 CaCl<sub>2</sub>·2H<sub>2</sub>O). Slices were then recovered in NMDG-based recovery solution for 10-15-min at 32 °C before being transferred to a chamber containing artificial cerebral spinal fluid (ACSF, in Mm: 119 NaCl, 2.5 KCl, 1.3 MgCl<sub>2</sub>·6H<sub>2</sub>O, 2.5 CaCl<sub>2</sub>·2H<sub>2</sub>O, 1.0 NaH<sub>2</sub>PO<sub>4</sub>·H<sub>2</sub>O, 26.2 NaHCO<sub>3</sub>, and 11 glucose; 287-295 mOsm). All experiments were performed using a Scientifica Slicescope Pro System with continuously-perfused 28-32 °C ACSF at 2 mL/min. MSNs in the NAc core were visualized using Scientifica PatchVision software and patched with 3–6 M $\Omega$  recording pipettes (P1000 Micropipette Puller) filled with K<sup>+</sup>-based intracellular solution: (in mM: 135 K<sup>+</sup>-gluconate, 5 NaCl, 2 MgCl<sub>2</sub>, 10 HEPES, 0.6 EGTA, 3 Na<sub>2</sub>ATP, 0.4 Na<sub>2</sub>GTP; 290 mOsm). D1(+) and D1(-) (putative D2) MSNs were differentiated according to the expression of the red tdTomato fluorophore via 530 nm LED light. D1(-) MSNs were distinguished from interneuron cell types based on morphological (size, shape) and biophysical properties (e.g., capacitance, membrane resistance, and AMPAR decay kinetics).

For *voltage-clamp* recordings, electrically-evoked excitatory postsynaptic currents (eEPSCs) were obtained at a command voltage of -70 mV and isolated by incorporating GABA<sub>A</sub>R antagonist, picrotoxin (PTX, 50  $\mu$ M), into the ACSF bath. In experiments examining local glutamatergic transmission, a bipolar electrode was placed at the corticoaccumbens interface and stimulated at 0.1 Hz. In mice stereotaxically injected with ChR2 in the PFC or MDT, optically-evoked glutamate release was sampled with a 0.3-0.5-ms stimulus duration at 10-30% stimulus intensity. Paired pulse ratios (PPR) were obtained within-experiment by delivering two 0.3-ms duration pulses with a 50-ms interstimulus interval and calculating the amplitude ratio of the second eEPSC to the first eEPSC (eEPSC<sub>2</sub>/eEPSC<sub>1</sub>) at the indicated time-point. Coefficient of variance (CV) analysis was conducted within-experiment by calculating  $\sigma/\mu$  of PSC amplitudes during specified time intervals. sEPSC analysis was performed with Clampfit 10.4 using a stringent best-fit template obtained from preliminary 10-min recording bouts in D1(+) and D1(-) MSNs. Each recording bout yielded a rise/decay time ( $\leq 3$ -ms) and amplitude ( $\geq 5$  pA) selection criteria that was reflected in the overall template score. RuBi-Glu experiments were obtained by field-illumination with 470 nm LED blue light with a 60-sec ISI and baseline RuBi-Glu oEPSC between 50-70 pA. For *current-clamp* recordings, cells were permitted 5-min after entering whole-cell configuration to equilibrate to the intracellular dialysate, after which a depolarizing plateau potential was established to maintain cells between -65 and -70 mV. Synaptically-evoked AP fidelity was assessed by first obtaining 15-20 mV EPSP amplitudes at resting membrane potential to permit between-cell analyses. A bipolar stimulating electrode was placed between 100-200  $\mu$ m from cells to prevent non-synaptic AP volleys. 12-15 stimulus trains were delivered at frequencies of 1, 5, 10, 20 and 30 Hz with a stimulus duration of 0.1 ms. Membrane resistance and series resistance ( $R_s$ ) were monitored

continuously during all experiments, with >20% change in  $R_s$  resulting in the omission of that experiment.

### *Stereotaxic surgery*

4–6 week male C57BL6 mice were anesthetized using ketamine (75 mg/kg I.P.) and dexdomitor (0.5 mg/kg I.P.). Craniotomies were performed using a drill, AmScope microscope, and World Precision Instruments Aladdin AI-2000 syringe pump hydraulic system. The following coordinates were used based on The Mouse Brain in Stereotaxic Coordinates: PFC (AP 1.4, ML  $\pm$  0.5, DV –2.9 mm) and MDT (AP –1.2, ML 0.3, DV –3.00 mm). Injection sites were located using Leica AngleTwo Stereotaxic software. AAV-CaMKII-ChR2-eYFP (UNC Vector Core) was injected at 100 nL/min. Mice were revived using antisedan (atipamezole, 0.5 mg/kg I.P.) and treated with ketoprofen (5 mg/kg I.P.) for 3 days post-operatively.

### *Pharmacology*

Histamine dihydrochloride, thioperamide, JNJ 5207852, cetirizine hydrochloride, ranitidine hydrochloride, (*R*)-(-)- $\alpha$ -methylhistamine dihydrobromide, RuBi-Glutamate, (*RS*)-baclofen, Akti<sub>1/2</sub>, CHIR 99021, gallein, forskolin, NBQX, and H89 dihydrochloride were each purchased from Tocris Biosciences. Picrotoxin was purchased from Sigma Aldrich.

### *Statistics and Data Analysis*

Electrophysiological experiments were analyzed using Clampfit 10.4 and GraphPad Prism v7.0. Changes in baseline EPSC (electric or optically-evoked) amplitude, coefficient of variance (CV), and PPR were calculated by comparing mean values during 5 min intervals specified in each time-

course to baseline PPR and CV values. A depression was defined as a significant difference in e/oEPSC amplitude from baseline calculated during the time interval specified in the recording. AP probability was assessed by calculating the percentage of APs evoked following each stimulus train. Gain was calculated by the slope of a linear regression function fitted to the AP probability quantified during each stimulus frequency. After obtaining each data set, Shapiro-Wilk tests were performed to assess normality. Data depicted in Figures 1-7 were determined to be normally distributed. Thus, paired or unpaired *t*-tests were used to analyze statistical differences between data sets. Sidak's post-hoc analyses were used for analyses requiring multiple comparisons. Power analyses were performed with preliminary data during the acquisition of each new data set. The sample size obtained from each power analysis calculation was then compared to sample sizes reported in the literature for similar experiments. Errors bars depicted in figures represent SEM. For all analyses,  $\alpha$  was set as 0.05, with P values  $< \alpha$  indicating a statistically significant difference.

#### A.4 Results

##### *Histamine recruits a presynaptic gain control mechanism that differentially modulates glutamatergic transmission onto D1(+) and D1(-) MSNs in the NAc core*

Histaminergic afferents from the tuberomammillary nucleus (TMN) of the hypothalamus have been identified in subcortical regions governing motivational behavior, including the nucleus accumbens (NAc) (Haas and Panula, 2003; Giannoni et al., 2009). To interrogate whether histamine (HA) modulates glutamatergic transmission onto MSNs in the NAc, we prepared *ex vivo* parasagittal brain slices from D1tdTomato bacterial artificial chromosome (BAC) transgenic mice (**Fig. A.1a**). Electrically-evoked excitatory postsynaptic currents (EPSCs) obtained at -70 mV were recorded from D1 [D1(+)] and putative D2 [D1(-)] dopamine (DA) receptor-expressing

MSNs, as described previously. Following a stable 10-min EPSC baseline, HA (10  $\mu$ M) was bath-applied for 15-min, resulting in a significant depression in EPSC amplitude at synapses onto D1(+) MSNs that persisted following drug wash-out (**Fig. A.1b,d,f**:  $64.55 \pm 4.03$ ,  $n=10$ ,  $p < 0.0001$ ). At D1(-) MSN synapses, HA elicited a modest reduction in EPSC amplitude that returned to baseline (**Fig. 1c,e,f**:  $92.94 \pm 4.47$ ,  $n=7$ ,  $p=0.126$ ). These data suggest that HA differentially regulates glutamatergic synaptic efficacy onto D1(+) and D1(-) MSN synapses in the NAc (**Fig. A.1.f**:  $p < 0.0001$ ).

To interrogate how HA scales excitatory gain onto D1(+) MSNs, we obtained an input-output function in which action potential (AP) probability was assessed at -70 mV following increasing stimulus frequencies (1, 5, 10, 20 and 30 Hz). We first confirmed that synaptically-evoked AP firing in D1(+) MSNs was due to AMPAR-mediated excitatory postsynaptic potentials (EPSPs). Bath-application of AMPAR antagonist, NBQX (50  $\mu$ M), completely blocked synaptically-evoked AP firing at all stimulus frequencies tested, indicating that increasing AP output in D1(+) MSNs is due to temporal summation of AMPAR-mediated EPSPs (data not shown). D1(+) MSNs in ACSF alone demonstrated a linear increase in AP fidelity following sequential increases in input frequency (**Fig. A.1.g, h**). In contrast, HA superfusion significantly reduced synaptically-evoked AP firing that coincided with a negative shift in gain (**Fig. A.1.g-i**). As a positive control, we replicated these experiments in ACSF containing GABA<sub>B</sub>R agonist, baclofen (BAC, 3  $\mu$ M), as recent work from our group demonstrates that GABA<sub>B</sub>R activity in the NAc elicits a robust decrease in glutamatergic synaptic efficacy. Consistent with the effects of HA, BAC application significantly reduced the gain of synaptically-evoked AP probability at D1(+) MSN synapses (**Fig.**

**A.1.i, j).** Together, these findings suggest that HA function in the NAc contributes to input-output inequities that alter D1(+) MSN output.

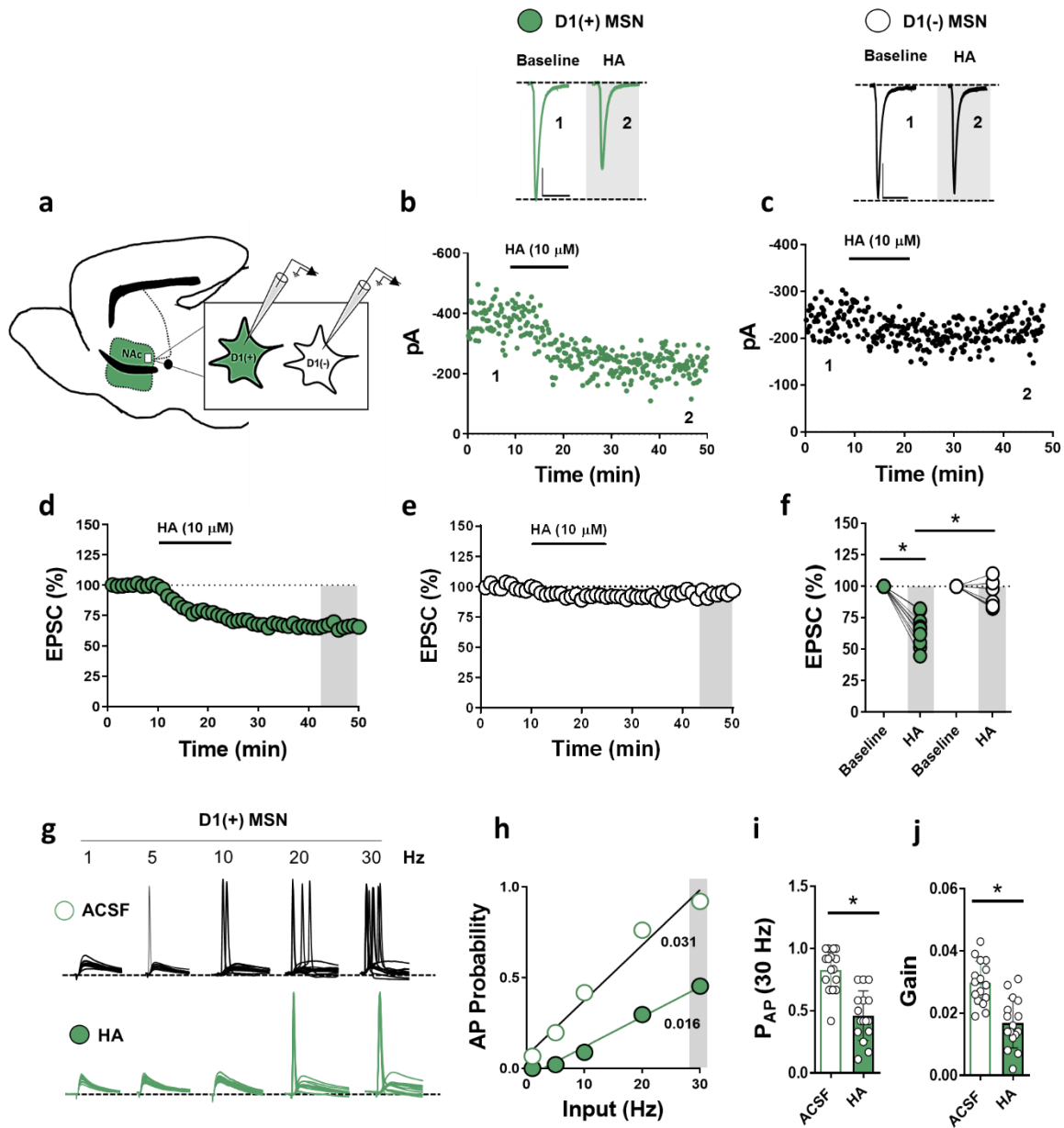


**Figure A.1. HA differentially modulates glutamatergic transmission onto D1(+) and D1(-) MSNs in the NAc core.** (a) Schematic of sagittal mouse brain slice depicting electrophysiological recording location in the dorsomedial NAc core. (b) Representative experiment and traces (above) of EPSCs obtained at baseline and in the presence of HA (10 μM) from tdTomato-expressing [D1(+)] MSNs. (c) Representative experiment and traces (above) of EPSCs obtained at baseline and in the presence of HA (10 μM) from tdTomato-negative [D1(-), putative D2] MSNs. (d) Time-course summary of normalized EPSCs in D1(+) MSNs depicting the HA-induced depression in EPSC amplitude that persists post-drug wash out. (e) Time-course summary of normalized EPSCs in D1(-) MSNs depicting a modest HA-induced depression in EPSC amplitude that returns to baseline. (f) Average EPSC amplitude in D1(+) (blue circles) and D1(-) MSNs (open circles) obtained at t(gray)= 45-50-min. Error bars indicate SEM with (\*) signifying  $p < 0.05$ .

To determine if HA modulates glutamatergic synaptic strength via pre- or postsynaptic mechanisms, we first examined the effects of HA on paired-pulse ratio (PPR) and coefficient of variance (CV). HA significantly increased PPR and CV at glutamatergic synapses onto D1(+) MSNs but not D1(-) MSNs, indicating a presynaptic locus of action that is restricted to D1(+) MSN synapses (**Fig. A.2.a-c**: D1(+) PPR baseline:  $1.10 \pm 0.05$ , D1(+) PPR HA:  $1.31 \pm 0.07$ ,  $n=11$ ,  $p=0.009$ ; D1(+) CV baseline:  $0.11 \pm 0.01$ ,  $n=5$ , D1(+) CV HA:  $0.17 \pm 0.02$ ,  $n=5$ ,  $p=0.012$ ; D1(-) PPR baseline:  $1.24 \pm 0.06$ , D1(-) PPR HA:  $1.31 \pm 0.06$ ,  $n=8$ ,  $p=0.187$ ; D1(-) CV baseline:  $0.15 \pm 0.007$ , CV HA:  $0.146 \pm 0.006$ ,  $n=5$ ,  $p=0.483$ ). Consistent with these findings, HA decreased spontaneous EPSC (sEPSC) frequency but not amplitude at D1(+) MSNs without significantly altering sEPSCs at D1(-) MSNs (**Fig. A.2.d,e**: *sEPSC frequency* = D1(+) baseline:  $1.97 \pm 0.304$  Hz,  $n=13$  D1(+) HA:  $0.80 \pm 0.09$  Hz,  $n=10$ ,  $p<0.001$ ; D1(-) baseline:  $1.54 \pm 0.316$  Hz,  $n=11$ , D1(-) HA:  $1.29 \pm 0.15$  Hz,  $n=8$ ,  $p=0.483$ ; *sEPSC amplitude* = D1(+) baseline:  $-18.8 \pm 1.09$  pA,  $n=13$ , D1(+) HA:  $-19.49 \pm 1.48$  pA,  $n=10$ ,  $p=0.3524$ ; D1(-) baseline:  $-18.99 \pm 1.04$  pA,  $n=11$ , D1(-) HA:  $-20.34 \pm 1.99$  pA,  $n=8$ ,  $p=0.2483$ ).

To discern the synaptic localization of HA function more clearly, we performed glutamate uncaging experiments with ruthenium-bipyridine-trimethylphosphine (RuBi) caged-glutamate (RuBi-Glu, 300  $\mu$ M), a caged-glutamate compound photochemically activated by 473-nm blue light (Fino et al., 2009). This strategy allows postsynaptic actions of HA to be examined in the absence of synaptically-evoked glutamate release. Optical stimulation ( $< 1$ -ms stimulus duration, 50-100 pA responses) of RuBi-Glu-containing ACSF faithfully elicited AMPA receptor

(AMPA)-mediated optical EPSCs (RuBi-Glu oEPSCs) in D1(+) and D1(-) MSNs, as responses were abolished by AMPAR antagonist, NBQX (50  $\mu$ M) (**Fig. A.2.f**). In line with a presynaptic site of action, HA had no effect on RuBi-Glu oEPSC amplitude at D1(+) or D1(-) MSNs (**Fig. A.2.f-h**: D1(+):  $101.26 \pm 1.96$ ,  $n=4$ ,  $p=0.5113$ ; D1(-)  $99.65 \pm 2.99$ ,  $n=4$ ,  $p=0.899$ ). Collectively, these data indicate that HA decreases glutamatergic synaptic efficacy in the NAc through a presynaptic mechanism that is preferentially expressed at D1(+) MSN synapses.

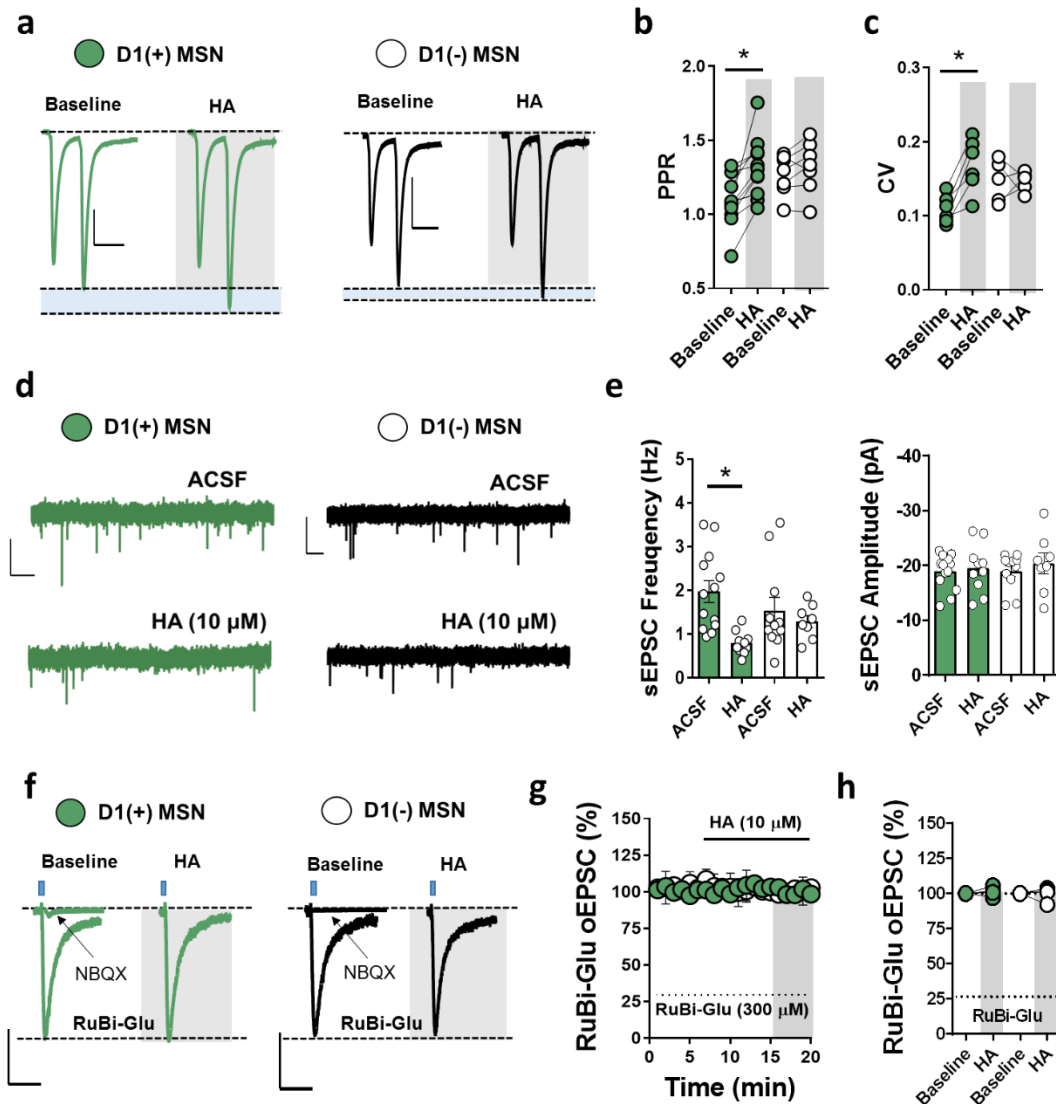


**Figure A.2. HA decreases glutamatergic synaptic efficacy onto D1(+) MSNs via a presynaptic locus of action.** (a) Representative traces of 50-ms ISI paired-pulse EPSCs obtained in D1(+) (blue circles) and D1(-) MSNs (open circles) at baseline and following HA (10  $\mu$ M) bath-application with light-blue shaded region indicating  $\Delta$ PPR. (b) Average PPR obtained at baseline and post-HA at in D1(+) and D1(-) MSNs. (c) Average coefficient of variance (CV) of EPSCs obtained during 10-min baseline and post-HA in D1(+) and D1(-) MSNs. (d) Representative traces of sEPSCs in D1(+) (blue traces) and D1(-) MSNs (black traces) in ACSF alone and in HA-containing ACSF. (e) Average sEPSC frequency (Hz) and amplitude (pA) in D1(+) (blue bars) and D1(-) (open bars) in ACSF alone and in the presence of HA. (f) Representative traces of optically-evoked RuBi-Glu EPSCs (RuBi-Glu oEPSCs) in D1(+) and D1(-) MSNs at baseline and in the presence of HA. Superimposed traces show that AMPAR-antagonist, NBQX, abolishes RuBi-Glu oEPSCs in both MSNs. (g) Time-course summary of RuBi-Glu oEPSCs in D1(+) (blue circles) and D1(-) MSNs (open circles) showing that HA has no effect on RuBi-Glu oEPSC amplitude. (h) Average RuBi-Glu oEPSC amplitude obtained at in D1(+) and D1(-) MSNs. Error bars indicate SEM with (\*) signifying  $p < 0.05$ .

*Histamine H<sub>3</sub> heteroreceptors trigger long-term depression of glutamatergic transmission onto D1(+) MSNs and is tonically active at D1(-) MSN synapses*

We next asked which HA receptor subtype mediates the effects of HA at glutamatergic synapses in the NAc. HA has been shown to modulate striatal circuit function through various HA receptor subtypes, including G<sub>αq</sub>- and G<sub>αs</sub>-coupled H<sub>1</sub> and H<sub>2</sub> receptors, respectively, and G<sub>αi</sub>-coupled H<sub>3</sub> receptors (Ellender et al., 2011; Aquino-Miranda et al., 2016; Zhuang et al., 2018). The observation that HA elicits more robust effects at glutamatergic synapses onto D1(+) MSNs led us to narrow our analysis to D1(+) MSN synapses, as this synapse is likely the principal site by which HA modulates afferent excitatory input to the NAc. To first assess the contribution of H<sub>1</sub> receptors (H<sub>1</sub>R) to the HA-induced depression in glutamatergic transmission, we superfused selective H<sub>1</sub>R antagonist, cetirizine (CTZ, 1 μM), into the ACSF bath prior to HA. Prior application of CTZ had no effect on the HA-induced decrease in EPSC amplitude at D1(+) MSN synapses (**Fig. A.3.a,g**: D1(+) HA: 58.12±2.60, n=6, p=0.247). Similarly, bath-application of selective H<sub>2</sub> receptor (H<sub>2</sub>R) antagonist, ranitidine (20 μM), failed to block the effects of HA at D1(+) MSN synapses, indicating that HA reduces glutamate release probability independently of H<sub>1</sub> and H<sub>2</sub> receptors (**Fig. A.3.b,g**: D1(+) HA: 67.11±3.76, n=6, p=0.656). To determine if HA instead functions through H<sub>3</sub> heteroreceptors, H<sub>3</sub>R antagonist, thioperamide (5 μM) or water-soluble H<sub>3</sub>R neutral antagonist, JNJ 5207852 (JNJ, 10 μM), was superfused into the ACSF bath for 30-min prior to HA. Thioperamide completely blocked the HA-induced depression in EPSC amplitude at glutamatergic synapses onto D1(+) MSNs (**Fig. A.3.c,g**: D1(+) HA: 100.98±2.24, n=5, p=0.005). Consistent with an H<sub>3</sub>R-mediated effect, selective H<sub>3</sub>R agonist, *R*-(-)-α-methylhistamine (RAMH, 1 μM),

recapitulated the HA-induced depression in EPSC amplitude at D1(+) MSN synapses (**Fig. A.3.d,g**: D1(+) RAMH:  $71.06 \pm 2.16$ ,  $n=9$ ,  $p < 0.001$ ). While H<sub>3</sub>R blockade had no effect on basal EPSC amplitude at synapses onto D1(+) MSNs, we observed a remarkable increase in EPSC amplitude at D1(-) MSN synapses. The increase in EPSC amplitude at D1(-) MSN synapses was accompanied by a significant reduction in PPR, indicating that tonic presynaptic H<sub>3</sub>R signaling is restricted to glutamatergic synapses onto D1(-) MSN synapses. To determine whether HA induces long-term depression (LTD) of glutamatergic transmission onto D1(+) MSNs, thioperamide was incorporated into the superfusate immediately following HA. The HA-induced depression in EPSC amplitude persisted in the presence of thioperamide, indicating that HA triggers H<sub>3</sub>R-dependent LTD of glutamatergic transmission (HA-LTD) onto D1(+) MSNs in the NAc (**Fig. A.3.e,f**: D1(+) HA:  $66 \pm 3.70$ , D1(+) thioperamide:  $79.68 \pm 4.86$ ,  $n=9$ ,  $p=0.002$ ).

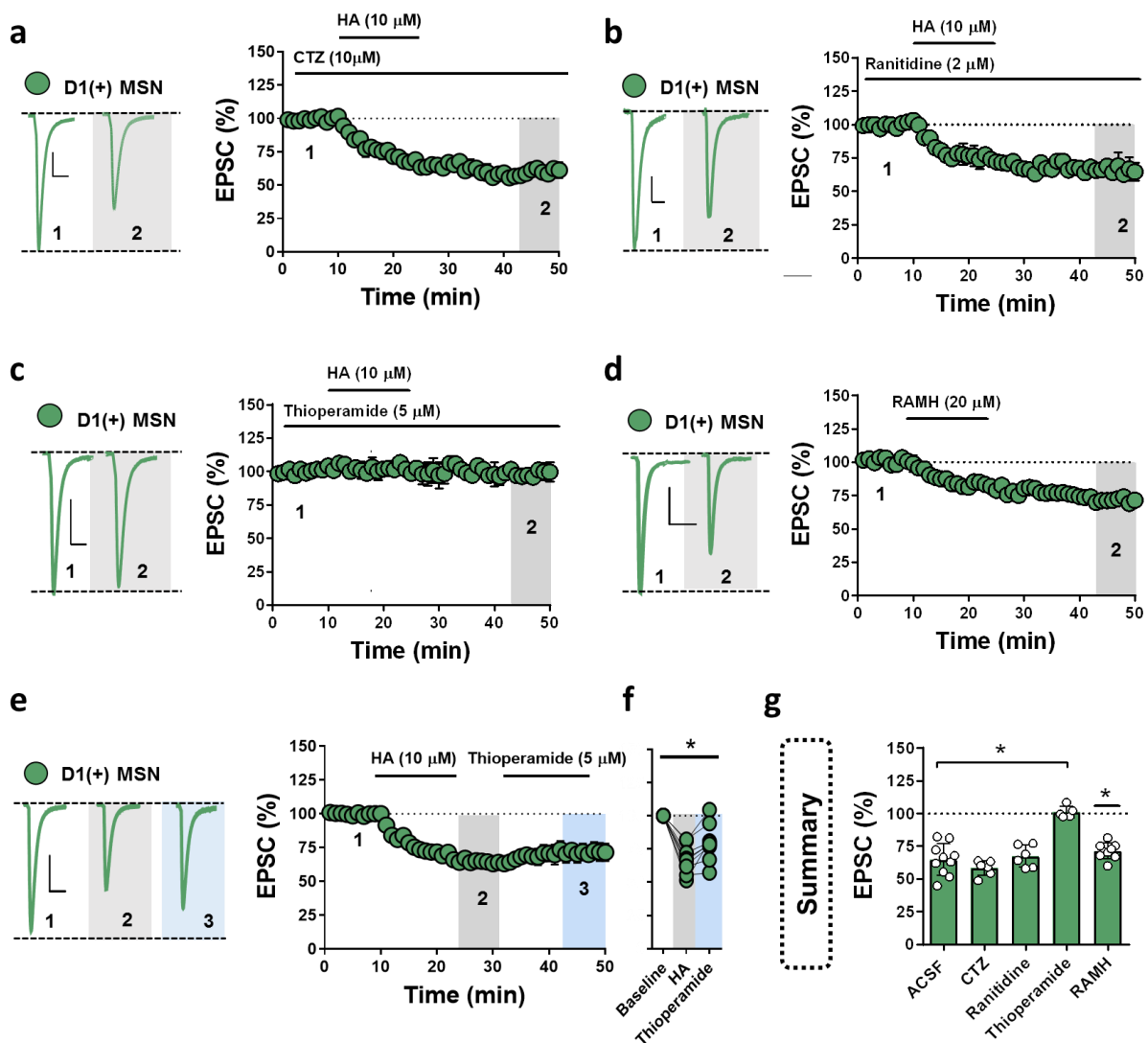


**Figure A.3. HA acts via H<sub>3</sub> heteroreceptors to elicit long-term depression of glutamatergic transmission onto D1(+) MSNs.** (a) Representative traces (left) and normalized time-course summary of EPSCs obtained in D1(+) MSNs (blue circles) showing the effects of HA in the presence of H<sub>1</sub>R antagonist, cetirizine (CTZ). (b) EPSCs obtained in D1(+) MSNs showing the effects of HA in the presence of H<sub>2</sub>R antagonist, ranitidine. (c) EPSCs obtained in D1(+) MSNs showing that H<sub>3</sub>R antagonist, thioperamide, completely blocks the effects of HA. (d) EPSCs obtained in D1(+) MSNs showing the effects of selective H<sub>3</sub>R agonist, R(-)- $\alpha$ -methylhistamine (RAMH). (e) Representative EPSCs obtained in D1(+) MSNs showing the effects of HA chased with H<sub>3</sub>R antagonist, thioperamide. (f) Average EPSC amplitude in D1(+) MSNs obtained at baseline, t(grey) = 25-30-min, and t(blue) = 45-50-min. (g) Summary table of average EPSC amplitude at D1(+) MSNs following each pharmacological treatment. Error bars indicate SEM with (\*) signifying p < 0.05.

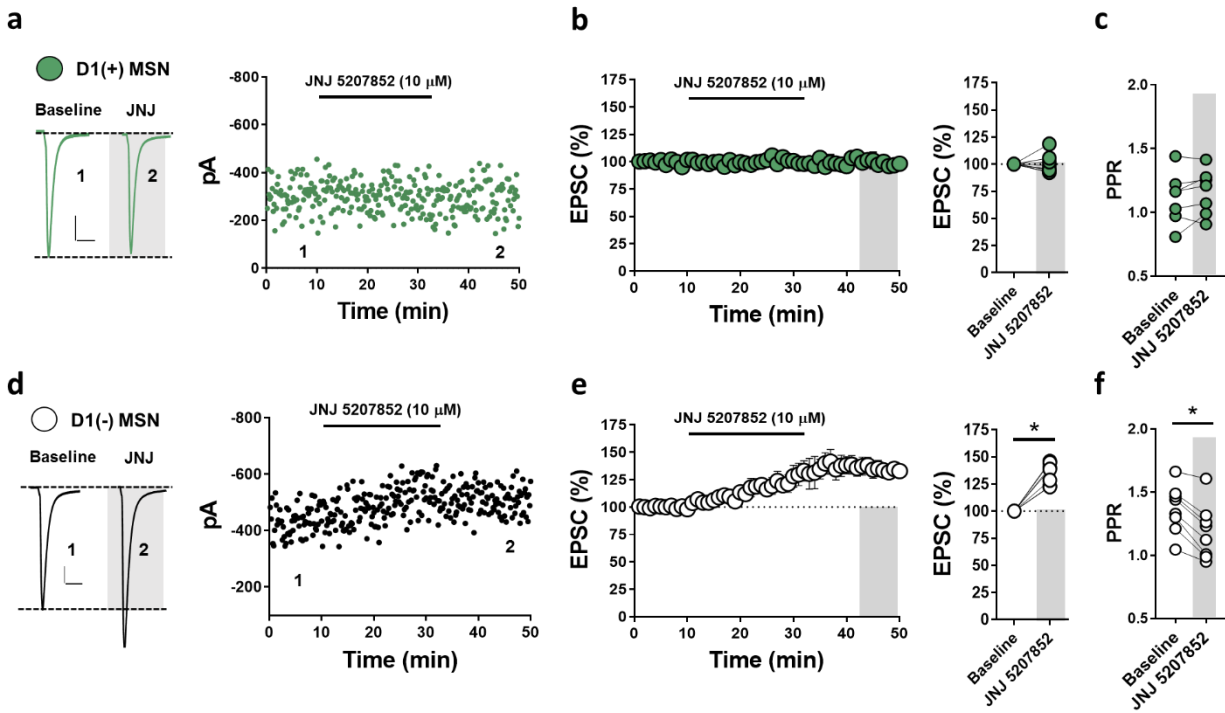


**Figure A.4. H<sub>3</sub>R activity tonically regulates glutamatergic synapses onto D1(-) MSNs but not D1(+) MSNs in the NAc.** (a) Representative traces (left) and experiments of EPSCs in D1(+) MSNs depicting the effects of H3 antagonist, JNJ. (b) Time-course summary and average EPSCs in D1(+) MSNs. (c) PPR in D1(+) MSNs at baseline and in the presence of JNJ. (d) Representative traces (left) and experiments of EPSCs in D1(-) MSNs depicting the effects of JNJ. (e) Time-course summary and average EPSCs in D1(-) MSNs. (f) PPR in D1(-) MSNs at baseline and in the presence of JNJ. Error bars indicate SEM with (\*) signifying p < 0.05.

*G<sub>βγ</sub>-directed recruitment of the PI3K-Akt-GSK3β axis mediates HA-LTD at glutamatergic synapses onto D1(+) MSNs in the NAc*

Presynaptic H<sub>3</sub> heteroreceptors recruit diverse intracellular effectors to reduce neurotransmitter release probability (Passani and Blandina, 2011; Nuutinen et al., 2012; Rapanelli et al., 2016). To interrogate the synaptic mechanism of HA-LTD at glutamatergic synapses onto D1(+) MSNs in the NAc, we first assessed the contribution of adenylyl cyclase (AC) and protein kinase A (PKA) activity. Bath-application of AC activator, forskolin (10 μM), had no effect on the HA-induced depression in EPSC amplitude at D1(+) MSN synapses (**Fig. A.5.a:** D1(+) HA in forskolin: 65.80±4.81, n=7, p<0.001) . If HA-LTD proceeds independently of AC /PKA signaling, then inhibiting downstream PKA function should also fail to occlude the expression of HA-LTD. Indeed, the HA-induced depression in EPSC amplitude remained intact in the presence of PKA inhibitor, H89 (1 μM) (**Fig. A.5.b:** D1(+) HA in H89: 67.12±3.76, n=6, p<0.001). These data suggest that the expression of HA-LTD at glutamatergic synapses onto D1(+) MSNs in the NAc does not require a reduction in AC/PKA activity.

To test if HA instead mobilizes G<sub>βγ</sub>, we incubated slices in cell-permeant G<sub>βγ</sub> complex inhibitor, gallein (20 μM). Pre-incubation in gallein completely blocked the HA-induced depression in EPSC amplitude at D1(+) MSN synapses, indicating that HA-LTD is mediated by an intracellular pathway targeted by the G<sub>βγ</sub> complex (**Fig. A.5.c:** D1(+) HA in gallein: 94.38±4.51, n=6, p=0.201). A downstream target of G<sub>βγ</sub> signaling associated with long-term changes in synaptic strength is the phosphoinositide 3-kinase (PI3K) pathway-Akt pathway. Intracellular recruitment of the PI3K-Akt signaling pathway underlies GPCR-induced synaptic plasticity in various regions, including the hippocampus and prefrontal cortex (Lüscher and Huber, 2010; Bradley et al., 2012; Joffe et

al., 2019). To determine if HA signaling engages this pathway, we superfused Akt-1/2 inhibitor, Akti<sub>1/2</sub> (10  $\mu$ M), into the ACSF bath prior to HA. While HA application induced a transient depression in EPSC amplitude, this depression returned to baseline following drug wash-out, indicating that Akt signaling contributes to the expression of HA-LTD at D1(+) MSN synapses in the NAc (**Fig. A.5d**: D1(+) HA in Akti<sub>1/2</sub> :  $91.38 \pm 3.01$ , n=4, p=0.111).

Several intracellular targets of Akt signaling can induce heterosynaptic forms of plasticity, most notably MAPKs (e.g., MEK<sub>1/2</sub>), glycogen synthase kinase-3 $\beta$  (GSK-3 $\beta$ ), and mammalian target of rapamycin (mTOR) (Horwood et al., 2006). To determine if MAPK signaling contributes to HA-LTD, HA was bath-applied in the presence of MEK<sub>1/2</sub> inhibitor, U0126 (1  $\mu$ M). HA-LTD at D1(+) MSNs was only partially disrupted following MEK<sub>1/2</sub> blockade, indicating that MAPK signaling likely serves as a parallel effector in the mechanism engaged by H<sub>3</sub>R (**Fig. A.5.e**: D1(+) HA in U0126:  $87.02 \pm 5.99$ , n=6, p=0.0317). Given the apparent contingency of G $\beta\gamma$ -directed Akt-MAPK function on HA-LTD, we postulated that HA requires a proximal shift in the activity GSK-3 $\beta$ , as phospho-inactivation of GSK-3 $\beta$  often mediates the expression of PI3K/Akt-dependent forms of LTD (Bradley et al., 2012; Rapanelli et al., 2016). To assess this possibility, we incubated slices in GSK-3 inhibitor, CHIR 99021 (2  $\mu$ M). Bath-application of HA in the presence of CHIR 99021 completely blocked the HA-induced depression in EPSC amplitude at D1(+) MSN synapses, suggesting that GSK-3 $\beta$  blockade likely occludes the expression of HA-LTD (**Fig. A.5.f**: D1(+) HA in CHIR 99021:  $92.45 \pm 3.45$ , n=6, p=0.0632). Together, these findings elucidate a novel form of plasticity in the NAc wherein H<sub>3</sub>R activation engages PI3K-Akt signaling to induce GSK-3 $\beta$ -dependent LTD of glutamatergic transmission onto D1(+) MSNs.

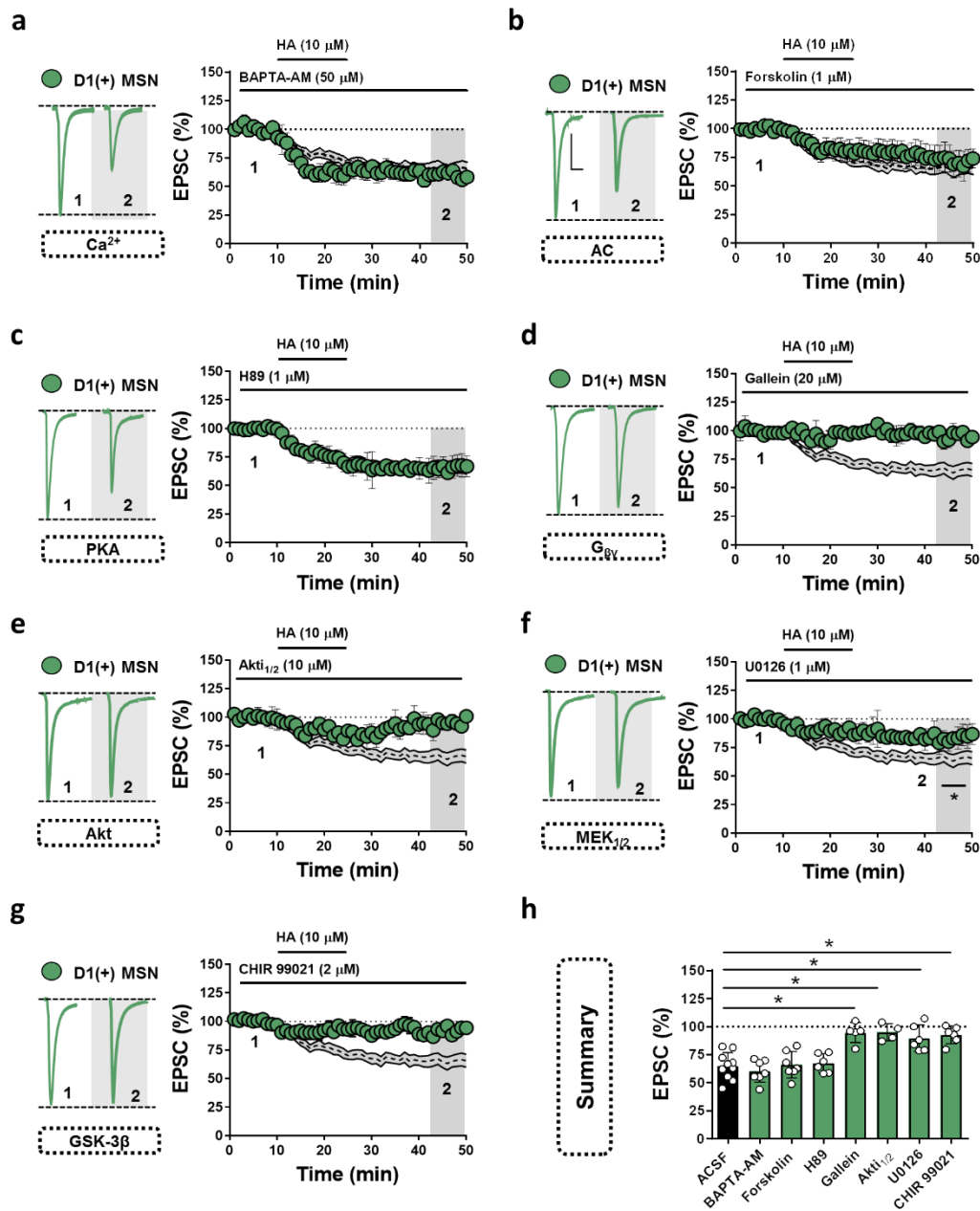


**Figure A.5.  $G_{\beta\gamma}$ -dependent recruitment of the PI3K-Akt-GSK3 $\beta$  axis mediates HA-LTD at glutamatergic synapses onto D1(+) MSNs.** (a) Representative traces (left) and normalized EPSCs obtained in D1(+) MSNs (blue circles) showing the effects of HA in AC activator, forskolin. (b) EPSCs obtained in D1(+) MSNs (blue circles) showing the effects of HA in the presence of PKA inhibitor, H89. (c) EPSCs obtained in D1(+) MSNs showing the effects of HA in the presence of  $G_{\beta\gamma}$  inhibitor, gallein. (d) EPSCs obtained in D1(+) MSNs showing the effects of HA in the presence of Akt-1/2 inhibitor, Akt<sub>1/2</sub>. (e) EPSCs obtained in D1(+) MSNs showing the effects of HA in the presence of MAPK (MEK1/2) inhibitor, U0126. (f) Representative traces (left) and time-course summary of EPSCs obtained in D1(+) MSNs showing the effects of HA in the presence of GSK-3 inhibitor, CHIR 99021.

*Thalamocortical drive onto D1(+) MSNs in the NAc is differentially regulated by histamine signaling*

We next hypothesized that HA acutely tunes MSN responsiveness to specific glutamatergic afferents to the NAc core. To test this hypothesis, we employed an optogenetic approach to determine if specific glutamatergic inputs onto D1(+) MSNs are differentially sensitive to the inhibitory actions of HA. We elected to examine inputs from the prefrontal cortex (PFC) and mediodorsal thalamus (MDT), as glutamatergic inputs from these regions exert behaviorally-divergent effects on NAc-dependent motivational states, with the PFC supporting reward-related behavioral outcomes and the MDT contributing to negative emotional valence. An adeno-associated virus (AAV) harboring a channelrhodopsin-2 (ChR2:H134R)-eYFP construct was stereotaxically injected into the medial PFC and periventricular MDT of D1tdTomato mice (**Fig. A.6A.**). Targeted expression of the AAV-CaMKII-ChR2-eYFP vector was validated empirically according to the presence of yellow-fluorescent protein (eYFP) in the PFC or MDT and optically-evoked EPSCs (oEPSCs) in MSNs in the NAc, as described previously (**Fig. A.6**).

To determine if PFC-to-NAc inputs are regulated by HA, oEPSCs were obtained in D1(+) MSNs from D1tdTomato mice expressing ChR2 in the medial PFC (**Fig. A.6b**). Following a 10-min oEPSC baseline, HA (10  $\mu$ M) was superfused into the ACSF bath for 15-min, resulting in a robust depression in oEPSC amplitude (**Fig. A.6b-f**: PFC-to-D1(+) HA:  $60.66 \pm 4.79\%$ ,  $n=10$ ,  $p < 0.001$ ). Similar to electrically-evoked EPSCs at D1(+) MSNs, the depression was accompanied by a significant increase in PPR and CV (data not shown), consistent with the presynaptic localization of H<sub>3</sub>R at glutamatergic synapses in the NAc core. We next examined whether MDT-to-NAc

synapses onto D1(+) MSNs are also sensitive to the inhibitory actions of HA. In contrast to PFC-to-NAc synapses, HA resulted in a significantly smaller depression in oEPSC amplitude at MDT-to-D1(+) MSN synapses (**Fig. A.6c-F**: MDT-to-D1(+) HA:  $80.25 \pm 5.15$ ,  $n=6$ ,  $p < 0.001$ ; 1-way RM-ANOVA, input effect:  $F_{3,28} = 39.4$ ,  $p=0.0017$ , Sidak's post-hoc analysis). These data suggest that HA modulates thalamocortical gain in the NAc such that MSN responsiveness is biased toward glutamatergic afferents originating from the MDT. To ensure that the differential effects of HA were indeed afferent-specific, we examined presynaptic GABA<sub>B</sub> receptor (GABA<sub>B</sub>R) function at both synaptic inputs, as GABA<sub>B</sub>R is highly expressed in the NAc and functionally restricted to presynaptic loci at glutamatergic synapses (Uchimura and North, 1991; Manz et al., 2019). Bath-application of selective GABA<sub>B</sub>R agonist, baclofen (BAC, 3  $\mu$ M), resulted in a robust depression in EPSC amplitude at PFC- and MDT-to-D1(+) MSN synapses that was indistinct between inputs (**Fig. A.6g-i**: PFC-to-D1(+) BAC:  $27.49 \pm 4.6\%$ ,  $n=6$ ,  $p < 0.001$ ; MDT-to-D1(+) BAC:  $30.10 \pm 5.28\%$ ,  $n=7$ ,  $p < 0.001$ ; 1-way RM ANOVA, input effect:  $F_{3,22} = 158$ ,  $p=0.994$  . Together, these data support the hypothesis that HA differentially regulates PFC- and MDT inputs to the NAc to orient MSN output toward information encoded by the MDT.

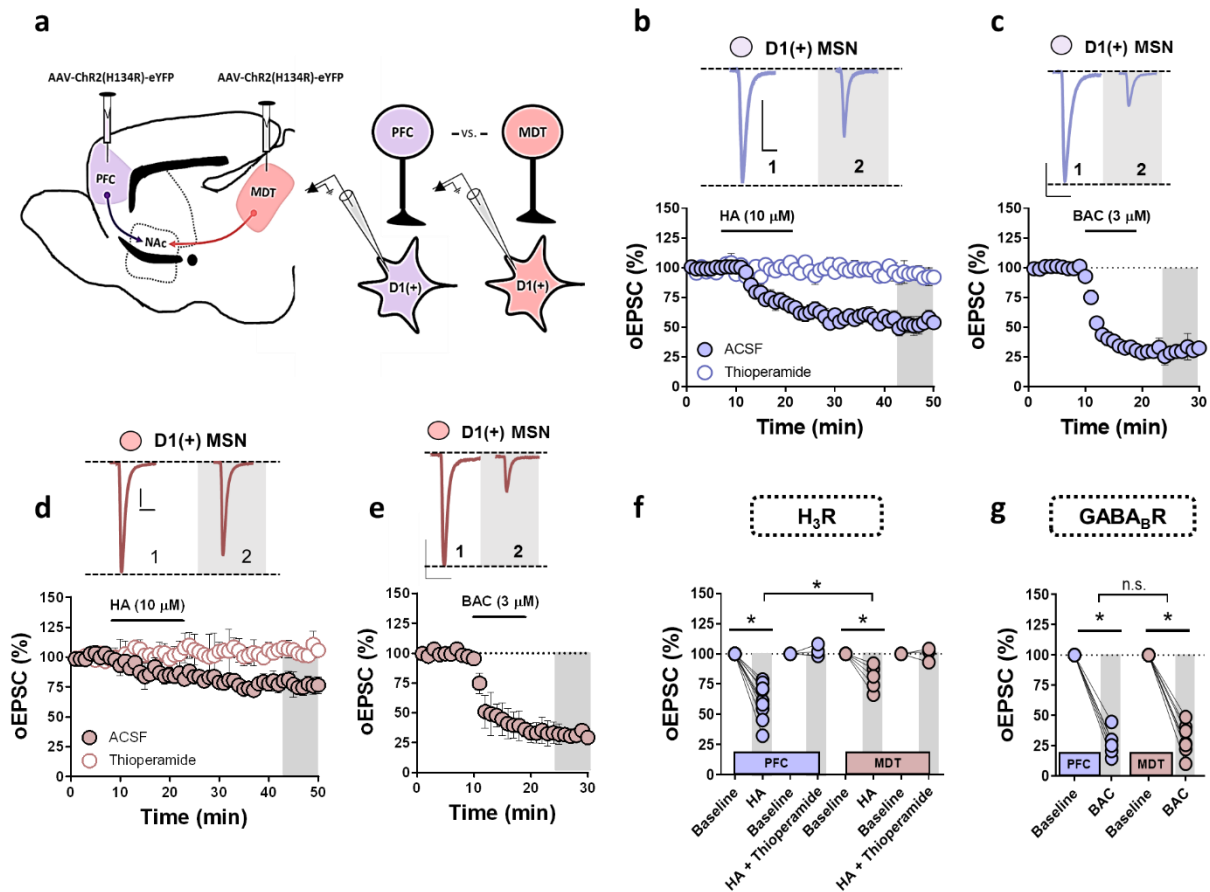


**Figure A.6. Thalamocortical drive onto D1(+) MSNs in the NAc is differentially regulated by histamine signaling.** (a) Schematic of (1) stereotaxic delivery of ChR2-eYFP-harboring viral vectors into the medial PFC or MDT. (b) Optically-evoked EPSCs (oEPSCs) from the PFC at baseline and in the presence of HA (10  $\mu$ M) in D1(+) MSNs. (c) oEPSCs from the MDT at baseline and in HA (10  $\mu$ M) in D1(+) MSNs. (d) Time-course summary of normalized oEPSCs in D1(+) MSNs showing the effect of HA at PFC-to-NAc synapses in ACSF alone (purple circles) and in the presence of H<sub>3</sub>R antagonist, thioperamide (open circles). (e) Time-course summary of oEPSCs in D1(+) MSNs showing the effect of HA at MDT-to-NAc synapses in ACSF alone (red circles) and in the presence of H<sub>3</sub>R antagonist, thioperamide (open circles). (f) Average oEPSC amplitude at PFC- and MDT-to-NAc D1(+) MSN synapses obtained at. (g, h) oEPSCs obtained in D1(+) MSNs showing the effects of GABA<sub>B</sub>R agonist, BAC (3  $\mu$ M), on oEPSC amplitude. (i) Average BAC-induced oEPSC amplitude at PFC- and MDT-to-NAc D1(+) MSN synapses obtained. Error bars indicate SEM with (\*) signifying  $p < 0.05$ .

*Acute stress recruits endogenous H<sub>3</sub>R signaling at glutamatergic synapses onto D1(+) MSNs in the NAc*

HA-containing TMN neuron output increases during behavioral states requiring heightened awareness of salient environment stimuli, including acute stress, fear learning, and systemic metabolic strain (e.g., fasting) (Taylor and Snyder, 1971; Dismukes and Snyder, 1974; Miklós and Kovács, 2003). Thus, we asked whether acute stress can recruit endogenous HA signaling at glutamatergic synapses in the NAc core. To answer this question, we employed an acute immobilization stress (AIS) paradigm in which mice were restrained for 30-min followed by a 15-min recovery period, after which acute brain slices were prepared for *ex vivo* electrophysiology (**Fig. A.7.a**). We hypothesized that AIS engages TMN-to-NAc volume transmission, thereby altering the expression of HA-LTD at glutamatergic synapses onto D1(+) MSNs. Similar to experiments performed in naïve mice, bath-application of HA in control mice elicited a robust depression in EPSC amplitude at D1(+) MSN synapses. However, in mice that underwent AIS, HA elicited a slight depression in EPSC amplitude that was significantly attenuated relative to control mice (**Fig. A.7.b,c**: D1(+) HA control:  $61.48 \pm 3.64\%$ ,  $n=5$ ,  $N(\text{animals})=4$ ; D1(+) HA AIS:  $87.88 \pm 4.13\%$ ,  $n=7$ ,  $N(\text{animals})=5$ ,  $p < 0.001$ ).

To determine if the reduction in HA-LTD was due to an experience-dependent shift in presynaptic H<sub>3</sub>R function, we repeated these experiments with H<sub>3</sub>R agonist, RAMH. In control mice, RAMH significantly decreased EPSC amplitude at D1(+) MSN synapses that persisted throughout the recording period. In contrast, bath-application of RAMH in AIS mice had no effect on EPSC amplitude, supporting the hypothesis that AIS modulates presynaptic H<sub>3</sub>R function at

glutamatergic synapses onto D1(+) MSNs (**Fig. A.7.d,e**: D1(+) RAMH control:  $66.78 \pm 3.61\%$ ,  $n=7$ ,  $N(\text{animals})=4$ ; D1(+) RAMH AIS:  $93.08 \pm 7.13\%$ ,  $n=7$ ,  $N(\text{animals})=5$ ,  $p=0.004$ ). A possible explanation for these findings is that endogenous TMN-to-NAc activity occludes subsequent HA-LTD assessed *ex vivo*. If this hypothesis is correct, *in vivo* blockade of H<sub>3</sub>R should restore HA-LTD at D1(+) MSN synapses in the NAc. Thus, 15-min prior to AIS, mice received an intraperitoneal (IP) injection of vehicle (VEH, saline) or brain-penetrant H<sub>3</sub>R antagonist, JNJ 5207852 (10 mg/kg) (**Fig. A.7.f**). Similar to prior experiments performed in AIS-exposed mice, HA-LTD in VEH-treated mice AIS mice was significantly attenuated. Interestingly, prior administration of JNJ 5207852 in AIS mice significantly increased HA-LTD relative to VEH-treated AIS mice (**Fig. A.7.g,h**: D1(+) HA-VEH:  $85.61 \pm 4.82\%$ ,  $n=10$ ,  $N(\text{animals})=5$ ; D1(+) HA-JNJ:  $66.85 \pm 5.38\%$ ,  $n=7$ ,  $N(\text{animals})=6$ ,  $p=0.008$ ). Together, these data suggest that AIS occludes HA-LTD at glutamatergic synapses onto D1(+) MSNs in the NAc by recruiting endogenous HA signaling via H<sub>3</sub>R.

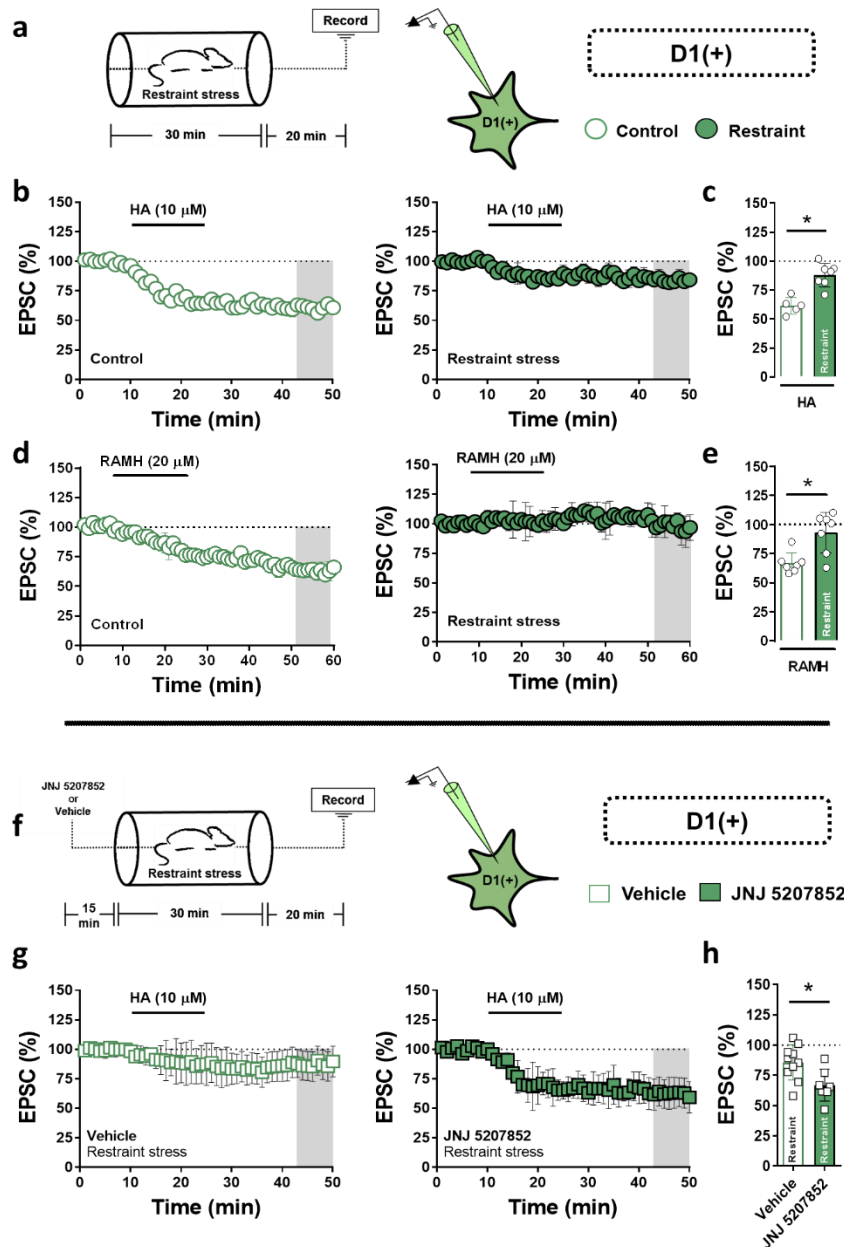


**Figure A.7. Acute stress recruits endogenous H<sub>3</sub>R signaling at glutamatergic synapses onto D1(+) MSNs in the NAc.** (a) Left: Schematic depicting immobilization stress (AIS) paradigm. Right: Recording strategy (b) EPSCs in control mice (left) and AIS-exposed mice (right) depicting the effects of HA at synapses onto D1(+) MSNs. (c) Average HA-induced EPSC amplitude obtained in control and AIS mice. (d) EPSCs in control mice (left) and AIS-exposed mice (right) depicting the effects of H<sub>3</sub>R agonist, RAMH, at synapses onto D1(+) MSNs. (e) RAMH-induced EPSC amplitude obtained at min in control and AIS mice. (f) Schematic depicting prophylactic treatment with water-soluble H<sub>3</sub>R antagonist, JNJ 5207852, or vehicle (saline) prior to AIS exposure. (g) EPSCs in D1(+) MSNs of vehicle-treated (open squares, left) and JNJ 5207852-treated (navy blue squares, right) AIS mice. (h) HA-induced EPSC amplitude obtained at in vehicle vs. JNJ 5207852-treated AIS mice.

## A.5 Discussion

In the present study, we elucidate a novel role for wake-promoting neurotransmitter, histamine (HA), in the NAc core. Utilizing D1-specific transgenic reporter mice, we report that HA recruits a presynaptic H<sub>3</sub>R-dependent gain control mechanism that differentially regulates glutamatergic synaptic strength onto D1(+) and D1(-) MSNs. At D1(+) MSN synapses, HA induces H<sub>3</sub>R-dependent LTD by mobilizing the G<sub>βγ</sub> complex to recruit the Akt-GSK3β effector pathway. While HA-LTD is functionally expressed at glutamatergic synapses onto D1(+) MSNs, we find that tonic presynaptic H<sub>3</sub>R activity negatively regulates synapses onto D1(-) MSN. Furthermore, HA differentially regulates glutamatergic synapses from the PFC and MDT, with PFC-to-D1(+) MSN synapses exhibiting exquisite sensitivity to the inhibitory actions of HA. Finally, AIS diminishes HA-LTD by recruiting endogenous HA signaling via H<sub>3</sub>R at D1(+) MSN synapses, suggesting that brief exposure to stressful stimuli can recruit heterosynaptic HA signaling at glutamatergic synapses in the NAc core.

### *Presynaptic HA signaling via H<sub>3</sub>R differentially modulates glutamatergic transmission onto D1(+) and D1(-) MSNs in the NAc core*

We report that HA decreases glutamatergic synaptic efficacy onto D1(+) MSNs with minimal effect at synapses onto D1(-) MSNs. The effect at D1(+) MSN synapses was completely abolished by selective H<sub>3</sub>R antagonist, thioperamide, and recapitulated with selective H<sub>3</sub>R agonist, RAMH, indicating that H<sub>3</sub>R mediates the effect of HA. Although we do not fully explain the cell-type specific actions of HA at these synapses, it is unlikely that histaminergic afferents from the TMN preferentially synapse onto D1(+) MSNs over D1(-) MSNs, as HA-containing varicosities rarely form direct synaptic connections in the striatum (Giannoni et al., 2009; Ellender et al., 2011).

Instead, HA signaling occurs predominately via volume transmission, where recipient structures dictate effects on circuit function according to the expression of specific HA receptor subtypes. Our findings demonstrate that glutamatergic synapses onto D1(-) exhibit tonic presynaptic H<sub>3</sub>R activity, as bath-application of water-soluble H<sub>3</sub>R antagonist, JNJ 5207852, unmasked a rapid and robust increase in glutamatergic transmission coincident with an increase in release probability. A plausible interpretation of these data is that H<sub>3</sub>R signaling engaged at D1(-) MSN synapses occludes any additional effects of HA applied *ex vivo* (Morisset et al., 2000, 2000). An intriguing possibility is whether glutamatergic afferents onto D1(+) and D1(-) MSNs in the NAc express varying levels or isoforms of H<sub>3</sub>R that couple to distinct intracellular effectors, or whether each input contains specialized specific H<sub>3</sub>R signaling states. Future studies will be needed to ascertain the functional difference of H<sub>3</sub>R at D1(+) and D1(-) MSN synapses in the NAc.

Our findings suggest that HA decreases glutamatergic transmission onto D1(+) MSNs via a presynaptic locus of action. This is supported by data showing that HA increases PPR and CV, metrics which inversely correspond to presynaptic release probability, and decreases sEPSC frequency but not amplitude. Although presynaptic H<sub>3</sub>R function has been shown to also negatively regulate glutamate release in the dorsal striatum, recent reports indicate that H<sub>3</sub>R is also expressed on striatal D1 and D2 MSNs (Moreno et al., 2011, 2014; Rapanelli et al., 2018). Thus, it is tempting to speculate that expression of HA-LTD incorporates a parallel effector pathway that is expressed postsynaptically. However, HA application has no effect on optically-uncaged AMPAR-mediated glutamate currents in D1(+) or D1(-) MSNs, corroborating a presynaptic locus of H<sub>3</sub>R function at these synapses. Alongside data showing a reduction in synaptically-evoked AP

fidelity, our data suggests that HA plays a critical role in regulating the gain of afferent information propagated by D1(+) MSNs in the NAc.

*HA induces H<sub>3</sub>R-dependent LTD at D1(+) MSN synapses by engaging Akt-MAPK-GSK3 $\beta$  signaling*

Although heterosynaptic HA function has been demonstrated elsewhere in the CNS, few studies define the temporal dynamics of H<sub>3</sub>R on synaptic transmission or the mechanism(s) engaged by H<sub>3</sub>R in native tissue preparations. Here, we delineate the synaptic mechanism by which HA depresses glutamatergic synapses onto D1(+) MSNs, showing that (a) HA triggers H<sub>3</sub>R-dependent LTD (HA-LTD) and (b) HA-LTD proceeds through a G <sub>$\beta\gamma$</sub> -directed Akt-GSK3 $\beta$  signaling pathway. While the HA-induced depression in glutamatergic transmission and increase in PPR and CV persisted following drug wash-out, interpreting this finding is complicated by reports that HA may linger in slices post-application (Brown and Reymann, 1996). Thus, we assessed whether HA induces LTD by chasing the application of HA with thioperamide. Thioperamide resulted in a modest uptrend toward baseline that remained depressed throughout the recording period, indicating that HA induces a presynaptic LTD of excitatory transmission onto D1(+) MSNs.

Our findings point to a critical role for the G <sub>$\beta\gamma$</sub>  effector arm in the induction of H<sub>3</sub>R-dependent LTD. While G <sub>$\beta\gamma$</sub>  signaling can activate multiple intracellular signaling pathways, we hypothesized that H<sub>3</sub>R couples to the PI3K-Akt pathway, as evidence *in vivo* suggests H<sub>3</sub>R activation engages striatal Akt-MAPK-GSK3 $\beta$  signaling without affecting AC/cAMP/PKA function, consistent with our electrophysiological findings (Jernigan et al., 2010; Rapanelli et al., 2016). Moreover, GSK-3 $\beta$  is commonly associated with H<sub>3</sub>R function and contributes to NAc-dependent motivational

behavior, yet few studies have identified upstream transduction events mediating synaptic GSK-3 $\beta$  activity (Xu et al., 2009; Bradley et al., 2012; Zhao et al., 2016). Our model proposes that H<sub>3</sub>R activation mobilizes the G $\beta\gamma$  complex, which activates the PI3K-Akt pathway, leading to the phosphorylation of MAPKs (MEK<sub>1/2</sub>) and GSK-3 $\beta$ . Given that GSK-3 $\beta$  functions highly under basal conditions and phosphorylation at Ser<sup>9</sup> inhibits GSK-3 $\beta$  activity, it is conceivable that inhibiting presynaptic GSK-3 $\beta$  activity shifts the phosphorylation state of exocytotic release machinery, leading to the expression of HA-LTD (Bradley et al., 2012). Indeed, multiple forms of presynaptic LTD, including cannabinoid receptor type-1 (CB<sub>1</sub>R)-dependent LTD in the NAc core, proceed through molecular alterations in SNARE-associated release machinery, such as RIM1 $\alpha$  (Heifets et al., 2008; Grueter et al., 2010). Altogether, we propose a form of LTD triggered by HA H<sub>3</sub>R function at glutamatergic synapses onto D1(+) MSNs in the NAc core.

*HA signaling biases the gain of glutamatergic inputs from the PFC and MDT onto D1(+) MSNs in the NAc core*

To better understand how presynaptic HA function may shift D1(+) MSN responsiveness to specific corticolimbic afferents, we speculated that HA differentially modulates glutamatergic afferents to the NAc that arise predominately from the medial PFC, MDT, basolateral amygdala (BLA), and ventral hippocampus (VHipp). We restricted our analysis to inputs from the PFC and MDT, as these regions densely innervate the NAc core and impose contrasting effects on NAc-directed motivational behavior (Pascoli et al., 2011; Britt et al., 2012). For example, MDT-to-NAc afferents drive real-time place aversion and negative affective states associated with morphine withdrawal, whereas other glutamatergic inputs, such as the PFC and BLA, contribute to the incubation of cocaine craving and are self-stimulated in intracranial self-stimulation (ICSS) tasks

(Lee et al., 2013; Zhu et al., 2016; Sweis et al., 2018). Our data suggests that PFC-to-NAc inputs onto D1(+) MSNs are exquisitely sensitive to the inhibitory actions of HA, whereas MDT-to-NAc synapses are only moderately affected by HA. Given that minimal differences exist between (a) the connectivity of these regions onto individual MSNs and (b) other presynaptic  $G_{i/o}$ -coupled receptor systems (e.g.,  $GABA_B$ R), these findings suggest that HA may selectively orient MSN responsiveness to inputs from the MDT. By improving the signal-to-noise element of MDT-to-NAc transmission and preferentially acting at D1(+) MSN synapses, the physiological actions of HA at these synapses could very well explain the “inhibitory” effects of central HA function on drug reward behavior and motivational output (Brabant et al., 2010; Blandina et al., 2012).

*Acute stress recruits endogenous HA signaling at glutamatergic synapses onto D1(+) MSNs in the NAc core*

HA is synthesized primarily in histidine decarboxylase (HDC)-expressing cells in the TMN of the posterior hypothalamus (Giannoni et al., 2009). Although HA is increasingly implicated in higher-order executive functions, such as learning, memory and motivation, a primary physiological role of HA is in sleep-wake transitions, arousal, and attentional control (Blandina et al., 2012; Yu et al., 2015; Venner et al., 2019). Accordingly, *in vivo* TMN activity is enhanced during bouts of acute stress, such as forced swim, foot shock, and acute immobilization stress (AIS) (Taylor and Snyder, 1971; Dismukes and Snyder, 1974). Thus, we employed AIS as means to recruit the TMN axis and assess whether endogenous HA signaling modulates the effects of  $H_3R$  function at glutamatergic synapses in the NAc core. Interestingly, we find that HA-LTD is reduced following AIS in an  $H_3R$ -dependent manner, as prophylactic treatment with an  $H_3R$  antagonist is sufficient to rescue this plasticity at D1(+) MSN synapses. Although HAergic afferents from the TMN are

the most likely source of endogenous HA signaling in the NAc, an alternative possibility is HA derived from mast cells, as several studies indicate that HA degranulation is triggered by acute stress (Theoharides et al., 1995; Baldwin, 2006). Nevertheless, while mast cell degranulation contributes to overall CNS HA content, direct synaptic effects of mast cell-derived HA remain to be determined. Future studies are needed to assess the functional contribution of TMN vs. mast cell-derived HA signaling to NAc-dependent reward behavior.

### *Concluding remarks*

The NAc receives dense input from mesencephalic regions containing high levels of monoamines, yet little is known how HA, another aminergic transmitter synthesized primarily in TMN neurons of the posterior hypothalamus, contributes to NAc circuit function. Here, we establish mechanisms by which HA modulates NAc circuit dynamics, with deliberate experimental attention on local and input-specific glutamatergic synapses onto D1(+) MSNs. Our findings suggest that HA elicits presynaptic H<sub>3</sub>R-dependent LTD that biases NAc output to information encoded by the MDT. Understanding the role of HA in the mesolimbic reward network may aid in the development of novel therapeutics for neuropsychiatric conditions characterized by stress-induced shifts in motivational behavior, such as depression and addiction.

## REFERENCES

- Allin R, Russell VA, Lamm MCL, Taljaard JJF (1988) Regional distribution of monoamines in the nucleus accumbens of the rat. *Neurochem Res* 13:937–942.
- Al-Muhtasib N, Forcelli PA, Vicini S (2018) Differential electrophysiological properties of D1 and D2 spiny projection neurons in the mouse nucleus accumbens core. *Physiol Rep* 6:e13784.
- Alsene KM, Fallace K, Bakshi VP (2010) Ventral striatal noradrenergic mechanisms contribute to sensorimotor gating deficits induced by amphetamine. *Neuropsychopharmacology* 35:2346–2356.
- Aquino-Miranda G, Escamilla-Sánchez J, González-Pantoja R, Bueno-Nava A, Arias-Montaña J-A (2016) Histamine H3 receptor activation inhibits dopamine synthesis but not release or uptake in rat nucleus accumbens. *Neuropharmacology* 106:91–101.
- Assous M, Tepper JM (2019) Excitatory extrinsic afferents to striatal interneurons and interactions with striatal microcircuitry. *Eur J Neurosci* 49:593–603.
- Atwood BK, Lovinger DM, Mathur BN (2014) Presynaptic long-term depression mediated by Gi/o-coupled receptors. *Trends Neurosci* 37:663–673.
- Augustin SM, Chancey JH, Lovinger DM (2018) Dual Dopaminergic Regulation of Corticostriatal Plasticity by Cholinergic Interneurons and Indirect Pathway Medium Spiny Neurons. *Cell Rep* 24:2883–2893.
- Augustin SM, Lovinger DM (2018) Functional Relevance of Endocannabinoid-Dependent Synaptic Plasticity in the Central Nervous System. *ACS Chem Neurosci* 9:2146–2161.
- Baimel C, McGarry LM, Carter AG (2019) The Projection Targets of Medium Spiny Neurons Govern Cocaine-Evoked Synaptic Plasticity in the Nucleus Accumbens. *Cell Rep* 28:2256–2263.e3.
- Baldwin AL (2006) Mast cell activation by stress. *Methods Mol Biol* 315:349–360.
- Barrientos C, Knowland D, Wu MMJ, Lilascharoen V, Huang KW, Malenka RC, Lim BK (2018) Cocaine-Induced Structural Plasticity in Input Regions to Distinct Cell Types in Nucleus Accumbens. *Biol Psychiatry* 84:893–904.
- Bassareo V, Cucca F, Frau R, Di Chiara G (2017) Changes in Dopamine Transmission in the Nucleus Accumbens Shell and Core during Ethanol and Sucrose Self-Administration. *Front Behav Neurosci* 11:71.
- Benuck M, Lajtha A, Reith ME (1987) Pharmacokinetics of systemically administered cocaine and locomotor stimulation in mice. *J Pharmacol Exp Ther* 243:144–149.

- Berridge CW, Stratford TL, Foote SL, Kelley AE (1997) Distribution of dopamine beta-hydroxylase-like immunoreactive fibers within the shell subregion of the nucleus accumbens. *Synapse* 27:230–241.
- Blandina P, Munari L, Provensi G, Passani MB (2012) Histamine neurons in the tuberomammillary nucleus: a whole center or distinct subpopulations? *Front Syst Neurosci* 6 Available at: <https://www.ncbi.nlm.nih.gov/pmc/articles/PMC3343474/> [Accessed October 27, 2019].
- Blomeley CP, Bracci E (2011) Opioidergic interactions between striatal projection neurons. *J Neurosci* 31:13346–13356.
- Bock R, Shin JH, Kaplan AR, Dobi A, Markey E, Kramer PF, Gremel CM, Christensen CH, Adrover MF, Alvarez VA (2013) Strengthening the accumbal indirect pathway promotes resilience to compulsive cocaine use. *Nat Neurosci* 16:632–638.
- Brabant C, Alleva L, Quertemont E, Tirelli E (2010) Involvement of the brain histaminergic system in addiction and addiction-related behaviors: a comprehensive review with emphasis on the potential therapeutic use of histaminergic compounds in drug dependence. *Prog Neurobiol* 92:421–441.
- Brabant C, Charlier Y, Navacerrada MES, Alleva L, Tirelli E (2016) Action of Pitolisant on the stimulant and rewarding effects of cocaine in mice. *Eur J Pharmacol* 791:552–559.
- Brabant C, Charlier Y, Quertemont E, Tirelli E (2005) The H3 antagonist thioperamide reveals conditioned preference for a context associated with an inactive small dose of cocaine in C57BL/6J mice. *Behav Brain Res* 160:161–168.
- Bradley CA, Peineau S, Taghibiglou C, Nicolas CS, Whitcomb DJ, Bortolotto ZA, Kaang B-K, Cho K, Wang YT, Collingridge GL (2012) A pivotal role of GSK-3 in synaptic plasticity. *Front Mol Neurosci* 5(34).
- Brimblecombe KR, Threlfell S, Dautan D, Kosillo P, Mena-Segovia J, Cragg SJ (2018) Targeted Activation of Cholinergic Interneurons Accounts for the Modulation of Dopamine by Striatal Nicotinic Receptors. *eNeuro* 5.
- Bristow LJ, Bennett GW (1988) Biphasic effects of intra-accumbens histamine administration on spontaneous motor activity in the rat; a role for central histamine receptors. *Br J Pharmacol* 95:1292–1302.
- Britt JP, Benaliouad F, McDevitt RA, Stuber GD, Wise RA, Bonci A (2012) Synaptic and behavioral profile of multiple glutamatergic inputs to the nucleus accumbens. *Neuron* 76:790–803.
- Brown RE, Reymann KG (1996) Histamine H3 receptor-mediated depression of synaptic transmission in the dentate gyrus of the rat in vitro. *J Physiol (Lond)* 496 ( Pt 1):175–184.
- Bunney BS, Aghajanian GK (1975) Evidence for drug actions on both pre- and postsynaptic catecholamine receptors in the CNS. *Psychopharmacol Bull* 11:8–10.

- Burke DA, Rotstein HG, Alvarez VA (2017) Striatal Local Circuitry: A New Framework for Lateral Inhibition. *Neuron* 96:267–284.
- Cai Y, Yang L, Niu F, Liao K, Buch S (2017) Role of Sigma-1 Receptor in Cocaine Abuse and Neurodegenerative Disease. *Adv Exp Med Biol* 964:163–175.
- Castro DC, Bruchas MR (2019) A Motivational and Neuropeptidergic Hub: Anatomical and Functional Diversity within the Nucleus Accumbens Shell. *Neuron* 102:529–552.
- Centonze D, Bracci E, Pisani A, Gubellini P, Bernardi G, Calabresi P (2002) Activation of dopamine D1-like receptors excites LTS interneurons of the striatum. *Eur J Neurosci* 15:2049–2052.
- Chen M, Zhao Y, Yang H, Luan W, Song J, Cui D, Dong Y, Lai B, Ma L, Zheng P (2015) Morphine disinhibits glutamatergic input to VTA dopamine neurons and promotes dopamine neuron excitation. *Elife* 4.
- Chen X, Liu Z, Ma C, Ma L, Liu X (2019) Parvalbumin Interneurons Determine Emotional Valence Through Modulating Accumbal Output Pathways. *Front Behav Neurosci* 13:110.
- Cheng J, Umschweif G, Leung J, Sagi Y, Greengard P (2019) HCN2 Channels in Cholinergic Interneurons of Nucleus Accumbens Shell Regulate Depressive Behaviors. *Neuron* 101:662-672.e5.
- Chevalyere V, Takahashi KA, Castillo PE (2006) Endocannabinoid-mediated synaptic plasticity in the CNS. *Annu Rev Neurosci* 29:37–76.
- Cohen K, Weizman A, Weinstein A (2019) Modulatory effects of cannabinoids on brain neurotransmission. *Eur J Neurosci* 50:2322–2345.
- Cole SL, Robinson MJF, Berridge KC (2018) Optogenetic self-stimulation in the nucleus accumbens: D1 reward versus D2 ambivalence. *PLoS ONE* 13:e0207694.
- Collins AL, Aitken TJ, Huang I-W, Shieh C, Greenfield VY, Monbouquette HG, Ostlund SB, Wassum KM (2019) Nucleus Accumbens Cholinergic Interneurons Oppose Cue-Motivated Behavior. *Biol Psychiatry* 86:388–396.
- Conti M, Spulber S, Raciti M, Ceccatelli S (2017) Depressive-like phenotype induced by prenatal dexamethasone in mice is reversed by desipramine. *Neuropharmacology* 126:242–249.
- Corre J, van Zessen R, Loureiro M, Patriarchi T, Tian L, Pascoli V, Lüscher C (2018) Dopamine neurons projecting to medial shell of the nucleus accumbens drive heroin reinforcement. *Elife* 7.
- Covey DP, Cheer JF (2019) Accumbal Dopamine Release Tracks the Expectation of Dopamine Neuron-Mediated Reinforcement. *Cell Rep* 27:481-490.e3.

- Cruz FC, Babin KR, Leao RM, Goldart EM, Bossert JM, Shaham Y, Hope BT (2014) Role of Nucleus Accumbens Shell Neuronal Ensembles in Context-Induced Reinstatement of Cocaine-Seeking. *J Neurosci* 34:7437–7446.
- Cruz FC, Koya E, Guez-Barber DH, Bossert JM, Lupica CR, Shaham Y, Hope BT (2013) New technologies for examining neuronal ensembles in drug addiction and fear. *Nat Rev Neurosci* 14:743–754.
- Cruz HG, Ivanova T, Lunn M-L, Stoffel M, Slesinger PA, Lüscher C (2004) Bi-directional effects of GABA(B) receptor agonists on the mesolimbic dopamine system. *Nat Neurosci* 7:153–159.
- Czubayko U, Plenz D (2002) Fast synaptic transmission between striatal spiny projection neurons. *Proc Natl Acad Sci USA* 99:15764–15769.
- Damodaran S, Evans RC, Blackwell KT (2014) Synchronized firing of fast-spiking interneurons is critical to maintain balanced firing between direct and indirect pathway neurons of the striatum. *J Neurophysiol* 111:836–848.
- Dautan D, Souza AS, Huerta-Ocampo I, Valencia M, Assous M, Witten IB, Deisseroth K, Tepper JM, Bolam JP, Gerdjikov TV, Mena-Segovia J (2016) Segregated cholinergic transmission modulates dopamine neurons integrated in distinct functional circuits. *Nat Neurosci* 19:1025–1033.
- Delfs JM, Zhu Y, Druhan JP, Aston-Jones GS (1998) Origin of noradrenergic afferents to the shell subregion of the nucleus accumbens: anterograde and retrograde tract-tracing studies in the rat. *Brain Res* 806:127–140.
- Delint-Ramirez I, Garcia-Oscos F, Segev A, Kourrich S (2018) Cocaine engages a non-canonical, dopamine-independent, mechanism that controls neuronal excitability in the nucleus accumbens. *Mol Psychiatry*.
- Deroche MA, Lassalle O, Manzoni OJ (2019) Cell-type and endocannabinoid specific synapse connectivity in the adult nucleus accumbens core. *bioRxiv*:613497.
- Dismukes K, Snyder SH (1974) Histamine turnover in rat brain. *Brain Res* 78:467–481.
- Dobbs LK, Kaplan AR, Lemos JC, Matsui A, Rubinstein M, Alvarez VA (2016) Dopamine Regulation of Lateral Inhibition between Striatal Neurons Gates the Stimulant Actions of Cocaine. *Neuron* 90:1100–1113.
- Dong Y, Taylor JR, Wolf ME, Shaham Y (2017) Circuit and Synaptic Plasticity Mechanisms of Drug Relapse. *J Neurosci* 37:10867–10876.
- Edwards NJ, Tejada HA, Pignatelli M, Zhang S, McDevitt RA, Wu J, Bass CE, Bettler B, Morales M, Bonci A (2017) Circuit specificity in the inhibitory architecture of the VTA regulates cocaine-induced behavior. *Nat Neurosci* 20:438–448.

- Eggermann E, Jonas P (2011) How the “slow” Ca(2+) buffer parvalbumin affects transmitter release in nanodomain-coupling regimes. *Nat Neurosci* 15:20–22.
- Elghaba R, Vautrelle N, Bracci E (2016) Mutual Control of Cholinergic and Low-Threshold Spike Interneurons in the Striatum. *Front Cell Neurosci* 10 Available at: <https://www.ncbi.nlm.nih.gov/pmc/articles/PMC4850159/> [Accessed October 27, 2019].
- Ellender TJ, Huerta-Ocampo I, Deisseroth K, Capogna M, Bolam JP (2011) Differential modulation of excitatory and inhibitory striatal synaptic transmission by histamine. *J Neurosci* 31:15340–15351.
- English DF, Ibanez-Sandoval O, Stark E, Tecuapetla F, Buzsáki G, Deisseroth K, Tepper JM, Koos T (2011) GABAergic circuits mediate the reinforcement-related signals of striatal cholinergic interneurons. *Nat Neurosci* 15:123–130.
- Fallon JH, Moore RY (1978) Catecholamine innervation of the basal forebrain. IV. Topography of the dopamine projection to the basal forebrain and neostriatum. *J Comp Neurol* 180:545–580.
- Faust TW, Assous M, Tepper JM, Koos T (2016) Neostriatal GABAergic Interneurons Mediate Cholinergic Inhibition of Spiny Projection Neurons. *J Neurosci* 36:9505–9511.
- Ferrario CR, Loweth JA, Milovanovic M, Ford KA, Galiñanes GL, Heng L-J, Tseng KY, Wolf ME (2011) Alterations in AMPA receptor subunits and TARPs in the rat nucleus accumbens related to the formation of Ca<sup>2+</sup>-permeable AMPA receptors during the incubation of cocaine craving. *Neuropharmacology* 61:1141–1151.
- Fino E, Araya R, Peterka DS, Salierno M, Etchenique R, Yuste R (2009) RuBi-Glutamate: Two-Photon and Visible-Light Photoactivation of Neurons and Dendritic spines. *Front Neural Circuits* 3:2.
- Fino E, Vandecasteele M, Perez S, Saudou F, Venance L (2018) Region-specific and state-dependent action of striatal GABAergic interneurons. *Nat Commun* 9 Available at: <https://www.ncbi.nlm.nih.gov/pmc/articles/PMC6104028/> [Accessed October 27, 2019].
- Fitzjohn SM, Collingridge GL (2002) Calcium stores and synaptic plasticity. *Cell Calcium* 32:405–411.
- Floresco SB, Ghods-Sharifi S, Vexelman C, Magyar O (2006) Dissociable Roles for the Nucleus Accumbens Core and Shell in Regulating Set Shifting. *J Neurosci* 26:2449–2457.
- Francis TC, Chandra R, Friend DM, Finkel E, Dayrit G, Miranda J, Brooks JM, Iñiguez SD, O'Donnell P, Kravitz A, Lobo MK (2015) Nucleus accumbens medium spiny neuron subtypes mediate depression-related outcomes to social defeat stress. *Biol Psychiatry* 77:212–222.
- Francis TC, Lobo MK (2017) Emerging Role for Nucleus Accumbens Medium Spiny Neuron Subtypes in Depression. *Biol Psychiatry* 81:645–653.

- Francis TC, Yano H, Demarest TG, Shen H, Bonci A (2019) High-Frequency Activation of Nucleus Accumbens D1-MSNs Drives Excitatory Potentiation on D2-MSNs. *Neuron* 103:432-444.e3.
- Gerachshenko T, Blackmer T, Yoon E-J, Bartleson C, Hamm HE, Alford S (2005) Gbetagamma acts at the C terminus of SNAP-25 to mediate presynaptic inhibition. *Nat Neurosci* 8:597–605.
- Giannoni P, Passani M-B, Nosi D, Chazot PL, Shenton FC, Medhurst AD, Munari L, Blandina P (2009) Heterogeneity of histaminergic neurons in the tuberomammillary nucleus of the rat. *Eur J Neurosci* 29:2363–2374.
- Gittis AH, Nelson AB, Thwin MT, Palop JJ, Kreitzer AC (2010) Distinct roles of GABAergic interneurons in the regulation of striatal output pathways. *J Neurosci* 30:2223–2234.
- Giustino TF, Fitzgerald PJ, Ressler RL, Maren S (2019) Locus coeruleus toggles reciprocal prefrontal firing to reinstate fear. *Proc Natl Acad Sci USA* 116:8570–8575.
- Graziane NM, Sun S, Wright WJ, Jang D, Liu Z, Huang YH, Nestler EJ, Wang YT, Schlüter OM, Dong Y (2016) Opposing mechanisms mediate morphine- and cocaine-induced generation of silent synapses. *Nat Neurosci* 19:915–925.
- Grueter BA, Brasnjo G, Malenka RC (2010) Postsynaptic TRPV1 triggers cell type-specific long-term depression in the nucleus accumbens. *Nat Neurosci* 13:1519–1525.
- Grueter BA, Rothwell PE, Malenka RC (2012) Integrating synaptic plasticity and striatal circuit function in addiction. *Curr Opin Neurobiol* 22:545–551.
- Gunter BW, Gould RW, Bubser M, McGowan KM, Lindsley CW, Jones CK (2018) Selective Inhibition of M5 Muscarinic Acetylcholine Receptors Attenuates Cocaine Self-Administration in Rats. *Addict Biol* 23:1106–1116.
- Haas H, Panula P (2003) The role of histamine and the tuberomammillary nucleus in the nervous system. *Nat Rev Neurosci* 4:121–130.
- Haber SN, Fudge JL, McFarland NR (2000) Striatonigrostriatal Pathways in Primates Form an Ascending Spiral from the Shell to the Dorsolateral Striatum. *J Neurosci* 20:2369–2382.
- Hainmüller T, Krieglstein K, Kulik A, Bartos M (2014) Joint CP-AMPA and group I mGlu receptor activation is required for synaptic plasticity in dentate gyrus fast-spiking interneurons. *Proc Natl Acad Sci U S A* 111:13211–13216.
- Harris NA, Isaac AT, Günther A, Merkel K, Melchior J, Xu M, Eguakun E, Perez R, Nabit BP, Flavin S, Gilsbach R, Shonesy B, Hein L, Abel T, Baumann A, Matthews R, Centanni SW, Winder DG (2018) Dorsal BNST  $\alpha$ 2A-Adrenergic Receptors Produce HCN-Dependent Excitatory Actions That Initiate Anxiogenic Behaviors. *J Neurosci* 38:8922–8942.

- He C, Chen F, Li B, Hu Z (2014) Neurophysiology of HCN channels: from cellular functions to multiple regulations. *Prog Neurobiol* 112:1–23.
- Hearing MC, Jedynak J, Ebner SR, Ingebretson A, Asp AJ, Fischer RA, Schmidt C, Larson EB, Thomas MJ (2016) Reversal of morphine-induced cell-type-specific synaptic plasticity in the nucleus accumbens shell blocks reinstatement. *Proc Natl Acad Sci U S A* 113:757–762.
- Heifets BD, Chevaleyre V, Castillo PE (2008) Interneuron activity controls endocannabinoid-mediated presynaptic plasticity through calcineurin. *Proc Natl Acad Sci USA* 105:10250–10255.
- Hoebel BG, Avena NM, Rada P (2007) Accumbens dopamine-acetylcholine balance in approach and avoidance. *Curr Opin Pharmacol* 7:617–627.
- Hoffman AF, Lupica CR (2001) Direct actions of cannabinoids on synaptic transmission in the nucleus accumbens: a comparison with opioids. *J Neurophysiol* 85:72–83.
- Holly EN, Davatolhagh MF, Choi K, Alabi OO, Vargas Cifuentes L, Fuccillo MV (2019) Striatal Low-Threshold Spiking Interneurons Regulate Goal-Directed Learning. *Neuron* 103:92-101.e6.
- Horwood JM, Dufour F, Laroche S, Davis S (2006) Signalling mechanisms mediated by the phosphoinositide 3-kinase/Akt cascade in synaptic plasticity and memory in the rat. *Eur J Neurosci* 23:3375–3384.
- Houchi H, Babovic D, Pierrefiche O, Ledent C, Daoust M, Naassila M (2005) CB1 receptor knockout mice display reduced ethanol-induced conditioned place preference and increased striatal dopamine D2 receptors. *Neuropsychopharmacology* 30:339–349.
- Hu H, Gan J, Jonas P (2014) Interneurons. Fast-spiking, parvalbumin<sup>+</sup> GABAergic interneurons: from cellular design to microcircuit function. *Science* 345:1255–1263.
- Huang C-C, Liang Y-C, Lee C-C, Hsu K-S (2015a) Cocaine Withdrawal Impairs mGluR5-Dependent Long-Term Depression in Nucleus Accumbens Shell Neurons of Both Direct and Indirect Pathways. *Mol Neurobiol* 52:1223–1233.
- Huang C-C, Yeh C-M, Wu M-Y, Chang AYW, Chan JYH, Chan SHH, Hsu K-S (2011) Cocaine withdrawal impairs metabotropic glutamate receptor-dependent long-term depression in the nucleus accumbens. *J Neurosci* 31:4194–4203.
- Huang YH, Schlüter OM, Dong Y (2015b) Silent Synapses Speak Up: Updates of the Neural Rejuvenation Hypothesis of Drug Addiction. *Neuroscientist* 21:451–459.
- Hwang E-K, Lupica CR (2019) Altered Corticolimbic Control of the Nucleus Accumbens by Long-term  $\Delta^9$ -Tetrahydrocannabinol Exposure. *Biol Psychiatry*.
- Ikemoto S (2007) Dopamine reward circuitry: two projection systems from the ventral midbrain to the nucleus accumbens-olfactory tubercle complex. *Brain Res Rev* 56:27–78.

- Ingebretson AE, Hearing MC, Huffington ED, Thomas MJ (2018) Endogenous dopamine and endocannabinoid signaling mediate cocaine-induced reversal of AMPAR synaptic potentiation in the nucleus accumbens shell. *Neuropharmacology* 131:154–165.
- Iremonger KJ, Bains JS (2009) Retrograde opioid signaling regulates glutamatergic transmission in the hypothalamus. *J Neurosci* 29:7349–7358.
- Jedynak J, Hearing M, Ingebretson A, Ebner SR, Kelly M, Fischer RA, Kourrich S, Thomas MJ (2016) Cocaine and Amphetamine Induce Overlapping but Distinct Patterns of AMPAR Plasticity in Nucleus Accumbens Medium Spiny Neurons. *Neuropsychopharmacology* 41:464–476.
- Jernigan KK, Cselenyi CS, Thorne CA, Hanson AJ, Tahinci E, Hajicek N, Oldham WM, Lee LA, Hamm HE, Hepler JR, Kozasa T, Linder ME, Lee E (2010) Gbetagamma activates GSK3 to promote LRP6-mediated beta-catenin transcriptional activity. *Sci Signal* 3:ra37.
- Ji M-J, Zhang X-Y, Peng X-C, Zhang Y-X, Chen Z, Yu L, Wang J-J, Zhu J-N (2018) Histamine Excites Rat GABAergic Ventral Pallidum Neurons via Co-activation of H1 and H2 Receptors. *Neurosci Bull* 34:1029–1036.
- Joffe ME, Grueter BA (2016) Cocaine Experience Enhances Thalamo-Accumbens N-Methyl-D-Aspartate Receptor Function. *Biol Psychiatry* 80:671–681.
- Joffe ME, Santiago CI, Stansley BJ, Maksymetz J, Gogliotti RG, Engers JL, Nicoletti F, Lindsley CW, Conn PJ (2019) Mechanisms underlying prelimbic prefrontal cortex mGlu3/mGlu5-dependent plasticity and reversal learning deficits following acute stress. *Neuropharmacology* 144:19–28.
- Joffe ME, Turner BD, Delpire E, Grueter BA (2018) Genetic loss of GluN2B in D1-expressing cell types enhances long-term cocaine reward and potentiation of thalamo-accumbens synapses. *Neuropsychopharmacology* 43:2383–2389.
- Kalivas PW (2009) The glutamate homeostasis hypothesis of addiction. *Nat Rev Neurosci* 10:561–572.
- Kashima DT, Grueter BA (2017) Toll-like receptor 4 deficiency alters nucleus accumbens synaptic physiology and drug reward behavior. *Proc Natl Acad Sci USA* 114:8865–8870.
- Kawaguchi Y (1993) Physiological, morphological, and histochemical characterization of three classes of interneurons in rat neostriatum. *J Neurosci* 13:4908–4923.
- Kawaguchi Y, Wilson CJ, Augood SJ, Emson PC (1995) Striatal interneurons: chemical, physiological and morphological characterization. *Trends Neurosci* 18:527–535.
- Kerfoot EC, Williams CL (2011) Interactions between brainstem noradrenergic neurons and the nucleus accumbens shell in modulating memory for emotionally arousing events. *Learn Mem* 18:405–413.

- Kim N, Li HE, Hughes RN, Watson GDR, Gallegos D, West AE, Kim IH, Yin HH (2019a) A striatal interneuron circuit for continuous target pursuit. *Nat Commun* 10:2715.
- Kim T, Capps RA, Hamade KC, Barnett WH, Todorov DI, Latash EM, Markin SN, Rybak IA, Molkov YI (2019b) The Functional Role of Striatal Cholinergic Interneurons in Reinforcement Learning From Computational Perspective. *Front Neural Circuits* 13:10.
- Knackstedt LA, Moussawi K, Lalumiere R, Schwendt M, Klugmann M, Kalivas PW (2010) Extinction training after cocaine self-administration induces glutamatergic plasticity to inhibit cocaine seeking. *J Neurosci* 30:7984–7992.
- Kononoff Vanhanen J, Nuutinen S, Tuominen M, Panula P (2016) Histamine H3 Receptor Regulates Sensorimotor Gating and Dopaminergic Signaling in the Striatum. *J Pharmacol Exp Ther* 357:264–272.
- Koob GF, Volkow ND (2016) Neurobiology of addiction: a neurocircuitry analysis. *Lancet Psychiatry* 3:760–773.
- Kourrich S (2017) Sigma-1 Receptor and Neuronal Excitability. *Handb Exp Pharmacol* 244:109–130.
- Kourrich S, Hayashi T, Chuang J-Y, Tsai S-Y, Su T-P, Bonci A (2013) Dynamic interaction between sigma-1 receptor and Kv1.2 shapes neuronal and behavioral responses to cocaine. *Cell* 152:236–247.
- Kreitzer AC, Malenka RC (2005) Dopamine modulation of state-dependent endocannabinoid release and long-term depression in the striatum. *J Neurosci* 25:10537–10545.
- Kupchik YM, Brown RM, Heinsbroek JA, Lobo MK, Schwartz DJ, Kalivas PW (2015) Coding the direct/indirect pathways by D1 and D2 receptors is not valid for accumbens projections. *Nat Neurosci* 18:1230–1232.
- Labouèbe G, Lomazzi M, Cruz HG, Creton C, Luján R, Li M, Yanagawa Y, Obata K, Watanabe M, Wickman K, Boyer SB, Slesinger PA, Lüscher C (2007) RGS2 modulates coupling between GABAB receptors and GIRK channels in dopamine neurons of the ventral tegmental area. *Nat Neurosci* 10:1559–1568.
- Laurent V, Bertran-Gonzalez J, Chieng BC, Balleine BW (2014)  $\delta$ -opioid and dopaminergic processes in accumbens shell modulate the cholinergic control of predictive learning and choice. *J Neurosci* 34:1358–1369.
- Lee BR, Ma Y-Y, Huang YH, Wang X, Otaka M, Ishikawa M, Neumann PA, Graziane NM, Brown TE, Suska A, Guo C, Lobo MK, Sesack SR, Wolf ME, Nestler EJ, Shaham Y, Schlüter OM, Dong Y (2013) Maturation of silent synapses in amygdala-accumbens projection contributes to incubation of cocaine craving. *Nat Neurosci* 16:1644–1651.
- Lee S-H, Ledri M, Tóth B, Marchionni I, Henstridge CM, Dudok B, Kenesei K, Barna L, Szabó SI, Renkecz T, Oberoi M, Watanabe M, Limoli CL, Horvai G, Soltesz I, Katona I (2015)

- Multiple Forms of Endocannabinoid and Endovanilloid Signaling Regulate the Tonic Control of GABA Release. *J Neurosci* 35:10039–10057.
- LeGates TA, Kvarita MD, Tooley JR, Francis TC, Lobo MK, Creed MC, Thompson SM (2018) Reward behaviour is regulated by the strength of hippocampus-nucleus accumbens synapses. *Nature* 564:258–262.
- Lemos JC, Shin JH, Alvarez VA (2019) Striatal Cholinergic Interneurons Are a Novel Target of Corticotropin Releasing Factor. *J Neurosci* 39:5647–5661.
- Lemos JC, Wanat MJ, Smith JS, Reyes BAS, Hollon NG, Van Bockstaele EJ, Chavkin C, Phillips PEM (2012) Severe stress switches CRF action in the nucleus accumbens from appetitive to aversive. *Nature* 490:402–406.
- Li G, Liu Z-L, Zhang W-N, Yang K (2016) Blockade of presynaptic 4-aminopyridine-sensitive potassium channels increases initial neurotransmitter release probability, reinstates synaptic transmission altered by GABAB receptor activation in rat midbrain periaqueductal gray. *Neuroreport* 27:50–55.
- Liu SQ, Cull-Candy SG (2000) Synaptic activity at calcium-permeable AMPA receptors induces a switch in receptor subtype. *Nature* 405:454–458.
- Logie C, Bagetta V, Bracci E (2013) Presynaptic control of corticostriatal synapses by endogenous GABA. *J Neurosci* 33:15425–15431.
- Lüscher C (2016) The Emergence of a Circuit Model for Addiction. *Annu Rev Neurosci* 39:257–276.
- Lüscher C, Huber KM (2010) Group 1 mGluR-Dependent Synaptic Long-Term Depression: Mechanisms and Implications for Circuitry and Disease. *Neuron* 65:445–459.
- Lüscher C, Malenka RC (2011) Drug-evoked synaptic plasticity in addiction: from molecular changes to circuit remodeling. *Neuron* 69:650–663.
- Malenka RC, Bear MF (2004) LTP and LTD: an embarrassment of riches. *Neuron* 44:5–21.
- Mamaligas AA, Ford CP (2016) Spontaneous synaptic activation of muscarinic receptors by striatal cholinergic neuron firing. *Neuron* 91:574–586.
- Mantsch JR, Baker DA, Funk D, Lê AD, Shaham Y (2016) Stress-Induced Reinstatement of Drug Seeking: 20 Years of Progress. *Neuropsychopharmacology* 41:335–356.
- Manvich DF, Petko AK, Branco RC, Foster SL, Porter-Stransky KA, Stout KA, Newman AH, Miller GW, Paladini CA, Weinshenker D (2019) Selective D2 and D3 receptor antagonists

- oppositely modulate cocaine responses in mice via distinct postsynaptic mechanisms in nucleus accumbens. *Neuropsychopharmacology* 44:1445–1455.
- Manz KM, Baxley AG, Zurawski Z, Hamm HE, Grueter BA (2019) Heterosynaptic GABA<sub>B</sub> receptor function within feedforward microcircuits gates glutamatergic transmission in the nucleus accumbens core. *J Neurosci*.
- Martín-García E, Bourgoin L, Cathala A, Kasanetz F, Mondesir M, Gutiérrez-Rodríguez A, Reguero L, Fiancette J-F, Grandes P, Spampinato U, Maldonado R, Piazza PV, Marsicano G, Deroche-Gamonet V (2016) Differential Control of Cocaine Self-Administration by GABAergic and Glutamatergic CB1 Cannabinoid Receptors. *Neuropsychopharmacology* 41:2192–2205.
- Mathur BN, Tanahira C, Tamamaki N, Lovinger DM (2013) Voltage drives diverse endocannabinoid signals to mediate striatal microcircuit-specific plasticity. *Nat Neurosci* 16:1275–1283.
- Mato S, Chevalyere V, Robbe D, Pazos A, Castillo PE, Manzoni OJ (2004) A single in-vivo exposure to delta 9THC blocks endocannabinoid-mediated synaptic plasticity. *Nat Neurosci* 7:585–586.
- Matsui A, Alvarez VA (2018) Cocaine Inhibition of Synaptic Transmission in the Ventral Pallidum Is Pathway-Specific and Mediated by Serotonin. *Cell Rep* 23:3852–3863.
- Maurice N, Mercer J, Chan CS, Hernandez-Lopez S, Held J, Tkatch T, Surmeier DJ (2004) D2 dopamine receptor-mediated modulation of voltage-dependent Na<sup>+</sup> channels reduces autonomous activity in striatal cholinergic interneurons. *J Neurosci* 24:10289–10301.
- McKittrick CR, Abercrombie ED (2007) Catecholamine mapping within nucleus accumbens: differences in basal and amphetamine-stimulated efflux of norepinephrine and dopamine in shell and core. *J Neurochem* 100:1247–1256.
- Meitzen J, Luoma JI, Stern CM, Mermelstein PG (2011)  $\beta$ 1-adrenergic receptors activate two distinct signaling pathways in striatal neurons. *J Neurochem* 116:984–995.
- Melendez-Zaidi AE, Lakshminarasimhah H, Surmeier DJ (2019) Cholinergic modulation of striatal nitric oxide-producing interneurons. *Eur J Neurosci*.
- Miklós IH, Kovács KJ (2003) Functional heterogeneity of the responses of histaminergic neuron subpopulations to various stress challenges. *Eur J Neurosci* 18:3069–3079.
- Mitrano DA, Schroeder JP, Smith Y, Cortright JJ, Bubula N, Vezina P, Weinshenker D (2012)  $\alpha$ -1 Adrenergic receptors are localized on presynaptic elements in the nucleus accumbens and regulate mesolimbic dopamine transmission. *Neuropsychopharmacology* 37:2161–2172.

- Moreno E, Hoffmann H, Gonzalez-Sepúlveda M, Navarro G, Casadó V, Cortés A, Mallol J, Vignes M, McCormick PJ, Canela EI, Lluís C, Moratalla R, Ferré S, Ortiz J, Franco R (2011) Dopamine D1-histamine H3 receptor heteromers provide a selective link to MAPK signaling in GABAergic neurons of the direct striatal pathway. *J Biol Chem* 286:5846–5854.
- Moreno E, Moreno-Delgado D, Navarro G, Hoffmann HM, Fuentes S, Rosell-Vilar S, Gasperini P, Rodríguez-Ruiz M, Medrano M, Mallol J, Cortés A, Casadó V, Lluís C, Ferré S, Ortiz J, Canela E, McCormick PJ (2014) Cocaine disrupts histamine H3 receptor modulation of dopamine D1 receptor signaling:  $\sigma$ 1-D1-H3 receptor complexes as key targets for reducing cocaine's effects. *J Neurosci* 34:3545–3558.
- Morisset S, Rouleau A, Ligneau X, Gbahou F, Tardivel-Lacombe J, Stark H, Schunack W, Ganellin CR, Schwartz JC, Arrang JM (2000) High constitutive activity of native H3 receptors regulates histamine neurons in brain. *Nature* 408:860–864.
- Moyer JT, Halterman BL, Finkel LH, Wolf JA (2014) Lateral and feedforward inhibition suppress asynchronous activity in a large, biophysically-detailed computational model of the striatal network. *Front Comput Neurosci* 8:152.
- Nakamura Y, Dryanovski DI, Kimura Y, Jackson SN, Woods AS, Yasui Y, Tsai S-Y, Patel S, Covey DP, Su T-P, Lupica C (2019) Cocaine-induced endocannabinoid signaling mediated by sigma-1 receptors and extracellular vesicle secretion. *Elife* 8.
- Neuhöfer D, Lassalle O, Manzoni OJ (2018) Muscarinic M1 Receptor Modulation of Synaptic Plasticity in Nucleus Accumbens of Wild-Type and Fragile X Mice. *ACS Chem Neurosci* 9:2233–2240.
- Neumann PA, Wang Y, Yan Y, Wang Y, Ishikawa M, Cui R, Huang YH, Sesack SR, Schlüter OM, Dong Y (2016) Cocaine-Induced Synaptic Alterations in Thalamus to Nucleus Accumbens Projection. *Neuropsychopharmacology* 41:2399–2410.
- Nicola SM, Malenka RC (1997) Dopamine depresses excitatory and inhibitory synaptic transmission by distinct mechanisms in the nucleus accumbens. *J Neurosci* 17:5697–5710.
- Nicola SM, Malenka RC (1998) Modulation of synaptic transmission by dopamine and norepinephrine in ventral but not dorsal striatum. *J Neurophysiol* 79:1768–1776.
- Nissen W, Szabo A, Somogyi J, Somogyi P, Lamsa KP (2010) Cell Type-Specific Long-Term Plasticity at Glutamatergic Synapses onto Hippocampal Interneurons Expressing either Parvalbumin or CB1 Cannabinoid Receptor. *J Neurosci* 30:1337–1347.
- Nuutinen S, Vanhanen J, Mäki T, Panula P (2012) Histamine H3 Receptor: A Novel Therapeutic Target in Alcohol Dependence? *Front Syst Neurosci* 6 Available at: <https://www.ncbi.nlm.nih.gov/pmc/articles/PMC3355329/> [Accessed October 27, 2019].

- O'Hare JK, Li H, Kim N, Gaidis E, Ade K, Beck J, Yin H, Calakos N (2017) Striatal fast-spiking interneurons selectively modulate circuit output and are required for habitual behavior. *Elife* 6.
- Orduz D, Bishop DP, Schwaller B, Schiffmann SN, Gall D (2013) Parvalbumin tunes spike-timing and efferent short-term plasticity in striatal fast spiking interneurons. *J Physiol (Lond)* 591:3215–3232.
- Owen SF, Berke JD, Kreitzer AC (2018) Fast-Spiking Interneurons Supply Feedforward Control of Bursting, Calcium, and Plasticity for Efficient Learning. *Cell* 172:683-695.e15.
- Owens MJ, Morgan WN, Plott SJ, Nemeroff CB (1997) Neurotransmitter receptor and transporter binding profile of antidepressants and their metabolites. *J Pharmacol Exp Ther* 283:1305–1322.
- Pancani T, Bolarinwa C, Smith Y, Lindsley CW, Conn PJ, Xiang Z (2014) M4 mAChR-Mediated Modulation of Glutamatergic Transmission at Corticostriatal Synapses. *ACS Chem Neurosci* 5:318–324.
- Pardo-Garcia TR, Garcia-Keller C, Penaloza T, Richie CT, Pickel J, Hope BT, Harvey BK, Kalivas PW, Heinsbroek JA (2019) Ventral Pallidum Is the Primary Target for Accumbens D1 Projections Driving Cocaine Seeking. *J Neurosci* 39:2041–2051.
- Park JW, Bhimani RV, Park J (2017) Noradrenergic Modulation of Dopamine Transmission Evoked by Electrical Stimulation of the Locus Coeruleus in the Rat Brain. *ACS Chem Neurosci* 8:1913–1924.
- Pascoli V, Terrier J, Espallergues J, Valjent E, O'Connor EC, Lüscher C (2014) Contrasting forms of cocaine-evoked plasticity control components of relapse. *Nature* 509:459–464.
- Pascoli V, Turiault M, Lüscher C (2011) Reversal of cocaine-evoked synaptic potentiation resets drug-induced adaptive behaviour. *Nature* 481:71–75.
- Passani MB, Blandina P (2011) Histamine receptors in the CNS as targets for therapeutic intervention. *Trends Pharmacol Sci* 32:242–249.
- Patton MH, Padgett KE, McKeon PN, Qadir H, Patton MS, Mu C, Roberts BM, Mathur BN (2019) TrkB-dependent disinhibition of the nucleus accumbens is enhanced by ethanol. *Neuropsychopharmacology* 44:1114–1122.
- Peng S-Y, Li B, Xi K, Wang J-J, Zhu J-N (2018) Presynaptic  $\alpha 2$ -adrenoceptor modulates glutamatergic synaptic transmission in rat nucleus accumbens in vitro. *Neurosci Lett* 665:117–122.
- Pennartz CM, Boeijinga PH, Kitai ST, Lopes da Silva FH (1991) Contribution of NMDA receptors to postsynaptic potentials and paired-pulse facilitation in identified neurons of the rat nucleus accumbens in vitro. *Exp Brain Res* 86:190–198.

- Pina MM, Cunningham CL (2014) Effects of dopamine receptor antagonists on the acquisition of ethanol-induced conditioned place preference in mice. *Psychopharmacology (Berl)* 231:459–468.
- Pisani A, Bonsi P, Centonze D, Martorana A, Fusco F, Sancesario G, De Persis C, Bernardi G, Calabresi P (2003) Activation of beta1-adrenoceptors excites striatal cholinergic interneurons through a cAMP-dependent, protein kinase-independent pathway. *J Neurosci* 23:5272–5282.
- Pisansky MT, Lefevre EM, Retzlaff CL, Trieu BH, Leipold DW, Rothwell PE (2019) Nucleus Accumbens Fast-Spiking Interneurons Constrain Impulsive Action. *Biol Psychiatry*.
- Pittenger C (2019) The histidine decarboxylase model of tic pathophysiology: a new focus on the histamine H3 receptor. *Br J Pharmacol*.
- Planert H, Szydlowski SN, Hjorth JJJ, Grillner S, Silberberg G (2010) Dynamics of synaptic transmission between fast-spiking interneurons and striatal projection neurons of the direct and indirect pathways. *J Neurosci* 30:3499–3507.
- Plenz D, Kitai ST (1998) Up and down states in striatal medium spiny neurons simultaneously recorded with spontaneous activity in fast-spiking interneurons studied in cortex-striatum-substantia nigra organotypic cultures. *J Neurosci* 18:266–283.
- Plotkin JL, Day M, Surmeier DJ (2011) Synaptically driven state transitions in distal dendrites of striatal spiny neurons. *Nat Neurosci* 14:881–888.
- Qi J, Zhang S, Wang H-L, Barker DJ, Miranda-Barrientos J, Morales M (2016) VTA glutamatergic inputs to nucleus accumbens drive aversion by acting on GABAergic interneurons. *Nat Neurosci* 19:725–733.
- Rapanelli M, Frick L, Bito H, Pittenger C (2017) Histamine modulation of the basal ganglia circuitry in the development of pathological grooming. *Proc Natl Acad Sci USA* 114:6599–6604.
- Rapanelli M, Frick L, Jindachomthong K, Xu J, Ohtsu H, Nairn AC, Pittenger C (2018) Striatal Signaling Regulated by the H3R Histamine Receptor in a Mouse Model of tic Pathophysiology. *Neuroscience* 392:172–179.
- Rapanelli M, Frick LR, Horn KD, Schwarcz RC, Pogorelov V, Nairn AC, Pittenger C (2016) The Histamine H3 Receptor Differentially Modulates Mitogen-activated Protein Kinase (MAPK) and Akt Signaling in Striatonigral and Striatopallidal Neurons. *J Biol Chem* 291:21042–21052.
- Rapanelli M, Frick LR, Pogorelov V, Ota KT, Abbasi E, Ohtsu H, Pittenger C (2014) Dysregulated intracellular signaling in the striatum in a pathophysiologically grounded model of Tourette syndrome. *Eur Neuropsychopharmacol* 24:1896–1906.

- Ribeiro EA et al. (2018) Transcriptional and physiological adaptations in nucleus accumbens somatostatin interneurons that regulate behavioral responses to cocaine. *Nat Commun* 9:3149.
- Ribeiro EA, Nectow AR, Pomeranz LE, Ekstrand MI, Koo JW, Nestler EJ (2019) Viral labeling of neurons synaptically connected to nucleus accumbens somatostatin interneurons. *PLoS ONE* 14:e0213476.
- Rice ME, Cragg SJ (2004) Nicotine amplifies reward-related dopamine signals in striatum. *Nat Neurosci* 7:583–584.
- Rothwell PE, Kourrich S, Thomas MJ (2011) Synaptic adaptations in the nucleus accumbens caused by experiences linked to relapse. *Biol Psychiatry* 69:1124–1126.
- Saito YC, Maejima T, Nishitani M, Hasegawa E, Yanagawa Y, Mieda M, Sakurai T (2018) Monoamines Inhibit GABAergic Neurons in Ventrolateral Preoptic Area That Make Direct Synaptic Connections to Hypothalamic Arousal Neurons. *J Neurosci* 38:6366–6378.
- Salgado S, Kaplitt MG (2015) The Nucleus Accumbens: A Comprehensive Review. *SFN* 93:75–93.
- Schultz W (1998) Predictive reward signal of dopamine neurons. *J Neurophysiol* 80:1–27.
- Scudder SL, Baimel C, Macdonald EE, Carter AG (2018) Hippocampal-Evoked Feedforward Inhibition in the Nucleus Accumbens. *J Neurosci* 38:9091–9104.
- Shang Y, Filizola M (2015) Opioid receptors: Structural and mechanistic insights into pharmacology and signaling. *Eur J Pharmacol* 763:206–213.
- Shin JH, Adrover MF, Alvarez VA (2017) Distinctive Modulation of Dopamine Release in the Nucleus Accumbens Shell Mediated by Dopamine and Acetylcholine Receptors. *J Neurosci* 37:11166–11180.
- Shin JH, Adrover MF, Wess J, Alvarez VA (2015) Muscarinic regulation of dopamine and glutamate transmission in the nucleus accumbens. *Proc Natl Acad Sci USA* 112:8124–8129.
- Shoblock J, O'Donnell P (2000) Histamine Modulation of Nucleus Accumbens Neurons. *Annals of the New York Academy of Sciences* 909:270–272.
- Siciliano CA, Jones SR (2017) Cocaine Potency at the Dopamine Transporter Tracks Discrete Motivational States During Cocaine Self-Administration. *Neuropsychopharmacology* 42:1893–1904.
- Smith ACW, Scofield MD, Heinsbroek JA, Gipson CD, Neuhofer D, Roberts-Wolfe DJ, Spencer S, Garcia-Keller C, Stankeviciute NM, Smith RJ, Allen NP, Lorang MR, Griffin WC, Boger HA, Kalivas PW (2017) Accumbens nNOS Interneurons Regulate Cocaine Relapse. *J Neurosci* 37:742–756.

- Soler-Llavina GJ, Sabatini BL (2006) Synapse-specific plasticity and compartmentalized signaling in cerebellar stellate cells. *Nat Neurosci* 9:798–806.
- Solís JM, Nicoll RA (1992) Pharmacological characterization of GABAB-mediated responses in the CA1 region of the rat hippocampal slice. *J Neurosci* 12:3466–3472.
- Sørensen G, Wegener G, Hasselstrøm J, Hansen TVO, Wörtwein G, Fink-Jensen A, Woldbye DPD (2009) Neuropeptide Y infusion into the shell region of the rat nucleus accumbens increases extracellular levels of dopamine. *Neuroreport* 20:1023–1026.
- Steidl S, Yeomans JS (2009) M5 muscarinic receptor knockout mice show reduced morphine-induced locomotion but increased locomotion after cholinergic antagonism in the ventral tegmental area. *J Pharmacol Exp Ther* 328:263–275.
- Straub C, Saulnier JL, Bègue A, Feng DD, Huang KW, Sabatini BL (2016) Principles of synaptic organization of GABAergic interneurons in the striatum. *Neuron* 92:84–92.
- Sullivan MA, Chen H, Morikawa H (2008) Recurrent inhibitory network among striatal cholinergic interneurons. *J Neurosci* 28:8682–8690.
- Sweis BM, Larson EB, Redish AD, Thomas MJ (2018) Altering gain of the infralimbic-to-accumbens shell circuit alters economically dissociable decision-making algorithms. *Proc Natl Acad Sci USA* 115:E6347–E6355.
- Szumliński KK, Ary AW, Lominac KD (2008) Homers regulate drug-induced neuroplasticity: Implications for addiction. *Biochem Pharmacol* 75:112–133.
- Szydlowski SN, Pollak Dorocic I, Planert H, Carlén M, Meletis K, Silberberg G (2013) Target selectivity of feedforward inhibition by striatal fast-spiking interneurons. *J Neurosci* 33:1678–1683.
- Takagi H, Morishima Y, Matsuyama T, Hayashi H, Watanabe T, Wada H (1986) Histaminergic axons in the neostriatum and cerebral cortex of the rat: a correlated light and electron microscopic immunocytochemical study using histidine decarboxylase as a marker. *Brain Res* 364:114–123.
- Takei H, Yamamoto K, Bae Y-C, Shirakawa T, Kobayashi M (2017) Histamine H3 Heteroreceptors Suppress Glutamatergic and GABAergic Synaptic Transmission in the Rat Insular Cortex. *Front Neural Circuits* 11:85.
- Tatsumi M, Groshan K, Blakely RD, Richelson E (1997) Pharmacological profile of antidepressants and related compounds at human monoamine transporters. *Eur J Pharmacol* 340:249–258.
- Taverna S, Canciani B, Pennartz CMA (2007) Membrane properties and synaptic connectivity of fast-spiking interneurons in rat ventral striatum. *Brain Res* 1152:49–56.

- Taylor KM, Snyder SH (1971) Brain histamine: rapid apparent turnover altered by restraint and cold stress. *Science* 172:1037–1039.
- Teal LB, Gould RW, Felts AS, Jones CK (2019) Selective allosteric modulation of muscarinic acetylcholine receptors for the treatment of schizophrenia and substance use disorders. *Adv Pharmacol* 86:153–196.
- Tejeda HA, Wu J, Kornspun AR, Pignatelli M, Kashtelyan V, Krashes MJ, Lowell BB, Carlezon WA, Bonci A (2017) Pathway- and Cell-Specific Kappa-Opioid Receptor Modulation of Excitation-Inhibition Balance Differentially Gates D1 and D2 Accumbens Neuron Activity. *Neuron* 93:147–163.
- Tepper JM, Koós T, Ibanez-Sandoval O, Tecuapetla F, Faust TW, Assous M (2018) Heterogeneity and Diversity of Striatal GABAergic Interneurons: Update 2018. *Front Neuroanat* 12:91.
- Theoharides TC, Spanos C, Pang X, Alferes L, Ligris K, Letourneau R, Rozniecki JJ, Webster E, Chrousos GP (1995) Stress-induced intracranial mast cell degranulation: a corticotropin-releasing hormone-mediated effect. *Endocrinology* 136:5745–5750.
- Thomas MJ, Beurrier C, Bonci A, Malenka RC (2001) Long-term depression in the nucleus accumbens: a neural correlate of behavioral sensitization to cocaine. *Nat Neurosci* 4:1217–1223.
- Threlfell S, Lalic T, Platt NJ, Jennings KA, Deisseroth K, Cragg SJ (2012) Striatal dopamine release is triggered by synchronized activity in cholinergic interneurons. *Neuron* 75:58–64.
- Turner BD, Kashima DT, Manz KM, Grueter CA, Grueter BA (2018a) Synaptic Plasticity in the Nucleus Accumbens: Lessons Learned from Experience. *ACS Chem Neurosci* 9:2114–2126.
- Turner BD, Rook JM, Lindsley CW, Conn PJ, Grueter BA (2018b) mGlu1 and mGlu5 modulate distinct excitatory inputs to the nucleus accumbens shell. *Neuropsychopharmacology* 43:2075–2082.
- Twomey EC, Yelshanskaya MV, Grassucci RA, Frank J, Sobolevsky AI (2017) Channel opening and gating mechanism in AMPA-subtype glutamate receptors. *Nature* 549:60–65.
- Twomey EC, Yelshanskaya MV, Vassilevski AA, Sobolevsky AI (2018) Mechanisms of Channel Block in Calcium-Permeable AMPA Receptors. *Neuron* 99:956-968.e4.
- Uchimura N, North RA (1991) Baclofen and adenosine inhibit synaptic potentials mediated by gamma-aminobutyric acid and glutamate release in rat nucleus accumbens. *J Pharmacol Exp Ther* 258:663–668.
- Vena AA, Mangieri R, Gonzales RA (2016) Regional Analysis of the Pharmacological Effects of Acute Ethanol on Extracellular Striatal Dopamine Activity. *Alcohol Clin Exp Res* 40:2528–2536.

- Venner A, Mochizuki T, De Luca R, Anaclet C, Scammell TE, Saper CB, Arrigoni E, Fuller PM (2019) Reassessing the role of histaminergic tuberomammillary neurons in arousal control. *J Neurosci*.
- Wang J, Ishikawa M, Yang Y, Otaka M, Kim JY, Gardner GR, Stefanik MT, Milovanovic M, Huang YH, Hell JW, Wolf ME, Schlüter OM, Dong Y (2018a) Cascades of Homeostatic Dysregulation Promote Incubation of Cocaine Craving. *J Neurosci* 38:4316–4328.
- Wang X, Gallegos DA, Pogorelov VM, O'Hare JK, Calakos N, Wetsel WC, West AE (2018b) Parvalbumin Interneurons of the Mouse Nucleus Accumbens are Required For Amphetamine-Induced Locomotor Sensitization and Conditioned Place Preference. *Neuropsychopharmacology* 43:953–963.
- Whitehead KJ, Rose S, Jenner P (2001) Involvement of intrinsic cholinergic and GABAergic innervation in the effect of NMDA on striatal dopamine efflux and metabolism as assessed by microdialysis studies in freely moving rats. *Eur J Neurosci* 14:851–860.
- Willett JA, Cao J, Dorris DM, Johnson AG, Ginnari LA, Meitzen J (2019) Electrophysiological Properties of Medium Spiny Neuron Subtypes in the Caudate-Putamen of Prepubertal Male and Female *Drd1a*-tdTomato Line 6 BAC Transgenic Mice. *eNeuro* 6.
- Williams RH, Chee MJS, Kroeger D, Ferrari LL, Maratos-Flier E, Scammell TE, Arrigoni E (2014) Optogenetic-mediated release of histamine reveals distal and autoregulatory mechanisms for controlling arousal. *J Neurosci* 34:6023–6029.
- Winder DG, Sweatt JD (2001) Roles of serine/threonine phosphatases in hippocampal synaptic plasticity. *Nat Rev Neurosci* 2:461–474.
- Winters BD, Krüger JM, Huang X, Gallaher ZR, Ishikawa M, Czaja K, Krueger JM, Huang YH, Schlüter OM, Dong Y (2012) Cannabinoid receptor 1-expressing neurons in the nucleus accumbens. *Proc Natl Acad Sci USA* 109:E2717-2725.
- Wise RA, Koob GF (2014) The development and maintenance of drug addiction. *Neuropsychopharmacology* 39:254–262.
- Witten IB, Lin S-C, Brodsky M, Prakash R, Diester I, Anikeeva P, Gradinaru V, Ramakrishnan C, Deisseroth K (2010) Cholinergic Interneurons Control Local Circuit Activity and Cocaine Conditioning. *Science* 330:1677–1681.
- Wolf ME (2016) Synaptic mechanisms underlying persistent cocaine craving. *Nat Rev Neurosci* 17:351–365.
- Wright WJ, Schlüter OM, Dong Y (2017) A Feedforward Inhibitory Circuit Mediated by CB1-Expressing Fast-Spiking Interneurons in the Nucleus Accumbens. *Neuropsychopharmacology* 42:1146–1156.

- Xu C-M, Wang J, Wu P, Zhu W-L, Li Q-Q, Xue Y-X, Zhai H-F, Shi J, Lu L (2009) Glycogen synthase kinase 3 $\beta$  in the nucleus accumbens core mediates cocaine-induced behavioral sensitization. *J Neurochem* 111:1357–1368.
- Yamamoto K, Ebihara K, Koshikawa N, Kobayashi M (2013) Reciprocal regulation of inhibitory synaptic transmission by nicotinic and muscarinic receptors in rat nucleus accumbens shell. *J Physiol (Lond)* 591:5745–5763.
- Yang H, de Jong JW, Tak Y, Peck J, Bateup HS, Lammel S (2018) Nucleus Accumbens Subnuclei Regulate Motivated Behavior via Direct Inhibition and Disinhibition of VTA Dopamine Subpopulations. *Neuron* 97:434-449.e4.
- Yorgason JT, Zeppenfeld DM, Williams JT (2017) Cholinergic Interneurons Underlie Spontaneous Dopamine Release in Nucleus Accumbens. *J Neurosci* 37:2086–2096.
- Yu J, Yan Y, Li K-L, Wang Y, Huang YH, Urban NN, Nestler EJ, Schlüter OM, Dong Y (2017) Nucleus accumbens feedforward inhibition circuit promotes cocaine self-administration. *Proc Natl Acad Sci USA* 114:E8750–E8759.
- Yu X, Franks NP, Wisden W (2018) Sleep and Sedative States Induced by Targeting the Histamine and Noradrenergic Systems. *Front Neural Circuits* 12:4.
- Yu X, Ye Z, Houston CM, Zecharia AY, Ma Y, Zhang Z, Uygun DS, Parker S, Vyssotski AL, Yustos R, Franks NP, Brickley SG, Wisden W (2015) Wakefulness Is Governed by GABA and Histamine Cotransmission. *Neuron* 87:164–178.
- Zahm DS (1999a) Functional-anatomical implications of the nucleus accumbens core and shell subterritories. *Ann N Y Acad Sci* 877:113–128.
- Zahm DS (1999b) Functional-anatomical implications of the nucleus accumbens core and shell subterritories. *Ann N Y Acad Sci* 877:113–128.
- Zhang C, Liu X, Zhou P, Zhang J, He W, Yuan T-F (2018) Cholinergic tone in ventral tegmental area: Functional organization and behavioral implications. *Neurochem Int* 114:127–133.
- Zhang L, Warren RA (2002) Muscarinic and Nicotinic Presynaptic Modulation of EPSCs in the Nucleus Accumbens During Postnatal Development. *Journal of Neurophysiology* 88:3315–3330.
- Zhang Y-F, Cragg SJ (2017) Pauses in Striatal Cholinergic Interneurons: What is Revealed by Their Common Themes and Variations? *Front Syst Neurosci* 11 Available at: <https://www.ncbi.nlm.nih.gov/pmc/articles/PMC5670143/> [Accessed October 27, 2019].
- Zhao R, Chen J, Ren Z, Shen H, Zhen X (2016) GSK-3 $\beta$  inhibitors reverse cocaine-induced synaptic transmission dysfunction in the nucleus accumbens. *Synapse* 70:461–470.
- Zhu Y, Wienecke CFR, Nachtrab G, Chen X (2016) A thalamic input to the nucleus accumbens mediates opiate dependence. *Nature* 530:219–222.

Zhuang Q-X, Xu H-T, Lu X-J, Li B, Yung W-H, Wang J-J, Zhu J-N (2018) Histamine Excites Striatal Dopamine D1 and D2 Receptor-Expressing Neurons via Postsynaptic H1 and H2 Receptors. *Mol Neurobiol* 55:8059–8070.